

On the Role of Endoplasmic Reticulum Homeostasis and Autophagy in Intestinal Inflammation

Dissertation
zur Erlangung des Doktorgrades
der Mathematisch-Naturwissenschaftlichen Fakultät
der Christian-Albrechts-Universität zu Kiel

vorgelegt von

Stephanie Tanja Stengel

Kiel, 2018

First referee (supervisor): Prof. Dr. Philip Rosenstiel
Second referee: Prof. Dr. Thomas Roeder
Examiner: Prof. Dr. Andre Franke
Chairperson: Prof. Stanislav Gorb

Date of the oral examination: 10 January 2019
Approved for publication on: 10 January 2019

Contents

List of Figures.....	7
List of Tables.....	8
1 Introduction.....	9
1.1 Inflammatory Bowel Disease.....	9
1.2 Genetic Risk Factors for IBD	9
1.3 The Gut Microbiome in Inflammatory Bowel Disease	11
1.4 ER Homeostasis, ER Stress & the Unfolded Protein Response.....	12
1.4.1 IRE1 Signaling	14
1.4.2 PERK Signaling	14
1.4.3 ATF6 α Signaling	14
1.5 Autophagy	15
1.5.1 The Molecular Core Machinery.....	15
1.5.2 Selective Autophagy.....	16
1.5.3 Xenophagy.....	17
1.5.4 ER-phagy.....	17
1.5.5 Crosstalk of the Autophagic Machinery and the Secretory Pathway.....	18
1.6 Crosstalk of ER Stress & Autophagy in Intestinal Inflammation.....	18
1.6.1 ER Stress & Intestinal Inflammation.....	18
1.6.2 ER Stress, Autophagy & Bacterial Sensing Converge in Intestinal Inflammation.....	20
1.7 The ORMDL Protein Family	21
1.7.1 ORMDL3 Modulates UPR Signaling	22
1.7.2 Regulation of Calcium Homeostasis by ORMDL3	22
1.7.3 ORMDL Proteins Regulate Sphingolipid Synthesis	22
1.7.4 ORMDL3 in Intestinal Inflammation.....	23
1.7.5 ORMDL3 & Autophagy	23
1.8 Aims of this Study and Thesis Outline	25
2 Material & Methods	26
2.1 Cell Biological Methods	26
2.1.1 Cell Lines.....	26
2.1.2 Preparation & Culture of Mouse Embryonic Fibroblasts (MEFs)	26
2.1.3 Generation of Immortalized MEFs (iMEFs)	26
2.1.4 Isolation of Crypts & Cultivation of Murine Small Intestinal Organoids	26
2.1.5 Establishment and Culture of Human Intestinal Organoids.....	27
2.1.6 Transient Transfection of Plasmid DNA.....	27

2.1.7 Transfection of siRNA	28
2.1.8 Promoter-Mediated Luciferase Reporter Assay	28
2.2 Molecular Biological Methods	29
2.2.1 Isolation of Total RNA	29
2.2.2 cDNA Synthesis	29
2.2.3 Endpoint Polymerase Chain Reaction	29
2.2.4 Agarose Gel Electrophoresis	30
2.2.5 Quantitative Real-Time Polymerase Chain Reaction	30
2.2.6 Plasmid DNA Isolation	30
2.3 Protein Biochemical Methods	31
2.3.1 Total Protein Lysate Preparation	31
2.3.2 Cell Fractionation	31
2.3.3 Protein Concentration Determination	31
2.3.4 Gel Electrophoresis of Proteins	31
2.3.5 Western Blot Analysis & Immunodetection	32
2.3.6 Co-Immunoprecipitations	32
2.4 Microbiology Techniques	33
2.4.1 Bacterial Strains	33
2.4.2 Bacterial Infection & CFU assay	33
2.4.3 Crypt Infection	33
2.5 Generation, Handling and Treatment of Mice	34
2.5.1 Generation of <i>Ormdl1</i> ^{-/-} , <i>Ormdl2</i> ^{-/-} , & <i>Ormdl3</i> ^{-/-} Mice	34
2.5.2 Animal Housing & Animal Care	35
2.5.3 Genotyping of Mice & iMEFs	35
2.5.4 Infection of Mice	36
2.6 Imaging	36
2.6.1 Immunofluorescence	36
2.6.2 Immunohistochemistry	36
2.6.3 Transmission electron microscopy	37
2.7 Statistical Analysis	37
2.8 High-Throughput RNAi Screening Procedure	37
3 Pharmacological Intervention Ameliorates Hyperactivation of the ATF6 α Branch in Impaired Autophagy and Endoplasmic Reticulum Stress Signaling in Intestinal Epithelial Cells	39
3.1 Results	39
3.1.1 Identification & Functional Network Analysis of ATF6 α Signaling Modulators	39
3.1.2 Chemical Interference with Selected Candidates Validates siRNA-Mediated Phenotypes	42

3.1.3 Nuclear p36ATF6 α Levels Partially Recapitulate ERSE Promoter Activity.....	42
3.1.4 Candidates <i>ACSL1</i> and <i>CSNK2B</i> Induce ATF6 α Signaling in Intestinal Epithelial Cells.....	44
3.1.5 Inhibition of Candidates Decreases Transcription of ATF6 α Target Genes in Human Organoids	44
3.1.6 <i>ACSL1</i> induction of ATF6 α signaling is independent of intramembrane cleavage & <i>CSNK2B</i> assists in COPII mediated transport of ATF6 α	45
3.1.7 The ATF α Branch of the UPR Modulates NF- κ B Signaling	47
3.1.8 Inhibition of ATF6 α Attenuates Pro-Inflammatory Profile in <i>Atg16l1</i> - & <i>Xbp1</i> -Deficient Intestinal Organoids	48
3.2 Discussion	53
3.2.1 Identification and Functional Network Analysis of ATF6 α Signaling Modulators	53
3.2.2 Chemical Interference with Selected Candidates Validates siRNA-Mediated Phenotypes .	54
3.2.3 Candidates <i>ACSL1</i> and <i>CSNK2B</i> are regulators of ATF6 α Signaling in Intestinal Epithelial Cells and Human Organoids	56
3.2.4 <i>ACSL1</i> Induction of ATF6 α Signaling is Independent of Intramembrane Cleavage and <i>CSNK2B</i> Facilitates ER-Golgi Trafficking of ATF6 α	56
3.2.5 The ATF6 α Branch of the UPR Modulates NF- κ B Signaling	57
3.2.6 Inhibition of ATF6 α Attenuates Pro-Inflammatory Profile in <i>Atg16l1</i> - and <i>Xbp1</i> -Deficient Intestinal Organoids	58
3.3 Conclusions & Future Perspectives	60
4 ORMDL3 Engages the Autophagy Machinery to Facilitate Endoplasmic Reticulum Turnover and Bacterial Clearance.....	62
4.1 Results	62
4.1.1 <i>Ormdl3</i> and <i>Ormdl1/3</i> Deficiency Impair Body Growth Whereas Simultaneous Deletion of <i>Ormdl1</i> , <i>Ormdl2</i> and <i>Ormdl3</i> Causes Embryonic Lethality.....	62
4.1.2 <i>Ormdl3</i> Expression is Shaped by the Microbial Community	64
<i>Ormdl3</i> -Deficient Mice Display Increased Susceptibility to Adherent-Invasive <i>E. coli</i> Colonization.	66
4.1.4 Critical Role of ORMDL Proteins for Structure & Function of Secretory Epithelial Cells in the Intestine.....	68
4.1.5 <i>Ormdl1/3</i> -Deficient Mice Display No Signs of Increased UPR Activation	70
4.1.6 Simultaneous Lack of ORMDL3 & ORMDL1 Causes Severe Motor Defects <i>in vivo</i>	71
4.1.7 <i>Ormdl3</i> - and <i>Ormdl1/3</i> Deficiency Impairs Autophagy in Intestinal Epithelial Cells.....	72
4.1.8 ORMDL Proteins Regulate ER Membrane Trafficking	75
4.2 Discussion	78
4.2.1 <i>Ormdl3</i> and <i>Ormdl1/3</i> Deficiency Impair Body Growth Whereas Simultaneous Deletion of <i>Ormdl1</i> , <i>Ormdl2</i> and <i>Ormdl3</i> Causes Embryonic Lethality.....	78
4.2.2 <i>Ormdl3</i> Expression is Regulated by Microbial Cues	79

4.2.3 <i>Ormdl3</i> -Deficient Mice Display Increased Susceptibility to Adherent-Invasive <i>E. coli</i> Colonization.....	80
4.2.4 Abnormalities in the Structure & Function of Highly Secretory Cells in the Intestine of <i>Ormdl3</i> - and <i>Ormdl1/3</i> -Deficient Mice Do Not Correlate with UPR Activation.....	80
4.2.5 Simultaneous Lack of ORMDL3 and ORMDL1 Causes Severe Motor Defects <i>in vivo</i>	81
4.2.6 <i>Ormdl3</i> - & <i>Ormdl1/3</i> Deficiency Impairs Autophagy in Intestinal Epithelial Cells	82
4.2.7 ORMDL Proteins Regulate ER membrane Trafficking.....	82
4.3 Conclusions & Future Perspectives	85
5 Summary.....	87
6 Zusammenfassung.....	89
7 References.....	91
8 Supplement	107
8.1 List of Abbreviations.....	107
8.2 Buffers and Solutions	110
8.3 Media.....	110
8.4 Chemicals.....	111
8.5 Enzymes & Inhibitors.....	112
8.6 Kits	112
8.7 Plasmids and Oligonucleotides.....	112
8.8 Antibodies.....	114
8.9 Devices & Consumables	115
8.10 Acknowledgments	125
8.11 Curriculum Vitae.....	126
8.12 Eidesstattliche Erklärung	128

List of Figures

Figure 1.1: Cellular responses to endoplasmic reticulum stress.....	13
Figure 1.2: Schematic overview of mammalian autophagy.....	16
Figure 2.1: Generation of <i>Ormdl1</i> ^{-/-} , <i>Ormdl2</i> ^{-/-} , and <i>Ormdl3</i> ^{-/-} mice.....	34
Figure 3.1: High-throughput RNAi screening approach for the identification of ATF6α signaling modulators.....	40
Figure 3.2: Systematic siRNA screening reveals modulators of ATF6α activation.....	41
Figure 3.3: Small molecule agents targeting candidate genes reflect the RNAi-mediated phenotype on ERSE promoter activity.....	43
Figure 3.4: <i>ACSL1</i> and <i>CSNK2B</i> are inducers of ATF6α signaling in the intestinal epithelial cell line Caco-2.....	44
Figure 3.5: Inhibition of <i>ACSL1</i> and <i>CSNK2B</i> represses ATF6α downstream signaling in human organoids.....	45
Figure 3.6: <i>CSNK2B</i> controls ATF6α signaling upstream of intramembrane cleavage.....	46
Figure 3.7: ATF6α regulates NF-κB signaling upon ER stress induction.....	47
Figure 3.8: Reduction of the hyperactivation of the ATF6α branch in <i>ATG16L1</i> -deficient intestinal epithelial cells alleviates levels of pro-inflammatory cytokines.....	49
Figure 3.9: Inhibition of the ATF6α branch in <i>Xbp1</i> -deficient intestinal epithelial cells alleviates transcription of pro-inflammatory cytokines.....	51
Figure 3.10: <i>ACSL1</i> stimulates ATF6α signaling downstream of the cleavage event and <i>CSNK2B</i> facilitates ER-Golgi trafficking of ATF6α.....	57
Figure 4.1: Generation and phenotype of <i>Ormdl3</i> - and <i>Ormdl1/3</i> -deficient mice.....	63
Figure 4.2: <i>Ormdl3</i> expression is regulated by the bacterial components.....	65
Figure 4.3: <i>Ormdl3</i> ^{-/-} mice display increased susceptibility to AIEC LF82 colonization.....	67
Figure 4.4: <i>ORMDL1</i> and <i>ORMDL3</i> regulate structure and function of highly secretory cells in the intestine.....	69
Figure 4.5: Critical role of <i>ORMDL1</i> and <i>ORMDL3</i> in the structure of Goblet cells and enterocytes ...	70
Figure 4.6: <i>Ormdl3</i> ^{-/-} mice do not exhibit any signs of increased UPR activation in the intestine.....	71
Figure 4.7: <i>Ormdl1</i> ^{-/-3} ^{-/-} mice exhibit severe motor defects.....	72
Figure 4.8: <i>ORMDL1</i> and <i>ORMDL3</i> regulate autophagic flux upon nutrient starvation and bacterial infection.....	74
Figure 4.9: <i>ORMDL</i> proteins as modulators of the secretory pathway and ER turnover.....	76

List of Tables

Table 1: Cell lines used in this study.....	26
Table 2: Overview of applied cell culture dishes for experiments with cell lines	26
Table 3: Formats and volumes for plasmid DNA transfections with FuGene 6.	27
Table 4: Formats and required volumes for siRNA transfection with siPORT.....	28
Table 5: Reverse transcription with the Maxima H Minus First Strand cDNA Synthesis Kit	29
Table 6: Reaction setup for PCR	29
Table 7: Cycling protocol for endpoint PCR.....	30
Table 8: License numbers for approved animal research	35
Table 9: Oligonucleotides for genotyping applied in this study	35
Table 10: PCR component and profile for genotyping	35
Table 11: List of applied buffers and solutions.	110
Table 12: List of applied media.....	110
Table 13: List of applied chemicals.....	111
Table 14: List of applied enzymes.	112
Table 15: List of applied small molecules.....	112
Table 16: List of applied kits.	112
Table 17: List of plasmids used in this study.	112
Table 18: List of applied oligonucleotides with their sequences.	113
Table 19: Overview of applied TaqMan probes.	113
Table 20: Primary antibodies used in this study.	114
Table 21: Secondary antibodies used in this study	114
Table 22: Devices used in this study.....	115
Table 23: List of consumables used in this study	116
Table 24: List of candidates identified in the primary screen.	117
Table 25: List of candidates identified in the second screen.	121
Table 26: List of final hits identified in the third screen.....	124

1 Introduction

1.1 Inflammatory Bowel Disease

Inflammatory bowel disease (IBD) is a group of chronic inflammatory disorders of the gastrointestinal tract comprising two main subentities: Crohn's disease (CD, OMIM #266600) and ulcerative colitis (UC, OMIM #266600). IBD is considered a multifaceted immunologically mediated disease caused by a dysregulated immune response to the intestinal microbiota in a genetically susceptible host. Both CD and UC are chronic, progressive diseases characterized by relapsing-remitting inflammatory episodes [1]. IBD usually becomes manifest between the 2nd and 4th decade of life (as defined by diagnostic criteria based on macroscopic lesions). The discontinuous inflammation in CD may occur at any part of the gastrointestinal tract from the mouth to the anus and may affect all layers of the intestine (transmural lesions). In contrast to CD, UC is continuous and restricted to the mucosal layer of the colon [2].

Clinical symptoms of both IBD subtypes include bloody diarrhea and abdominal pain often accompanied by malnutrition and inflammatory extraintestinal manifestations (e.g. arthritis, uveitis) [1]. Beyond local manifestations IBD is characterized by an increased mortality due to complications in the intestine (e.g. increased risk for malignancies such as colorectal carcinoma) and chronic involvement of other organs such as the liver (e.g. primary sclerosing cholangitis or non-alcoholic steatohepatitis) [3].

Treatment of IBD aims to induce and maintain remission. Most therapeutic approaches are based on anti-inflammatory agents and therapies that modulate the immune system. Despite the recent progress, no medical or surgical cure is available [4] and there is still a large unmet need for more efficient therapies as many patients do not respond satisfactorily to existing treatments [5-7]. Moreover, we face a dramatic increase in incidence rates worldwide. While incidence of IBD has traditionally been highest in North America and Western Europe, we have experienced a dramatic rise in incidence over the past 50 years. IBD affects approximately 1.5 million Americans and 2.2 million Europeans [8, 9]. In addition, incidence of IBD in low-risk populations (including Japan and India) is increasing [10], suggesting that environmental factors (e.g. a life style of Western industrialized countries) play an important role in disease pathogenesis.

The past three decades have tremendously contributed to our understanding of the complex development of IBD. Genetic risk factors have been studied in detail and with the research approach shifting from positional cloning to systematic analyses, genome wide association studies (GWAS) enabled the identification of more than 160 validated and replicated loci [11-14]. In addition, progress in microbiome analysis revealed that the genetic risk factors do not act in isolation but interact with the gut microbiota by shaping the immune response.

1.2 Genetic Risk Factors for IBD

A role of genetics in IBD pathogenesis was initially supported by familial aggregation studies and twin studies indicating a crucial hereditary factor [15-17]. Between 2-14 % of CD and 8-14% UC patients show a family history of the condition and the relative risk of developing IBD for first-degree relatives of CD patients is estimated to be around 5%, whereas that for UC is 1.6% [18]. The risk of children of diseased parents to develop IBD before the age of 30 years is calculated to be one-in-three [16]. Twin

studies have also provided evidence for an impact of genetics in IBD. For CD, concordance rates in monozygotic twins are estimated to be 20-50% and in dizygotic twins 10%. In UC, corresponding numbers are 16% for monozygotic and 4% for dizygotic twins [16, 19, 20].

Most disease loci linked to IBD have been detected by GWAS. GWAS identify common risk alleles, which are significantly more frequent in patients compared to healthy controls. The so far largest genetic association study for IBD included genome-wide association data of over 75,000 patients and controls [14]. This collaborative effort identified 163 loci associated with IBD. Although the disease variances explained by the 163 loci only amount to 13.6 % and 7.5 % for CD and UC, respectively, the identified loci and related candidate genes contributed significantly to our understanding of IBD pathogenesis and the involved signaling pathways.

Most loci are associated with both CD and UC, although some loci such as *NOD2* (*Nucleotide-binding oligomerization domain-containing protein 2*) and *ATG16L1* (*autophagy related 16 like 1*) are specifically linked to CD alone and others only to UC [14]. In 2001, *NOD2* was the first gene to be associated with CD [21, 22], and despite the expansion in the number of genetic loci connected to IBD, *NOD2* remains the genetic risk factor conferring the highest risk for the development of CD. Heterozygosity at the *NOD2* locus is associated with a 2-4 fold increase and homozygosity confers a 20-40 fold increase in disease risk [21, 22]. The association of *NOD2* with CD demonstrates the importance of microbe sensing and defense in IBD pathogenesis. The intracellular sensor *NOD2*, which detects bacterial peptidoglycan, activates host responses to restrict bacterial infection.

Several studies have demonstrated that *NOD2* induces autophagy in response to bacterial infection. Autophagy is required for the degradation and recycling of cytosolic contents and organelles, as well as for the removal of intracellular microbes (for more details see chapter 1.5.3). *NOD2* recruits *ATG16L1* to the plasma membrane at the site of bacterial entry [23]. *ATG16L1* is essential for autophagy serving as adaptor protein for the formation of double-membraned autophagosomes around cargoes. The discovery of a coding variant (T300A) in *ATG16L1* associated with Crohn's disease initially reported by Hampe et al. [24] and later independently reported by other groups [25, 26] brought this pathway into the spotlight in IBD. The detected coding polymorphism in *ATG16L1* increases caspase-mediated cleavage of *ATG16L1*, thereby drastically reducing the levels of full-length protein [27]. Patients carrying homozygous *ATG16L1* risk alleles and *Atg16l1*-hypomorphic mice show structural alterations in Paneth and Goblet cells [28, 29].

Further support for an involvement of autophagy in IBD derived from an association of the regulatory autophagy gene *IRGM* with Crohn's disease [30, 31]. Immunity-related GTPase M (*IRGM*) is required for autophagosome formation in response to intracellular pathogens [32] and the Crohn's disease-associated *IRGM* has been shown to interfere with bacterial clearance [33].

An association of *CALCOCO2/NDP52* (*calcium binding and coiled-coil domain 2/ nuclear dot protein 52kDa*) with CD, which encodes a specific autophagy cargo adaptor, further emphasizes the importance of this pathway in disease pathogenesis. The identified rare variants of *NDP52* affect the stability of the protein and therefore reduce proteolysis of ubiquitinated adaptor molecules, resulting in enhanced NF- κ B (nuclear factor κ B) activation and induction of pro-inflammatory genes [34].

In addition to autophagy, dysfunctional endoplasmic reticulum (ER) stress induced by the accumulation of incorrectly folded proteins in the ER has been linked to IBD pathophysiology. Autophagy is directly induced by ER stress serving a compensatory function to limit ER stress [35].

Autophagy and the unfolded protein response (UPR) activated in response to ER stress are two essential processes for maintaining cellular homeostasis and, finally, resolution of ER stress (for details see chapter 1.4 and 1.5).

Genes involved in the UPR, including *XBP1* (*X-box binding protein-1*) [36], *AGR2* (*anterior gradient protein-2*) [37], and *ORMDL3* (*orosomucoid-1-like 3*) [38, 39], have been associated with increased risk for IBD. In mouse models, genetic deletion of the transcription factor *Xbp1* specifically in the intestinal epithelium results in spontaneous small intestinal inflammation and a pronounced hyper-reactivity of intestinal epithelial cells (IECs) towards microbes and cytokines [36]. In IECs, defects in XBP1 signaling result in dysfunction of antimicrobial peptide-secreting Paneth cells and in a reduction of Paneth cell numbers, culminating in impaired bacterial handling [36].

Polymorphisms in *ORMDL3* have been first associated with asthma [40], and later also with IBD [39]. *ORMDL3* is an ER-associated highly conserved protein that regulates sphingolipid synthesis and is functionally linked to the UPR, sensitivity to stress, and ER-to-Golgi transport.

Another ER stress-related risk gene is *AGR2*, which encodes an ER-resident protein disulfide isomerase involved in protein folding. Detected *AGR2* variants are linked to reduced *AGR2* mRNA expression and confer risk for both CD and UC [37]. *Agr2* deficient mice spontaneously develop ileocolitis and exhibit increased ER stress in IECs, lack of mucus in Goblet cells and an expansion of Paneth cells [41].

1.3 The Gut Microbiome in Inflammatory Bowel Disease

Despite the advances in the identification of genetic risk factors for IBD, the described risk loci explain less than one-quarter of the heritability of IBD, suggesting a strong role of the (internal and external) environment [14, 15, 42]. An association between the growing incidence of IBD and changed environmental factors related to Western lifestyle has been proposed. Western-style diet with high intake of animal proteins and saturated fat affects the gut microbiome by altering the microbial composition, which in turn might enhance disease risk [43, 44]. Furthermore, cohort studies have suggested that breastfeeding, larger family size and early life exposure to farm animals and pets are protective against IBD [45, 46]. The mentioned protective factors, characteristic for a more traditional lifestyle, have been shown to shape the gut microbiota, pointing towards a role of the intestinal microbes in disease pathogenesis. Indeed, dysbiosis of the intestinal microbiome, that is quantitative and qualitative changes in composition, represents a common hallmark of IBD [47-49]. Microbial composition of patients with IBD shows a reduced diversity and decreased stability compared with healthy individuals [48, 50]. Moreover, a shift from predominant protective microbes to potential harmful microbes has been observed in IBD patients [51].

Several bacterial species, most notably the *Bifidobacterium*, *Lactobacillus*, and *Faecalibacterium* genera, have been proposed to exhibit protective effects against mucosal inflammation. Noteworthy, these species have been found to be underrepresented in IBD [50, 52, 53]. Various strains, generally considered as beneficial, such as *Lactobacillus casei*, *Lactobacillus plantarum* and *Faecalibacterium prausnitzii* downregulate the expression of pro-inflammatory cytokines [54]. Likewise, other bacterial strains induce the production of anti-inflammatory cytokines such as interleukin 10 (IL-10) [52].

In contrast to these beneficial bacteria, certain members of the intestinal microbiota might aggravate inflammation. Up to now, no single causative microorganism has been identified, however many studies have described a role of pathogens such as *Clostridium difficile* [55], *Helicobacter* species [56],

and *Campylobacter* species [57] in IBD. Moreover, in the last 20 years functionally altered commensal bacteria including adherent-invasive *Escherichia coli* (AIEC) have been associated with disease pathogenesis [58]. The AIEC strain used in this study, namely LF82 (for Lille-France), was isolated from the ileum of patients with CD by Darfeuille-Michaud et al. [59]. LF82 is considered as AIEC reference strain being one of the most studied AIEC strains with the complete genome available [60]. Surprisingly, genome analysis also revealed that AIEC strains lack common virulence factor-encoding genes [59]. Instead, AIEC strains, categorized as pathobionts, interfere indirectly with the host by stimulating an immune response [61-63]. AIEC strains adhere to IECs via binding of the bacterial type 1 pili to the cell adhesion molecule 6 (CEACAM6) receptor expressed on ileal enterocytes. Following adhesion, AIEC strains induce actin polymerization and microtubule recruitment triggering bacterial internalization [64]. Moreover, AIEC are able to survive and replicate within macrophages [65]. In response to the high replication rates of AIEC, tumor necrosis factor α (TNF- α) and other proinflammatory cytokines are released promoting dysbiosis and proliferation of AIEC without inducing host cell death [66-68].

Currently, it is unclear whether AIEC strains cause intestinal inflammation promoting IBD or whether AIEC colonization in the intestinal mucosa is a consequence of pre-existing inflammation favoring disease pathogenesis [69]. In mice, studies revealed that successful colonization with AIEC requires pre-existing dysbiosis or gut inflammation as induced by DSS or antibiotic treatment [70-72]. In humans, host defects that result in an abnormal mucosal immunity or in intestinal barrier dysfunction may favor bacterial colonization and invasion of mucosal cells. Indeed, autophagy-related risk polymorphisms that impair sensing and handling of intracellular bacteria, favor AIEC replication [67, 73, 74]. In this context, mutations in *NOD2* and *ATG16L1* have been linked to defects in bacterial clearance [23, 75].

1.4 ER Homeostasis, ER Stress & the Unfolded Protein Response

ER stress is a tightly controlled cellular process responsible for maintaining and restoring protein homeostasis in the cell. Defects in this pathway are linked to IBD, where ER stress-related genetic risk loci have been associated to increased disease risk. The ER, arranged in a dynamic tubular network, is the major site of protein synthesis and folding of secreted and transmembrane proteins. Proteins synthesized in the secretory pathway constitute approximately 30% of all proteins made in the eukaryotic cell. Additionally, the ER serves as the major intracellular calcium reservoir in the cell, which contributes to lipid and sterol synthesis and the biogenesis of autophagosomes [76-78]. Following translation on ER membrane-associated ribosomes, proteins are transported into the ER lumen. In the ER, protein folding is facilitated by chaperones and post-translational modifications such as *N*-linked glycosylation and disulfide bond formation and proline *cis-trans* isomerization occurs [79-82]. ER-to-Golgi transport is the first step in the secretory pathway. At the ER, correctly folded and assembled secretory and membrane proteins are selectively incorporated into COPII-coated vesicles that transport them to the Golgi apparatus. COPII-coated vesicles bud from specialized regions of the ER known as ER exit sites (ERESs) [83, 84]. The COPII coat consists of five subunits including Sar1-GTP, dimeric Sec23/Sec24, and tetrameric Sec13/Sec31 [85].

Various stress conditions, such as enhanced synthesis of secretory proteins, disturbed calcium homeostasis and redox balance induce ER stress. The protein-folding machinery is particularly challenged in highly secretory cells, such as IECs (particularly Paneth cells and Goblet cells), due to their high demand for protein synthesis [35]. Upon ER stress, the UPR, a highly conserved cytoprotective

signaling pathway, is activated. The UPR enables the cell to respond to ER stress and aims at restoring cellular homeostasis. Specifically, ER stress triggers the activation of three proteins located in the ER membrane that sense the presence of unfolded proteins in the ER lumen, inositol-requiring enzyme 1 (IRE1), double-stranded RNA-dependent protein kinase (PKR)-like ER kinase (PERK) and activating transcription factor 6 α (ATF6 α) [82, 86, 87] (Fig. 1.1). Under homeostatic conditions, the luminal domains of IRE1, PERK and ATF6 α are retained through association with immunoglobulin heavy chain binding protein (BIP), also known as glucose-regulated protein 78 (GRP78). However, in the presence of misfolded proteins, GRP78 dissociates from the ER stress sensors due to its higher affinity to exposed hydrophobic domains of misfolded proteins, thereby initiating the downstream signaling cascades. Activation of the three UPR signaling branches restricts protein translation, stimulates the synthesis of chaperones assisting in protein folding and initiates the degradation of irreversibly misfolded proteins.

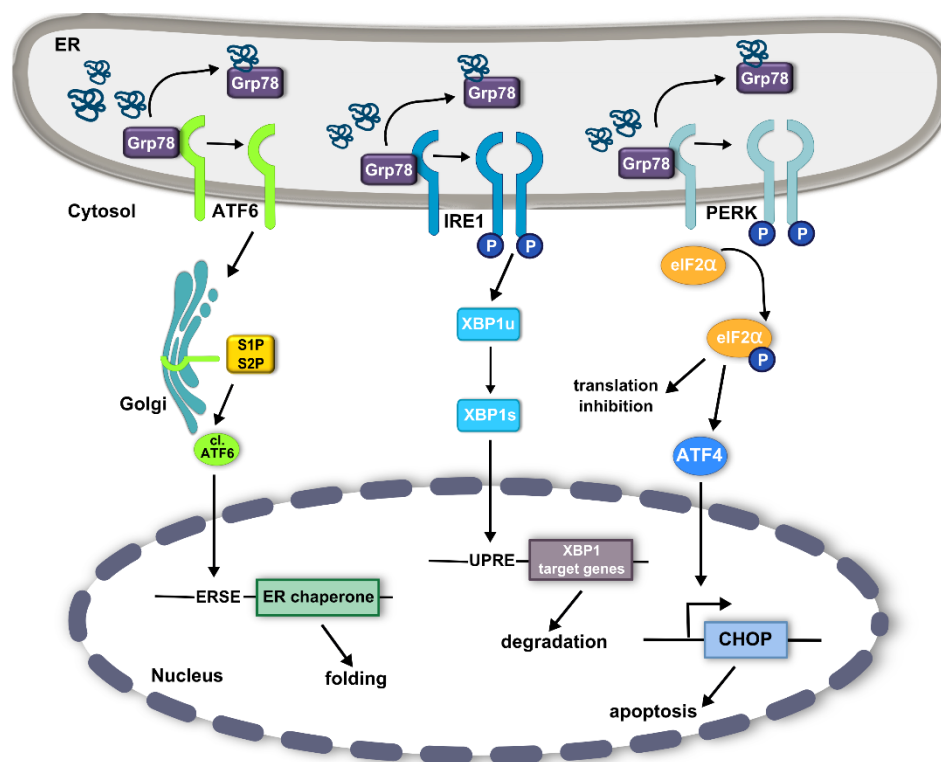


Figure 1.1: Cellular responses to endoplasmic reticulum stress. ER stress induces the unfolded protein response (UPR). Three stress sensors control UPR-dependent responses: activating transcription factor 6 α (ATF6 α), inositol-requiring enzyme 1 (IRE1) and double-stranded RNA-dependent protein kinase (PKR)-like ER kinase (PERK). Under homeostatic conditions, PERK, IRE1 and ATF6 α are bound by the glucose-regulated protein 78 (GRP78), which suppresses their activity. In response to ER stress, GRP78 is recruited away from PERK, IRE1 and ATF6 α activating the ER stress sensors. ATF6 α translocates to the Golgi complex where it is cleaved by the site 1 (S1P) and site 2 protease (S2P) releasing its cytosolic domain (cleaved ATF6 = cl. ATF6). Cleaved ATF6 induces the transcription of chaperones. In response to ER stress, IRE1 splices the mRNA encoding the transcription factor X-box binding protein 1 (XBP1). Spliced XBP1 (XBP1s) induces UPR target genes related to protein folding and ER-associated protein degradation. Activation of PERK attenuates general protein synthesis through phosphorylation of eIF2 α while selectively inducing the translation of activating transcription factor 4 (ATF4), which controls the expression of the pro-apoptotic C/EBP homologous protein (CHOP). ERSE= ER stress response element, UPRE= unfolded protein response element.

1.4.1 IRE1 Signaling

Signaling via the type 1 transmembrane protein IRE1 is the evolutionarily most conserved pathway of the UPR [88]. Mammalian cells possess two highly conserved isoforms, the ubiquitously expressed IRE1 α [89] and IRE1 β , which is restricted to gut and lung epithelial cells [90]. Upon activation, IRE1 dimerizes and autophosphorylates, activating its endoribonuclease activity. The endoribonuclease activity excises a 26-nucleotide intron of *XBP1* mRNA resulting in a frame shift and generation of a transcriptionally active isoform known as XBP1s ('s' for 'spliced') [91, 92]. Xbp1s functions as a potent transactivator of UPR target genes, inducing the transcription of genes implicated in protein folding, trafficking, and ER-associated degradation (ERAD) [93, 94]. During ERAD, misfolded or misassembled proteins are subjected to degradation by the ubiquitin-proteasome machinery. In addition to the specific endoribonuclease activity that splices *XBP1*, IRE1 α exhibits a nonspecific endonuclease activity responsible for degradation of ER membrane-associated mRNAs, a process termed regulated IRE1-dependent decay (RIDD). RIDD reduces the amount of protein that enters the secretory pathway [95].

1.4.2 PERK Signaling

Similar to IRE1, PERK is an ER stress-activated kinase that homodimerizes and autophosphorylates upon dissociation of GRP78. Activated PERK in turn phosphorylates the translation initiation factor eIF2 α [96, 97], attenuating the synthesis of secretory proteins by inhibiting the assembly of the 80S ribosome [98]. While the translation of most mRNAs is attenuated under ER stress conditions, the translation of the mRNA encoding the transcription factor ATF4 is favored [99]. ATF4 controls the transcription of UPR target genes involved in amino acid metabolism, oxidative stress resistance and autophagy [100]. At the same time, ATF4 induces the expression of *PPP1R15A*, encoding GADD34, the regulatory subunit of the protein phosphatase 1 (PP1). PP1 mediates dephosphorylation of eIF2 α to override the translation block. However, under conditions of prolonged, excessive ER stress, ATF4 activates the transcription of C/EBP homologous protein (CHOP; also known as DDIT3) [100] [101], which promotes ER-stress-mediated apoptotic cell death [102, 103].

1.4.3 ATF6 α Signaling

ATF6 is a type II ER-transmembrane protein with its carboxy-terminal stress-sensing domain facing the ER lumen and a cytosolic amino-terminal domain with a bZIP (basic leucine zipper) transcription factor motif [104, 105]. Mammals have two ATF6 homologues, ATF6 α and ATF6 β . Interestingly, *Atf6 α /Atf6 β* double deficiency causes embryonic lethality in mice, indicating an overlapping function of the two isoforms in early embryonic development. Surprisingly, while *Atf6 β* -deficient mice develop normally and do not exhibit a prominent phenotype when exposed to ER stress, *Atf6 α* -null animals are highly susceptible to intraperitoneal injections with the ER stress-inducing reagent Tunicamycin (TM) demonstrating the role of ATF6 α in ER stress regulation and proteostasis [106, 107].

ER stress induces the dissociation of GRP78 from ATF6 α , which in turn is released and transported from the ER to the Golgi apparatus via coat protein complex II (COPII) vesicles. At the Golgi, ATF6 α is sequentially cleaved by the site 1 (S1P) and the site 2 protease (S2P) releasing the cytoplasmic domain of ATF6 α . The cleaved cytoplasmic fragment migrates into the nucleus where it binds to the ER stress response element (ERSE) sequence, originally discovered in the gene encoding GRP78 [108] [109]. The consensus sequence of ERSE is CCAAT-N(9)-CCACG, which acts in *cis* of many UPR-related genes such as *BIP*, *HSP90B1* (encoding the 94 kDa glucose-regulated protein, GRP94) and *DNAJC3* (encoding the protein kinase inhibitor of 58 kDa, P58^{IPK}) [110]. Gene expression patterns observed upon ATF6 α

signaling overlap to some extent with genes induced by the IRE1 α and PERK branch [106, 111]. Additionally, ATF6 α is able to form heterodimers with XBP1 resulting in the expression of ERAD components, such as EDEM, HERP and HRD1 [107].

1.5 Autophagy

A functional link between ER stress and autophagy is important for maintaining cellular homeostasis. Recent studies have demonstrated that activation of the UPR induces autophagy and that autophagy in turn is able to resolve ER stress [28, 35, 36, 112-116].

Autophagy (from Greek, αὐτός (*autós*, "self") and φαγεῖν, (*phagein*, "to eat") is a firmly controlled cellular process present in all eukaryotic cells, which involves the delivery of cytoplasmic cargo (e.g. aged organelles, larger protein complexes or intracellular pathogens) to lysosomes for their degradation. While the ubiquitin-proteasome system controls degradation of cytoplasmic short-lived proteins [117], autophagy facilitates the degradation and recycling of long-term proteins and organelles [118]. Based on their function and mode of cargo delivery to the lysosome, autophagy is classified in three types - macroautophagy, microautophagy and chaperone-mediated autophagy. Macroautophagy refers to the engulfment of cytoplasmic proteins and organelles by double membrane-bound vesicles (termed autophagosomes) which fuse with lysosomes resulting in cargo degradation [119]. In microautophagy, whole cytosolic regions are encircled by autophagosomes, which then fuse with late endosomes/multivesicular bodies (MVBs) [120]. In chaperone-mediated autophagy, the cargo is recognized by the cytosolic chaperone heat shock cognate 70 kDa protein (HSC70). HSC70 together with the lysosomal-associated membrane protein 2A (LAMP2A) receptor enables the translocation of the cargo into the lysosomal lumen [121]. The present study focuses on mammalian macroautophagy, which is hereafter termed autophagy.

1.5.1 The Molecular Core Machinery

The autophagy machinery depends on a set of evolutionarily conserved autophagy-related proteins (ATG proteins), that regulate the initial steps of autophagosome formation (Fig. 1.2). As a first step, a cup-shaped isolation membrane forms around cytoplasmic components. The isolation membrane elongates and generates the phagophore. The phagophore eventually closes forming the double-membraned autophagosome. After membrane fusion, the autophagosome fuses with lysosomes generating the so-called autolysosome enabling the proteolytic degradation and recycling of the autophagic content [122-125]. For phagophore formation, the ULK1 complex (ULK1, ATG13, FIP200, ATG101) translocates from the cytoplasm to the ER providing the source of the autophagosome membrane. Then, the ULK1 complex recruits the autophagosome-specific PI3 kinase (phosphatidylinositol 3-kinase) complex, which comprises ATG14L, BECLIN1, VPS15 and VPS34 [119, 126]. The PI3K complex generates phosphatidylinositol 3-phosphate (PI3P) required for canonical autophagy [119, 127]. In addition to the ULK1 and the PI3 kinase complex, two ubiquitin-like modification systems are required for mammalian autophagy.

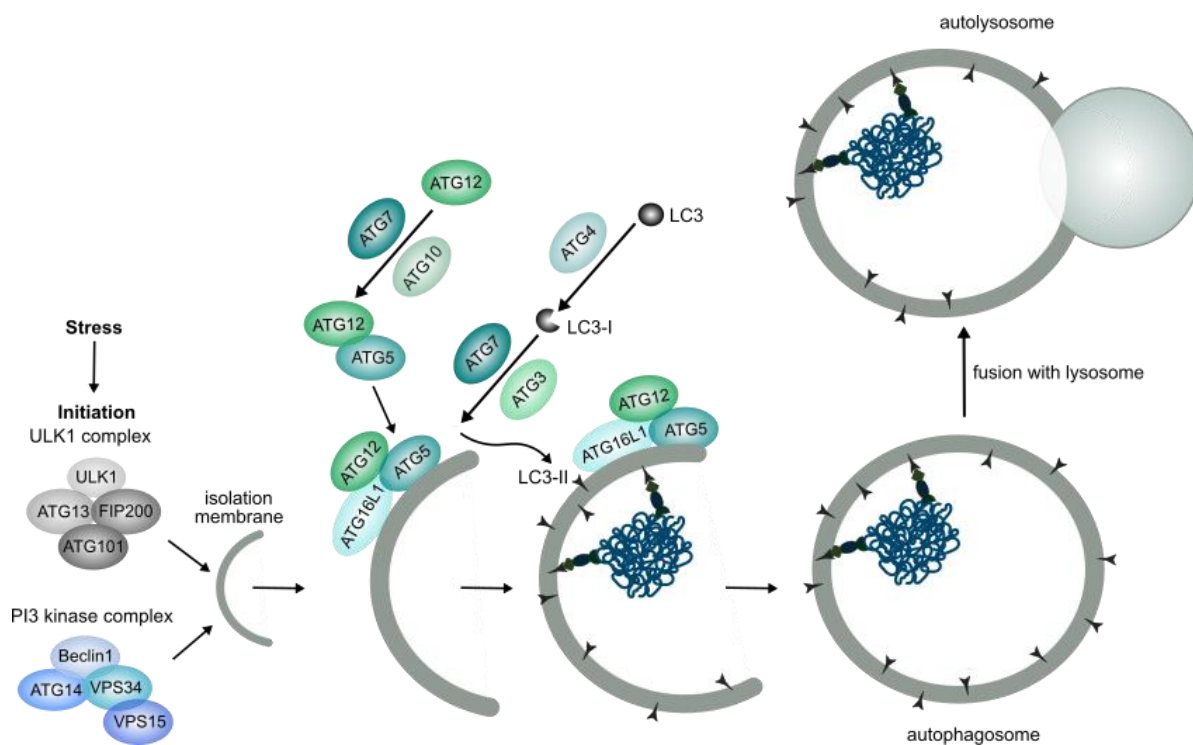


Figure 1.2: Schematic overview of mammalian autophagy. The autophagic process is typically initiated by cellular stress triggered by starvation, hypoxia, oxidative stress, protein aggregation, ER stress and others. The common target of these signaling pathways is the Unc-51-like kinase 1 (ULK1) complex, which comprises ULK1, autophagy-related protein 13 (ATG13), FAK family kinase interacting protein of 200 kDa (FIP200) and ATG101. Further nucleation requires the PI3 kinase complex, which consists of the vacuolar protein sorting 34 (VPS34), VPS15; ATG14L and Beclin 1. Phagophore membrane elongation is dependent on a ubiquitin-like conjugation pathway, which produces the ATG5–ATG12 conjugate forming a multimeric complex with ATG16L. The ATG12-ATG5-ATG16L1 complex enhances ATG3-mediated conjugation of microtubule-associated protein light chain 3 (LC3) to membrane-resident phosphatidylethanolamine (PE), thus forming the membrane-bound, lipidated form of the microtubule-associated protein 1 light chain 3 LC3-II. In selective autophagy, LC3 mediates the sequestration of cargo into autophagosomes. Autophagy cargo receptors (depicted as oval shapes in dark blue) interact with both the autophagic substrate (shown in blue) and the maturing autophagosome via LC3-interacting regions (shown in dark green, ●). The resulting autophagosome fuses with the lysosome, generating the autolysosome. The autophagic cargo is degraded by acidic hydrolases in the lysosome.

In a first step, the ubiquitin-like protein ATG12 is activated by ATG7 and transferred to the E2 ubiquitin conjugating enzyme-like protein ATG10 [128]. Subsequently, ATG12 is conjugated to ATG5 generating a complex with ATG16L1 [128]. Acting in an E3 ubiquitin ligase-like manner, the ATG12-ATG5-ATG16L1 then facilitates the lipidation of microtubule-associated protein 1 light chain 3 (LC3) with phosphatidylethanolamine [129]. Synthesized as precursor, LC3 is cleaved by ATG4 generating LC3-I [130]. Like ATG12, LC3-I is activated by ATG7 and transferred to the E2 ubiquitin conjugating enzyme-like protein ATG3 [131]. Finally, LC3-I is conjugated to phosphatidylethanolamine (PE) giving rise to the membrane-bound form of LC3, namely LC3-II. LC3-II localizes to the autophagosome membrane and is subsequently degraded by hydrolytic enzymes within the autolysosome [132, 133]. Functional defects in ATG7 or one of the constituents of the ATG12-ATG5-ATG16L1 complex impair the conversion of LC3 causing an accumulation of LC3-I. Turnover of LC3-I to LC3-II is monitored to quantify autophagic flux in mammalian cells [134].

1.5.2 Selective Autophagy

Previously considered as being a non-selective process of bulk degradation, it is increasingly being appreciated that autophagy is highly specific for certain cargos to be degraded. Up to now, numerous autophagic pathways have been described and named according to their type of targeted cellular

material. These include aggrephagy (protein aggregates), xenophagy (pathogens), mitophagy (mitochondria), ribophagy (ribosomes) and endoplasmic reticulum autophagy (ER-phagy or reticulophagy) [135-140]. Selective autophagy requires, in addition to the core autophagy machinery, selective autophagy receptors (SARs), which label the specific cargo for degradation.

SARs establish a link between their cargo and the autophagosome by simultaneously interacting with the cargo and LC3-like proteins on autophagic compartment [141, 142]. SARs bind to their cargo labelled with degradation signals, most commonly ubiquitin, via their ubiquitin-binding domain (UBD). The interaction of SARs with autophagosomes is established via LC3-interacting regions (LIR) [141, 143].

1.5.3 Xenophagy

Xenophagy is a type of selective macroautophagy that targets intracellular pathogens for lysosomal degradation. Mechanistically, xenophagy resembles canonical macroautophagy (see Fig. 1.2) including steps of initiation, elongation, substrate targeting, and lysosomal fusion [119]. Xenophagy is induced by cytoplasmic recognition of pathogen-associated molecular patterns (PAMPs) or damage-associated molecular patterns (DAMPs) [23, 144-147]. Subsequent to phagophore formation, bacteria are ubiquitinated or ubiquitin co-localization with the bacteria is mediated by ubiquitin ligases such as PARKIN [145]. As a result, autophagy receptors are able to recognize and bind to ubiquitin. These autophagy receptors interact with LC3 targeting the bacteria to autophagosomes [148]. Autophagy receptors include SQSTM1 (sequestosome-1)/p62, NDP52, and OPTN (Optineurin). The autophagosome matures and fuses with lysosomes degrading the invading pathogens.

Bacterial pathogens have developed different strategies to evade xenophagy. Bacteria such as *Listeria monocytogenes* interfere with bacterial detection via autophagy factors to avoid xenophagy. Other bacteria including *Salmonella enterica* serovar Typhimurium are able to interfere with autophagosome formation and LC3 targeting. Another strategy commonly used by bacteria to evade xenophagy is to block autophagosome maturation and fusion with lysosomes. Interestingly, it was shown that AIEC infection specifically induces microRNAs that diminish the levels of ATG5 and ATG16L1, thereby restricting autophagy [73]. Additionally, during infection of neutrophil-like PLB-985 cells, AIEC are able to inhibit autophagy at the autolysosomal step, enabling bacterial survival and replication [149].

1.5.4 ER-phagy

The fragmentation and delivery of ER fragments to lysosomal compartments for their degradation is termed ER-phagy [112]. The ER volume must be maintained under constitutive conditions, while regulated ER turnover aims to prevent or end excessive ER expansion in cells exposed to certain stress conditions. ER stress, nutrient deprivation, infection, accumulation of misfolded proteins, and activators of macroautophagy have been shown to induce ER-phagy [150-154]. The selectivity of this process is mediated by specific ER membrane-localized ER-phagy receptors such as FAM134B (family with sequence similarity 134), SEC62 (translocation protein SEC62), RTN3 (Reticulon 3), and CCPG1 (Cell-cycle progression gene 1) that engage the macroautophagy machinery via LC3- interacting regions [150-154].

1.5.5 Crosstalk of the Autophagic Machinery and the Secretory Pathway

The secretory and autophagic pathways are two fundamental, evolutionary highly conserved endomembrane processes that are intimately linked [155]. The process of transporting cargo-containing vesicles is not only characteristic for autophagy but also for the secretory pathway. There is mounting evidence that secretory and autophagy pathways are closely connected. First, membranes of the secretory pathway serve as sources and platforms for autophagosome biogenesis. Second, there are several proteins such as ULK1 and ULK2 that participate in both pathways [156]. For instance, the small GTPases Rab1, known for its role in ER-Golgi trafficking, has been shown to be required for autophagosome formation [157]. Moreover, *Saccharomyces cerevisiae* strains deficient in genes essential for COPII vesicle formation, show impaired autophagosome formation [158, 159]. Similarly, in mammals, defective function of the GTPase Sar1, which controls traffic from the ER to the Golgi, affects autophagy [157]. ULK1 and ULK2 were long thought to exclusively modulate autophagy. Recently, it was shown that ULK1/2 play a role in ER-Golgi trafficking by phosphorylating Sec16A, a protein involved in the biogenesis and maintenance of ERES [156, 160]. Phosphorylation of SEC16A enables ER export of specific cargo proteins.

1.6 Crosstalk of ER Stress & Autophagy in Intestinal Inflammation

The UPR is crucial for maintaining cellular homeostasis and highly secretory IECs such as Paneth and Goblet cells are prone to dysfunctional UPR [28, 161]. Consistent with this, the small intestine, which contains high numbers of Paneth and Goblet cells, exhibits higher baseline expression levels of UPR-related gene in comparison to the colon [162]. Paneth cells, located at the crypt bottom, regulate intestinal microbiota composition, protect against intestinal pathogens and provide signals required for proliferation of the stem cell compartment [163]. In particular, Paneth cells secrete antimicrobial peptides (AMPs) such as α -defensins and lysozyme into the lumen, thereby shaping the gut microbiota composition and modulating acquired immunity [164] [165]. Goblet cells secrete mucins, which form the mucus layer protecting the host from (opportunistic) pathogens. Further, most intestinal epithelial cells secrete a large array of cytokines and chemokines influencing the composition of the gut microbiota and the mucosal immune system [166]. Consequently, IECs face a large secretory burden, which in turn illustrates the importance of ER homeostasis.

1.6.1 ER Stress & Intestinal Inflammation

Several studies have demonstrated that genetic deletions of ER stress related genes are associated with either spontaneous intestinal inflammation and/or increased sensitivity to chemical-induced colitis.

Atf6 α -deficient mice showed a more severe course of disease following DSS administration indicated by a more pronounced body weight loss, increased rectal bleeding and more severe mucosal damage compared to their wild type littermates. Interestingly, *Atf6 α* ^{-/-} mice exhibited reduced levels of ER chaperones, including GRP78, GRP94 and p58IPK compared to the control mice, indicating that the lack of ATF6 α impairs UPR signaling in IECs in response to intestinal inflammation [167]. Similar to *Atf6 α* -deficient mice, *P58*^{IPK}^{-/-} mice showed increased sensitivity to DSS-induced colitis illustrated by a more severe body weight loss, enhanced rectal bleeding, more pronounced shortening of the large intestine and increased mucosal damage compared with their wild type littermates. Mice lacking P58IPK exhibited enhanced expression of ER chaperone GRP78 and pro-apoptotic CHOP and enhanced

phosphorylation of IRE1 [167]. A tamoxifen-inducible deletion of the ATF6 α target *Grp94* severely impairs intestinal homeostasis. *Grp94*-deficient mice experienced rapid, severe body weight loss, loss of intestinal villus structure and, ultimately, death 12–14 days post tamoxifen injection [168]. Additionally, mice with a hypomorphic allele of the membrane-bound transcription factor S1P-encoding gene *Mbtps1* exhibited an elevated susceptibility to dextran sodium sulfate (DSS)-induced colitis. The loss-of-function mutation in the site 1 protease (S1P), crucial for the generation of the transcriptionally active form of ATF6 results in reduced expression of the ER chaperones GRP78 and GRP94 in the colon upon DSS treatment [169]. However, due to the broad substrate specificity of S1P including not only ATF6, but also additional transcription factors such as CREB-H, SREBP and OASIS [170], the observed phenotype might not be solely ATF6-dependent.

Besides the role of ATF6 signaling in intestinal homeostasis, the PERK branch exerts a crucial role in regulating ER stress *in vivo*. Mice with a non-phosphorylatable Ser51A1a mutant of eIF2 α in IECs displayed defective UPR signaling in IECs resulting in disrupted protein secretion of Paneth cells. Additionally, lack of p-eIF2 α caused an increased sensitivity to DSS-induced colitis and augmented susceptibility to *Salmonella enterica* serovar Typhimurium infection [171]. In contrast to the above-mentioned ER stress related genes, deletion of the pro-apoptotic factor *Chop*, a downstream target of the PERK branch, was observed to be protective both in a DSS- and TNBS (trinitrobenzene sulfonic acid)-induced colitis model [172].

Both IRE1 α (encoded by *Ern1*) and IRE1 β (encoded by *Ern2*) have been extensively studied to shed light on their role in intestinal inflammation. IRE1 α is ubiquitously expressed and deletion causes early embryonic lethality [173]. To circumvent embryonic lethality, resulting from disturbed placenta development, conditional knockout mice that express IRE1 α only in the placenta were generated [174]. *Ern1* conditional knockout mice displayed a decrease in spliced *Xbp1* mRNA and reduced GRP78 expression. However, Goblet cells of *Ern1*-deficient mice did not show any abnormalities [175]. Strikingly, mice lacking both *Xbp1* and *Ern1* in intestinal epithelial cells (*Ern1/Xbp1* ^{Δ IEC}) revealed less NF- κ B phosphorylation and reduced ileitis in comparison with *Xbp1* ^{Δ IEC} mice, suggesting that NF- κ B activation is mediated by IRE1 α [35].

In contrast to IRE1 α , the expression of IRE1 β is restricted to the gastrointestinal tract, and its knockout mice develop normally [176]. However, *Ern2*^{-/-} mice exhibit elevated levels of the ER stress marker GRP78 in the colonic epithelium and they are highly sensitive to DSS-induced colitis [177]. In contrast to IRE1 α deficient mice, *Ern2*^{-/-} mice exhibit aberrant mucin 2 (MUC2) accumulation in the ER of goblet cells, ER distension and increased ER stress indicated by enhanced *Xbp1* mRNA splicing [175].

Mice with conditional deletion of XBP1 in the intestinal epithelium (*Xbp1* ^{Δ IEC} mice) developed spontaneous mild enteritis when exposed to an SPF (Specific Pathogen Free) flora [36]. *Xbp1* ^{Δ IEC} mice exhibit increased ER stress and enhanced autophagic flux in the small intestine. The phenotype of the *Xbp1*-deficient mice is characterized by a significant reduction in Paneth cells accompanied by lack of lysozyme and cryptdins. In addition, *Xbp1* deficiency resulted in a decline of mucus-producing Goblet cells. Consistent with a defect in Paneth and Goblet cells, mucosal defense is impaired and *Xbp1* ^{Δ IEC} mice are highly susceptible to *Listeria monocytogenes* infection and DSS-induced colitis [36]. Moreover, *Xbp1* deficiency in IECs induces IRE1-dependent NF- κ B and JNK activation causing increased transcription of pro-inflammatory cytokines favoring intestinal inflammation [36].

Agr2, another ER stress related IBD risk gene, encodes a protein disulfide isomerase (PDI) localized in the ER. *Agr2* is expressed in Goblet, Paneth and entero-endocrine cells in the small intestine [178] and reduced expression levels have been associated with CD and UC [37]. *Agr2*^{-/-} mice developed spontaneous ileocolitis with increased levels of ER stress markers such as spliced XBP1, CHOP and GRP78, decreased *Muc2* expression in goblet cells and abnormal localization and expansion of Paneth cells in the small intestine [41]

In summary, numerous studies have demonstrated that the intestinal epithelium is highly susceptible to defects in UPR. Depending on the effect a specific mutation has on the UPR, spontaneous or induced enterocolitis might develop. While *Xbp1* or *Agr2* deficiency favors spontaneous intestinal inflammation in the presence of the commensal microbiota, other mouse models require additional environmental triggers. Moreover, the mentioned studies emphasize the increased sensitivity of the small intestine relative to the colon to impaired ER stress signaling.

1.6.2 ER Stress, Autophagy & Bacterial Sensing Converge in Intestinal Inflammation

Increasing evidence has emerged that the so far identified IBD risk genes converge in interconnected pathways such as the UPR, autophagy, and intracellular bacterial sensing. The intersection between autophagy and bacterial sensing was revealed by the functional link of the CD risk genes *ATG16L1* and *NOD2*. Both *NOD2* and *ATG16L1* have been suggested to be required for autophagy induction upon bacterial entry into the cell [23]. A pathway closely intertwined with both bacterial sensing and autophagy is the UPR, which is genetically linked to both CD and UC (*XBP1* and *ORMDL3*). ER stress and autophagy are reciprocally interconnected. Deficiency of either UPR or autophagy in the intestinal epithelium and especially in Paneth cells promotes each other's compensatory engagement and defects in both signaling pathways promote spontaneous enteritis.

A missense mutation in the autophagy-related *ATG16L1* gene is associated with CD [24] and mice hypomorphic for *ATG16L1* protein expression show a spontaneous phenotype in their intestinal epithelium accompanied by abnormalities in Paneth cell function [28]. Using a conditional mouse model with the *Atg16l1* deletion only in IECs (*Atg16l1*^{ΔIEC}), Adolph et al. [35] could demonstrate that ER stress is induced upon dysfunctional autophagy due to the lack of *ATG16L1*. Paneth cells of *Atg16l1*^{ΔIEC} mice exhibit not only reduced number of granules, but also enhanced secretion of inflammatory cytokines. Strikingly, *Atg16l1*^{ΔIEC} mice developed spontaneous enteritis under SPF conditions accompanied by large cluster formation of activated IRE1α [179]. During persistent ER stress, hyper-activated IRE1α favors pro-inflammatory signaling instead of resolving ER stress by activating the XBP1 branch of the UPR. Importantly, a selective *ATG16L1*-dependent autophagy process is crucial for the removal of IRE1α clusters and termination of pro-inflammatory signaling [179]. Indeed, in patients with *ATG16L1*^{T300A} a similar accumulation of IRE1α has been observed in Paneth cells [179] emphasizing the importance of autophagy as a regulator of IRE1α activity. At the same time, IRE1 signaling is involved in lipid conjugation of LC3 crucial for autophagy [116]. Similarly, signaling of *NOD2* initiates IKKα (IκB kinase α) activation, which in turn induces phosphorylation and stabilization of *ATG16L1*. Disrupted IKKα activation impairs the removal of accumulated IRE1α [114].

Evidence that autophagy may function as a compensatory mechanism in intestinal epithelial cells upon sustained ER stress was provided by studies of ER stress-induced small intestinal inflammation. Deletion of epithelial *ATG7* and epithelial XBP1 (*Atg7/Xbp1*^{ΔIEC}) resulted in increased ER stress and severe transmural Crohn's disease-like enteritis. *Atg7/Xbp1*^{ΔIEC} mice demonstrated a complete absence

of UPR-induced autophagy and in contrast to *Xbp1^{ΔIEC}* mice, *Atg7/Xbp1^{ΔIEC}* mice developed discontinuous submucosal or transmural inflammation. Similar to *Atg7/Xbp1^{ΔIEC}* animals, *Atg16l1/Xbp1^{ΔIEC}* mice lack UPR-induced autophagy and develop severe spontaneous ileitis [36]. These studies underline the compensatory role exerted by autophagy and in particular by ATG16L1 in protecting against inflammation due to sustained ER stress.

Abnormal Paneth cell function accompanied by impaired lysozyme secretion represents a shared feature of disturbed ATG16L1 and NOD2 signaling [28, 180]. Such lysozyme distribution abnormalities favor abnormal responses to pathogenic and commensal bacteria. As recently demonstrated by Diamanti et al. [114], antimicrobial lysozyme is released via secretory autophagy from Paneth cells during ER stress. ER stress induced by infection with *Salmonella enterica* serovar Typhimurium disrupts the secretory pathway in Paneth cells causing impaired lysozyme secretion. Instead, induction of PERK signaling triggers secretory autophagy of lysozyme from Paneth cells into the intestinal lumen.

1.7 The ORMDL Protein Family

In 2002, Hjelmqvist et al. described for the first time the ORM1 (*Saccharomyces cerevisiae*)-like (*ORMDL*) gene family. The *ORMDL* gene family in mouse and man is comprised of *ORMDL1* (*ORM1-like 1*), *ORMDL2* (*ORM1-like 2*) and *ORMDL3* (*ORM1-like 3*). Comparison of the human *ORMDL1*, 2 and 3 revealed amino-acid identities of 77 %, whereas pairwise comparisons showed more than 95% identity between human and murine *ORMDL* orthologs [181]. Human *ORMDL1*, *ORMDL2*, and *ORMDL3* are found on chromosomes 2q32, 12q13.2, and 17q21, whereas murine *Ormdl1*, *Ormdl2*, and *Ormdl3* are located on chromosomes 1, 10, and 11, respectively. Human *ORMDL* proteins are composed of 153 amino acids and possess a molecular mass of around 17.4 kDa. *ORMDL* proteins are predicted to form two transmembrane domains, with a loop facing the ER lumen and the N- and C-terminus within the cytoplasm [182]. *ORMDL* proteins are ubiquitously expressed in fetal as well as adult tissues [181].

The most extensively studied member of the *ORMDL* family *ORMDL3* was originally described as a major locus contributing to the genetic risk for bronchial asthma [40]. However, soon after, *ORMDL3* was identified as overlap risk gene for both CD and UC [38, 39]. In both bronchial asthma and CD, the detected genetic variants elevate *ORMDL3* expression levels [38, 183]. The identified putatively causative variant represents one of the most significant CD-associated expression quantitative trait loci (eQTL) in the European population [38]. Additionally, single nucleotide polymorphisms (SNPs) in close proximity to the *ORMDL3* are associated with type 1 diabetes [184], rheumatoid arthritis [185], glioma [186], allergic rhinitis [187], primary biliary cirrhosis [188] and ankylosing spondylitis [189]. Strikingly, GWAS have not identified any association of *ORMDL1* or *ORMDL2* with IBD. However, analysis of gene expression associated SNPs detected *ORMDL1* as eQTL related to hypertension [190].

Phylogenetically, *ORMDL* genes are highly conserved and found in eukaryotes ranging from yeast to human. In yeast, absence of ORM1 and ORM2 impairs protein quality control, growth and sphingolipid synthesis [191]. Yeast cells lacking ORM1 and ORM2 are highly sensitive to stress and show constitutive activation of the UPR accompanied by slow ER-to-Golgi transport. Remarkably, deletion of only one *ORM* gene does not affect stress resistance, proposing at least partial overlapping function of the two yeast homologues. Strikingly, the phenotype of the double knockout mutants was alleviated by functional complementation with human *ORMDL3* [181, 191].

1.7.1 ORMDL3 Modulates UPR Signaling

Similar to ORM1 and ORM2 in yeast, human ORMDL proteins seem to modulate UPR signaling, however in these studies, some discrepancies have been noticed.

Cantero-Recasens et al. [182] reported that overexpression of ORMDL3 in HEK-293 cells resulted in increased levels of phosphorylated eIF2 α . In contrast, no changes in IRE1 signaling (such as *XBP1* splicing) have been observed in this study. In fibroblast-like cells (Cos-7), ORMDL3 overexpression restricted the UPRE promoter activity both under basal conditions and after ER stress induction, suggesting less *XBP1* splicing [39]. Miller et al. [192] described augmented activation of the ATF6 branch in ORMDL3 overexpressing A549 airway epithelial cells, whereas no changes in IRE1 and PERK signaling were monitored. In another study, no differences in UPR activation were observed in human airway epithelial cells (1HAE) upon ORMDL3 knockdown [183]. The stated inconsistencies point towards a complex role of ORMDL3 in regulating the UPR. These studies might indicate that the function of ORMDL3 is not only dependent on the cell type but also on the extent and duration of ER stress. Recently, our group could demonstrate that *in vitro* the general silencing of ORMDL3 reduces ATF6 α cleavage upon ER stress induction. *Vice versa*, overexpression of ORMDL3 promoted ATF6 α processing followed by the induction of ERSE target genes (unpublished data). In agreement with our findings, Miller et al. [192] demonstrated that ORMDL3 overexpression induces *SERCA2B*, a target gene of ATF6 α . In addition, we revealed a direct physical interaction between ORMDL3 and ATF6 α by co-immunoprecipitation studies. Moreover, we observed that ORMDL3 stimulates signaling via PERK. Overexpression of ORMDL3 provoked enhanced ATF4 promoter activities and increased levels of the pro-apoptotic transcription factor CHOP. In contrast, in our hands ORMDL3 overexpression resulted in inhibition of the IRE1 pathway as indicated by diminished *XBP1* splicing and UPRE promoter activity (unpublished data).

1.7.2 Regulation of Calcium Homeostasis by ORMDL3

Tightly controlled Ca²⁺ levels in the ER are essential for generating favorable conditions for correct protein folding. Altered Ca²⁺ levels impair protein folding, thereby inducing ER stress and activating the UPR [193]. The import of Ca²⁺ into the ER lumen is mediated by sarco/endoplasmic-reticulum Ca²⁺ ATPase (SERCA) proteins [194]. So far, studies linking ORMDL3 to calcium homeostasis have been inconsistent. Miller et al. [192] showed that overexpression of ORMDL3 increased *SERCA2b* mRNA levels in lung epithelial cells. Moreover, supporting their previous findings, overexpression of human *ORMDL3* in transgenic mice was shown to increase expression of *SERCA2B* [195]. By contrast, Cantero-Recasens et al. [182] reported that *ORMDL3* overexpression resulted in elevated cytosolic Ca²⁺ levels and reduced ER-mediated Ca²⁺ signaling in HEK-293 cells suggesting an inhibitory effect on SERCA activity.

Furthermore, a study in a T-cell line (Jurkat cells) states that ORMDL3 modifies lymphocyte activation by decreasing store-operated Ca²⁺ entry, which is crucial for calcium homeostasis and lymphocyte activation [196]. These findings suggest that higher ORMDL3 expression is associated with decreased activation of T-cells and provides insights into the functional link between *ORMDL3* and IBD.

1.7.3 ORMDL Proteins Regulate Sphingolipid Synthesis

Sphingolipids are essential components of eukaryotic cell membranes. Sphingolipids contain a sphingoid backbone that is *N*-acylated with various fatty acids generating several ceramide species, which can have numerous distinct head groups. Sphingolipid metabolites such as ceramide, ceramide-1-phosphate (C1P) and sphingosine-1-phosphate regulate a diverse set of cellular processes related to immunity and inflammation [197]. *De novo* sphingolipid synthesis starts in the ER with the

condensation of serine and palmitoyl coenzyme A (CoA) by serine palmitoyltransferase (SPT), the rate-limiting step, forming 3-ketosphinganine. A series of reactions then generates ceramide and subsequently sphingomyelin and glycosphingolipids.

Noteworthy, in yeast ORM proteins are negative regulators of SPT activity [198]. Cells deficient in both ORM1 and ORM2 displayed enhanced levels of long-chain-based sphingolipids and inhibition of SPT in ORM1/ORM2-deficient cells restores normal growth [191, 198]. Additionally, increased expression of *ORM1* or *ORM2* diminished levels of the *long-chain base 1 (LCB1)* and *2 (LCB2)*, encoding the SPT in yeast. In agreement with these findings, deletions of *ORM1* or *ORM2* augmented levels of *LCB1* and *LCB2* [156]. Regulation of SPT activity is established via phosphorylation of ORM proteins relieving their inhibitory activity [198]. However, ORMDL proteins in mammalian cells lack the motif, which is phosphorylated in yeast to regulate the formation of SPT-ORM complexes [191]. In mammalian cells, balanced expression levels of ORMDL family members were proposed as regulatory mechanism for sphingolipid biosynthesis [199, 200]. In this study, Kiefer et al. induced *de novo* synthesis of ceramides by treatment of cells with palmitate, substrate for the SPT reaction. Only siRNA mediated downregulation of all three ORMDL proteins resulted in changes in ceramide production. Furthermore, only simultaneous overexpression of the three ORMDLs inhibited SPT completely, whereas single knockdown showed only a slight inhibitory effect. Structure-function studies revealed that ORMDL proteins form oligomeric complexes that change conformation depending on cellular sphingolipid levels [191, 199, 201].

1.7.4 ORMDL3 in Intestinal Inflammation

The role of the IBD risk gene *ORMDL3* [38, 39] in intestinal inflammation was investigated in both an acute and chronic DSS-colitis model using *Ormdl3*-deficient mice (unpublished data). We observed an increased susceptibility to acute DSS-induced colitis in *Ormdl3*-deficient mice compared to their wild-type littermates, as indicated by a more severe body weight loss and higher disease activity indices (DAI). In contrast, *Ormdl3* deficiency was protective in the course of chronic colitis. Compared to their wild-type littermates, *Ormdl3*^{-/-} mice showed less body weight loss and an improved survival rate (unpublished data). Our *in vivo* studies suggest that ORMDL proteins constitute a precise fine-tuning mechanism in response to disturbed cellular homeostasis determining cell fate decisions in intestinal inflammation.

1.7.5 ORMDL3 & Autophagy

As illustrated above, ORMDL3 is involved in various cellular processes including the regulation of ER stress, ER-mediated calcium homeostasis, sphingolipid synthesis, and intestinal inflammation. Strikingly, ER stress, inflammation and dysregulated sphingolipid synthesis have been shown to induce autophagy [127, 197, 202, 203] pointing towards a functional link between ORMDL3 and autophagy.

A previous work by Ma et al. [204] postulated a role of ORMDL3 in basal and oxidized low-density lipoprotein-induced autophagy in endothelial cells. Another study reported that both ORMDL1 and ORMDL3 are translocated out of the ER upon free cholesterol loading. Subsequently, autophagy induced by free cholesterol loading degraded ORMDL1 resulting in increased sphingomyelin biosynthesis [205]. Recent findings suggested that ORMDL3 might mediate autophagy via the ATF6 branch of the UPR [206]. In agreement with these findings, it has been proposed that ATF6 is required for induction of autophagy [207]. IFN- γ -induced cleavage of ATF6 and ERK1/2-dependent phosphorylation of C/EBP- β induce the expression of *Dapk1* (Death-associated kinase 1), a Ca²⁺/calmodulin-regulated serine/threonine kinase. DAPK1 itself has been shown to induce

autophagosome formation through phosphorylation of Beclin 1 [208]. ATF6 α deficient cells displayed reduced expression of DAPK1 and reduced autophagosome formation. Consistent with these observations, *Atf6 α* -deficient mice were more susceptible to *Bacillus anthracis* infection compared to wild-type animals. These findings provide a first link between autophagy and ORMDL3.

1.8 Aims of this Study and Thesis Outline

The aim of this thesis was to decipher the role of endoplasmic reticulum homeostasis and autophagy in intestinal epithelial homeostasis. This thesis elucidates the function of the two ER membrane-localized proteins ATF6 α and ORMDL3 in the context of intestinal inflammation.

More specifically, we addressed the following major questions:

- What is the molecular regulatory network controlling ATF6 α signaling?

The intestinal epithelium of IBD patients characteristically displays ER stress and activation of the UPR [36, 209-212]. The role of the ATF6 α branch in intestinal inflammation is illustrated by augmented ATF6 α cleavage and increased expression of the ATF6 α target genes *GRP78* and *GRP94* in the intestine of IBD patients compared to healthy controls [36, 209-212]. However, while the modulatory signaling network of the other two branches of the UPR has been extensively studied, the regulation of the ATF6 α arm is poorly understood.

The present study is designed to shed light on the molecular regulatory network modulating ATF6 α signaling using a high-throughput siRNA screening approach. Identified candidates will be subjected to a more detailed analysis, exploring the specific molecular mechanisms of ATF6 α signaling regulation. Moreover, we experimentally examine whether interfering with the ATF6 α branch by modifying the activity of ATF6 α modulators might represent a feasible therapeutic approach in IBD treatment.

- What is the function of ORMDL3 in shaping host-microbe interactions and cellular homeostasis in the intestine?

Genome-wide association studies (GWAS) have identified *ORMDL3* as a genetic risk factor of IBD [38, 39]. At present, there are no studies exploring the function of ORMDL3 in intestinal homeostasis and its contribution to IBD pathogenesis. While impaired bacterial handling is assumed to underlie disease pathogenesis, the role of the IBD risk gene ORMDL3 in determining host-microbe interactions has not been assessed.

To elucidate the function of ORMDL3 in the intestine, we use both *in vitro* and *in vivo* models. As a first step, due to the high amino acid identity between ORMDL1 and ORMDL3, which suggests functional redundancies of these proteins, a phenotype analysis of both *Ormdl3*- and *Ormdl1/3* double deficient mice will be performed.

Moreover, we will assess whether antibacterial defense mechanism including the synthesis and secretion of antimicrobial peptides and xenophagy are affected by the absence of ORMDL3. In this context, the structure and function of secretory intestinal epithelial cells will be explored. We will explore the role of ORMDL3 in maintaining ER homeostasis and based on these findings, the function of ORMDL proteins in regulating ER turnover will be addressed.

This thesis consists of a general introduction (*Chapter 1*), followed by the material and methods section, and two chapters (*Chapter 3 & 4*) presenting the core research of the PhD, and a summary of the key findings (*Chapter 5*).

2 Material & Methods

2.1 Cell Biological Methods

2.1.1 Cell Lines

Cell lines used in this study were purchased from the German Collection of Microorganisms and Cell Cultures (DSMZ). Cells were cultured in respective media (Gibco/Life Technologies, Darmstadt, Germany) and incubated at 37 °C with 5 % (v/v) carbon dioxide (Table 1).

Table 1: Cell lines used in this study.

cell line	company	product nr.	species	tissue	nutrition medium
HEK-293	DSMZ	ACC-305	human	embryonic kidney	DMEM, 10 % (v/v) FCS
Caco-2	DSMZ	ACC-169	human	colon	MEM, 20 % (v/v) FCS

To split cells, cells were washed with PBS and treated with a trypsin/EDTA solution (Life Technologies, Darmstadt, Germany) for 5 min at 37 °C for dissociation. After complete detachment, trypsin was neutralized by adding full culture media. Cell suspensions were spun down at 300 g for 5min, resuspended in fresh nutrition media and replated at the needed concentration (Table 2). All steps were carried out in a laminar flow hood under sterile conditions (Thermo Scientific, Bremen, Germany).

Table 2: Overview of applied cell culture dishes for experiments with cell lines.

experiment	cell culture dish	cell number/well	medium [ml]
cell fractionation	10 cm dish	5 x 10 ⁶	10
co-immunoprecipitation	10 cm dish	5 x 10 ⁶	10
protein lysates	6-well plate	2 x 10 ⁵	2
RNA isolation	6-well plate	2 x 10 ⁵	2
fluorescence microscopy	12-well plate	1 x 10 ⁵	1
reporter gene assay	96-well plate	2 x 10 ⁴	0.1

2.1.2 Preparation & Culture of Mouse Embryonic Fibroblasts (MEFs)

Primary cultures of MEFs were generated from embryonic day 13.5 (E13.5) embryos by trypsinization, followed by mechanical dissociation using the gentleMACS Dissociator (Miltenyi Biotec). Primary MEFs were cultured in Dulbecco's modified Eagle's medium (DMEM with GlutaMax supplement and pyruvate) supplemented with 10 % fetal bovine serum, 100 U/ml penicillin and 100 µg/ml streptomycin.

2.1.3 Generation of Immortalized MEFs (iMEFs)

Immortalized MEFs (iMEFs) were generated by transfecting primary mouse embryonic fibroblasts with a vector (pMSSVLT) harboring the SV40 large T antigen (kindly provided by Paul Saftig, University of Kiel). Immortalized MEFs were cultured in Dulbecco's modified Eagle's medium (DMEM with GlutaMax supplement and pyruvate) supplemented with 10 % fetal bovine serum, 0.1 mM non-essential amino acids (Thermo Scientific), 100 U/ml penicillin and 100 µg/ml streptomycin at 37°C in a humidified 5% CO₂ atmosphere.

2.1.4 Isolation of Crypts & Cultivation of Murine Small Intestinal Organoids

Crypts were isolated from mouse small intestine by EDTA-based Ca²⁺/Mg²⁺ chelation and intestinal organoids were cultivated as described by Sato et al. [213]. Isolated crypts form 3D organoids,

characterized by a central lumen that is surrounded by a simple, polarized epithelial layer. Multiple crypt-like structures project outward. The basal side of the epithelial cells is oriented towards the outside, whereas the apical side is orientated towards the lumen [214].

In brief, small intestine was removed and cut longitudinally. The washed intestine was laterally cut into pieces of 0.5 cm. Intestinal pieces were incubated in cold PBS supplemented with 10 nM EDTA for 10 min intermitted by vigorous shaking. Supernatant was removed and fresh PBS-EDTA solution was added. This procedure was repeated 4 times. The resulting crypt suspension was passed through a 100 µm strainer and centrifuged at 1200 rpm at 4 °C. Supernatant was removed and epithelial crypts were resuspended in Matrigel (5-10 crypts/1µl Matrigel) (BD Bioscience/Heidelberg, Germany). Matrigel provides 3D laminin- and collagen-rich matrix resembling the basal lamina. Crypts were embedded in 24-well plates and cultivated in IntestiCult Organoid Growth Medium (STEMCELL, Köln, Germany). Medium was changed twice per week and organoids were stimulated after 7 days of cultivation.

2.1.5 Establishment and Culture of Human Intestinal Organoids

Human intestinal biopsy specimens were obtained from patients who underwent enteroscopic examination for the diagnosis of digestive symptom or the evaluation of diseases such as Crohn's disease and ulcerative colitis. Two or three biopsies were taken from an endoscopically normal and active diseased mucosa of IBD patients. The study was approved by the Ethics Committee of B231/98 and written informed consent was obtained from each patient. Isolation of the crypts and the subsequent establishment of intestinal organoids were performed as previously described [215]. Briefly, crypts were collected by rigorously shaking biopsy specimens in 2.5 mM EDTA. Isolated crypts were embedded in 40 µl of Matrigel at a density of 100-200 crypts per well and placed in 24-well culture dish. Crypts were maintained in 50 % L-WRN conditioned medium supplemented with recombinant human EGF (50 ng/ml, PeproTech, Hamburg, Germany), Y-27632 (10 µM, Sigma-Aldrich St.Louis, USA), A83-01 (500 nM, Tocris, Bristol,UK), Nicotinamide (10 mM, Sigma-Aldrich St.Louis, USA), N2 supplement and B12 suppelement (ThermoFischer Scientific, Steineich, Germany) and SB202190 (10 µM, Enzo Lörrach, Germany). 50 % L-WRN conditioned media was generated as previously described using the L-WRN cell line [216]. Organoids were passed every 6-7 days.

2.1.6 Transient Transfection of Plasmid DNA

For transfection of plasmid DNA into cultured cells, FuGENE 6 (Promega, Mannheim, Germany) was used. Briefly, the appropriate volume of the FuGENE 6 Transfection Reagent is diluted in Opti-MEM (Life Technologies, Darmstadt, Germany), mixed and incubated for 5 min at room temperature (Table 3). Plasmid DNA was added to the transfection mix to allow complex formation. After 15 min of incubation, the transfection mix was added to the cells.

Table 3: Formats and volumes for plasmid DNA transfections with FuGene 6.

Cell culture dish	Opti-MEM volume [µl]	DNA [µg]	FuGENE [µl]
10 cm	500	5	15
6-well plate	100	1	3
96-well plate	5	0.05	0.15

2.1.7 Transfection of siRNA

For transfection of small interfering RNA (siRNA) into cultured cells the polyamine-based transfection agent siPORT Amine (Life Technologies, Darmstadt, Germany) was employed. The positively charged reagent functions by complexing with negatively charged siRNA enabling the fusion with the cell membrane and the transfer of siRNA into cells.

In this study, reverse transfection was performed according to the manufacturers protocol. siPORT amine was diluted with Opti-MEM (Table 4) and incubated for 10 min at room temperature. Target-specific siRNA diluted with Opti-MEM was combined with the transfection agent and incubated for 10 min enabling the formation of transfection complexes. Cells were pipetted into the culture plate wells containing transfection complexes.

Table 4: Formats and required volumes for siRNA transfection with siPORT.

Cell culture dish	Opti-MEM volume [μ l]	siPORT [μ l]	siRNA [μ M]
6-well plate	100	5	7.5
96-well plate	5	0.25	0.375

2.1.8 Promoter-Mediated Luciferase Reporter Assay

To measure the activation of the ATF6 signaling branch, a luciferase reporter construct was used. The reporter construct comprises three ERSE (ER stress response element; consensus sequence CCAATN₉CCACG) sites of the human *GRP78* promoter fused to a firefly luciferase. The ERSE acts a *cis*-element critical for transcriptional induction of human GRP78 [108].

For the assay, the ERSE-dependent firefly luciferase (pGL3-ERSE) and the luciferase from *Renilla reniformis* driven by thymidine kinase promoter (pRL-TK; Clontech) were used. Bioluminescence from the *Renilla* luciferase was used as internal control for transfection efficiency and cell viability. HEK-293 cells were seeded into a 96-well plates at a density of 2×10^4 cells per well. After 24 h, cells were transfected with 12 ng plasmid DNA of pGL3-ERSE and 3 ng of pRL-TK. Cells were subjected to dual-luciferase assay 24 h after stimulation with Tunicamycin (5 μ g/ml). For cell lysis, 25 μ l of passive lysis buffer was used and cells were subjected to a freeze-thaw cycle. Cell lysates were analyzed on a 96-well microplate reader (Tecan, Männedorf, Switzerland) and dual-luciferase activity was expressed as relative light units (RLU).

2.2 Molecular Biological Methods

2.2.1 Isolation of Total RNA

The RNA extraction was performed using the RNeasy Mini Kit (Qiagen, Hilden, Germany) according to the manufacturer's protocol. Murine tissue was disrupted and homogenized using the TissueLyser II (Qiagen, Hilden, Germany) in the presence of 350 μ L RLT buffer containing 1% β -mercaptoethanol. Alternatively, cells were lysed directly in the cell-culture vessel and transferred into a microcentrifuge tube. For homogenization, lysates were loaded onto QIAshredder spin columns. To avoid contaminations by genomic DNA, on-column DNase digestion using the RNase-Free DNase Set (Qiagen, Hilden, Germany) was performed. RNA was eluted in 10-30 μ L RNase-free water and RNA concentration was measured using the NanoDrop ND-1000 spectrophotometer (PiqLab Biotechnologie GmbH, Erlangen, Germany). Purified RNA was stored at -80 °C.

2.2.2 cDNA Synthesis

For reverse transcriptase, 100-1000 ng total RNA was transcribed into complementary DNA (cDNA) by reverse transcription using the Maxima H Minus First Strand cDNA Synthesis Kit (Thermo Scientific, Bremen, Germany). Reverse transcription was performed according to the manufacturer's protocol (see also Table 5). The synthesized cDNA was diluted 1:10 with nuclease-free water and stored at -20°C.

Table 5: Reverse transcription with the Maxima H Minus First Strand cDNA Synthesis Kit.

step	component	quantity	temperature	time
1	RNA	100-1000ng	65 °C	5 min
	Oligo(dt)18 oligonucleotide	0.125 μ l		
	dNTP mix (10 Mm each)	0.5 μ l		
2	nuclease-free water	to 7.5 μ l	25°C	10 min
	5x RT buffer	2 μ l	50°C	15 min
	Maxima H Minus RT	0.5 μ l	85°C	5 min

2.2.3 Endpoint Polymerase Chain Reaction

The Polymerase Chain Reaction discovered by Mullis et al. [217] more than 20 years ago has become one of the most important tools in molecular biology allowing the amplification of DNA *in vitro*. In this work, endpoint PCRs were performed for semi-quantitative analysis of mRNA transcript levels. The list of oligonucleotides is provided in the supplementary material (Table 18). PCRs were set up according to the scheme depicted in Table 6 using the GoTaqTM polymerase (Promega, Mannheim, Germany).

Table 6: Reaction setup for PCR.

component	volume [μ l]
cDNA	2
dNTPs (10 mM)	1
oligonucleotides (10 μ M)	1
5x GoTaq buffer	5
GoTaq polymerase	0.4
nuclease-free water	ad 20

The amplification of DNA was conducted in a 96-well thermocycler (Applied Biosystems, Carlsbad, USA) carrying out denaturation, annealing and elongation according to steps listed in Table 7. For semi-quantitative analysis, amplification was performed with low cycle numbers to guarantee amplification in the exponential range and not in plateau phase.

Table 7: Cycling protocol for endpoint PCR.

temperature [°C]	time	cycles
95	3 min	1
95	30 s	
T _{anneal}	30 s	25-33
72	30 s	
72	7 min	1
4	∞	1

2.2.4 Agarose Gel Electrophoresis

For the separation of DNA fragments and verification of PCR product size agarose gel electrophoresis was carried out. 0.5 % TAE gels containing 1 % (w/v) agarose were run at a constant voltage of 120 V and a maximum current of 300 mA for 30-60 min using Bio-Rad Power Pac 300 power supply (Bio-Rad, Munich, Germany). SYBR Safe DNA gel stain was mixed into the agarose gel enabling nucleic acid visualization by UV excitation. Images were taken using Molecular Imager ChemiDoc XRS Imaging System (Bio-Rad, Munich, Germany). As molecular weight standard, SmartLadder MW-1700-10 (Eurogentec, Cologne, Germany) was utilized.

2.2.5 Quantitative Real-Time Polymerase Chain Reaction

Quantitative real-time PCRs (qPCRs) enabled the amplification and simultaneous quantification of mRNA levels using target-specific oligonucleotides. In this work, predesigned TaqMan probes, obtained from Applied Biosystems (Carlsbad, USA), were used. TaqMan probes are listed in the supplementary material (Table 19). All qPCR experiments were performed on the 7900HT Fast Real Time PCR System (Applied Biosystems, Darmstadt, Germany) and samples were run in duplicates on 384-well plates. 5-10 ng cDNA and 0.5 µL of the specific TaqMan® gene expression assay were used for the PCR mixture. PCR program was carried out according to the TaqMan Gene Expression Master Mix protocol (Applied Biosystems, Darmstadt, Germany). Cycle threshold (Ct) values of the target genes were normalized to the respective mRNA levels of *Gapdh* or β -*Actin*.

2.2.6 Plasmid DNA Isolation

For the isolation of genetically modified plasmids from *E. coli*, alkaline lysis of the cells was performed. In this work, the PureLink® HiPure Plasmid Filter Midiprep Kit (Life Technologies, Darmstadt, Germany) was used and plasmid preparation was carried out according to the manufacturer's protocol. DNA concentration was measured using the NanoDrop ND-1000 spectrophotometer (PeqLab Biotechnologie GmbH, Erlangen, Germany). Plasmid DNA was stored at -20 °C for further usage.

2.3 Protein Biochemical Methods

2.3.1 Total Protein Lysate Preparation

Culture medium was removed from adherent cells. Cells were washed twice with cold PBS and cell lysis was performed using cold RIPA buffer (Thermo Scientific, Bremen, Germany) supplemented with Halt Protease and Phosphatase Inhibitor Cocktail (Thermo Scientific, Bremen, Germany) enabling protein extraction from cytoplasmic, membrane and nuclear proteins. Lysates were incubated at 4°C for 5 min to achieve complete cell lysis. Lysates were gathered to one side using a cell scraper and collected lysates were centrifuged at 14,000 x g for 15 min at 4°C to pellet cell debris. For further analysis, supernatant was transferred to a new tube and protein lysates were stored at -80°C.

2.3.2 Cell Fractionation

To enrich cytosolic, membrane and nuclear proteins, cell fractionation was performed. Cells were washed with cold PBS and incubated on ice for 10 min with cell fractionation buffer 1 (250µl/6well). Cells were scraped and transferred into a microcentrifuge tube. The lysate was passed through a 26G needle 15 times using a 1 ml syringe and centrifuged at 1,000 x g for 10 min at 4°C. While the supernatant 1 includes cytosolic and membrane proteins, the pellet 1 is enriched for nuclear proteins. For further separation, the supernatant 1 was centrifuged at 16,000 x g for 45 min at 4°C to enrich for cytosolic proteins (supernatant 2) and the membrane fraction (pellet 2, resuspended in RIPA buffer).

To isolate the nuclear fraction, pellet 1 obtained from the first centrifugation step was resuspended in cell fractionation buffer 2 and incubated overnight at 4°C. The suspension was centrifuged at 16,000 x g for 15 min at 4°C to obtain the nuclear fraction. All buffers were supplemented with Halt Protease and Phosphatase Inhibitor Cocktail.

2.3.3 Protein Concentration Determination

Protein concentration was measured using the copper-based DC Protein Assay (Bio-Rad, Munich, Germany) according to the manufacturer's protocol.

This colorimetric assay, adapted from Lowry [218], is based on the biuret reaction. In an alkaline environment, copper ions react with peptide bonds resulting in the formation of monovalent copper ion. Copper ions immediately react with the Folin reagent, which is reduced into a blue colored substance with a maximum absorbance at 750 nm.

Briefly, 5 µl of protein lysate were diluted with 5 µl of aqua bidest. and mixed with the assay reagents. After 15 min, absorbance at 750 nm was quantified using the microplate reader Infinite M200 Pro (Tecan, Männedorf, Switzerland) and the associated software i-control 1.9 (Tecan, Männedorf, Switzerland) and correlated with protein concentrations using a bovine serum albumin (BSA) standard curve.

2.3.4 Gel Electrophoresis of Proteins

The separation of proteins by their molecular weight was performed using precast gradient polyacrylamide gels for improved separation of a wide range of proteins under denaturing conditions. The precast NuPAGE® 4-12 % Bis-Tris gels (Life Technologies, Darmstadt, Germany), optimized for the separation of proteins with a molecular weight range between 14 and 260 kDa, provide a neutral pH environment minimizing protein modifications.

Protein lysates were supplemented with NuPAGE LDS Sample Buffer (Thermo Scientific, Bremen, Germany) and incubated for 10 min at 70 °C before electrophoresis. SDS-PAGE was performed at 160 V (maximum current of 300 mA) for 2 h at room temperature in the XCell SureLock Mini Cell system (Life Technologies, Darmstadt, Germany). For running the gels, NuPAGE MOPS SDS Running Buffer was used. Prestained PageRuler plus protein ladder 10-250 K (Thermo Scientific, Bremen, Germany) was utilized for protein size estimation.

2.3.5 Western Blot Analysis & Immunodetection

For further analysis, separated proteins were transferred onto a polyvinylidene difluoride (PVDF) membrane enabling immunodetection of proteins by specific antibodies.

PVDF membranes (Bio-Rad, Munich, Germany) were activated under mild agitation with methanol for 10 sec, washed for 5 min in H₂O and then transferred for 5 min into anode puffer 1. Protein transfer was carried out by semi-dry blotting using the Trans-Blot Turbo™ Transfer System (Bio-Rad, Munich, Germany) with a discontinuous buffer system of one cathode buffer and two anode buffers at 0.1 A and a maximum voltage of 25 V for 45 min.

To avoid unspecific binding of the antibodies PVDF membranes were blocked for 1 h at room temperature with 5 % (w/v) blotting grade blocker (non-fat dry milk) or bovine serum albumin (BSA) in Tris-buffered saline (TBS) supplemented with 0.1 % (v/v) Tween 20. Membranes were probed with the appropriate primary (Table 20) and secondary (Table 21) antibodies. The primary antibody was diluted in TBS-T according to manufacturers' instructions and incubated overnight at 4 °C under mild agitation. To remove excess antibody, three washing steps (each 15 min) with TBS-T were carried out. A horseradish peroxidase (HRP) conjugated secondary antibody, which recognizes the Fc region of the primary antibody, was diluted in TBS-T following manufacturers' recommendations and incubated for 1 h at room temperature. Proteins were detected using a chemiluminescent substrate kit (Thermo Scientific) and recorded with an automated developer machine (Agfa, Mortsel, Belgium).

2.3.6 Co-Immunoprecipitations

In this study, co-Immunoprecipitations (co-IP) were performed to demonstrate a potential interaction of ORMDL3 and LC3. Briefly, Caco-2 cells were co-transfected with HA-tagged ORMDL3 and GFP-tagged LC3. After 48 h, cells were subjected to starvation (2h EBSS) in the presence of Bafilomycin A (100 nM). Cells were lysed using 500 µl RIPA buffer containing 1X Halt™ combined protease and phosphatase inhibitor. For complete cell lysis, cells were vortexed three times for 45 sec each. Lysates were centrifuged at 16,000 g for 15 min at 4 °C and the supernatant was subjected to the co-IP. For the co-IP, anti-HA Magnetic Beads (Thermo Fisher) were used and immunoprecipitation was performed according to the manufacture's protocol.

2.4 Microbiology Techniques

2.4.1 Bacterial Strains

E. coli LF82 [59] and K12 MG1655 were cultivated aerobically in lysogeny broth (LB) medium. 15 g/l agar was added to the liquid medium to obtain solid medium plates. Where appropriate, liquid and solid media were supplemented with antibiotics. To isolate *E. coli* LF82, medium was supplemented with 100 µg/ml ampicillin (Sigma, Munich, Germany) and 20 µg/ml erythromycin (Munich, Germany). For detection of *E. coli* K12, 300 µg/ml rifampicin (Roth, Karlsruhe, Germany) was added to the medium.

2.4.2 Bacterial Infection & CFU assay

iMEFs (1×10^6 cells per well) were seeded 24 hr prior to infection in a 6-well plate. Overnight cultures of *E. coli* LF82 or K12 MG1655 were diluted 1:100 in fresh LB medium and grown for 14 h without shaking. Bacteria were harvested by centrifugation at $3.000 \times g$, washed with PBS and resuspended in PBS. To enable efficient bacterial infection, cell culture medium supplemented with antibiotics was removed and changed to fresh antibiotic-free culture medium. iMEFs were infected with *E. coli* LF82 at indicated MOIs (MOI = multiplicity of infection). After addition of bacteria, cells were centrifuged at $300 g$ for 5 min followed by 1 h incubation at $37^\circ C$ in 5% CO_2 , humidified atmosphere. The medium was replaced with fresh medium containing gentamicin (100 µg/ml) to kill extracellular bacteria. Following 60 min incubation, the medium was replaced with fresh medium containing 10 µg/ml gentamicin for the remaining of the experiment.

To quantify *E. coli* LF82 intracellular replication (CFU assay), 2 h after infection, cells were washed with PBS and lysed with PBS supplemented with 0.2% Triton-X-100. Samples were serially diluted in PBS and plated on LB plates and incubated 14–16 hr. The number of colonies formed from the invasive bacteria was counted.

2.4.3 Crypt Infection

Intestinal crypts were isolated as described in 2.1.4. Crypts were counted and transferred into 1.5 ml tubes (20,000 crypts per tube). When indicated, crypts were pretreated with Bafilomycin A (100 nM) for 20 min at $37^\circ C$. The crypts were then inoculated with 10^8 CFU *E. coli* LF82 grown overnight as described in the previous chapter. 2 h post infection, crypts were collected.

2.5 Generation, Handling and Treatment of Mice

2.5.1 Generation of *Ormdl1*^{-/-}, *Ormdl2*^{-/-}, & *Ormdl3*^{-/-} Mice

The murine *Ormdl1* gene, located on chromosome 1, consists of 4 exons separated by 3 introns. For the generation of the knockout of *Ormdl1*, exon 2 containing the translation initiation codon (NM_145517) was targeted in collaboration with genOway SA (Lyon, France). The targeting vector containing the cDNA of exon 2 flanked by *loxP* sites and a neomycin resistance gene cassette flanked by flippase recognition target (FRT) sites (Fig. 2.1) was electroporated into 129Sv embryonic stem cells. Positive recombined embryonic stem cells were microinjected into C57BL/6 blastocysts. Blastocysts were transferred into pseudo-pregnant mice and resulting male chimeras were bred to C57BL/6 Flp deleter mice (C57BL/6-Tg(CAG-Flpe)2) for germline transmission and *in vivo* removal of selection markers. To obtain *Ormdl1*^{-/-} mice, animals were bred to Cre deleter mice (C57BL/6-*Gt(ROSA)26Sortm9(Cre/ESR1)*) resulting in the excision of exon 2 by recombination of the two *loxP* site. Obtained mice were backcrossed for nine generations to a C57BL/6J background.

The murine *Ormdl2* gene is located in chromosome 10 and consists of 4 exons. *Ormdl2*^{-/-} mice were engineered by the UC Davis Mouse Biology Program (California, USA). The targeting vector designed with two *loxP* sites flanking exon 2 and 3, was electroporated into C57BL/6N embryonic stem cells. Positive recombined embryonic stem cells were microinjected into C57BL/6 blastocysts. Chimeras were bred with C57BL/6N-A^{tmBrd}.

Ormdl3^{-/-} mice were generated in collaboration with TaconicArtemis GmbH (Cologne, Germany). The targeting vector with exon 2 to 4 of the murine *Ormdl3* gene (ensemble gene ID: ENSMUSG00000038150) flanked by *loxP* sites was electroporated into C57BL/6N Tac embryonic stem cells. Positive embryonic stem cells were identified by double positive selection with puromycin and neomycin. Chimeras were bred with Flp deleter mice (C57BL/6-Tg(CAG-Flpe)2Arte) for germline transmission and removal of selection markers. *Ormdl3*^{-/-} mice were generated by breeding *Ormdl3* conditional mice to Cre deleter mice (C57BL/6-*Gt(ROSA)26Sortm9(Cre/ESR1)Arte*). To avoid unspecific side effects, mice with a constitutive knockout allele were bred with C57BL/6N wild-type mice to remove the Cre recombinase

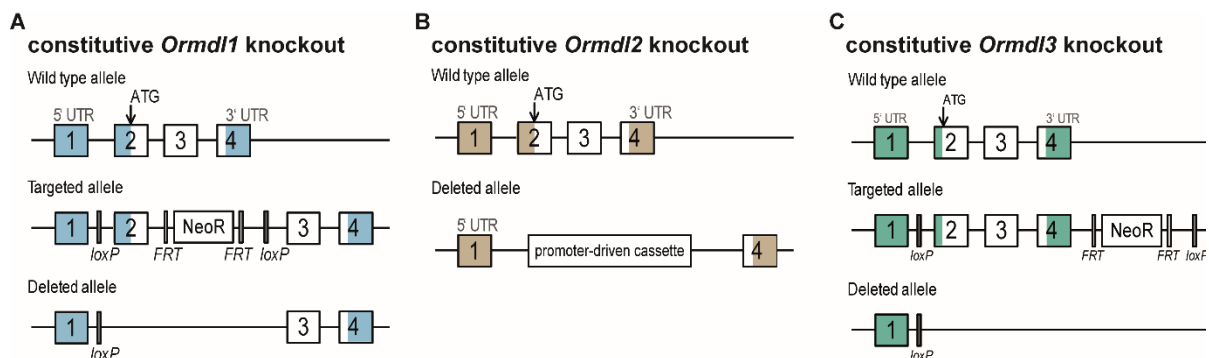


Figure 2.1: Generation of *Ormdl1*^{-/-}, *Ormdl2*^{-/-}, and *Ormdl3*^{-/-} mice. The targeting strategy for the generation of *Ormdl1*^{-/-} (A), *Ormdl2*^{-/-} (B) and *Ormdl3*^{-/-} (C) mice is depicted schematically.

2.5.2 Animal Housing & Animal Care

Mice were housed under specific pathogen-free (SPF) conditions in individually ventilated cages (IVCs) at the Central Animal Facility of the Schleswig-Holstein University Hospital Kiel, Germany. Animals were maintained in a 12 h light-dark cycle at 21°C ± 2°C and 60% ± 5% humidity. Food and water were provided *ad libitum*. All animal experiments were approved by the Animal Investigation Committee of the University Hospital Schleswig-Holstein (Table 8)

Table 8: License numbers for approved animal research.

license number	designated use
V 312-7224-121-33	sacrifice for tissue harvesting
V 242-66465/2016 (124-10/16)	infection of mice

2.5.3 Genotyping of Mice & iMEFs

Genotyping was conducted by polymerase chain reaction (PCR) using the primers listed in Table 9. Isolation of genomic DNA from iMEFs was performed using the DNeasy Blood & Tissue Kit (Qiagen, Hilden, Germany) according to the manufacturer's protocol. Genomic DNA from mice was extracted from tail biopsies by boiling with 100 µl of 50 mM NaOH for 1 h. Samples were centrifuged and the supernatant containing the genomic DNA was submitted to two independent touch-down PCRs per mouse line using the GoTaq DNA polymerase (Promega, Mannheim, Germany). Details of the PCR reaction and profile are shown in Table 10. Size of the amplified PCR products was determined by gel electrophoresis.

Table 9: Oligonucleotides for genotyping applied in this study.

target	species	forward primer	reverse primer
<i>Ormdl1</i> WT (1632 bp)	murine	5'-AACGTTAGTGCTGTTTGGACACACG	5'-AACATGCTTCCCTATACTGTGCCACT
<i>Ormdl1</i> KO (2015 bp)	murine	5'-CCCCAAAAGTATGCTCAGACA	5'-TCCCTATACTGTGCCACTACCCATTGT
<i>Ormdl2</i> (WT 407 bp, KO 872 bp)	murine	5'-ACACCTCCCCCTGAACCTGAAA	5'-AATACCATGGAACCAGCAAGGAATGC
<i>Ormdl3</i> WT (194 bp)	murine	5'-CTTCATCCGTTGTTGCTTGC	5'-TCCCCTACAGATCTCCTGAGG
<i>Ormdl3</i> KO (277 bp)	murine	5'-CTTCATCCGTTGTTGCTTGC	5'-TCACAGTGCCAGTAGGAAACC

Table 10: PCR component and profile for genotyping.

component	volume [µl]	number of cycles	temp [°C]	time
DNA	1	1	95	2 min
5X GoTaq Green Buffer	4		95	30 s
dNTPs (10 mM each)	0.5	10	65 to 55 (-1°C/cycle)	5 s
oligonucleotide for (10µM)	0.25		72	4 min
oligonucleotide rev (10µM)	0.25		95	10 s
GoTaq Polymerase	0.5	33	55	5 s
Nuclease-free water	13.5		72	4 min
		1	72	7 min
		1	4	∞

2.5.4 Infection of Mice

Ormdl3^{-/-} and their *Ormdl3^{+/+}* littermates received 0.25% (wt/vol) of dextran sulfate sodium (DSS; molecular mass = 36,000-50,000 daltons; MP Biomedicals) in drinking water starting 3 d before infection to increase adherence to the epithelial layer and invasion of bacteria. 12-16 wk-old male mice (body weight, 25-30 g) were pretreated with the broad-spectrum antibiotic streptomycin (20 mg intragastric per mouse; Sigma Munich, Germany) to disrupt bacterial flora in the intestinal tract. 24 h later, mice were orally challenged with 2×10^9 AIEC LF82 or K12 MG1655 bacteria by gavage. Fresh fecal samples were collected at day 1, 2, 3, 5 and 7 post-infection and resuspended in PBS to determine CFUs. At day 7 post-infection, mice were sacrificed and tissue was collected for further analysis.

Ileal, colonic, spleen, liver and kidney tissues were collected to quantify associated bacteria. Briefly, tissue was transferred into gentleMACS M Tubes with strainer and homogenized in 1 ml PBS using the Gentle-MACS Dissociator (Miltenyi Biotec, Bergisch-Gladbach, Germany). After serial dilution, samples were plated on LB agar plates supplemented with 100 µg/ml ampicillin and 20 µg/ml erythromycin (Sigma, Munich, Germany) to isolate *E. coli* LF82 bacteria, or with 300 µg/ml rifampicin (Euromedex, 1059-B) to isolate *E. coli* K12 MG1655 bacteria. Plates were incubated at 37°C overnight and CFUs were determined.

2.6 Imaging

2.6.1 Immunofluorescence

Cells were grown on cover slips overnight. Cells were washed with PBS and fixed in 4 % (w/v) paraformaldehyde for 20 min at room temperature. After washing with PBS, cells were permeabilized for 3 min at room temperature with 1 % (v/v) Triton X-100 in PBS supplemented with 5 % (w/v) BSA. To prevent unspecific binding, blocking with 5 % (v/v) goat serum for 60 min was carried out at room temperature. Incubation with the primary antibody (see Table 20) was performed overnight at 4 °C using a dilution of 1:100. Cells were washed three times with PBS and incubated for 45 min at room temperature with the respective secondary antibody coupled to a fluorophore. Cells were washed with PBS and stained for 10 min with the fluorescent stain DAPI which binds strongly to A-T rich regions in DNA. Cover slips were washed with PBS followed by washing with H₂O and mounted onto glass slides covered with mounting medium (Roth, Karlsruhe, Germany). Stained cells were examined using a Zeiss AxioImager.Z1 apotome fluorescence microscope and AxioVision Rel 4.9 software (ZEISS, Oberkochen, Germany).

2.6.2 Immunohistochemistry

2.6.2.1 Tissue Processing

Murine tissue was removed and immediately fixed in 10 % (w/v) formalin for 24 h at 4 °C. For complete dehydration, tissue was immersed in a series of ethanol solutions of increasing concentrations until 100%. In a next step, the ethanol was gradually replaced with xylene, which is then replaced by paraffin. The paraffin embedded tissue was dissected into 3.5 - 4.5 µm sections using the RM2255 microtome (Leica, Wetzlar, Germany).

2.6.2.2 Hematoxylin and Eosin (H&E) Staining

Samples were rehydrated in decreasing xylene and ethanol solutions followed by washing steps with distilled water. Slides were stained for 2 - 5 min in hematoxylin. Haematoxylin in complex with

aluminium salts is positively charged and reacts with negatively charged, basophilic cell components including nucleic acids which are stained blue. Counterstaining of the cytoplasm was achieved with 1 % (v/v) eosin solution for 2 min. Eosin is negatively charged and therefore reacts with positively charged, acidophilic components such as amino groups in proteins in the cytoplasm, which are stained pink. Slides were dehydrated and embedded in Roti-Histo-Kit mounting medium (Roth, Karlsruhe, Germany). Slides were examined with a Zeiss AxioImager.Z1 apotome fluorescence microscope and the AxioVision Rel 4.9 software (ZEISS, Oberkochen, Germany).

2.6.2.3 3,3'-Diaminobenzidine (DAB) staining

After rehydration of the slides, slides were boiled for 20 min in citrate buffer (pH 6.0) for antigen retrieval. Blocking of unspecific binding sites was achieved by incubating the slides with 5 % (v/v) goat serum in PBS. Naturally occurring peroxidases were inactivated by treatment with 3 % hydrogen peroxide. Antibody incubation and 3,3'-diaminobenzidine (DAB) staining was performed as described in the manufacturer's instructions of the Vectastain Elite ABC Kit (Vector Labs, Peterborough, United Kingdom). Briefly, the signal of the primary antibody was amplified by incubation with a biotinylated secondary antibody. Colorimetric reaction of DAB was achieved by adding a horseradish peroxidase-conjugated streptavidin antibody. DAB is oxidized by the horseradish peroxidase in the presence of hydrogen peroxide resulting in the deposition of a brown precipitate. Antibodies are listed in Table 20.

2.6.3 Transmission electron microscopy

0.5 cm long pieces of the ileum were fixed in 3 % glutaraldehyde in PBS at 4°C overnight. Transmission electron microscopy of semi thin ileal sections was performed at Institute of Anatomy (AG Lucius) as described previously [219].

2.7 Statistical Analysis

Statistical analysis was performed using the GraphPad Prism 5 software package (GraphPad Software Inc., La Jolla, USA). Unless otherwise stated, the Student's unpaired t-test was performed. Data are shown as mean \pm standard error of the mean (SEM). A p-value of ≤ 0.05 was considered as significant (*). A p-value of ≤ 0.01 was considered as strongly significant (**) and p-value of ≤ 0.001 as highly significant (***).

2.8 High-Throughput RNAi Screening Procedure

To elucidate the regulatory network (inducers/inhibitors) that modulates ATF6 α signaling, we initially screened 23,349 unique siRNAs targeting 7,783 genes using the Silencer Human Druggable Genome (HDG) siRNA library V3 (Ambion). HEK-293 cells (6×10^3 cells per well in 96-well plates) were reverse transfected with either single siRNAs (Ambion; primary and secondary screen) or siRNA pools (siGENOME; SMARTpool; Dharmacon; tertiary screen) complexed with siPORT Amine (Ambion).

Specifically, the Ambion HDG library consists of three siRNAs per gene that are screened individually, whereas the Dharmacon library are pools of four siRNAs. The applied siRNA concentration was 20 nM. Transfection of plasmid DNA was carried out using FuGENE 6 (Roche) as described in chapter 2.1.6. The dual-luciferase reporter assay was employed as read-out system (for details see chapter 2.1.8). Cells were transfected with 12 ng of plasmid encoding the ERSE-dependent firefly luciferase (pGL3-ERSE) and 3 ng of plasmid containing the luciferase from *Renilla reniformis* driven by thymidine kinase promoter (pRL-TK; Clontech). 24 h after plasmid transfection, cells were stimulated with Tunicamycin

(5 µg/ml) to induce ER stress. Cell lysis was performed after 24 h of exposure to Tunicamycin using 25 µl 1x passive lysis buffer (Promega). Cell lysates were analyzed on a 96-well microplate reader (Tecan, Männedorf, Switzerland) and dual-luciferase activity was detected (relative light units (RLU)).

As positive control for silencing, siRNA targeting the Firefly Luciferase was employed (Silencer Firefly Luciferase GL2 + GL3 siRNA; LifeTechnologies). Additionally, siRNA targeting ATF6α (Silencer siRNA 115888, LifeTechnologies) was included as positive control for the specific pathway and the screening phenotype. Silencer Negative Control No. 1 siRNA (LifeTechnologies) was employed as non-targeting control to ensure that there are no changes in gene expression due to siRNA delivery.

For initial data normalization, pre-processing and off-target analysis of screening data the web-based Comprehensive Analysis of RNAi-screen Data (CARD) application [220], available at <https://card.niaid.nih.gov>, was used. RLU values were normalized to the plate median (not considering RLU values of controls for determination of the median) and robust z-scores and fold-induction values were calculated. The robust z-score, which is more resistant to outliers than the z-score, is calculated from the plate median ($\mu_{1/2}$) and median absolute deviation (MAD):

$$\text{robust z score} = \frac{x - \mu_{1/2}}{\text{MAD} \times 1.4826}$$

The MAD is defined as the median of the absolute deviation from the median of data points X_1 to X_n :

$$\text{MAD} = \text{median}_i(|X_i - \text{median } X_{1..n}|)$$

Plates with systematic bias such as row, column or edge effects were discarded and repeated. Additional criteria for successful plate measurements were a knockdown efficiency > 2 fold (firefly siRNA and ATF6 control siRNA) and robust z-score means for the three non-targeting control siRNAs within the range ± 1.25 . To level out potential experimental fluctuations and to reduce the false positive rate, the third screen (Dharmacon) was measured three times independently and the robust z-score mean was calculated. Candidate genes passing this final stage were considered as final hits when robust z-score induction values were ≥ 2 (inhibitor) or ≤ -2 (inducer).

The normalized data from CARD was analyzed in R version 3.3.3. Functional profiles in screen hits were analyzed using the R package clusterProfiler v3.0.4 [221].

3 Pharmacological Intervention Ameliorates Hyperactivation of the ATF6 α Branch in Impaired Autophagy and Endoplasmic Reticulum Stress Signaling in Intestinal Epithelial Cells

The endoplasmic reticulum (ER) provides a critical environment for secretory protein folding. The accumulation of unfolded or misfolded proteins within the ER provokes ER stress, which in turn induces the unfolded protein response (UPR) mediated by the two transmembrane protein kinases protein kinase (PKR)-like ER kinase (PERK) and inositol-requiring enzyme 1 (IRE1 α), and the membrane-bound activating transcription factor 6 α (ATF6 α). Upon UPR activation, ATF6 α translocates to the Golgi apparatus where it undergoes regulated intramembrane proteolysis mediated by the site 1 and site 2 protease (S1P/S2P). The released cytosolic N-terminal portion of ATF6 α migrates to the nucleus and induces the expression of genes containing ER stress response elements (ERSE-I and -II) present in many chaperones (e.g. in glucose-regulated protein 78 kDa; *GRP78/BIP*) [108, 109]. While the downstream transcriptional program induced by ATF6 α signaling has been extensively studied in the context of ER homeostasis [106, 107], the knowledge regarding the molecular regulation of the ATF6 α branch is still limited.

3.1 Results

3.1.1 Identification & Functional Network Analysis of ATF6 α Signaling Modulators

To identify modulators of the ATF6 α signaling pathway, we targeted 7,783 genes using a commercially available “druggable” genome siRNA library. The screen was performed in human embryonic kidney cells (HEK-293) transfected with siRNA and a dual ERSE luciferase reporter construct (Fig. 3.1A,B). Luciferase activity was measured 24 h after stimulation with the ER stress inducer Tunicamycin (Fig. 3.1B). Non-targeting siRNA was included to establish a baseline reference for the screen and to discriminate sequence-specific silencing from non-specific changes induced by siRNA delivery. Additionally, knockdown of the firefly luciferase and *ATF6 α* itself served as internal controls for silencing (Fig. 3.1C).

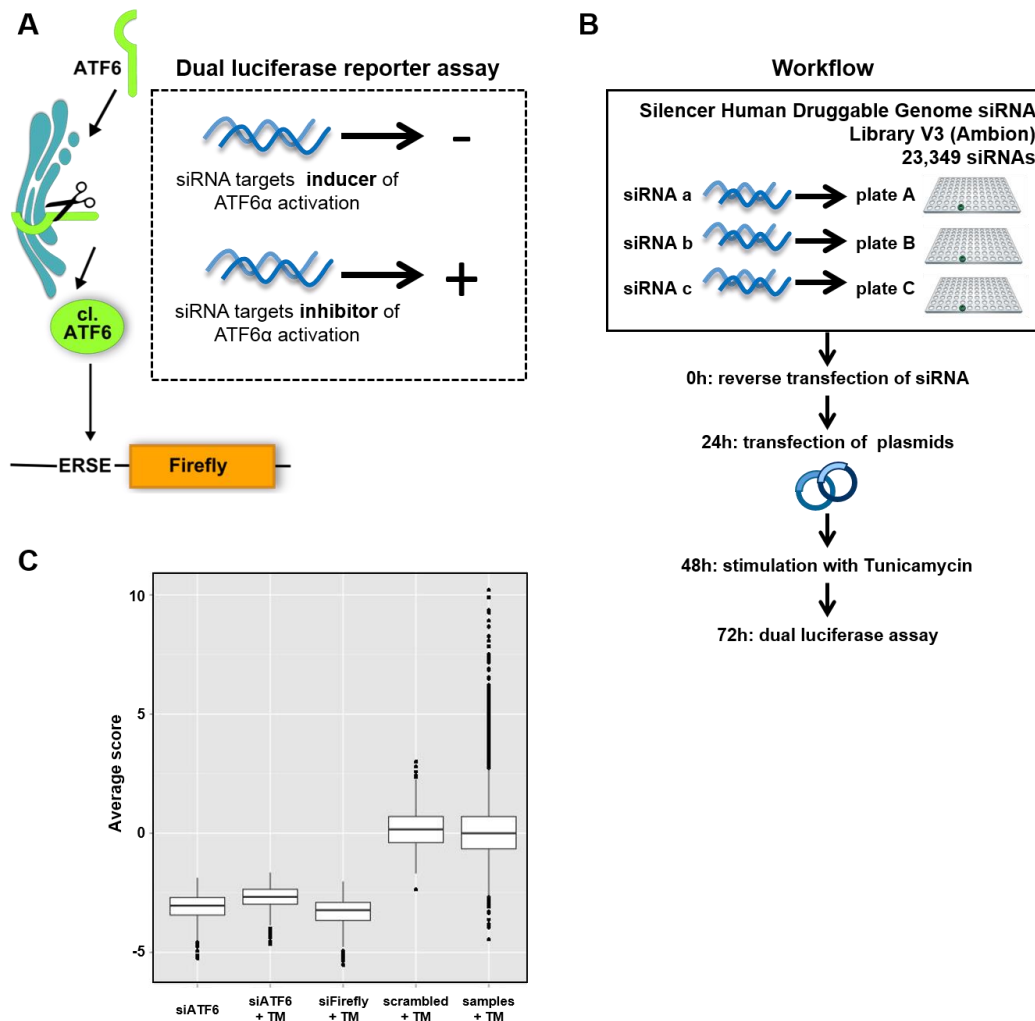


Figure 3.1: High-throughput RNAi screening approach for the identification of ATF6 α signaling modulators.

(A) Schematic representation of the luciferase reporter assay-based screening approach. (B) HEK-293 cells were reverse-transfected with siRNA and 24 h later transfected with the reporter plasmids for ATF6 (pGL3-ERSE) and thymidine kinase (pRL-TK). Luciferase activity was measured 24 h after Tunicamycin stimulation (5 μ g/ml). (C) Scores of primary screen samples and controls. Scrambled siRNA was used as non-targeting negative control, siRNA directed against firefly luciferase (siFirefly) was used as technical control, siRNA targeting ATF6 (siATF6) was employed as biological control. TM=Tunicamycin, 5 μ g/ml.

Each transcript was targeted using three different siRNAs, resulting in a total number of 23,349 assays for ATF6 activation (Fig. 3.2A). Genes with a normalized, averaged fold-induction higher than 2.0 or lower than -2.0 were considered as candidate genes. Among the 157 candidate genes identified in the primary screen, bioinformatics analysis demonstrated an enrichment of candidate genes in different functional groups (based on Gene Ontology terms) such as RNA processing and splicing (Fig. 3.2B). To narrow down the number of candidate genes, the 157 genes were rescreened using the same experimental setup. The remaining 104 candidate genes were validated in a third screen altering the application of individual siRNAs to a pool of four siRNAs per transcript, which differed in their respective target sequences (Fig. 3.2A). This approach resulted in 22 validated hits, including 15 suppressors and 7 activators of ATF6 α signaling (Fig. 3.2C). Remarkably, a STRING-database network analysis of the 22 confirmed candidates revealed a strong connection of the identified regulators of ATF6 α signaling (Fig. 3.2D).

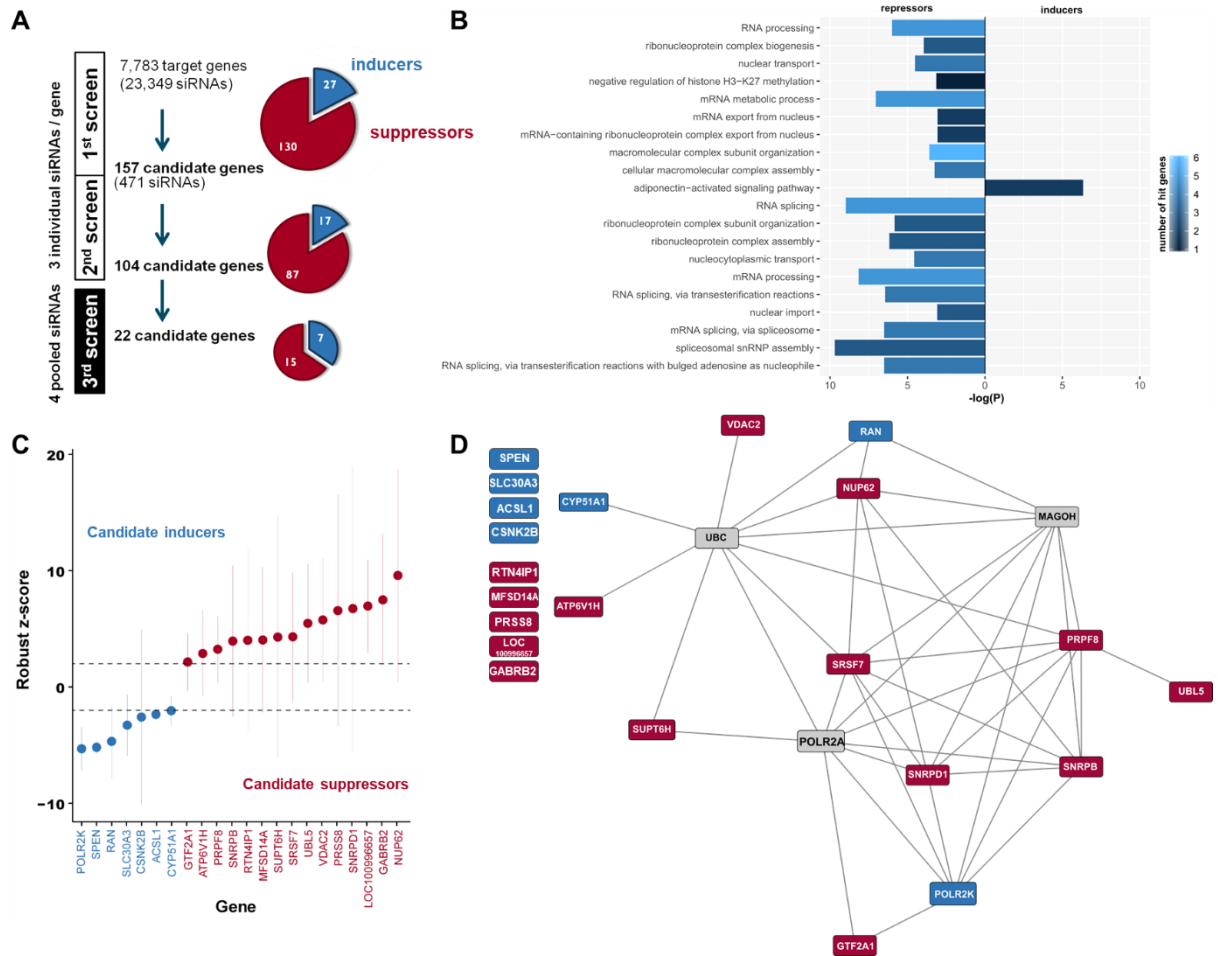


Figure 3.2: Systematic siRNA screening reveals modulators of ATF6 α activation. (A) Screening procedure and number of candidate genes at different screening stages. In the primary and secondary screens each gene was targeted with three individual siRNAs tested separately. Pools of four siRNAs were used for the third screen. Candidate genes with an inducing or repressing effect on ATF6 activation are indicated in blue or red, respectively. (B) Enrichment of candidate genes in different functional groups (GO Biological Process) after the primary screen. (C) Final set of 22 candidates after the third screen. Bars depict mean and 95th confidence interval (3 replicates). (D) STRING Network of candidate genes after the third screen. Only interactions with a confidence score >0.9 were considered. Inducers are depicted in blue, repressors are shown in red and connecting proteins not identified in the screen in grey.

3.1.2 Chemical Interference with Selected Candidates Validates siRNA-Mediated Phenotypes

From the 22 validated ATF6 α signaling regulators, the following criteria were applied to select the candidates for detailed functional characterization: (1) biological function, (2) cellular localization, (3) availability of specific inhibitors or inducers and (4) antibody availability. This selection resulted in 6 candidates. To independently validate them and to exclude any siRNA-mediated off-target effects, the 6 candidates were rescreened using corresponding inhibitors or inducers (Fig 3.3A-D). Notably, direct inhibition of the identified ATF6 signaling inducers ACSL1 (Acyl-CoA Synthetase Long Chain Family Member 1) and CSNK2B (Casein Kinase 2 β) using TC (Triacsin C) and TBB (4,5,6,7-Tetrabromo-2-azabenzimidazole), respectively, significantly reduced ERSE promoter activity upon ER stress induction (Fig. 3.3A). In contrast, treatment of cells with TPEN (N,N,N',N'-Tetrakis(2-pyridylmethyl)ethylenediamine), a Zn²⁺ chelator, known to increase the expression of the identified ATF6 inducer *SLC30A3* [222], elevated the activity of the ATF6 α branch validating our previous results (Fig. 3.3B). As indicated by the siRNA screen, direct inhibition of the serine protease 8 (PRSS8) activity by exposure to Camostat mesylate (CM) augmented ATF6 α signaling (Fig. 3.3C). Similarly, indirect inhibition of RTN4IP1 signaling with Simvastatin, which blocks RhoA signaling, a downstream target of RTN4 [223], resulted in increased ERSE promoter activity verifying RTN4IP1 as repressor of ATF6 α signaling (Fig. 3.3C). Treatment of cells with the VDAC2 (voltage dependent anion channel 2) binding small molecule Erastin, known to induce *VDAC2* expression [224], diminished ATF6 α signaling and verified VDAC2 as repressor of this signaling branch (Fig. 3.3D). In summary, chemical interference with selected candidates confirmed the phenotypic effect of siRNA demonstrating the reliability of our approach.

3.1.3 Nuclear p36ATF6 α Levels Partially Recapitulate ERSE Promoter Activity

To investigate the effect of our candidates on the translocation of ATF6 α , enrichment of the nuclear fraction was performed. In addition to the 50 kDa cleavage product of ATF6 α , a 60 kDa and a 36 kDa fragment of ATF6 α have been described to induce the ERSE promoter during ER stress [225, 226]. Here, nuclear levels of the 36 kDa ATF6 α fragment (p36ATF6 α) were measured. Inhibition of ACSL1 and CSNK2B by the small molecules TC and TBB, respectively, caused slightly reduced levels of nuclear p36ATF6 α (Fig. 3.3E). On the contrary, upregulation of the inducer *SLC30A3* by exposure to TPEN generated elevated amounts of cleaved ATF6 α in the nuclear enriched fraction (Fig. 3.3F). Small molecule-mediated inhibition of the repressors PRSS8 and RTN4IP1 resulted in higher p36ATF6 α levels (Fig. 3.3G). In contrast, upregulation of the repressor VDAC2 decreased p36ATF6 α protein levels in the nuclear enriched fraction both under basal conditions and upon exposure to Tunicamycin (Fig. 3.3H). Thus, nuclear levels of p36ATF6 α supported our findings from the ERSE dual luciferase reporter assays.

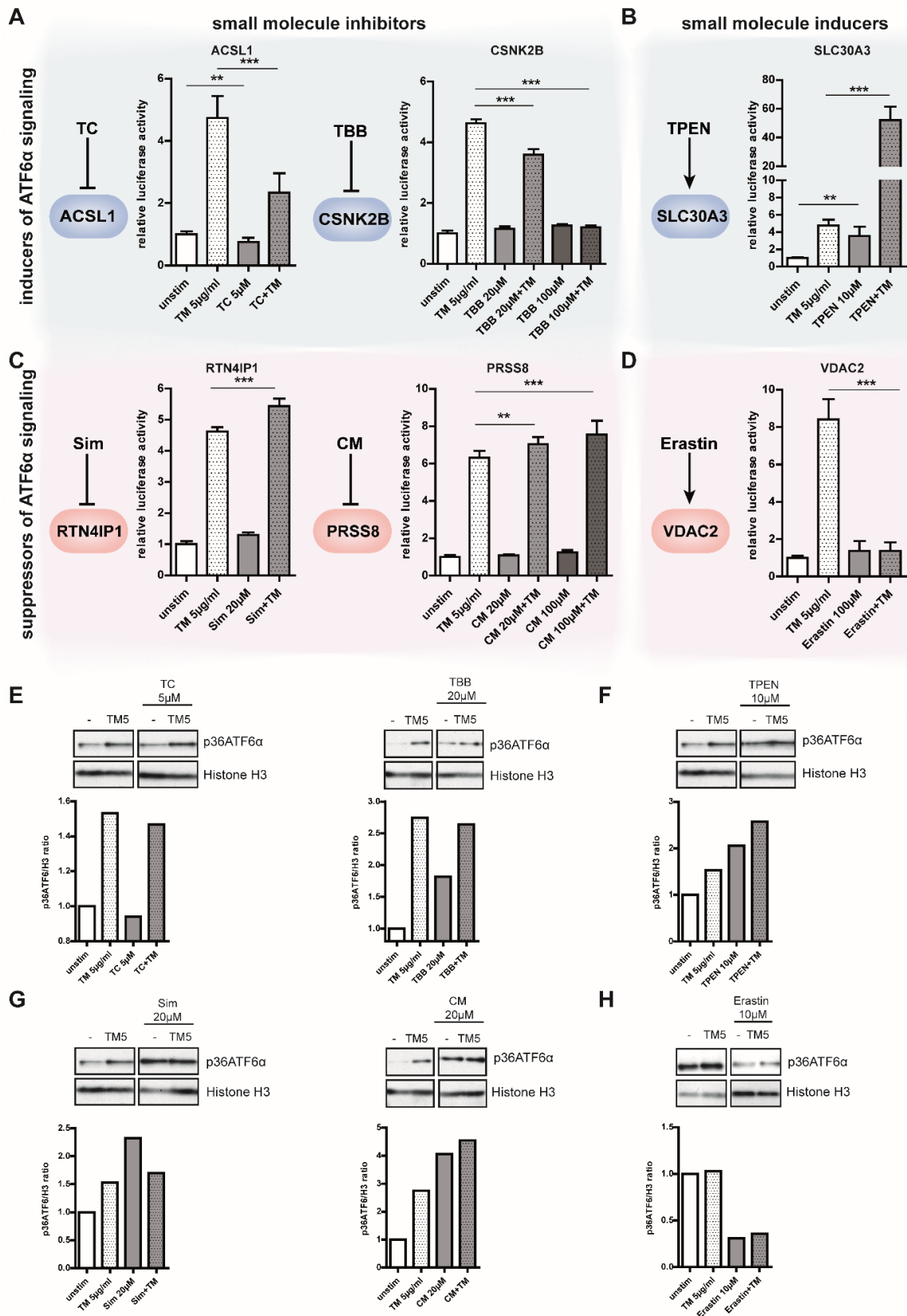


Figure 3.3: Small molecule agents targeting candidate genes reflect the RNAi-mediated phenotype on ERSE promoter activity. (A-D) ERSE promoter activity was quantified by dual luciferase reporter assay in HEK-293 cells. Cells were exposed to Tunicamycin (5 μ g/ml) and small molecule agents for 24 h as indicated. (E-F) HEK-293 cells were treated with Tunicamycin and small molecules for 5h. Immunoblotting of nuclear lysates for the 36 kDa fragment of ATF6 α (p36ATF6 α) and corresponding quantifications of nuclear ATF6 α . TC=Triacsin C; TBB=4,5,6,7-Tetrabromo-2-azabenzimidazole; TPEN=N,N,N',N'-Tetrakis(2-pyridylmethyl)ethylenediamine; CM=Camostat mesylate; Sim=Simvastatin.

3.1.4 Candidates *ACSL1* and *CSNK2B* Induce ATF6 α Signaling in Intestinal Epithelial Cells

Due to their pronounced effect on ATF6 α signaling (Fig. 3.3), *ACSL1* and *CSNK2B* were selected for further functional studies. To confirm the relevance of *ACSL1* and *CSNK2B* on ATF6 α signaling in the intestinal epithelium, we rescreened *ACSL1* and *CSNK2B* using the intestinal epithelial cell line Caco-2. Knockdown of the two genes in Caco-2 cells resulted in a significantly reduced ERSE promoter activity (Fig. 3.4A) and reduced mRNA levels of *HSP90B1*, a target gene of ATF6 α (Fig. 3.4B).

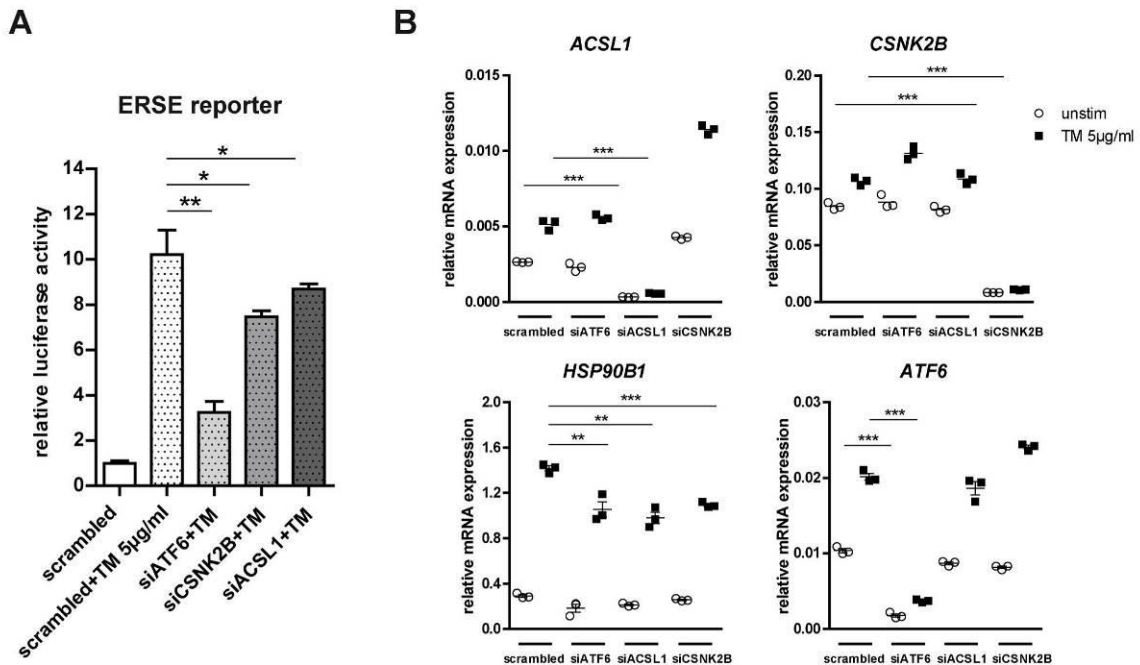


Figure 3.4: *ACSL1* and *CSNK2B* are inducers of ATF6 α signaling in the intestinal epithelial cell line Caco-2. siRNA-mediated knockdown of *ACSL1* (*siACSL1*), *CSNK2B* (*siCSNK2B*) and *ATF6 α* (*siATF6*) in Caco-2 cells. scrambled= non-targeting control siRNA. (A) ERSE promoter activity was quantified by luciferase reporter assays. Cells were co-transfected with the firefly luciferase reporter pGL3B-ERSE and a Renilla luciferase for normalization. After 24 h, cells were left untreated or stimulated with 5 μ g/ml Tunicamycin (TM) for additional 24 h. (B) mRNA levels of ATF6 α target gene *HSP90B1* (*GRP94*) were measured by quantitative PCR (n=3) 24 h after TM stimulation.

3.1.5 Inhibition of Candidates Decreases Transcription of ATF6 α Target Genes in Human Organoids

To determine the biological relevance of the findings, small intestinal human organoids derived from a Crohn's disease (CD) patient were exposed to the ER stress inducer Tunicamycin. Indeed, reduced downstream signaling of ATF6 α was monitored upon exposure to the *ACSL1* inhibitor Triacsin C (Fig. 3.5A) or the *CSNK2B* inhibitor TBB (Fig. 3.5B), respectively.

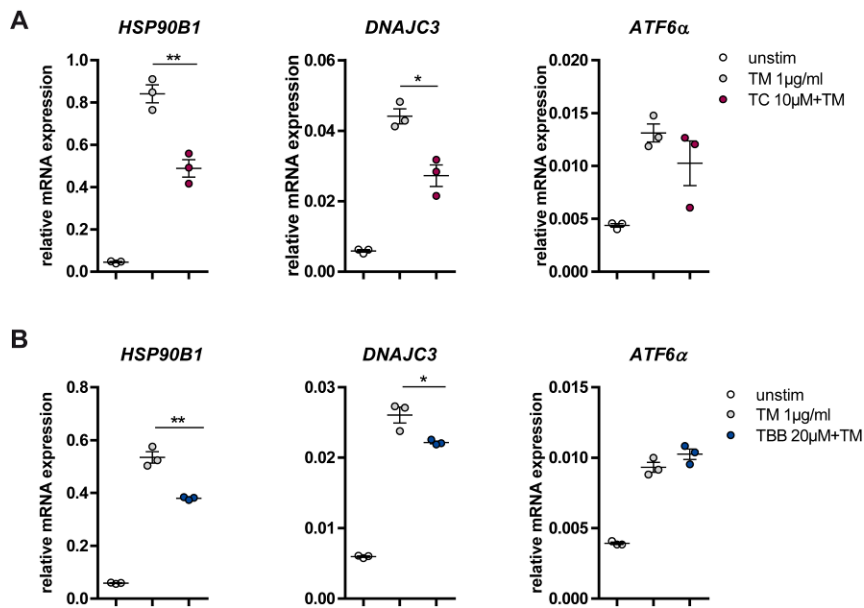


Figure 3.5: Inhibition of ACSL1 and CSNK2B represses ATF6 α downstream signaling in human organoids. Human organoids derived from inflamed ileal tissue (CD patient) were exposed to 1 μ g/ml Tunicamycin for 24 h in presence or absence of (A) ACSL1 inhibitor Triacsin C (TC, 10 μ M) or (B) CSNK2B inhibitor TBB (20 μ M). Transcript levels of ATF6 α target gene *HSP90B1* (*GRP94*) and *DNAJC3* (*P58IPK*) were determined by quantitative PCR (n=3).

3.1.6 ACSL1 induction of ATF6 α signaling is independent of intramembrane cleavage & CSNK2B assists in COPII mediated transport of ATF6 α

To get insights into how ACSL1 and CSNK2B specifically mediate effects on ATF6 α downstream signaling, we transfected Caco-2 cells either with a plasmid encoding the transcriptionally active N-terminal ATF6 α fragment or with the empty plasmid. We found that Triacsin C treatment repressed ERSE activation in cells overexpressing N-terminal ATF6 α , whereas treatment with TBB did not inhibit promoter activity (Fig. 3.6A). Similarly, in intestinal organoids derived from Villin-Cre-driven IEC-specific transgenic mice overexpressing the activated form of ATF6 α (*nAtf6 α ^{IEC}*), TBB treatment did not diminish mRNA levels of *Atf6 α* target genes upon exposure to Tunicamycin. In contrast, inhibition of ACSL1 with Triacsin C resulted in reduced mRNA levels of *Atf6 α* target genes *Hsp90b1* (*Grp94*) and *Hspa5* (*Grp78*) (Fig. 3.6B,C). These results might imply that ACSL1 mediates its inducing effect on ATF6 α signaling downstream of the cleavage event at the Golgi apparatus. While the exact mechanisms of how ACSL1 affects ATF6 α signaling needs to be explored in more detail, fluorescence microscopy revealed co-localization of ACSL1 and GFP-ATF6 α in Tunicamycin-exposed cells (Fig. 3.6D), suggesting that these proteins might directly interact. Moreover, treatment of intestinal epithelial cells with Palmitoyl coenzyme A, product of the enzymatic reaction catalyzed by ACSL1, caused increased ERSE reporter activity (Fig. 3.6F) supporting the role of ACSL1 as inducer of ATF6 α signaling. Importantly, the abolishing effect of TBB on ATF6 α downstream signaling implies that CSNK2B regulates ATF6 α signaling upstream of the intramembrane proteolysis. We therefore hypothesized that CSNK2B might be involved in the transport of ATF6 α from the ER to the Golgi apparatus. Indeed, it was shown that ATF6 α trafficking is dependent on COPII vesicles [227]. Moreover, Koreishi et al. [228] demonstrated that the casein kinase 2, composed of CSNK2B and CSNK2A, phosphorylates the COPII constituent Sec31, thereby facilitating ER-Golgi trafficking. Indeed, depletion of SEC31 by siRNA in intestinal epithelial cells abolished the inhibitory effect of TBB on ERSE promoter activity (Fig. 3.6F). In agreement with these findings, inhibition of ER-Golgi trafficking by treatment with FLI-06 [229] diminished the inhibitory effect of TBB on ERSE promoter activity (Fig. 3.6E).

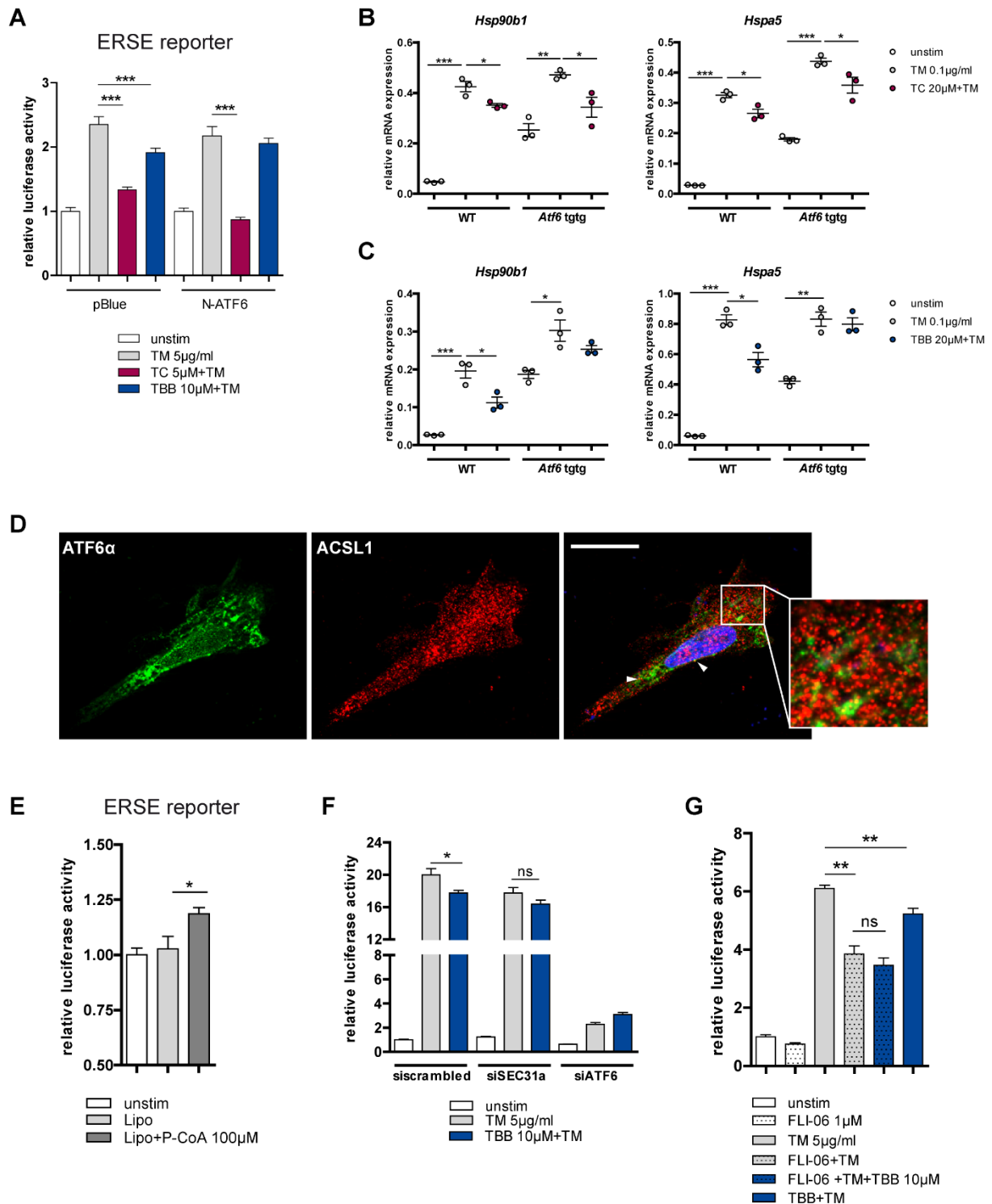


Figure 3.6: CSNK2B controls ATF6 α signaling upstream of intramembrane cleavage. (A) Effects of TC and TBB treatment on ERSE promoter activity in Caco-2 cells quantified by dual luciferase reporter assays. Caco-2 cells were transfected either with N-ATF6 α or with the empty plasmid (pBlue) and stimulated with Tunicamycin and inhibitors for 24 h. (B) and (C) Transcript levels of *Atf6* α target genes *Hsp90b1* (*Grp94*) and *Hspa5* (*Grp78*) in WT and *Atf6* α transgenic (*Atf6 tggt*) small intestinal organoids treated with Tunicamycin (TM 0.1 μ g/ml) and TC (B) or TBB (C) for 24 h. (D) Fluorescence microscopy of ACSL1 and GFP-ATF6 α . Caco-2 cells were transfected with GFP-ATF6 α and stimulated with Tunicamycin (1 μ g/ml) for 4 h. Cells were fixed and stained with an α -ACSL1 antibody (red). DAPI staining depicted in blue. Scale bar, 20 μ m. (E) Caco-2 cells were stimulated with lipofectamine-complexed Palmitoyl coenzyme A (100 μ M) or lipofectamine alone (Lipo) for 24 h and ERSE dual luciferase reporter activity was measured. (F) ERSE promoter activity in Caco-2 cells upon siRNA-mediated depletion of SEC31a (siSEC31a). (G) ER-Golgi transport was inhibited in Caco-2 cells with FLI-06 (1 μ M) in presence or absence of Tunicamycin and TBB, respectively. Cells were stimulated for 24 h and ERSE promoter activity was quantified by dual luciferase reporter assay.

3.1.7 The ATF α Branch of the UPR Modulates NF- κ B Signaling

Unresolved ER stress in intestinal epithelial cells has emerged as an important mechanism favoring intestinal inflammation [36]. It was shown that *Xbp1* deletion in mouse IECs initiates ER stress and promotes hypersensitivity to inflammatory signals. This hypersensitivity is caused by increased JNK and NF- κ B signaling accompanied by elevated IRE1 kinase activity [230]. In contrast, the contribution of the ATF6 α branch in NF- κ B signaling has not been investigated in the context of intestinal inflammation. Here, we examined NF- κ B signaling overexpressing the N-terminal ATF6 α fragment in intestinal epithelial cells upon ER stress induction (Fig. 3.7A). In line with our previous findings, enhanced NF- κ B promoter activity in cells overexpressing the transcriptionally active ATF6 α fragment was ameliorated in the presence of TC, while TBB treatment did not have any effect on NF- κ B reporter activity. To better understand the role of the ATF6 α branch in NF- κ B signaling, we next stimulated intestinal organoids derived from *nAtf6*^{IEC} mice encoding the cleaved form of ATF6 α with Tunicamycin. Upon UPR activation, organoids expressing the N-terminal ATF6 α fragment exhibited increased mRNA levels of *Tnfa* compared to wild type organoids, pointing towards augmented NF- κ B signaling (Fig. 3.7B). Likewise, inhibition of the site 1 protease required for ATF6 α cleavage at the Golgi complex and siRNA mediated downregulation of *Atf6 α* , *Acs1* or *Csnk2b*, respectively, reduced NF- κ B promoter activity in the presence of Tunicamycin (Fig. 3.7C,D). In agreement with these findings, stimulation with the ACSL1 product Palmitoyl coenzyme A caused increased NF- κ B activity (Fig. 3.7E).

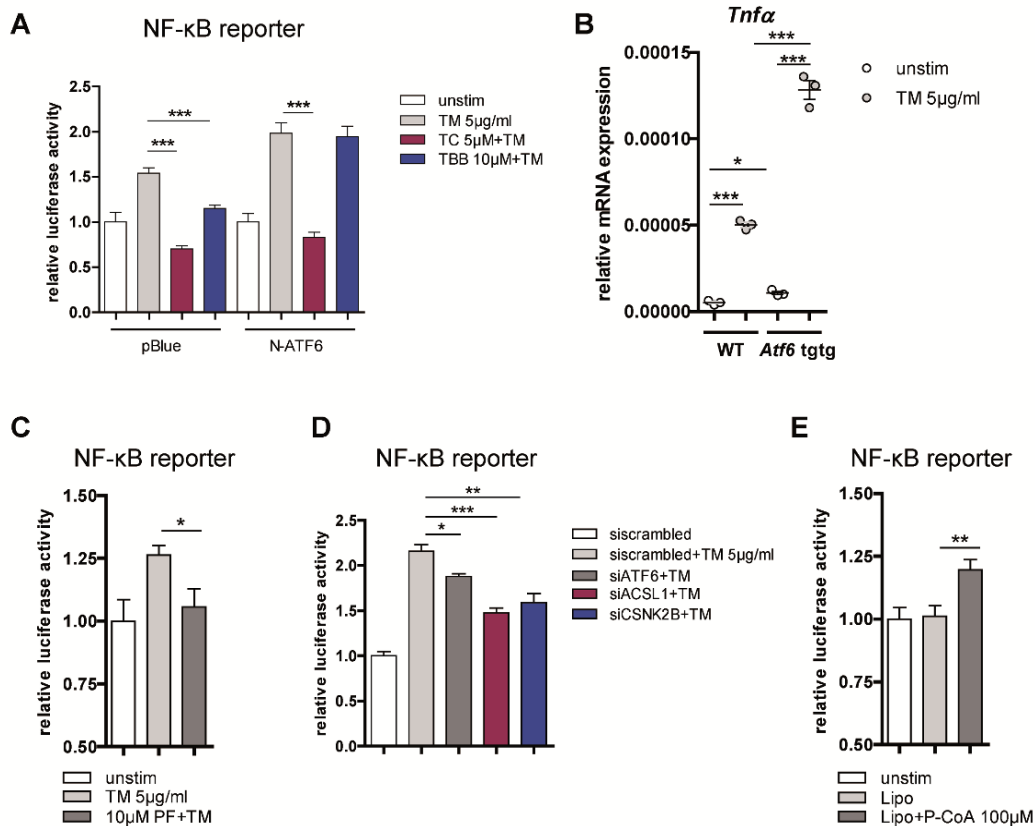


Figure 3.7: ATF6 α regulates NF- κ B signaling upon ER stress induction. (A) NF- κ B promoter activity in Caco-2 cells quantified by dual luciferase reporter assays. Caco-2 cells were transfected either with N-ATF6 α or with the empty plasmid (pBlue) and exposed to Tunicamycin for 24 h. Average relative luciferase activity of unstimulated cells was set to 1. (B) Transcript levels of *Tnfa* in WT and in *Atf6 α* transgenic (*Atf6 tgg*) small intestinal organoids stimulated with Tunicamycin (TM 0.1 μ g/ml) for 24 h. (C) and (D) NF- κ B promoter activity in Caco-2 cells upon (C) inhibition of the site 1 protease (S1P) with PF-429242 (10 μ M) or (D) siRNA-mediated depletion of ATF6 α (siATF6), ACSL1 (siACSL1) or CSNK2B (siCSNK2B). (E) NF- κ B dual luciferase reporter assay in Caco-2 cells stimulated with lipofectamine-complexed Palmitoyl coenzyme A (100 μ M) or lipofectamine alone (Lipo) for 24 h.

3.1.8 Inhibition of ATF6 α Attenuates Pro-Inflammatory Profile in *Atg16l1*- & *Xbp1*-Deficient Intestinal Organoids

CD patients and healthy individuals homozygous for the *ATG16L1*^{T300A} single-nucleotide polymorphism (SNP) exhibit high expression of the chaperone GRP78 in their Paneth cells indicating ER stress [113]. Similarly, mice with IEC-specific deletion of *Atg16l1* demonstrate increased levels of this chaperone [35]. High levels of GRP78, a target gene of the ATF6 α branch, might point towards an engagement of the ATF6 branch in this context. However, the specific contribution of the ATF6 α branch to this phenotype has not been studied in detail. We hypothesized that increased GRP78 expression at least partially might be due to hyper-activation of the ATF6 branch in ATG16L1-deficient cells. Indeed, we observed a significantly increased activation of the ATF6 α branch in cells lacking the autophagy gene ATG16L1 (Fig. 3.8).

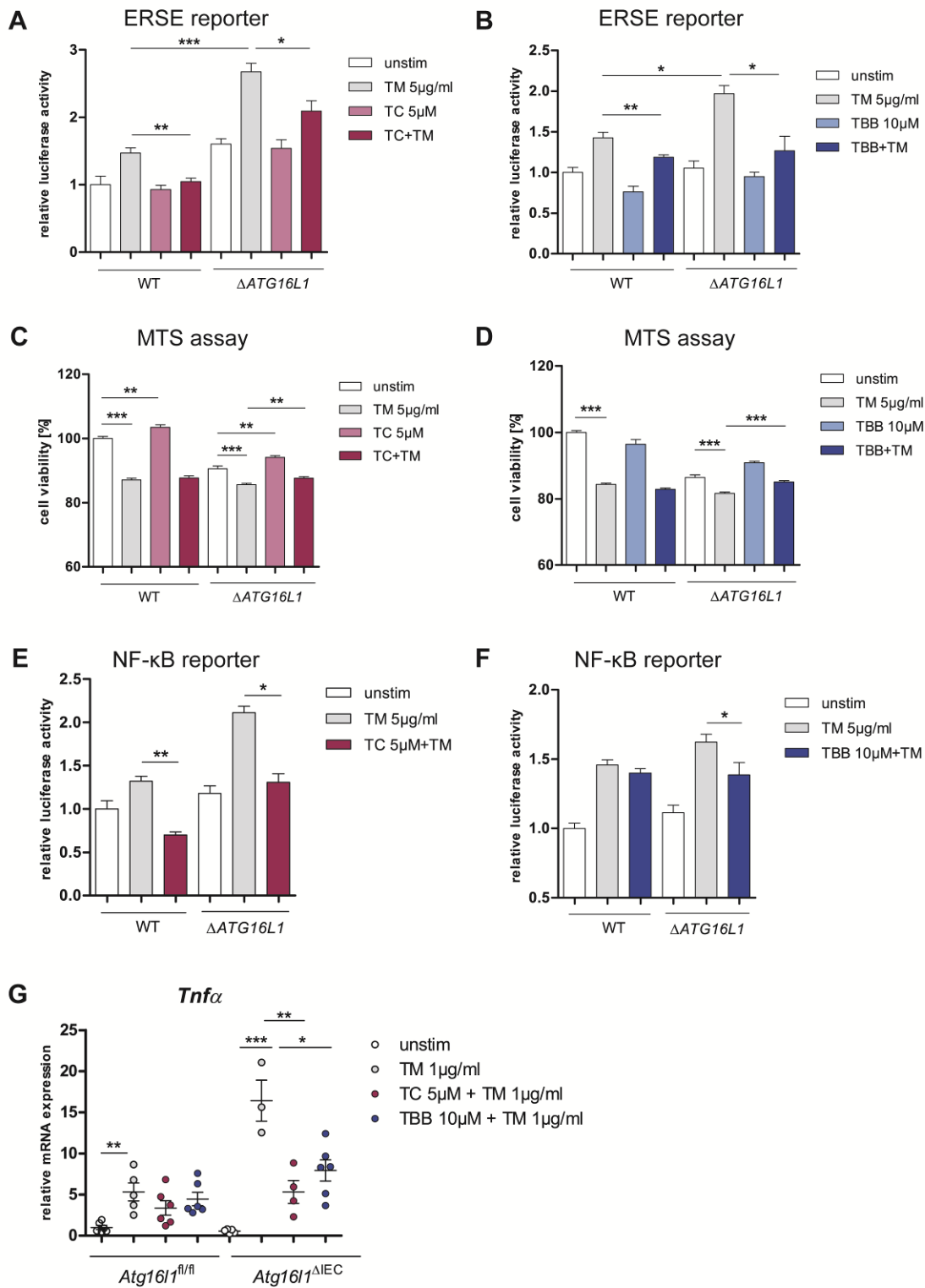


Figure 3.8: Reduction of the hyperactivation of the ATF6 α branch in *ATG16L1*-deficient intestinal epithelial cells alleviates levels of pro-inflammatory cytokines. (A) Effects of TC and (B) TBB treatment on the ERSE promoter in Caco-2 cells were measured by dual luciferase reporter assays. Cell viability of Caco-2 WT and Δ *ATG16L1*-deficient cells was quantified by MTS assay in the presence of TC (C) and TBB (D) after 24 h of Tunicamycin stimulation (5 μ g/ml). (E) and (F) NF- κ B Luciferase activity in Caco-2 WT and *ATG16L1*-deficient cells. Cells were stimulated with Tunicamycin (5 μ g/ml) for 24 h in the presence or absence of (E) ASCL1 inhibitor Triascin C (TC, 5 μ M) or (F) Casein kinase 2 inhibitor TBB (10 μ M) as indicated. (G) Transcript levels of *Tnfa* in small intestinal organoids (*Atg16l1^{fl/fl}* and *Atg16l1^{ΔIEC}*) treated with Tunicamycin (100 ng/ml) and inhibitor TC or TBB for 24 h as indicated (n=3).

To investigate the effect of the ATF6 α inhibitors on the hyper-activation of the ATF6 α branch upon ER stress induction in *ATG16L1*-deficient intestinal epithelial cells, the activity of the ATF6 α branch was measured in the presence or absence of Triascin C and TBB, respectively (Fig. 3.8A,B). We measured a significantly reduced ERSE dual luciferase activity upon stimulation with Tunicamycin in the presence of both Triascin C and TBB. In addition, as indicated by the results of an MTS assay, cell viability upon ER stress induction of *ATG16L1*^{-/-} Caco-2 cells was significantly improved by treatment with the two ATF6 inhibitors (Fig. 3.8C,D). Next, we studied the effect of inhibition of the ATF6 α branch on NF- κ B signaling. NF- κ B induces the expression of various pro-inflammatory genes, and dysregulated NF- κ B activation is a hallmark of inflammatory bowel disease [231]. *ATG16L1*-deficient cells exhibited increased NF- κ B activity upon Tunicamycin stimulation compared to wild type Caco-2 cells (Fig. 3.8E,F). Notably, treatment with both TBB and Triascin significantly reduced NF- κ B activation. Additionally, increased mRNA levels of TNF α observed in the *Atg16l1*-deficient organoids were reduced upon treatment with the ACSL1 and the CSNK2B inhibitor, respectively (Fig. 3.8G).

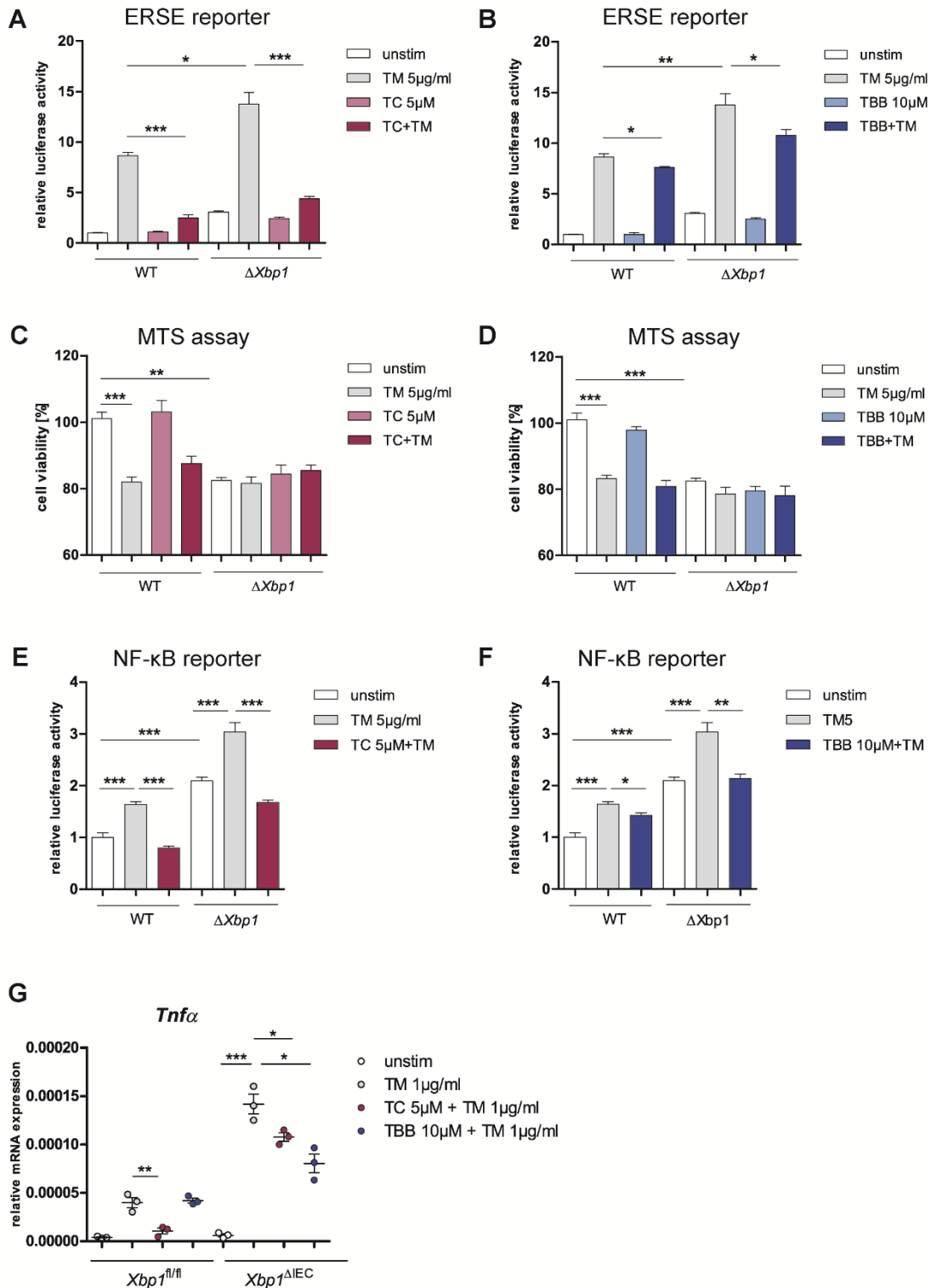


Figure 3.9: Inhibition of the ATF6 α branch in *Xbp1*-deficient intestinal epithelial cells alleviates transcription of pro-inflammatory cytokines. Activation of the ATF6 α branch upon ER stress induction (Tunicamycin, 24 h, 5 μ g/ml) was quantified in the presence of (A) TC and (B) TBB in MODE-K.*iXbp1* ($\Delta Xbp1$) and MODE-K.*iCtrl* (WT) cells by dual luciferase reporter assays. Effects of TC (C) and TBB (D) on cell viability were quantified by MTS assay after 24 h of exposure to Tunicamycin (5 μ g/ml) in MODE-K.*iCtrl* (WT) and MODE-K.*iXbp1* ($\Delta Xbp1$) cells. (E, F) NF- κ B luciferase activity in WT and *Xbp1*-deficient Mode-K cells. Cells were exposed to Tunicamycin (5 μ g/ml) for 24 h in the presence or absence of (E) Triacsin C (TC, 5 μ M) or (F) TBB (10 μ M) as indicated. (G) qPCR of *Tnfa* of intestinal organoids (*Xbp1*^{fl/fl}, *Xbp1* ^{Δ IEC}) treated with or without Tunicamycin (100 ng/ml) and inhibitors (TC 5 μ M; TBB 10 μ M) for 24 h (n=3).

As another ER stress model, Xbp1-deficient cells were employed. Deletion of the UPR transcription factor X-box binding protein-1 (*Xbp1*) in intestinal epithelial cells results in ER stress, Paneth cell impairment and spontaneous enteritis [36]. Importantly, similar to *Atg16l1*-deficient mice, *XBP1*^{-/-} small intestinal epithelial cells exhibit elevated Grp78 levels indicating increased ER stress [36]. Notably, we found elevated activation of the ATF6 α arm of the UPR in the small intestinal epithelial cell line MODE-K stably transduced with a short hairpin *Xbp1* (*shXbp1*) lentiviral vector (Fig. 3.9A,B). Inhibition of ATF6 α signaling by treatment with Triascin C or TBB alleviated ERSE promoter activity (Fig. 3.9A,B) and improved cell viability upon ER stress induction in MODE-K.*iXbp1* (Δ *Xbp1*) cells (Fig. 3.9C,D). Moreover, both augmented NF- κ B activity (Fig. 3.9E,F) and *Tnfa* levels (Fig. 3.9G) were reduced in the presence of the inhibitors upon Tunicamycin treatment in *Xbp1*-deficient cells compared to wild type cells.

In conclusion, we provide evidence that impairment in either UPR (*Xbp1* ^{Δ IEC}) or the autophagic machinery (*Atg16l1* ^{Δ IEC}) in intestinal epithelial cells triggers the upregulation of the ATF6 α arm. Our findings indicate that hyper-activation of the ATF6 α branch may function as compensatory mechanism in intestinal epithelial cells with impaired autophagy or defective UPR signaling.

3.2 Discussion

ER stress and UPR activation are commonly found characteristics of intestinal epithelial cells from UC and CD patients [36, 209-212]. Importantly, Treton et al. [211] detected increased cleavage of ATF6 α and augmented expression of the ATF6 α target genes *GRP78* and *GRP94* in IECs from UC patients compared to controls implicating a crucial role of ATF6 α signaling in intestinal inflammation. However, while the regulation of the PERK and the IRE1 pathway of the UPR and their role in intestinal inflammation have been extensively studied, the regulation of ATF6 α signaling has remained poorly understood. Defining the mechanisms of physiological ATF6 α signaling is pivotal not only to our understanding of ATF6 α signaling in intestinal inflammation but also to identify targets to modulate signaling of the ATF6 α arm.

3.2.1 Identification and Functional Network Analysis of ATF6 α Signaling Modulators

The discovery of RNAi, conserved in most eukaryotic species, has enabled high-throughput gene silencing. Upon the binding of a sequence-specific siRNA to its target transcript, the mRNA is cleaved and degraded [232]. RNAi screening has made it possible to identify new genes, or gene networks, that are involved in a wide variety of biological processes [233, 234]. In this study, we identified regulators of ATF6 α signaling using a stringent high-throughput siRNA screening approach targeting 7,783 human transcripts. Importantly, to monitor activation of the ATF6 α branch, we used the ERSE reporter construct. Noteworthy, the ERSE promoter shows a certain sensitivity to all three branches of the UPR, however, ATF6 α has the most pronounced effect on the ERSE promoter [107, 235]. Nevertheless, it cannot be completely excluded, that the identified hits might modify signaling of the other two UPR branches to a certain degree. Noteworthy, our screening approach was designed to reveal modulators of the ATF6 α branch but not regulators of ATF6 β signaling. While ATF6 α regulates stress-dependent activation of genes containing ER stress response elements (ERSE) such as the chaperone *GRP78* [107-109], ATF6 β deletion does not induce ERSE-target genes [107] permitting the specificity of our RNAi screening for ATF6 α . In the primary and secondary screen, single siRNAs were used resulting in 157 and 104 candidates, respectively. In contrast, in the third screen, pools of four siRNAs per transcript, which differed in their respective target sequences, were used. This approach resulted in 22 validated hits. The observed reduction of remaining hits suggests that a lot of false-positive hits, possibly due to off target effects, were removed in the third round. Remarkably, we detected a pronounced interaction of the confirmed 22 hits performing a STRING network analysis suggesting the reliability of our final candidates. For siRNA screening, we employed the human embryonic kidney cells (HEK-293) as epithelial cell line. This cell line was chosen due to technical considerations such as high growth rates, transfection efficacy and costs, and high reproducibility of results. To ensure the relevance of our findings, identified hits were validated in the intestinal epithelial cell line Caco-2 cells and in small intestinal organoids derived from human tissue. Interestingly, while we discovered 15 suppressors of ATF6 α signaling, only 7 activators were confirmed. These results might reflect biological requirements of the ATF6 α pathway. However, this observed bias might also be due to technical limitations. In our screening set-up, the measured signal range for repressors was wider than for the inducers, increasing the detection probability. Interestingly, a bias in the ratio of identified inducers and repressors is commonly found in RNAi screening approaches [236-238]. To our surprise, we neither detected the S1P nor the S2P, required for ATF6 α cleavage, in our screening approach. However, in previous studies (data not shown), we noticed that both proteins exhibit a long half-life and that the conditions used

for siRNA-mediated knockdown most likely have not been sufficient to induce a significant reduction of the two proteases.

3.2.2 Chemical Interference with Selected Candidates Validates siRNA-Mediated Phenotypes

RNAi screening technologies have provided insights into gene function and molecular networks. However, due to technical limitations such as off-target effects, identified hits should be confirmed and followed-up to independently validate the observed biological effect in various cellular contexts. The unintended down-regulation of targets, known as off-target effect, represents a major problem of RNAi-based screening approaches and may contribute to the discovery of false positive candidates [239-241]. Three types of off-target effects have been described. First, if the siRNA sequence is nearly identical to a sequence found in another mRNA, the unrelated mRNA may be degraded causing a false-positive hit. However, the siRNAs used in this study were developed to minimize this phenomenon. Second, if the 'seed region' of an siRNA is partially complementary with a sequence in the 3' untranslated region of another mRNA, the siRNA may function similar to a microRNA inducing mRNA degradation finally resulting in the depletion of non-target proteins [239]. To avoid off-target effects, multiple siRNA species should be used for each target gene. In this study, we used three different siRNAs per gene in the primary and secondary screen. Additionally, pools of 4 different siRNAs that differed from the sequences used in the first and second screen were used in the third screen. Third, in mammalian cells, even short siRNA may act as potent inducers of the antiviral type I interferon response in a sequence-independent way [242]. Additional unintended effects may arise through the activation of Toll-like receptors such as Toll-like receptor 3 (TLR3), which detects dsRNA [243]. This recognition is assumed to be cell-specific and primarily a concern when working with immune cells. To confirm the siRNA-mediated phenotype, we used pharmacological inhibitors or small molecules interfering with the signaling of the identified candidates. Importantly, pharmacological intervention does not necessarily produce identical phenotypes observed with RNAi-mediated knockdown. Whereas RNAi-mediated knockdown causes the absence of the protein, pharmacological interference might alter the enzymatic activity of the protein. However, the protein might still fulfill cellular functions independent from its enzymatic activity. Based on their (1) biological function, (2) their cellular localization, (3) the availability of specific inhibitors or inducer and (4) antibody availability, the following 6 candidates were selected for a more detailed analysis: the acyl-CoA synthetase long-chain family member 1 (ACSL1), the Casein Kinase 2 Beta (CSNK2B), the solute carrier family 30 member 3 (SLC30A3), the reticulon 4 interacting protein 1 (RTN4IP1), the protease Prostaticin (PRSS8), and the voltage-dependent anion channel 2 (VDAC2).

ACSL1 (acyl-CoA synthetase long-chain family member 1), one of the identified inducers of ATF6 α signaling, is a 78-kDa intrinsic membrane protein. ACSL1, together with the other long-chain acyl-CoAs ACSL3, ACSL4, ACSL5, and ACSL6, mediates the conversion of fatty acids (FAs) to acyl-CoAs. Acyl-CoAs are engaged in lipid formation and remodeling, activation of transcription factors, and oxidation to provide cellular energy. Importantly, ACSL1 localizes to the endoplasmic reticulum and to mitochondria-associated membranes. In this study, Triacsin C was used as inhibitor of ACSL1. Of note, Triacsin C inhibits not only ACSL1, but also ACSL3 and ACSL4 [244, 245]. To our surprise, none of the other ACSL family members was identified in our screening approaches, suggesting that ACSL1 might exert a unique function during ER stress. Moreover, upon Tunicamycin injection, ATF6 α -deficient mice demonstrated reduced levels of ACSL1 compared to controls indicating the existence of a positive feedback loop between ATF6 α and ACSL1 [246]. Notably, ACSL1 is a downstream target of SREBP2, which is, like ATF6 α , a substrate of the site 1- and site 2-protease [247].

Second, *CSNK2B*, encoding the regulatory subunit of the casein kinase 2 and identified as inducer of ATF6 α signaling, was selected for a more detailed analysis. The casein kinase 2 is a tetrameric serine/threonine-selective protein kinase composed of two catalytic α - or α' -subunits and two regulatory β -subunits. The casein kinase 2 localizes to the endoplasmic reticulum and the Golgi complex [248]. Notably, a plethora of different substrates are phosphorylated by the enzyme [249], which has been shown to modulate various cellular processes such as cell growth and apoptosis [250-252]. Importantly, in line with our findings, various studies have described a modulatory function of the casein kinase 2 on the UPR [253, 254]. However, to our knowledge, none of these studies have provided a mechanistic link between the ATF6 α branch of the UPR and *CSNK2B*. In this study, we used TBB, a highly selective, ATP/GTP-competitive inhibitor of casein kinase-2 to inhibit the enzyme activity. TBB binds to the Val66 residue of casein kinase-2 and inhibits the binding of ATP/GTP [255].

In addition, we selected SLC30A3 (ZnT3), identified as activator of ATF6 α signaling in our screening approach, for a more detailed analysis. SLC30A3 belongs to the solute-linked carrier 30 (SLC 30) protein family of zinc transporters, which consists of 10 members (ZnT1 to ZnT10) in mammals [256]. These zinc transporters allow zinc ions to permeate from the cytoplasm to the intercellular space, as well as intracellular organelles [257]. Importantly, Zinc is a co-factor of the site 2 protease (S2P). Knockdown of SLC30A3 might lower intracellular zinc concentrations and thus inhibit S2P activity [258]. Due to the lack of any pharmacological inhibitor, we used TPEN (N,N,N',N'-Tetrakis(2-pyridylmethyl)ethylenediamine), a Zn²⁺ chelator, which was shown to increase the expression SLC30A3 [222].

RTN4IP1, identified as suppressor of ATF6 α signaling in our siRNA screen, encodes a highly conserved and ubiquitously expressed mitochondrial ubiquinol oxido-reductase. RTN4IP1 interacts with reticulon 4 (RTN4), which is a potent inhibitor of regeneration following spinal cord injury. Mutations in RTN4IP1 have been associated with a deficit of mitochondrial respiratory complex I and IV activities [259]. The RTN4 gene produces several transcripts, which have been shown to repress axonal growth. To date, three isoforms including RTN4-A, RTN-B, and RTN-C have been described [260, 261]. RTN4 proteins are mainly found in the endoplasmic reticulum, suggesting that RTN4IP1 localizes to the ER as well. Strikingly, RTN4 inhibits the membrane-bound aspartyl protease BACE1 [262]. Therefore, we hypothesized that RTN4 in collaboration with RTN4IP1 might inhibit the proteases involved in ATF6 cleavage. Many studies have shown that RTN4 signaling triggers activation of the small GTPase RHOA and its effector protein Rho-associated, coiled-coil containing protein kinase 1 (ROCK) in different cell types [263-265]. Due to the lack of any direct inhibitor of RNT4IP1, we used Simvastatin known to inhibit the RhoA/ROCK pathway.

PRSS8 (Prostasin), identified as repressor of ATF6 α signaling, encodes a glycosyl-phosphatidyl-inositol (GPI)-anchored extracellular serine protease. Originally, PRSS8 was found to be expressed in ducts of the prostate [266]. Importantly, it is also localized to the apical surface of (intestinal) epithelial cells [267]. PRSS8 triggers the proteolytic activation of epithelial sodium channels *in vitro*, regulating sodium balance [268]. Moreover, it was described that activation of the UPR triggers the downregulation of PRSS8 [269]. In this study, Camostat mesylate (CM) was used to inhibit PRSS8 activity. However, Camostat mesylate is a reversible inhibitor of various endopeptidases with trypsin-like specificity [270] including not only PRSS8 but also other proteases such as matriptase [271]. How PRSS8 interferes with ATF6 α signaling is not clear. One might speculate that PRSS8 is involved in the cleavage of the S1P or

S2P. In addition, PRSS8 exhibits protease-independent functions, therefore PRSS8-mediated repression of ATF6 α signaling might be indeed complex.

Our RNAi screening approach identified the voltage-dependent anion channel 2 (VDAC2) as repressor of ATF6 α signaling. VDAC2 is ubiquitously expressed and integrated into the mitochondrial outer membrane. The N-terminus resides inside the pore controlling permeability [272]. Notably, VDAC2 not only regulates mitochondrial apoptosis [273, 274] but has also been proposed to form a complex with the ER Ca²⁺ release channel IP3Rs, which might facilitate Ca²⁺ transfer from the ER to the mitochondria [275, 276]. Assuming that VDAC2 might be critical for Ca²⁺ homeostasis of the ER, VDAC2 might modulate ATF6 α signaling by interfering with UPR activation upstream of ATF6 α . Interestingly, VDAC2 forms a complex with ACSL1. This complex is supposed to be involved in the transfers of activated fatty acids via the mitochondrial outer membrane [277]. In this study, we used Erastin to interfere with VDAC2 mediated signaling. Erastin was shown to directly bind to VDAC2 [278] and treatment with Erastin causes enhanced expression of VDAC2 [279].

In summary, we could validate the siRNA-mediated phenotype using small molecule agents illustrating the reliability of our approach: First, measuring ERSE promoter activity after stimulation with small molecule agents produced similar effects observed for siRNA mediated knockdown. Second, levels of cleaved ATF6 (p36ATF6) in the nuclear-enriched fraction partially recapitulated our previous findings when treated with the pharmacological agents. Of note, upon cleavage of ATF6 α mediated by the Site-1 protease (S1P) and Site-2 protease (S2P) not only a 50 kDa product of ATF6 α , but also a 60 kDa and 36 kDa fragment of ATF6 α were detected. The observed fragments of ATF6 α have all been described to induce the ERSE promoter during ER stress [225, 226]. However, the various ATF6 cleavage fragments might exert specific characteristics, functions and kinetics, possibly explaining the less pronounced effect of small molecule agents on nuclear p36ATF6 levels when compared to the strong effects on ERSE promoter.

3.2.3 Candidates *ACSL1* and *CSNK2B* are regulators of ATF6 α Signaling in Intestinal Epithelial Cells and Human Organoids

Due to their strong, reproducible effect on ATF6 α signaling and due to technical considerations, such as antibody specificity, *ACSL1* and *CSNK2B* were selected for further functional studies. We confirmed the biological relevance of *ACSL1* and *CSNK2B* using the intestinal epithelial cell line Caco-2 and small intestinal human organoids derived from a CD patient. siRNA-mediated knockdown or exposure to pharmacological inhibitors, respectively, confirmed the inducing capacities of our candidates on ATF6 α signaling. Interestingly, our group found that *ACSL1* is differently expressed in tissues of IBD patients compared to controls [280] suggesting a role of this protein in IBD pathogenesis. Likewise, genome-wide association studies have identified an IBD-predisposing allele in the gene encoding *CSNK2B* [12] and the enzymatically active subunit of the casein kinase 2 was found to be less expressed in and translocated into the nucleus of colonic crypts from IBD patients [281, 282]. These findings point towards an involvement of the casein kinase 2 in disease pathogenesis.

3.2.4 *ACSL1* Induction of ATF6 α Signaling is Independent of Intramembrane Cleavage and *CSNK2B* Facilitates ER-Golgi Trafficking of ATF6 α

We discovered Triacsin C-mediated repression of ERSE promoter activity in cells overexpressing N-terminal ATF6 α , whereas TBB exposure did not repress promoter activity. Similarly, in intestinal organoids overexpressing the N-terminal ATF6 α fragment, TBB treatment did not affect expression of

Atf6α target genes. In contrast, inhibition of ACSL1 resulted in reduced mRNA levels of *Atf6α* target genes.

These findings indicate that ACSL1 possibly mediates its effect on ATF6α signaling independently of the cleavage event at the Golgi complex (Fig. 3.10). While the exact mechanisms of how ACSL1 facilitates ATF6α signaling needs to be explored in more detail, fluorescence microscopy revealed partial co-localization of ACSL1 and ATF6α, suggesting that these proteins act in close proximity to each other. Whether a direct interaction between these two proteins exists, is part of ongoing investigations. Since we observed that the inducing capacity of ACSL1 on ATF6α signaling is independent of the intramembrane proteolysis, ACSL1 might assist in nuclear translocation or the binding of the transcriptionally active ATF6α fragment to the ERSE promoter region. However, a more detailed analysis is required to provide insights into the regulation ATF6α signaling via ACSL1.

The abolishing effect of TBB on ATF6α downstream signaling led us to speculate that CSNK2B might facilitate ATF6α signaling upstream of the cleavage event. Importantly, ATF6α transport from the ER to the Golgi complex is mediated by COPII vesicles [227]. Upon ER stress induction, ATF6α is released from its association with GRP78 forming an interaction with COPII. Interestingly, the casein kinase 2 has been shown to be responsible for the phosphorylation of the COPII component Sec31, which initiates membrane trafficking [228]. They demonstrate that casein kinase 2-mediated Sec31 phosphorylation reduces the association of Sec31 with the ER membrane as well as with Sec23 enabling the formation of COPII vesicles. Indeed, we could demonstrate that the depletion of SEC31 or inhibition of ER-Golgi trafficking by treatment with FLI-06 [229], respectively, diminishes the inhibitory effect of TBB on ERSE promoter activity. Our findings support the notion that CSNK2B induces ATF6α signaling by facilitating the transport of ATF6α from the ER to the Golgi complex (Fig. 3.10).

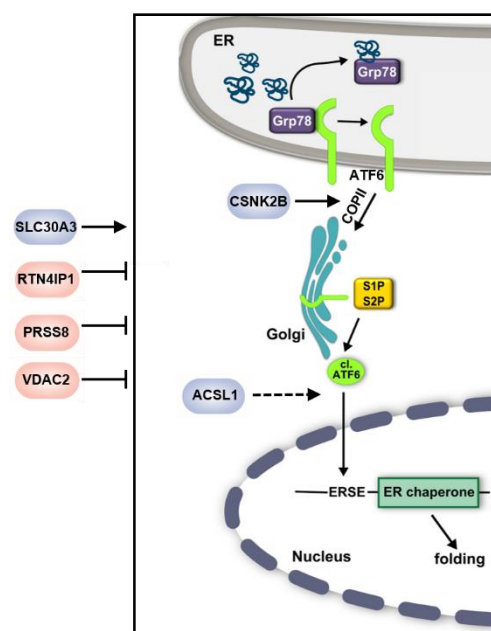


Figure 3.10: ACSL1 stimulates ATF6α signaling downstream of the cleavage event and CSNK2B facilitates ER-Golgi trafficking of ATF6α. Schematic representation of. Genes, identified and confirmed as inducers of ATF6α signaling are depicted in blue (SLC30A3, CSNK2B, and ACSL1), hits identified as suppressors are shown in red (RTN4IP1, PRSS8, and VDAC2). Our data indicates that CSNK2B induces ATF6α signaling by facilitating the trafficking of ATF6α from the ER to the Golgi complex via COPII mediated transport. ACSL1 induces ATF6α signaling downstream of the intramembranous cleavage at the Golgi complex. COPII=

3.2.5 The ATF6α Branch of the UPR Modulates NF-κB Signaling

Unresolved ER stress in intestinal epithelial cells has emerged as an important mechanism favouring intestinal inflammation [36]. Noteworthy, NF-κB is a key transcriptional regulator with a critical role in the onset of inflammation [231]. In the absence of any stimuli, NF-κB is kept in an inactive state through binding to IκB. Phosphorylation of IκB results in its degradation and exposes the nuclear-localization

signal of NF- κ B enabling the translocation of NF- κ B to the nucleus, where it induces the transcription of numerous inflammatory genes. Activation of the UPR has been shown to result in the activation of NF- κ B [283, 284]. Likewise, *Xbp1* deficiency in the intestinal epithelium generates ER stress accompanied by increased NF- κ B signaling due to increased IRE1 kinase activity [230]. In response to ER stress, the auto-phosphorylation of IRE1 α induces a conformational change in its cytosolic domain, enabling the binding of the adaptor protein tumour-necrosis factor- α -receptor-associated factor 2 (TRAF2) [285]. IRE1 α interaction with TRAF2 ultimately leads to the recruitment of I κ B kinase (IKK) and the phosphorylation and subsequent degradation of I κ B which in turn releases NF- κ B for translocation to the nucleus [286]. On the contrary, activation of the PERK branch of the UPR activates NF- κ B via attenuation of translation. PERK-mediated inhibition of protein synthesis increases the ratio of NF- κ B to I κ B, owing to the shorter half-life of I κ B, thereby releasing NF- κ B from its inhibition to translocate to the nucleus [287, 288]. In contrast, the contribution of the ATF6 α branch in NF- κ B signaling has not been investigated in detail. The ATF6 branch of the UPR has been proposed to induce the phosphorylation of AKT to finally activate NF- κ B signaling [289, 290]. In our study, we observed ATF6 α -induced activation of NF- κ B signaling. Augmented NF- κ B signaling was accompanied by enhanced *Tnfa* expression in organoids overexpressing the N-terminal ATF6 α fragment compared to control intestinal organoids (Fig. 2.7B). In line with our previous findings, treatment with TC but not with TBB reduced NF- κ B activation upon overexpression of the N-terminal ATF6 α fragment. Noteworthy, siRNA-mediated downregulation of *ACSL1* or *CSNK2B* reduced NF- κ B promoter activity more effectively than knockdown of *ATF6 α* indicating that both *ACSL1* and *CSNK2B* might execute additional functions in modulating NF- κ B signaling. Indeed, it has been shown that the casein kinase 2 is able to phosphorylate I κ B at its C-terminus inducing I κ B degradation [291]. Vice versa, an enzymatically inactive form of the casein kinase 2 can block NF- κ B activation [292]. Similar to the here proposed role of ATF6 α signaling in inducing NF- κ B signaling, Coleman et al. [293] reported increased cytokine levels in aged mice (older than 20 weeks) overexpressing the transcriptionally active ATF6 α fragment.

3.2.6 Inhibition of ATF6 α Attenuates Pro-Inflammatory Profile in *Atg16l1*- and *Xbp1*-Deficient Intestinal Organoids

Strikingly, genetic impairment of UPR-related genes or mutations that affect the autophagic machinery have been described to exhibit high levels of the chaperone GRP78, a main target gene of the ATF6 α branch. Paneth cells of CD patients and healthy individuals homozygous for the *ATG16L1*^{T300A} single-nucleotide polymorphism (SNP) display high levels of GRP78 [113]. Similarly, mice with IEC-specific deletion of *Atg16l1* demonstrate augmented levels of GRP78 [35]. Likewise, small intestinal epithelial cells that lack the UPR gene *Xbp1* exhibit elevated Grp78 [36]. High levels of GRP78 might point towards an engagement of the ATF6 branch when UPR signaling or autophagy are compromised. However, the specific contribution of the ATF6 α branch to this phenotype has not been studied in detail. We hypothesized that the reported increased GRP78 expression might be at least partially due to hyper-activation of the ATF6 branch in *Atg16l1*- or *Xbp1*-deficient cells, respectively.

Indeed, we observed a significantly increased activation of the ATF6 α branch in cells lacking the autophagy gene *Atg16l1* or the unfolded protein response gene *Xbp1* illustrated by increased ERSE promoter activity. Importantly, inhibition of ATF6 α signaling using the small molecule inhibitors Triacsin C/TBB was able to diminish the observed hyper-activation of ATF6 α signaling in *Atg16l1/Xbp1*-deficient cells. These findings support the notion, that upon defective autophagy or UPR signaling, compensatory engagement of the ATF6 α branch occurs. Moreover, based on the here described function of the ATF6 α pathway in NF- κ B signaling, we hypothesized that increased NF- κ B activation

accompanied by enhanced *Tnfa* levels observed in *Atg16l1*- and *Xbp1*-deficient cells could be mitigated by inhibition of the ATF6 α branch. Indeed, treatment with TBB or Triacsin C, respectively, significantly attenuated NF- κ B hyper-activation and *Tnfa* levels.

Noteworthy, the compensatory engagement of other UPR branches upon genetic deletion of specific components has been described. Similarly, impaired UPR signaling compensatory engages the autophagy machinery (IRE1/ATG16L1).

Ire1 β -deficient mice not only exhibit augmented Grp78 levels in their crypts but also show a compensatory upregulation of IRE1 α [177]. Conversely, mice that lack *Ire1 α* show increased amounts of IRE1 β in their crypts. Notably, *Xbp1* splicing is markedly increased in crypt lysates of *Ire1 β* -deficient mice, suggesting IRE1 α over-activation in the absence of functional IRE1 β . Similarly, deletion of P58^{PK} is accompanied by increased expression of Grp78, increased phosphorylation of IRE1 α , and activation of the PERK branch indicated by augmented CHOP levels [167].

As mentioned above, although expression of the ER chaperone Grp78 is to a certain extent under the control of *Xbp1*, *Xbp1*^{-/-} deletion is accompanied by elevated Grp78 levels in intestinal epithelial cells [36]. Importantly, while Grp78 shows some sensitivity to all three branches of the UPR, ATF6 α has a more pronounced effects on common targets compared with IRE1 α [107, 235]. These observations support the idea of a compensatory engagement of ATF6 α signaling upon deletion of UPR genes. Moreover, *Xbp1* deletion results in IRE1 α over-activation indicated by IRE1 α accumulation and phosphorylation [230]. Evidence for a compensatory engagement of the UPR branch upon impaired autophagy function, and vice versa, was provided by Adolph et al. [35]. Mice with *Atg16l1* deletion in intestinal epithelial cells show IRE1 α accumulation in their Paneth cells, and humans homozygous for *ATG16L1*^{T300A} exhibit augmented IRE1 α levels in their crypts. Notably, deletion of both *Atg16l1* and *Xbp1* show profoundly increased IRE1 α expression and phosphorylation compared with intestinal epithelial lysates from *Xbp1* ^{Δ IEC} mice [35].

Here we show that impairment in either UPR (*Xbp1* ^{Δ IEC}) or autophagy function (*Atg16l1* ^{Δ IEC}) in intestinal epithelial cells results in the compensatory upregulation of ATF6 α signaling. Our findings suggest that engagement of the ATF6 α branch may represent a compensatory mechanism in intestinal epithelial cells with defective autophagy or impaired UPR signaling. Noteworthy, ER stress and UPR activation have been described as characteristic features of intestinal epithelial cells isolated from IBD patients [36, 209-212]. Likewise, increased cleavage of ATF6 α accompanied by elevated expression of the ATF6 α target genes *GRP78* and *GRP94* were observed in IECs from non-inflamed tissues of patients with UC compared to healthy controls [211]. Moreover, Coleman et al. [293] detected genetic alterations and aberrant expression levels of ATF6 α as the only clinically relevant UPR mediator in colorectal cancer patients and revealed a tumor promoting role of activated ATF6. Notably, tumorigenesis in N-ATF6 α overexpressing mice was accompanied by enhanced expression of pro-inflammatory cytokines such as *Tnfa* [293]. Similarly, elevated levels of pro-inflammatory cytokines such as TNF- α have been measured in serum and intestinal mucosa of IBD patients [294] and anti-tumor necrosis factor (TNF)- α agents are commonly used in IBD treatment. Thus, interfering with hyperactive ATF6 α signaling via inhibition of the identified ATF6 α signaling inducers ACSL1 and CSNK2B using the small molecules Triacsin C or TBB, respectively, might represent a suitable pharmacological approach in intestinal inflammation.

3.3 Conclusions & Future Perspectives

Intestinal epithelial cells from IBD patients typically exhibit ER stress and UPR activation illustrated by enhanced ATF6 α cleavage and increased expression of the ATF6 α target genes *GRP78* and *GRP94* compared to healthy controls implicating a crucial function of the ATF6 α branch in intestinal inflammation [36, 209-212]. In this study, we elucidate the regulation of ATF6 α signaling using a high-throughput siRNA screening approach targeting 7,783 human transcripts. This approach identified 15 suppressors and 7 activators of ATF6 α signaling. We identified the regulatory subunit of the casein kinase 2 (CSNK2B) as inducer of ATF6 α signaling. Our data suggests that CSNK2B mediates its effect on the ATF6 α pathway upstream of the cleavage event at the Golgi complex. Based on our findings, we propose that CSNK2B facilitates the transport of ATF6 α from the ER to the Golgi apparatus by promoting COPII vesicle formation. On a molecular level, a more detailed analysis will reveal the exact mechanisms of CSNK2B-facilitated ATF6 trafficking. Moreover, we identified the acyl-CoA synthetase long chain family member 1 (ACSL1) as activator of the ATF6 α pathway. While we observed co-localization of ATF6 α and ACSL1, it still needs to be elucidated whether these two proteins physically interact. Our findings imply that ACSL1 facilitates ATF6 α signaling downstream of and independently from the cleavage event. However, further studies are required to reveal the molecular mechanisms of ACSL1 mediated activation of ATF6 α signaling. In this context, it would be interesting to systematically assess the effects of specific fatty acids on the activation of the ATF6 α branch.

Strikingly, in our experiments, we noticed a strong downregulation of the identified ATF6 α modulators ACSL1 and VDAC2 on protein level in *Atg16l1*-deficient cells. It might be promising to study the regulatory crosstalk of these two proteins with ATG16L1. Apart from this, future research may focus on the other identified, promising ATF6 signaling regulators such as RTN4IP1.

Another so far neglected aspect is to determine the specific function of the different ATF6 cleavage products. To our knowledge, it is still unclear, whether the specific ATF6 α fragments fulfil specific functions in ATF6 α signaling. In this context, it may be determined whether the different cleavage fragments vary in their inducing capacities and induce similar gene expression patterns.

This study reveals that impairment in either UPR or autophagy function in intestinal epithelial cells triggers a compensatory upregulation of ATF6 α signaling. In this context, it might be interesting to assess the role of the ATF6 α branch in mice that lack either *Atg16l1* or *Xbp1* in the intestinal epithelium. It will be exciting to see whether inhibition of the ATF6 α branch by targeting ACSL1 or CSNK2B, respectively, ameliorates intestinal inflammation under basal condition and inflammation in these mice. In case of ACSL1, it might be worth to assess whether inhibition of the ATF6 α arm using Triacsin C restricts tumorigenesis.

Notably, we observed that the ATF6 α branch stimulates NF- κ B signaling. Restriction of ATF6 α signaling by inhibition of the inducers ACSL1 or TBB was able to limit NF- κ B activation in *Atg16l1*- and *Xbp1*-deficient organoids, respectively. Importantly, increased levels of pro-inflammatory cytokines such as TNF- α are commonly found in sera and intestinal tissue of UC and CD patients [294]. Thus, it might be exciting to assess whether human organoids carrying the mutation in the *Atg16l1* gene (T300A) or a hypomorphic *Xbp1* variant show compensatory hyper-activation of the ATF6 α branch. If so, interfering with hyperactive ATF6 α pathway via inhibition of the identified ATF6 α signaling inducers ACSL1 and

CSNK2B, respectively, might represent a reasonable pharmacological approach in limiting intestinal inflammation.

4 ORMDL3 Engages the Autophagy Machinery to Facilitate Endoplasmic Reticulum Turnover and Bacterial Clearance

Genome-wide association studies (GWAS) have identified *ORMDL3* as a genetic risk factor of CD and UC [38, 39], and asthma [40], another disease of a mucosal barrier. *ORMDL3*, which localizes to the ER [39, 182], has been suggested to be involved in calcium homeostasis [182, 192, 195, 196], in regulating the UPR [39, 182, 192] and in sphingolipid metabolism [191, 198, 199, 201]. However, at present, there are no studies elucidating the role of *ORMDL3* in intestinal homeostasis and IBD pathogenesis. Moreover, molecular functions of *ORMDL* proteins, in this regard, are largely unknown. Strikingly, the association of *ORMDL3* with bronchial asthma [40] and IBD [38, 39] points towards a role of *ORMDL3* in shaping host-microbe interactions bearing in mind that both lung and intestinal epithelial cells are continuously exposed to microbes. Therefore, we aimed to investigate how *ORMDL3* may shape host-microbe interactions in the intestine and modulate disease progression.

4.1 Results

4.1.1 *Ormdl3* and *Ormdl1/3* Deficiency Impair Body Growth Whereas Simultaneous Deletion of *Ormdl1*, *Ormdl2* and *Ormdl3* Causes Embryonic Lethality

To explore a possible function of *ORMDL* proteins in intestinal homeostasis, we generated *Ormdl3*^{-/-} and *Ormdl1/3* double-deficient mice (see chapter 2.5.1). While *Ormdl3*^{-/-} mice were born at the expected Mendelian ratio (Fig. 4.1A) and showed normal life expectancy, *Ormdl1/3* double-deficient mice were born at sub-Mendelian ratios (Fig. 4.1B) and exhibited a reduced lifespan. Strikingly, *Ormdl3*^{-/-} and even more pronounced *Ormdl1*^{-/-}*3*^{-/-} animals exhibited decreased overall body size (Fig. 4.1C) accompanied by reduced body weight when compared to the wild type mice (Fig. 4.1D). Deficiency in *Ormdl3* had no effect on the histological morphology of the ileum or the colon, as determined by inspection of HE stained sections (Fig. 4.1E). No signs of spontaneous intestinal inflammation were observed in *Ormdl3*^{-/-} and *Ormdl1*^{-/-}*3*^{-/-} animals up to 25 weeks of age. Noteworthy, because of the significant amino acid identity between the three murine *ORMDL* proteins [181], we hypothesized that there could be functional redundancy, however, we did not detect any compensatory upregulation of *Ormdl1* and *Ormdl2* in ileal and colonic tissues of *Ormdl3*-deficient animals (Fig. 4.1F,G). Next, we aimed to produce triple constitutive knockout mice of *Ormdl1*, *Ormdl2* and *Ormdl3* (*Ormdl1*^{-/-}*2*^{-/-}*3*^{-/-}). As shown in Fig. 4.1H, several breeding attempts to obtain a triple-negative mouse failed. These results suggest that *ORMDL1*, *ORMDL2* and *ORMDL3* exert overlapping functions essential for mouse development.

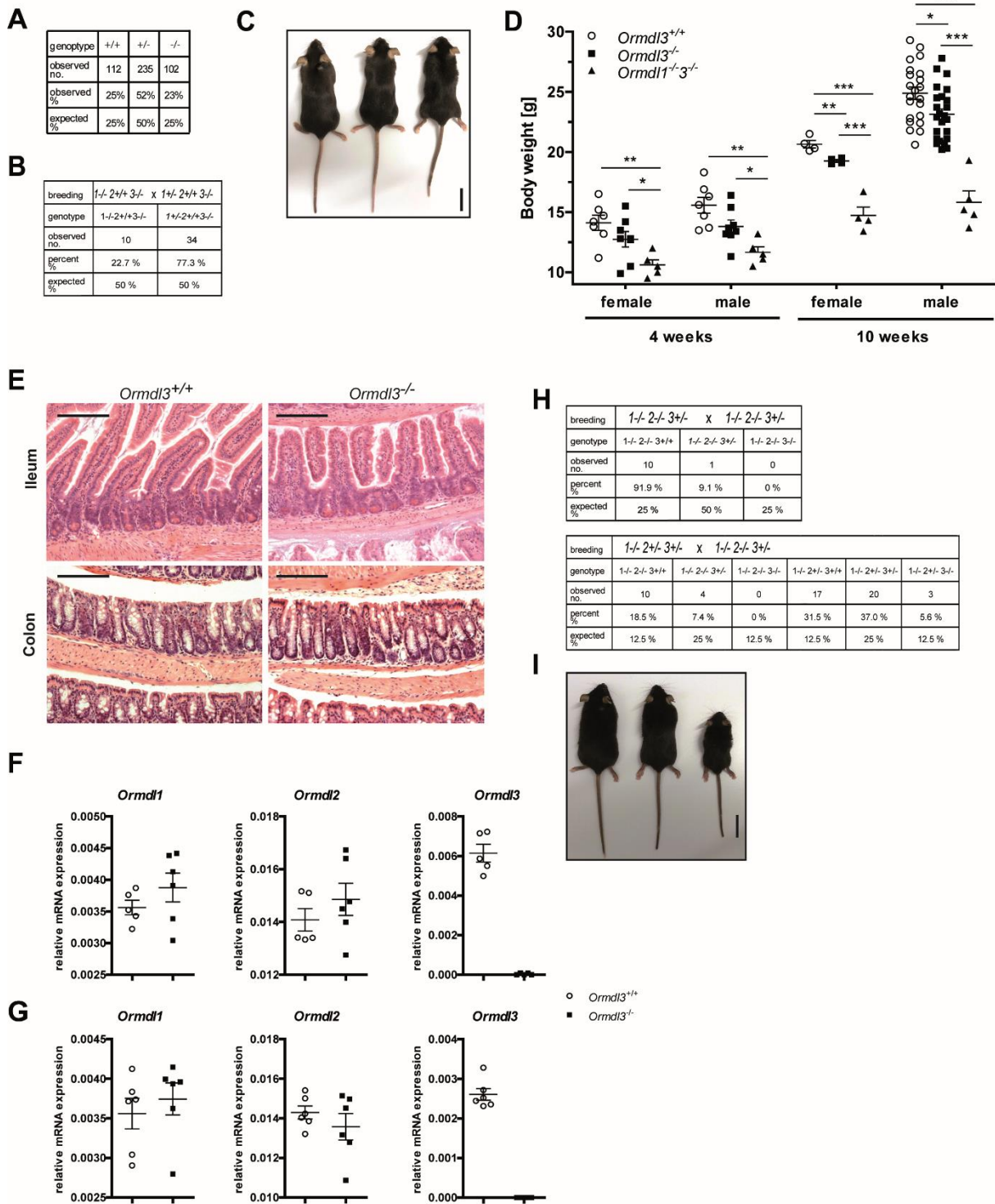


Figure 4.1: Generation and phenotype of *Ormdl3*- and *Ormdl1/3*-deficient mice. (A) Genotypes of pups from *Ormdl3*^{-/-} intercrosses were tabulated and compared against expected percentages. (B) Genotypes of pups from breeding of *Ormdl1*^{-/-}2^{+/-}3^{-/-} and *Ormdl1*^{+/-}2^{+/-}3^{-/-} mice are tabulated and percentages of observed and expected pups are shown. (C) Representative picture of a male wild type (left), *Ormdl3*^{-/-} (middle) and *Ormdl1*^{-/-}3^{-/-} (right) animal at 15 weeks of age. Scale bar, 2 cm. (D) Body weight of *Ormdl3*^{+/-}, *Ormdl3*^{-/-} and *Ormdl1*^{-/-}3^{-/-} mice at 4 and 10 weeks of age. (E) H&E staining of ileal and colonic sections of 20 week old animals. (F) and (G) mRNA levels of *Ormdl1*, *Ormdl2* and *Ormdl3* in ileal (F) and colon (G) tissues of 20 week-old *Ormdl3*^{+/-} and *Ormdl3*^{-/-} mice assessed by qPCR. (H) *Ormdl1*^{-/-}2^{+/-}3^{+/-} mice were crossed with *Ormdl1*^{-/-}2^{-/-}3^{+/-} mice (upper panel) or with *Ormdl1*^{-/-}2^{+/-}3^{+/-} mice (lower panel). Genotypes of all pups were determined and are indicated as observed percentages together with expected percentages. (I) Exemplary picture of a wild type (left), *Ormdl1*^{-/-}2^{+/-}3^{+/-} (middle) and *Ormdl1*^{-/-}2^{-/-}3^{+/-} (right) mouse at 10 weeks of age.

4.1.2 *Ormdl3* Expression is Shaped by the Microbial Community

To determine the dynamics of *Ormdl3* gene expression during postnatal development and to explore potential effects of the gut microbiota on *Ormdl3* expression, we analyzed RNAseq data from intestinal epithelial cells of conventionally raised and germ-free mice at three different stages during postnatal development- week 1, week 4, and week 12-16 [295]. We observed generally higher levels of *Ormdl3* in 1 week old newborn mice compared to 4 week or 12-16 week old mice (Fig. 4.2A) indicative of an important role of *Ormdl3* in postnatal development. Notably, we detected a microbiota-dependent expression pattern of *Ormdl3* demonstrated by a significantly decreased expression in conventionally raised mice compared to germ-free mice at 12-16 weeks of age (Fig. 4.2A,B). *In vitro* we detected a robust repressive effect of both *E. coli* LF82 and *E. coli* lipopolysaccharide (LPS) on *Ormdl3* promoter activity in immortalized wild type mouse embryonic fibroblasts (WT iMEFs) (Fig. 3.2C,D), suggesting a role of TLR4 signaling in regulating *Ormdl3* expression. In agreement with these findings, we measured decreased *Ormdl3* mRNA levels upon *E. coli* LF82 infection (Fig. 4.2E). In contrast, bacteria-derived muramyl dipeptide (MDP) and flagellin exhibited only mild inhibitory activity on *Ormdl3* promoter activity (Fig. 4.2C). Additionally, we monitored protein levels of all three ORMDL homologues upon *E. coli* LF82 infection in iMEF and intestinal epithelial cells by immunoblotting with a pan-specific ORMDL1/2/3 antibody (Fig. 4.2F-H). Consistent with reduced *Ormdl3* promoter activity and decreased mRNA levels upon LF82 exposure, we found a time-dependent reduction in ORMDL protein levels upon infection.

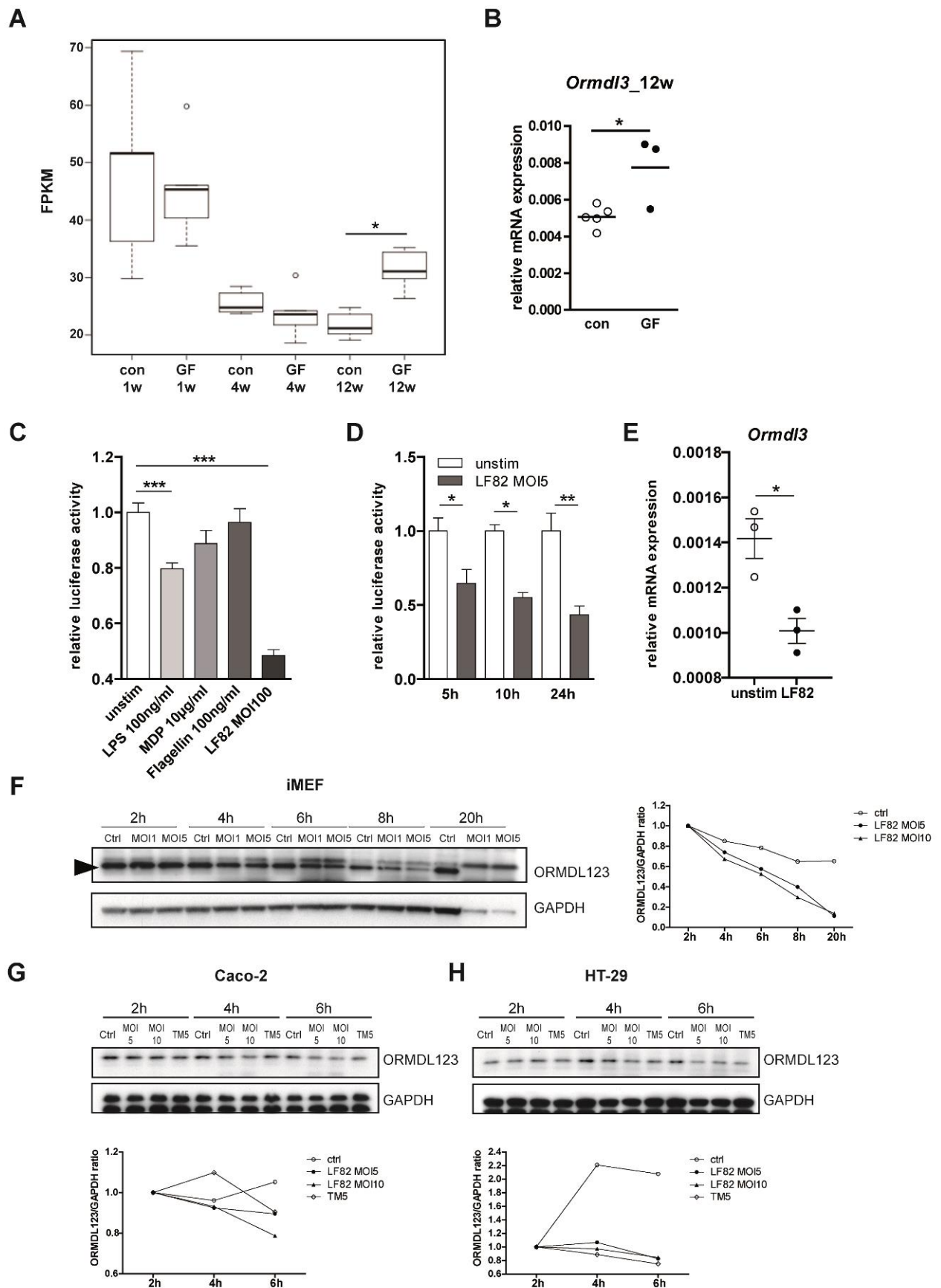


Figure 4.2. Ormdl3 expression is regulated by the bacterial components. (A) and (B) Conventionally (con) or germ-free (GF) raised mice were sacrificed at 1 week, 4 weeks, and between 12-16 weeks of age and intestinal epithelial cells (IECs) from the ileum were collected and *Ormdl3* expression was determined. (A) by RNA seq and (B) by qPCR. (C) Immortalized wild type MEF cells (iMEF) were stimulated with indicated bacterial components

(LPS= Lipopolysaccharide, MDP= α -muramyl dipeptide) or with *E. coli* LF82 (multiplicity of infection, MOI100) for 24 h. For bacterial infection, Gentamicin was added 2 h post infection to limit LF82 replication. *Ormdl3* promoter activity was measured by promoter-mediated luciferase reporter assays. (D) *Ormdl3* promoter activity 5 h, 10 h and 24 h post infection quantified by promoter-mediated luciferase reporter assays in iMEFs. (E) *Ormdl3* transcript levels upon *E. coli* LF82 infection (MOI5, 8 h p.i.). Upper band: non-specific binding; arrow indicates ORMDL123 band. *E. coli* LF82 infection diminishes ORMDL protein levels in (F) iMEFs and in the intestinal epithelial cell lines (G) Caco-2 and (H) HT-29. Cells were infected with indicated MOI. Western blots and quantification of ORMDL123 are depicted.

***Ormdl3*-Deficient Mice Display Increased Susceptibility to Adherent-Invasive *E. coli* Colonization.**

In chapter 4.1.2, we could show that *Ormdl3* expression is shaped by bacterial components. Similar to *ORMDL3*, other IBD risk genes such as *NOD2* and *ATG16L1* have been described to be differentially regulated in germ-free compared to conventionally raised mice [295, 296]. Importantly, defects in *NOD2* and *ATG16L1* signaling impair control of intracellular bacteria [23]. Therefore, we hypothesized that ORMDL3 might also play a role in bacterial handling. In a colonization model, we analyzed the colonization susceptibility of *Ormdl3*^{-/-} and control mice using the adherent-invasive *E. coli* (AIEC) strain LF82, a pathotype of *E. coli* associated with the ethiopathogenesis of Crohn's disease [58]. In detail, *Ormdl3*^{+/+} and *Ormdl3*^{-/-} mice were orally challenged with 10⁹ bacteria, and bacterial numbers in the feces were monitored to determine *E. coli* LF82 colonization rate. We observed a higher bacterial burden at day 5 and day 7 post infection in *Ormdl3*^{-/-} mice compared with their WT littermates (Fig. 4.3A). In line with this observation, at day 7 post infection, *Ormdl3*-deficient mice revealed a significantly higher load of AIECs in their ileal and colonic tissue accompanied by increased numbers of punctate *E. coli* LPS staining in the ileum compared with their control littermates (Fig. 4.3B,C). Increased colonization in *Ormdl3*-deficient mice was accompanied by elevated levels of epithelial cell death as depicted by increased numbers of terminal deoxynucleotidyl transferase dUTP nick end labeling (TUNEL)⁺ cells both in the ileal (though not significant) and colonic crypt regions (Fig. 4.3D,E), when compared to *Ormdl3*^{+/+} mice.

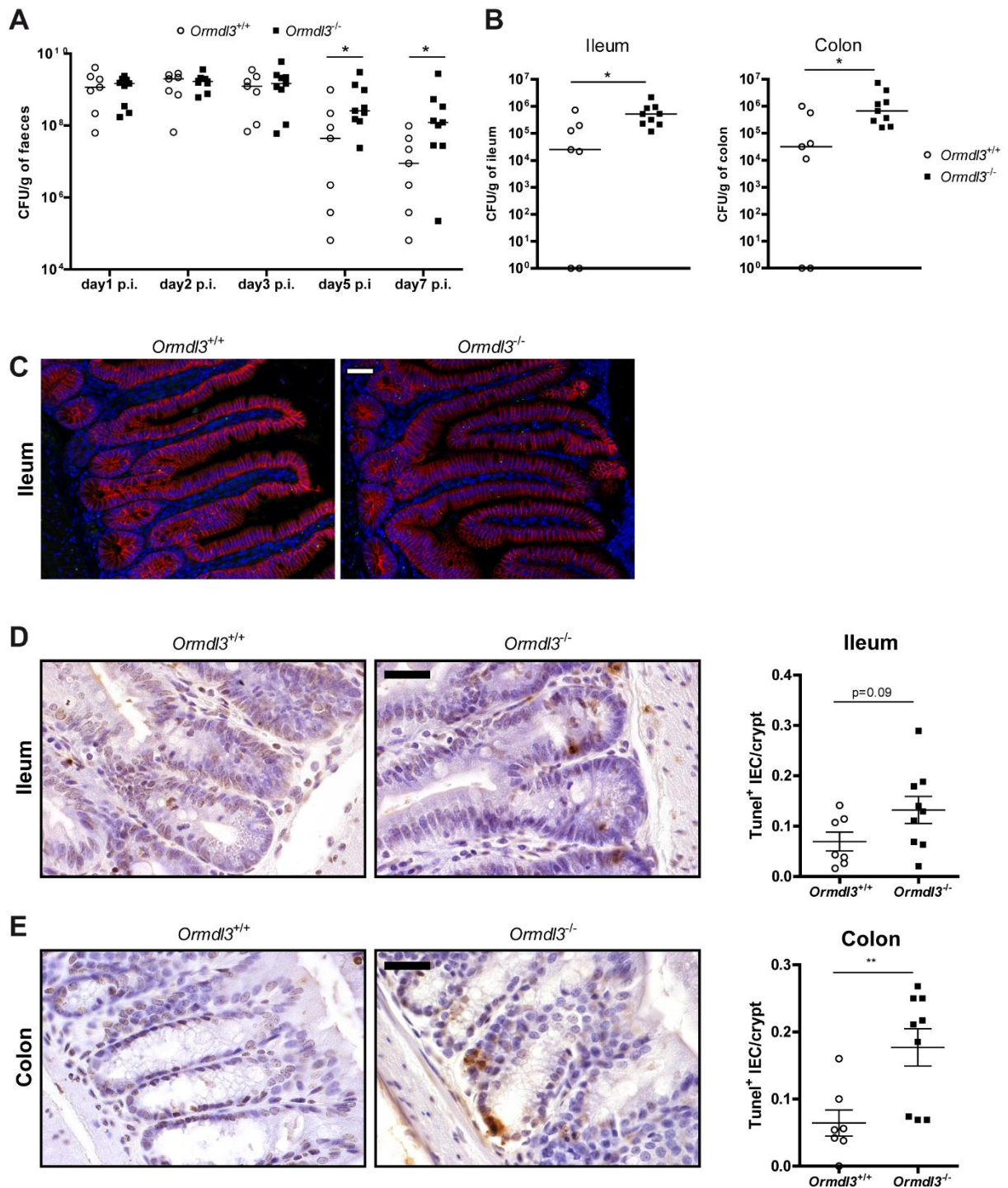


Figure 4.3: *Ormdl3*^{-/-} mice display increased susceptibility to AIEC LF82 colonization. Mice were pretreated by oral administration of streptomycin (20 mg) and received 0.25% (wt/vol) of dextran sulfate sodium (DSS) in drinking water. *Ormdl3*^{+/+} and *Ormdl3*^{-/-} mice were infected with 10⁹ CFU of AIEC LF82 by gavage for 7 days. **(A)** Quantification of AIEC LF82 in the feces of *Ormdl3*^{-/-} mice and their littermates. **(B)** Quantification of ileal and colonic mucosal-associated AIEC LF82 bacteria at day 7 after oral infection. **(C)** Immunofluorescence staining of ileal section from WT or *Ormdl3*-deficient mice at day 7 after AIEC LF82 colonization. *E. coli* LPS is depicted in green and E-Cadherin is shown in red, DAPI=blue. Scale bar, 20 μ m. Histological evaluation of ileal **(D)** and colonic sections **(E)** with representative pictures and absolute quantification for TUNEL⁺ cells per crypt. For quantification, a minimum of 100 crypts/intestine were analysed. Scale bar, 20 μ m.

4.1.4 Critical Role of ORMDL Proteins for Structure & Function of Secretory Epithelial Cells in the Intestine

Paneth cells limit bacterial invasion by secreting antimicrobial proteins including lysozyme and the appearance of dysfunctional Paneth cells is a remarkably consistent consequence when Crohn's disease susceptibility genes, such as *Atg16l1* [28, 29], *Nod2* [297, 298], *Irgm1* [299], and *Xbp1* [36] are mutated. We hypothesized that the increased colonization susceptibility observed in *Ormdl3*-deficient mice might at least partially be due to a defect in Paneth cell function. We examined Paneth cells by transmission electron microscopy (TEM). Although we did not detect any accumulation of the atypical membranous structures or abnormal mitochondria that are seen with deficiency of other autophagy-related genes [300-302], the endoplasmic reticulum (ER) compartment was expanded (Fig. 4.4A). Notably, the dilation of the ER was even more pronounced in *Ormdl1^{-/-}Ormdl3^{-/-}* double-deficient Paneth cells compared to *Ormdl3* singly deficiency. Immunostaining against lysozyme showed a significant decrease in the number of Paneth cells in the ileum of *Ormdl3^{-/-}* and *Ormdl1^{-/-}Ormdl3^{-/-}* mice when compared to controls (Fig. 4.4B), suggesting an abnormality of Paneth cell function. To further test this idea, we isolated Paneth cell-containing crypts and infected them *in vitro* with *E. coli* LF82 and quantified bacterial numbers two hours post infection. Strikingly, crypts from *Ormdl3^{-/-}* and *Ormdl1^{-/-}Ormdl3^{-/-}* mice showed reduced bacterial killing compared with their control littermates suggesting reduced levels and/or secretion of antimicrobial peptides such as lysozyme (Fig. 4.4C). Next, we examined Goblet cells, another major secretory cell type in the intestine [303]. Goblet cells secrete high-molecular-weight glycoproteins called mucins which represent the main structural components of the mucus layer. Light microscopy analysis of colonic sections of *Ormdl3^{-/-}* and *Ormdl1^{-/-}Ormdl3^{-/-}* mice revealed a decrease in the number of Periodic Acid Schiff (PAS) positive Goblet cells when compared to controls (Fig. 4.4D). Consistent with these observations, we observed decreased *Muc2* expression in the ileum and colon of *E. coli* LF82 infected *Ormdl3^{-/-}* mice compared to WT mice (Fig. 4.4E).

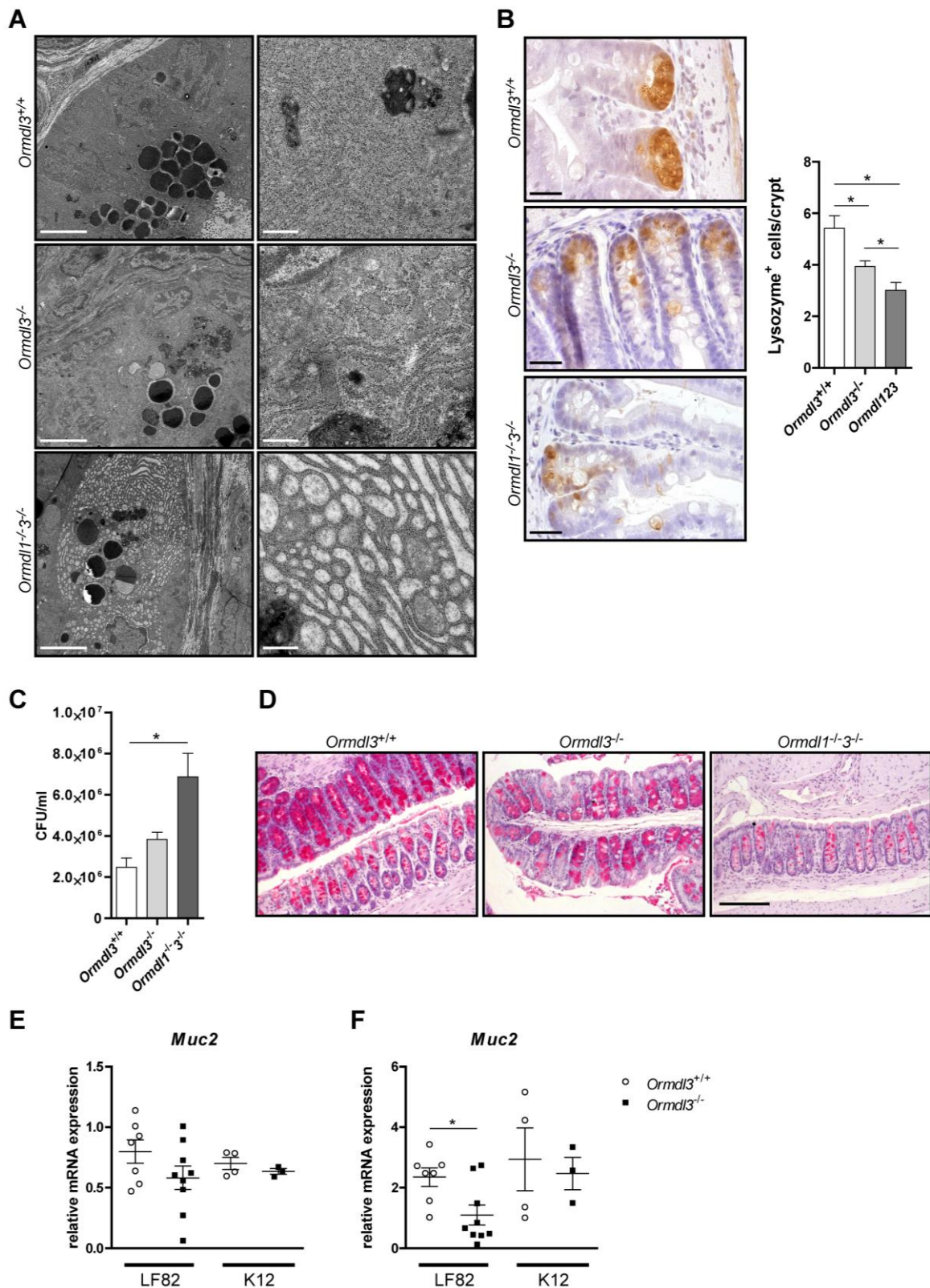


Figure 4.4: ORMDL1 and ORMDL3 regulate structure and function of highly secretory cells in the intestine. (A) Transmission electron microscopy (TEM) of ileal crypts of 12-week old *Ormdl3*^{+/+}, *Ormdl3*^{-/-} and *Ormdl1*^{-/-3}^{-/-} mice. Left panel: scale bar, 4 μ m; right panel: scale bar, 500 nm. (B) Representative images of mouse ileal sections (n=4 per genotype) stained for lysozyme (scale bar, 20 μ m) and quantification. For quantification, a minimum of 100 crypts/intestine were assessed. (C) Bacterial killing assay. Freshly isolated crypts (~20,000) were infected with *E. coli* LF82 (1×10^8 bacterial cells) and colony forming units (CFU) were determined 2h post infection. n=3. (D) Representative pictures of Periodic acid-Schiff (PAS)-stained colonic sections (scale bar, 50 μ m). Downregulation of *Muc2* in ileal (E) and colonic tissue (F) of *E. coli* LF82 infected *Ormdl3*-deficient mice (7d p.i.) as demonstrated by real-time PCR. No significant differences were observed in the control groups infected with *E. coli* K12.

Remarkably, we noted a dilated ER lumen by TEM in Goblet cells in ileal sections of *Ormdl3*^{-/-} and *Ormdl1*^{-/-}*3*^{-/-} mice resembling the phenotype observed in Paneth cells (Fig. 4.5A). Additionally, ER expansion was also observed in enterocytes of *Ormdl1*^{-/-}*3*^{-/-} mice but not in *Ormdl3*^{-/-} mice (Fig. 4.5B) indicating a more pronounced phenotype in double-deficient animals, which might suggest overlapping functions of ORMDL1 and ORMDL3 in the intestine.

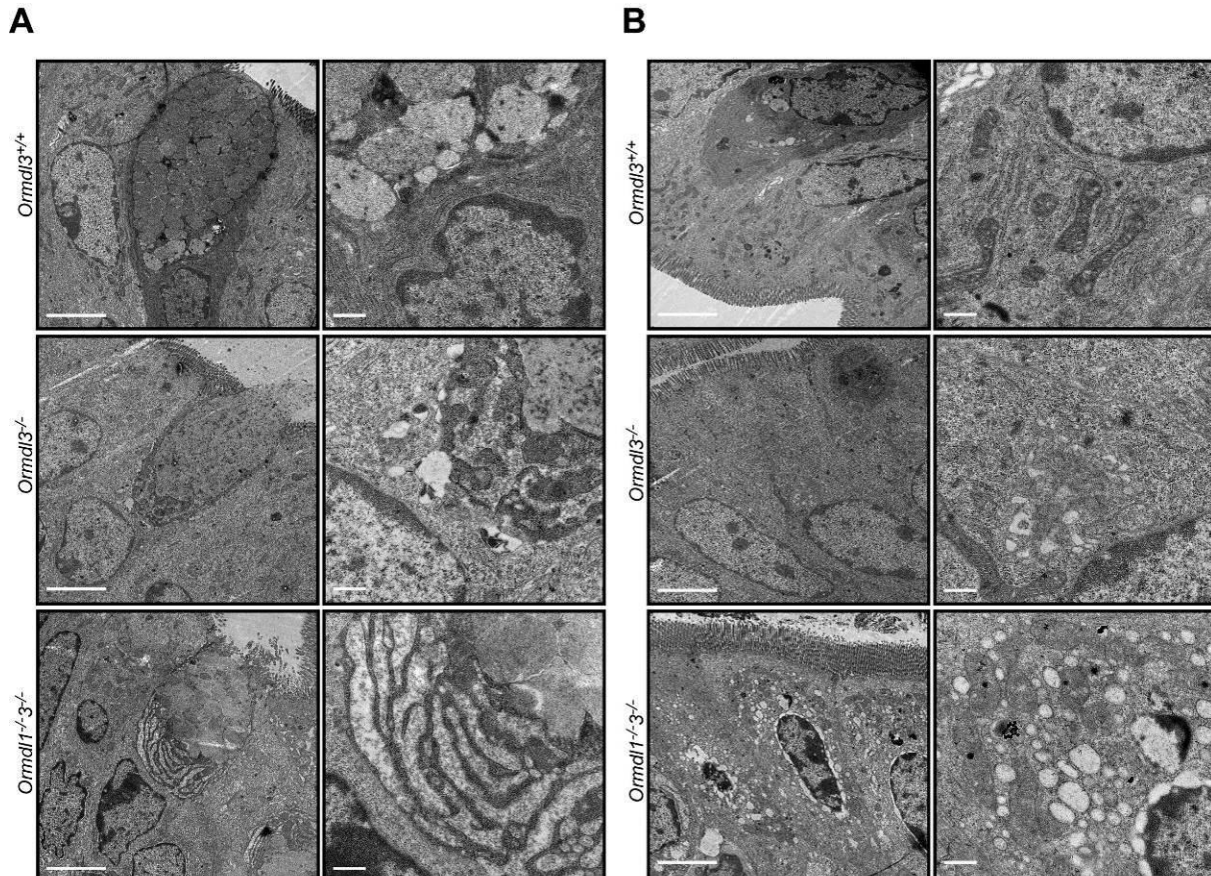


Figure 4.5: Critical role of ORMDL1 and ORMDL3 in the structure of Goblet cells and enterocytes. Transmission electron microscopy (TEM) of ileal (A) Goblet cells and (B) enterocytes of 12-week old *Ormdl3*^{+/+}, *Ormdl3*^{-/-} and *Ormdl1*^{-/-}*3*^{-/-} mice. Left panel: scale bar, 4 μm; right panel: scale bar, 500 nm.

4.1.5 *Ormdl1/3*-Deficient Mice Display No Signs of Increased UPR Activation

A dilated ER lumen often suggests an ER stress response [112, 304]. To our surprise, we did not observe any significant increase of ER stress markers such as GRP78 or GRP94 neither on protein nor on mRNA level in younger (up to 20-week-old) *Ormdl3*^{-/-} and *Ormdl1*^{-/-}*3*^{-/-} animals compared to controls (Fig. 4.6A,B). Additionally, we did not detect increased activation of the UPR in freshly isolated crypts of *Ormdl3*^{-/-} and *Ormdl1*^{-/-}*3*^{-/-} animals upon *E. coli* LF82 infection as external ER stress trigger (Fig. 4.6C). Based on these findings, we hypothesized that, similar to aged *Atg16l1*^{ΔIEC} mice, which eventually exhibit increased signs of ER stress [179], intestinal epithelial cells of *Ormdl3*- and *Ormdl1/3*-deficient mice might become increasingly prone to ER stress over time. However, 1 year old *Ormdl3*^{-/-} and *Ormdl1*^{-/-}*3*^{-/-} mice exhibited reduced expression of the ER stress markers *Hsp90b1* (*Grp94*), *Atf6a* and *Atf4* in ileal tissue compared with control mice (Fig. 4.6D). Similarly, we did not detect elevated basal GRP94 levels in ileal sections of aged *Ormdl3*- and *Ormdl1/3*-deficient mice compared to their littermates (data not shown).

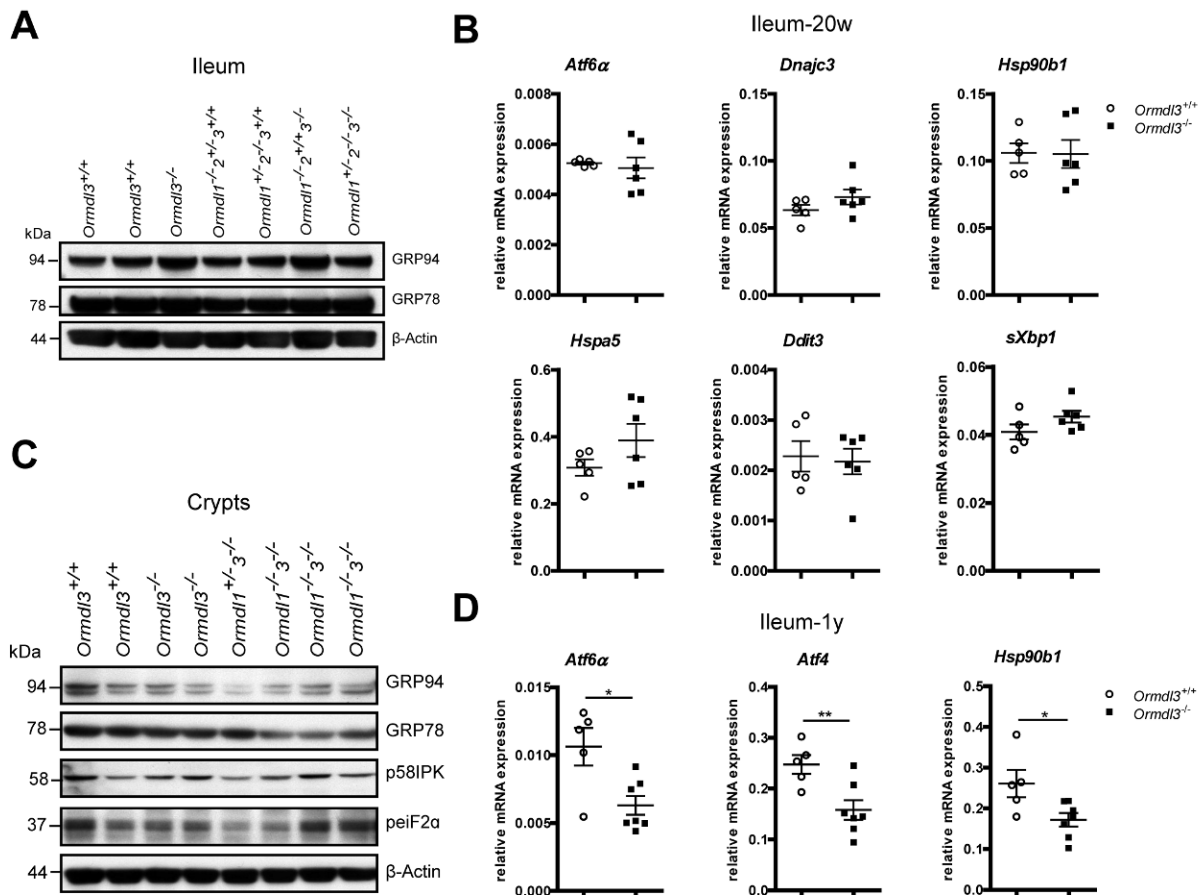


Figure 4.6: *Ormdl3*^{-/-} mice do not exhibit any signs of increased UPR activation in the intestine. (A) Immunoblot analysis of ileal sections of 20-week old mice from the indicated genotypes. **(B)** mRNA levels of ER stress markers in 20-week-old *Ormdl3*^{+/+} and *Ormdl3*^{-/-} mice. **(C)** Immunoblot of small intestinal crypts from wild-type, *Ormdl3*^{-/-} and *Ormdl1*^{-/-}3^{-/-} mice (20 w) *ex vivo* infected for 2h with LF82 (1x10⁸ cells). **(D)** qPCR of ileal tissue of 1-year-old animals.

4.1.6 Simultaneous Lack of ORMDL3 & ORMDL1 Causes Severe Motor Defects *in vivo*

However, both male and female *Ormdl1*^{-/-}3^{-/-} mice displayed abnormal limb-clasping reflexes (Fig. 4.7A), they had difficulty walking in a straight line (Fig. 4.7B,C) and showed impaired motor coordination ability (Fig. 4.7D). The observed defects are often observed in mouse models of neurodegenerative disease [305, 306] and have also been described in *Atg5*- and *Atg7*-conditional knockout mice [300, 301]. To identify the neurologic deficits in *Ormdl1*^{-/-}3^{-/-} mice, histological stainings of brain sections were inspected at various time points. We detected a progressive degeneration of the basal ganglia accompanied by a diffuse and progressive astrogliosis (data not shown). Consistent with glial activation in response to neuronal damage, immunoblotting for the glial marker GFAP (glial fibrillary acidic protein) and microglial marker IBA1 (ionized calcium-binding adapter molecule 1) was increased in *Ormdl1/3* double-deficient mice (Figure 4.7E). These results highlight the functional redundancy of ORMDL1 and ORMDL3 in the central nervous system and the sensitivity of neurons to loss of ORMDL1 and ORMDL3. In line with our previous findings, we did not detect increased levels of ER stress markers such as GRP78 (BIP) and p58IPK in brain sections of 18-23w old mice. However, immunoblotting of brain tissue revealed a significant increase in p62 (SQSTM1, sequestosome 1) (Fig. 4.7E) pointing towards defective autophagy in *Ormdl3*- and *Ormdl1/3*-deficient mice. Notably, we

found increased levels of p62 not only in brain sections but also in other tissues such as lung, liver and ileum (Fig. 4.7F).

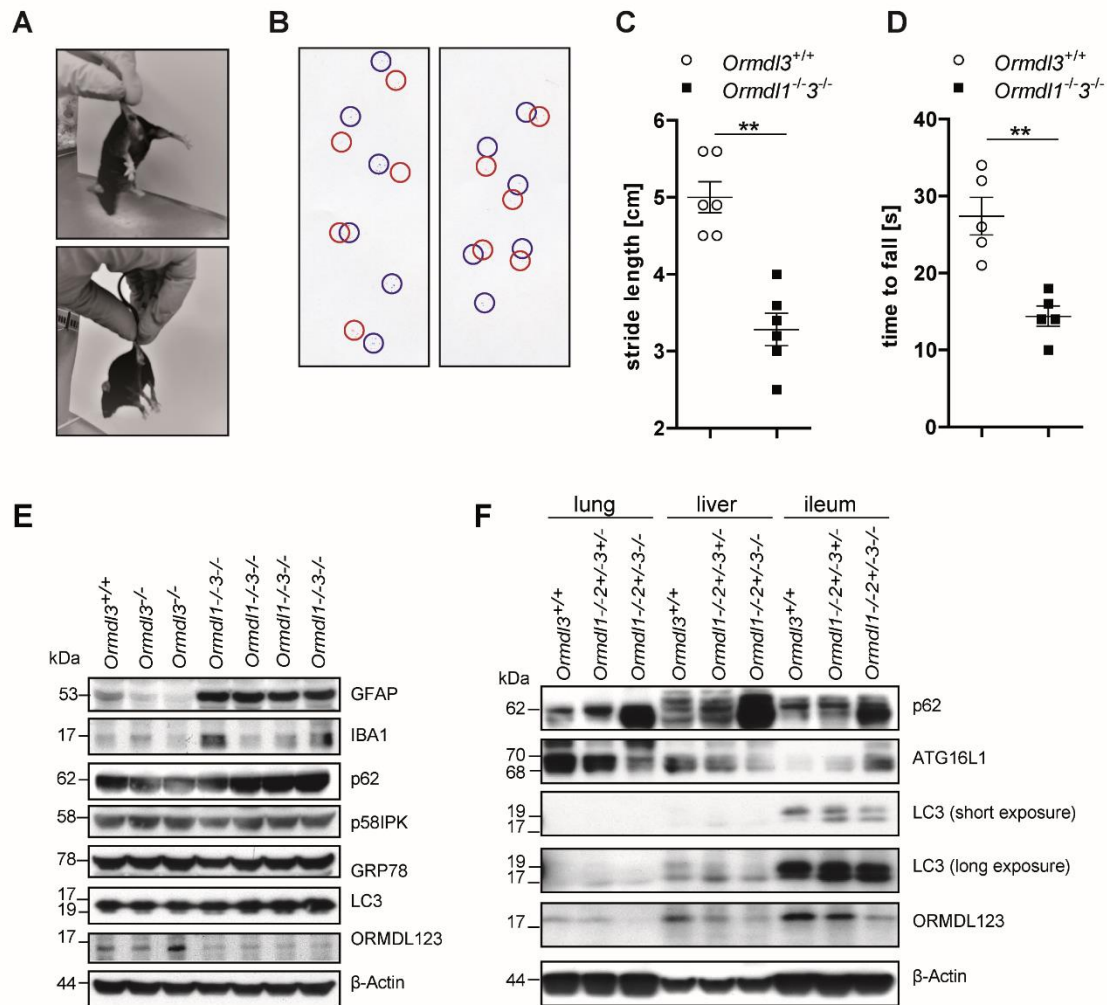


Figure 4.7: *Ormdl1*^{-/-3}^{-/-} mice exhibit severe motor defects. (A) Limp-clasping reflexes in a wild type mouse (upper panel). Abnormal limb-clasping reflexes in a 10-week-old *Ormdl1*^{-/-3}^{-/-} mouse (lower panel). (B) The ink paw-print test, in which the fore paws were marked in blue ink (blue circles) and the hind paws in red ink (red circles), revealed abnormal gait pattern in *Ormdl1*^{-/-3}^{-/-} deficient mice. (C) Stride length was measured in *Ormdl3*^{+/+} and *Ormdl1*^{-/-3}^{-/-} animals (n=6). (D) Motor coordination was tested using a rotarod assay. *Ormdl3*^{+/+} (n=5) and *Ormdl1*^{-/-3}^{-/-} (n=6) mice were placed on a rotating rod and the time spent on the rod was measured. (E) Immunoblotting of brain tissue of 18-23w old wild-type, *Ormdl3*^{-/-} and *Ormdl1*^{-/-3}^{-/-} animals. (F) Immunoblot of lung, liver and ileal tissue of 8w old mice.

4.1.7 *Ormdl3*- and *Ormdl1/3* Deficiency Impairs Autophagy in Intestinal Epithelial Cells

To study autophagic flux, we quantified the turnover of LC3BI to its phosphatidylethanolamine-conjugated form LC3BII (Fig. 4.8A), a marker for autophagosome formation, in *Ormdl1*^{-/-3}^{-/-} and *Ormdl1*^{-/-2}^{+/3}^{-/-} immortalized MEFs (iMEFs). Autophagy was induced by nutrient starvation and chemically by stimulation with the mTOR inhibitor rapamycin. *Ormdl1*^{-/-3}^{-/-} and *Ormdl1*^{-/-2}^{+/3}^{-/-} iMEFs showed a marked reduction in LC3 turnover and elevated p62 levels compared to WT iMEFs upon autophagy induction. Likewise, simultaneous siRNA mediated knockdown of *Ormdl1* and *Ormdl3* in intestinal epithelial cells resulted in reduced LC3 conversion upon autophagy induction by rapamycin compared to control cells (Fig. 4.8B). We next determined whether markers of autophagy were

abnormal in iMEFs upon bacterial autophagy induction. Recently, it was shown that functional autophagy is required to limit intracellular AIEC replication [74]. Indeed, LC3 conversion in *Ormdl3*-deficient iMEFs was impaired upon infection with *E. coli* LF82 compared to *Ormdl3*^{+/+} cells (Fig. 4.8C). Functionally, LF82 infected *Ormdl3*^{-/-} and *Ormdl1*^{-/-}*3*^{-/-} iMEFs showed reduced bacterial killing in a gentamicin protection assay (Fig. 4.8D). Accordingly, *E. coli* LF82 infection of iMEFs resulted in higher numbers of bacteria localized within *Ormdl3*- and *Ormdl13*-deficient iMEFs compared to WT cells as determined by immunofluorescence staining of *E. coli* LPS and of cell membranes using AlexaFluor 555-conjugated wheat germ agglutinin (Fig 4.8E). To further test this idea in primary cells, we isolated crypts, infected them *in vitro* with LF82 and monitored protein levels of the adaptor protein p62 and the autophagy protein ATG16L1 (Autophagy-related 16-like 1). We observed increased levels of both p62 and ATG16L1 accompanied by a reduced LC3 conversion in *Ormdl3*^{-/-} and *Ormdl1*^{-/-}*3*^{-/-} infected crypt lysates supporting the role of ORMDL proteins in autophagy (Fig. 4.8F).

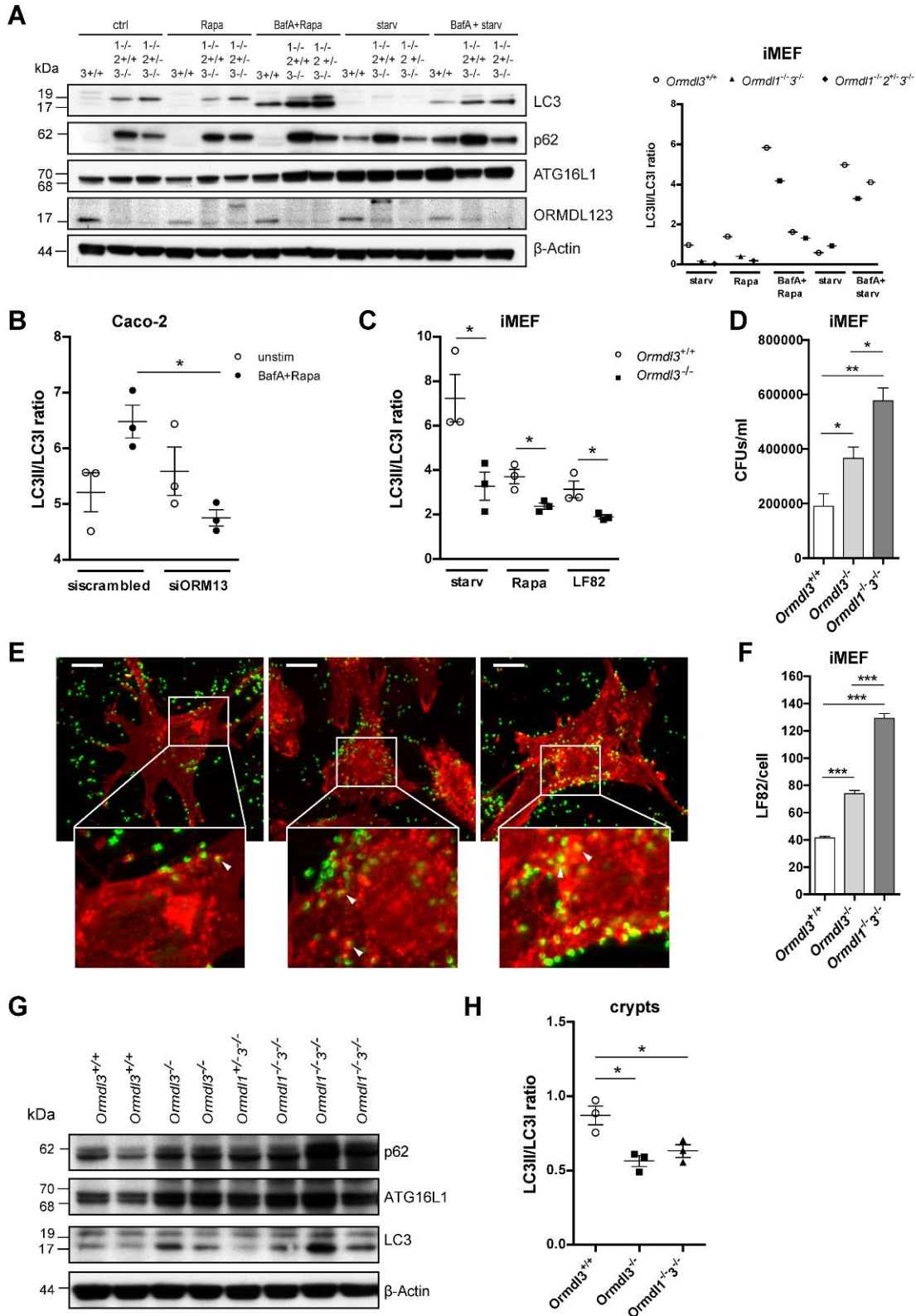


Figure 4.8: ORMDL1 and ORMDL3 regulate autophagic flux upon nutrient starvation and bacterial infection. (A) WT, *Ormdl1*^{-/-}3^{-/-} and *Ormdl1*^{-/-}2^{+/-}3^{-/-} iMEFs were stimulated with Rapamycin (100 nM) or nutrient-starved with EBSS for 2 h in the presence of Bafilomycin A (BafA, 100 nM). Protein lysates were probed by immunoblot for levels of the indicated proteins and the ratio of LC3II to LC3I was quantified. EBSS: Earle's Balanced Salt Solution. (B) Caco-2 cells were treated with siRNA targeting *Ormdl1* and *Ormdl3* (siORM13) or with non-targeting siRNA (siscrambled) and autophagy was induced by exposure to rapamycin (100 nM, 2h) in the presence of BafA, 100 nM. The LC3II/LC3I ratio is depicted. (C) iMEFs were infected with *E. coli* LF82 (multiplicity of infection MOI25) in the presence of BafA (100 nM) and LC3 turnover was quantified 2 h post infection. Starvation with HBSS and Rapamycin treatment (100 nM) served as positive control for autophagy induction. (D) Gentamicin protection assay.

iMEFs were infected with *E. coli* LF82 (MOI25) for 2h and colony forming units (CFU) were counted. n=3. (E) Immunofluorescence of *E. coli* LPS in *E. coli* LF82-infected wild-type, *Ormdl3*^{-/-} and *Ormdl1*^{-/-}*3*^{-/-} iMEFs. Cell membranes were visualized using AlexaFluor 555-conjugated wheat germ agglutinin (WGA). Scale bars, 10 μm. (F) For quantification, 30 cells/genotype were assessed. (G) Immunoblot of *ex vivo* small intestinal crypts from wild-type, *Ormdl3*^{-/-} and *Ormdl1*^{-/-}*3*^{-/-} mice infected for 2 h with LF82 (1×10⁸ cells). (H) Crypts (20,000), pretreated for 20 min with BafA (100 nM), were *ex vivo* infected with *E. coli* LF82 (1×10⁸ cells). LC3 conversion was quantified by immunoblotting 2 h post infection.

4.1.8 ORMDL Proteins Regulate ER Membrane Trafficking

In recent years, an intense crosstalk between autophagy and the secretory pathway has been described and several proteins have been identified, which play pleiotropic roles in both cellular processes [156, 157, 160, 307, 308]. The first indication that core components of the ER export machinery regulate autophagy came from the observation that yeast strains with genetic defects in certain COPII components are unable to generate autophagosomes [309]. To study the role of ORMDL proteins in ER-Golgi trafficking, we followed the delivery of the ts045 mutant strain of vesicular stomatitis virus envelope glycoprotein G (VSVG) from the ER to the Golgi complex [310]. Due to protein misfolding, VSVG-GFP localizes exclusively to the ER in cells incubated at 41°C. A temperature shift to 32°C induces the transport of VSVG-GFP from the ER to the Golgi apparatus, where it acquires a complex glycan structure that is resistant to Endoglycosidase H (Endo H) treatment [310]. Strikingly, we observed enhanced transport of VSVG-GFP from the ER to the Golgi apparatus in *Ormdl3*- and *Ormdl1/3*-deficient iMEFs compared to wild type cells both under basal conditions and after exposure to Tunicamycin (Fig. 4.9A,B,C). Enhanced ER-Golgi trafficking combined with the dilation of the ER in intestinal epithelial cells, the lack of ER stress in *Ormdl3*-deficient mice, and defective autophagy, led us to hypothesize that ORMDL proteins might be involved in regulating ER turnover. ORMDL proteins might act as a molecular switch determining the fate of ER membrane towards the autophagy machinery or towards secretory pathway. Therefore, we first analysed whether ORMDL proteins are regulated in an autophagy dependent manner. Indeed, starvation-induced autophagy in the presence of protein synthesis inhibitor Cycloheximide caused a reduction of ORMDL protein levels (Fig. 4.9D). To follow the fate of ORMDL3 proteins upon autophagy induction, we immuno-stained autophagosomes with anti-ATG16L1 or anti-LC3, respectively, and lysosomes with anti-LAMP2 in iMEFs overexpressing ORMDL3. After 3 h of starvation, ORMDL3 co-localized with ATG16L1, LC3 and LAMP2 (Fig. 4.9E). In agreement with these findings, co-immunoprecipitation revealed an interaction between overexpressed ORMDL3 and LC3 in iMEFs (Fig. 4.9F) suggesting a possible interaction of ORMDL3 with the macroautophagy machinery. Importantly, while the signaling pathways that increase the ER volume and expression of ER-resident proteins have been studied in detail, insights into the selective degradation of ER fragments, termed ER-phagy, have only recently emerged. ER-phagy is considered as fragmentation and delivery of ER fragments to lysosomal compartments for clearance. The selectivity of this poorly characterized catabolic pathway is ensured by ER-phagy receptors that engage autophagy components via LC3-interacting regions [150-152, 154]. To test whether the lack of ORMDL3 or ORMDL1/3 affects ER turnover, iMEFs were starved and the ER sheet marker TRAPα was visualized (Fig. 4.9G). Remarkably, *Ormdl3*- and *Ormdl1/3*-deficient iMEFs showed an altered ER morphology upon starvation similar to changes observed in iMEFs deficient in the ER-phagy receptor FAM134B [150]. Next, we investigated how ORMDL3 or ORMDL1/3 absence influences ER-phagy. The lack of ORMDL proteins affected starvation induced turnover of the ER sheet marker proteins TRAPα and CLIMP63 and the ER tubules marker RTN4B (Fig. 4.9H). Both in *Ormdl3*^{-/-} and *Ormdl1*^{-/-}*3*^{-/-} iMEFs, degradation of TRAPα, CLIMP63, and RTN4B was impaired upon starvation induced autophagy induction.

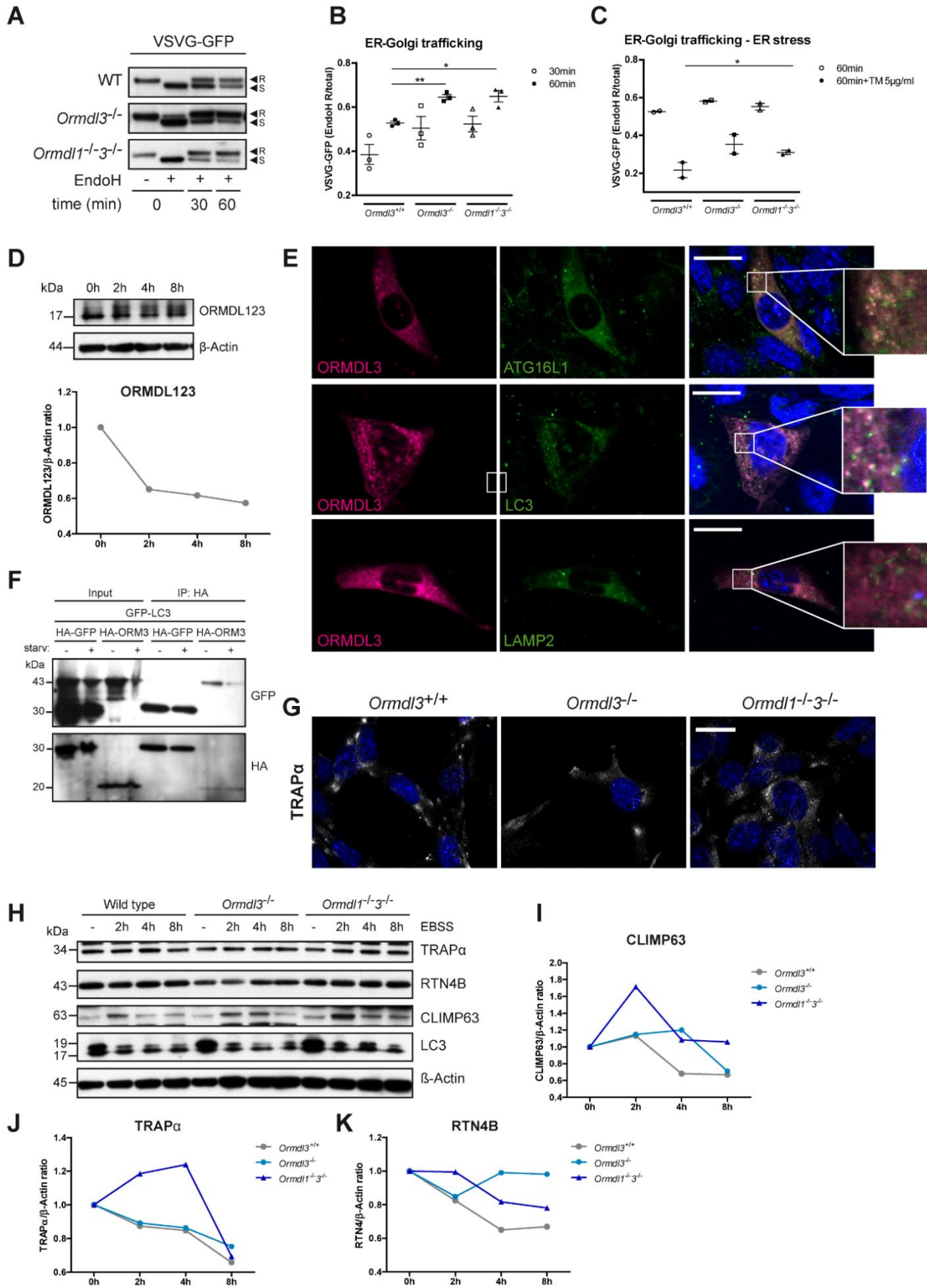


Figure 4.9: ORMDL proteins as modulators of the secretory pathway and ER turnover. (A) Representative immunoblots of WT, *Ormdl3*^{-/-} and *Ormdl1*^{-/-3}^{-/-} iMEFs transfected with VSVG(ts045)-GFP and incubated for 24 h at 41°C. Cells were transferred to 32°C for the indicated times (30 min/60 min) before whole-cell extracts were prepared. Lysates were treated with or without endoglycosidase H (EndoH) and subjected to immunoblot analysis. R= EndoH-resistant; S= EndoH-sensitive. (B) Ratios of EndoH-R VSVG to total VSVG from 3 independent

experiments are depicted. **(C)** iMEFs transfected with VSVG(ts045)-GFP were incubated for 24 h at 41°C. Upon transfer to 32°C, cells were stimulated with Tunicamycin (5 µg/ml). Ratios of EndoH-R VSVG to total VSVG from 2 independent experiments. **(D)** Western blot analysis and quantification of ORMDL123 protein turnover in wild-type iMEFs. Cells were starved with EBSS for the indicate time in the presence of 100 µM Cycloheximide to inhibit protein synthesis. **(E)** Immunofluorescence of RFP-ORMDL3 and ATG16L1 (upper panel)/LC3B (middle panel)/LAMP2 (lower panel) in iMEFs in presence of 100 nM Bafilomycin A1. Cells were starved with EBSS for 4 hr. Scale bars, 20 µm. **(F)** Co-IP of LC3B with ORMDL3. Cells were transfected with GFP-LC3B and HA-ORMDL3/HA-GFP. Cells were starved for 2 h (EBSS) in the presence of Bafilomycin A1 (100 nM). **(G)** Immunofluorescence staining of TRAPα in iMEFs. Cells were starved (EBSS) for 4h. Scale bars, 20 µm. **(H)** Western blot analysis and quantification **(I-K)** of ER protein turnover in wild-type, *Ormdl3*^{-/-} and *Ormdl1*^{-/-}*3*^{-/-} iMEFs. Cells were starved (EBSS) for the indicate time in the presence of 100 µM Cycloheximide. Data are representative of three independent biological replicates.

Thus, our findings in *Ormdl3*^{-/-} and *Ormdl1*^{-/-}*3*^{-/-} cells suggest an important role of the ORMDL protein family in regulating ER membrane trafficking. Dependent on the cellular requirements, ORMDL proteins might function as selective ER-phagy receptors directing ER fragments towards degradation via the autophagic machinery.

4.2 Discussion

IBD, with its two main forms CD and UC, is characterized by chronic inflammation of the gastrointestinal tract. IBD has long been known to have a genetic basis and likely involves aberrant immune responses to environmental factors. Importantly, little is known about the mechanism of action of alleles that favor disease pathogenesis. Although the inability to control intestinal bacteria is considered to underlie IBD, the role of ORMDL3, associated with both CD and UC [38, 39], in shaping host-microbe interaction is unclear. This study sheds light on the role of ORMDL3 in shaping host-microbe interactions. We find that *Ormdl3*-deficient mice are more susceptible to bacterial colonization with an adherent-invasive *E. coli* strain. Specifically, we show that the lack of ORMDL3 affects ER structure and cellular function of highly secretory cell types including Paneth and Goblet cells, thereby compromising mucosal defense against entry of pathogenic bacteria. We demonstrate that autophagy, essential for host defense against bacterial infection, is impaired in the absence of ORMDL3. Moreover, our study suggests a possible role of ORMDL proteins in regulating ER turnover, thereby determining the fate of ER membrane fragments. We propose that ORMDL proteins might function as molecular switch directing ER fragments towards the autophagy machinery for degradation or towards the secretory pathway.

4.2.1 *Ormdl3* and *Ormdl1/3* Deficiency Impair Body Growth Whereas Simultaneous Deletion of *Ormdl1*, *Ormdl2* and *Ormdl3* Causes Embryonic Lethality

To shed light on the function of ORMDL proteins in intestinal homeostasis, we analyzed *Ormdl3*^{-/-} and *Ormdl1*^{-/-}*3*^{-/-} double-deficient mice.

Ormdl3^{-/-} and even more pronounced *Ormdl1*^{-/-}*3*^{-/-} mice exhibited decreased overall body size accompanied by reduced body weight when compared to the wild type mice implying growth retardation in the absence of ORMDL proteins. Remarkably, genetic deletions of other UPR components have been shown to affect body growth revealing a link between UPR components and body growth. Deletion of the ATF6α target *Hsp90b1* (encoding GRP94) is essential for postnatal body growth [311, 312]. Likewise, deletion of Perk causes growth retardation accompanied by reduced body weight at the age of 3 weeks [313, 314]. In contrast, in yeast, a single knockout of one of the two ORMDL homologues ORM1/2 does not cause any growth abnormalities [181]. However, ORM1/2-double deficient yeast display impaired cell growth, pointing towards functional redundancy of the ORMDL proteins and a possible dosage-dependent effect. In line with these findings, *Ormdl1/3* double-deficient mice exhibited more severe growth retardation compared to *Ormdl3* single-deficient mice.

Under physiological conditions, 20-week old *Ormdl3*^{-/-} mice did not show any signs of spontaneous intestinal inflammation, indicating that ORMDL3 is dispensable for intestinal homeostasis. Likewise, genetic deletion of the ER stress related genes *Atf6α* or *Ddit3* (encoding Chop) does not cause intestinal inflammation [167, 172], suggesting that single deletions of UPR components do not compromise intestinal homeostasis under basal conditions. Similarly, *Atg16l1*^{ΔIEC} and *Atg16l1*^{HM} mice do not develop intestinal inflammation until week 35 [28, 35, 161, 315], indicating that additional environmental triggers are involved in disease pathogenesis.

Importantly, while *Ormdl1/3* double-deficient mice were born at sub-Mendelian ratios and showed a reduced lifespan, *Ormdl3*^{-/-} did not exhibit any abnormalities in life expectancy and breeding. Failed breeding attempts to obtain a triple-negative mouse (*Ormdl1*^{-/-}*2*^{-/-}*3*^{-/-}) strongly suggest that ORMDL1, ORMDL2 and ORMDL3 exert overlapping functions essential for organogenesis and embryonic

development and might again point towards a dosage-dependent effect since *Ormdl1*^{-/-}*3*^{-/-} are viable. Interestingly, it was shown that ORMDL proteins form homo- and hetero-oligomers that change conformation depending on cellular sphingolipid levels [191, 199]. Kiefer et al. observed that a coordinated overexpression of all three ORMDL proteins efficiently blocks the serine palmitoyltransferase (SPT), involved in sphingolipid biosynthesis, whereas single ORMDL proteins were not as effective. Additionally, in yeast, while the single knockout of ORM1 or ORM2 does not affect stress resistance, double knockout mutants are highly sensitive towards stress [181, 191]. Remarkably, the human ORMDL3 is able to rescue the phenotype of ORM1/2-deficient yeast [181], indicating a highly conserved function even throughout different species. Similar to the observed embryonic lethality in triple-negative mice, several other UPR related genes have been shown to exert a crucial function in embryonic and postnatal development. Lack of IRE1 α or its target gene *Xbp1* results in embryonic lethality in mice [173, 316]. Similarly, deletion of *Hspa5* (*Grp78*) or *Hsp90b1* (*Grp94*), both encoding ER chaperones, leads to embryonic lethality in mice [317, 318]. Similar to *Ormdl1*^{-/-}*3*^{-/-} mice, embryonic lethality has been observed in mice that lack both *Atf6 α* and *Atf6 β* [106, 107]. However, the exact function of ORMLD proteins in embryonic development and organogenesis in mammals remains to be elucidated and is subject of ongoing investigation.

4.2.2 *Ormdl3* Expression is Regulated by Microbial Cues

Our findings indicate that ORMDL proteins are not only important during embryonic developmental, but also during post-natal development as indicated by high expression levels of *Ormdl3* in 1-week old compared to 4-week and 12-16-week old mice. Moreover, the detected microbiota-driven transcriptional repression of *Ormdl3* in germ free raised mice compared to wild type mice correlates with our *in vitro* data, where we detected a repressive effect of both *E. coli* LF82 and *E. coli* lipopolysaccharide (LPS) on *Ormdl3* promoter activity in iMEFs. The strong effect of LPS on *Ormdl3* promoter activity suggests a role of TLR4 signaling in negatively regulating *Ormdl3* expression levels. Similarly, Kiefer et al. [199] reported a significant decrease in *Ormdl3* expression levels 4 h and 8 h after LPS stimulation in RAW264.7 monocytes. Importantly, TLR4 agonists have been shown to induce de novo sphingolipid biosynthesis in RAW264.7 cells [202]. Subsequently, changes in sphingolipid composition might adjust *Ormdl3* transcription. Of note, in contrast to our observations, Kiefer et al observed *Ormdl3* upregulation 24 h after LPS stimulation. These discrepancies might be due to cell type-specific differences between RAW264.7 cells and iMEFs. Regarding the transcriptional regulation of *ORMDL3* little is known. Jin et al. [319] reported that *ORMDL3* gene expression might be regulated by multiple transcriptional factors such p300 (E1A Binding Protein P300), ETS-1 (ETS Proto-Oncogene 1) and CREB (cAMP response element binding protein). Moreover, it was reported that a protein complex formed by STAT6 and p300 binds to the promoter of *ORMDL3* inducing its expression [320]. Strikingly, several studies have described that STAT DNA binding activity can be repressed by IL-1R or TLR4 signaling [321-323], suggesting that reduced *ORMDL3* expression upon LPS exposure in iMEFs might be due to diminished STAT6 binding within its promoter region. Additionally, it was shown that CREB binds to the CRE element within the *ORMDL3* gene promoter and trans-activates its expression [324]. Recently, Wang et al. [325] identified an IRF-3 (interferon-regulatory factor-3) binding site within the *ORMDL3* promoter region. Importantly, a repressive function of TLR4 signaling on UPR components was described for ATF4 [326, 327]. Translation of *Atf4* mRNA is repressed by TLR4 signaling, which in turn decreases CHOP levels in activated macrophages.

4.2.3 *Ormdl3*-Deficient Mice Display Increased Susceptibility to Adherent-Invasive *E. coli* Colonization

Two hypotheses have emerged regarding the role of the intestinal microbiota in the pathogenesis of IBD. Several lines of evidence support the notion that primary dysregulation of the mucosal immune system provokes overshooting immune response to gut commensal organisms [328]. Another hypothesis proposes that changes in the microbiota composition cause excessive immune response. In IBD patients, an increase in pathogenic mucosa-associated *E. coli* is observed [58, 59, 64, 65]. These bacteria are able to adhere to and invade intestinal epithelial cells and to replicate within macrophages [59, 64, 329]. To mimic increased colonization with pathogenic *E. coli*, *Ormdl3*^{-/-} mice and their wild-type littermates were infected with the adherent-invasive *E. coli* (AIEC) strain LF82. *Ormdl3*^{-/-} mice, compared to control mice, exhibited increased susceptibility to *E. coli* LF82. In line with these findings, a recent study showed that *Atf6α*-deficient mice are highly susceptible to *Bacillus anthracis* infection. *Atf6α*^{-/-} mice showed reduced autophagic bacterial degradation due to decreased expression of *Dapk1* (death-associated protein kinase 1) which promotes autophagy [207]. Moreover, deletion of *Xbp1* in intestinal epithelial cells results in diminished levels of antimicrobial peptides such as lysozyme favoring *Listeria monocytogenes* infection [36]. Moreover, it was demonstrated that CHOP is involved in antimicrobial defense. RNAi mediated knockdown of *Ddit3* (Chop) during *Mycobacterium tuberculosis* infection results in increased numbers of intracellular bacteria [330].

4.2.4 Abnormalities in the Structure & Function of Highly Secretory Cells in the Intestine of *Ormdl3*- and *Ormdl1/3*-Deficient Mice Do Not Correlate with UPR Activation

In addition to the increased susceptibility to *E. coli* LF82 colonization in *Ormdl3*-deficient mice, we found ER expansion in highly secretory cell types such as Paneth and Goblet cells. Paneth cells secrete antimicrobial peptides including lysozyme and limit bacterial invasion. Importantly, Paneth cells dysfunction is commonly observed upon deletion of Crohn's disease susceptibility genes including *Atg16l1* [28, 29], *Nod2* [297, 298], *Irgm1* [299], and *Xbp1* [36]. In detail, decreased expression of *Atg16l1* in the intestinal epithelium causes abnormalities in the ultrastructure of Paneth cells with an altered architecture of secretory vesicles loaded with antimicrobial peptides. *Xbp1*-deficient mice have reduced numbers of Paneth cells and remaining Paneth cells contained compressed ER demonstrating the role of ER homeostasis for Paneth cell biology [36]. In addition to Paneth cells, mucin-secreting goblet cells are involved in antimicrobial defense by containing microbes within the intestinal lumen. *Muc2*-deficient mice are highly susceptible to infection [331], emphasizing the critical role of functional goblet cells in antibacterial defense. Interestingly, Goblet cells in IBD patients show decreased *Muc2* expression [332, 333]. Consistent with these observations, we observed decreased *Muc2* expression upon *E. coli* LF82 colonization in the intestine of *Ormdl3*^{-/-} mice compared to WT mice, which might in part explain increased colonization. In this context, characterizing the effect of Goblet cell dysfunction on the structure and thickness of the mucus layer is part of ongoing research. Importantly, functional defects of Paneth and Goblet cells might alter the microbiome in *Ormdl3*^{-/-} and *Ormdl1*^{-/-}*3*^{-/-} mice compared with control animals. Thus, the increased colonization susceptibility in *Ormdl3*-deficient mice might be at least in part due to changes in the microbial composition. Of note, prior to *E. coli* LF82 infection, mice were pre-treated by oral administration of the broad-spectrum antibiotic streptomycin to deplete the commensal intestinal microbiota. Nevertheless, to exclude the effect of an altered gut microbiome composition on bacterial handling, we are currently performing 16S rDNA profiling of *Ormdl3*^{+/+}, *Ormdl3*^{-/-} and *Ormdl1*^{-/-}*3*^{-/-} feces.

Interestingly, defects in highly secretory cells are commonly found in mice deficient in UPR related genes. Deletion of the ER-resident disulfide isomerase anterior gradient 2 (*Agr2*) causes Paneth and

goblet cell dysfunction [41]. Likewise, intestinal deletion of *Xbp1* results in reduced goblet cell numbers accompanied by reduced *Muc2* mRNA levels [36]. While intestinal deletion of *Xbp1*, recently linked to ER biogenesis [334, 335], results in collapsed ER [36], we observed ER dilation in *Ormdl3*^{-/-} and *Ormdl1*^{-/-}*3*^{-/-} mice. Interestingly, knockout of *Atg5* or *Atg7* in pancreatic acinar cells causes dilation of the ER [336, 337]. Thus, the massive expansion of the ER in highly secretory cells of *Ormdl3*^{-/-} and *Ormdl1*^{-/-}*3*^{-/-} mice might rather point to a defect in autophagy than to excessive UPR signaling.

Despite the massive expansion of the ER lumen, we did not detect any signs of elevated ER stress in ileal or colonic tissue of *Ormdl3*^{-/-} or *Ormdl1*^{-/-}*3*^{-/-} mice. On the contrary, we measured reduced levels of ER stress markers in 1-year old *Ormdl3*^{-/-} mice. Remarkably, in yeast, Schuck et al. [338] demonstrated that ER membrane expansion alleviates endoplasmic reticulum stress independently of an increase in ER chaperone levels. Our observations are in strong contrast to previous findings in mice with intestinal deletion of *Atg16l1*, that show ER expansion accompanied by enhanced UPR activation in aged mice. For the UPR component ATF6 α , the ability to trigger ER expansion was reported. This ATF6 α -induced ER expansion is assumed to be dependent on the induction of phospholipid biosynthesis [335]. Likewise, expression of the transcriptionally active form of XBP1 triggers lipid biosynthesis and augments the ER volume [334, 339]. Conversely, defects in *Xbp1* signaling compromise ER membrane expansion during the development of highly secretory cells [340, 341].

In summary, while *Ormdl3*- and *Ormdl1/3*-deficient cells exhibit an expanded ER membrane and volume, they show basal chaperone levels. This finding might suggest that defects in ORMDL signaling uncouples membrane expansion from an increase in ER chaperone levels.

4.2.5 Simultaneous Lack of ORMDL3 and ORMDL1 Causes Severe Motor Defects *in vivo*

We detected a progressive degeneration of the basal ganglia and a diffuse, progressive astrogliosis accompanied by reduced life expectancy in *Ormdl1/3*-deficient mice. However, the exact cause of death in *Ormdl1*^{-/-}*3*^{-/-} mice remains unknown and requires further studies. In line with our previous findings, no upregulation of ER stress markers was detected in brain tissue. Interestingly, deletion of the ER chaperone GRP78 in Purkinje cells causes ER dilatation, growth retardation, motor defects and cerebellar atrophy [342] partially resembling the phenotype of *Ormdl1/3*-deficient animals. Considering the pronounced ER expansion in *Ormdl3*- and *Ormdl1/3*-deficient mice, it is noteworthy that ER shaping and remodeling are proposed to play a fundamental role during development. The great plasticity of the ER is illustrated during the differentiation of B lymphocytes into plasma cells. To handle the enormous folding load during antibody synthesis, differentiating lymphocytes massively expand their ER membrane [343]. In the same way, activation of the cytochrome P450 detoxification in hepatocytes initiates a massive dilatation of the ER membrane [344]. Several proteins are involved in shaping and remodeling the architecture of the ER, which is comprised of ER tubules and sheets. While the reticulon domain-containing proteins (RTNs) and receptor expression enhancing proteins (REEPs) modulate ER tubule formation, cytoskeleton-linking membrane protein 63 (CLIMP63) and family with sequence similarity 134, member B (FAM134B) control ER sheet formation [150, 151, 345, 346]. Several ER-shaping proteins including RTN2, REEP1 and FAM134B have been implicated in neurodegenerative diseases accompanied by the degeneration specific neurons [347, 348]. Deletion of the selective autophagy receptor *Fam134b* in mice causes ER expansion, inhibits ER turnover and ultimately leads to degeneration of sensory neurons [150]. These studies illustrate the importance of a functional ER in neuronal homeostasis and illustrate that ER homeostasis and autophagy are closely intertwined processes.

Accumulation of the autophagy receptor p62 (SQSTM1, sequestosome 1) in several tissues points towards compromised autophagy in *Ormdl3*- and *Ormdl1/3*-deficient mice. Noteworthy, motor defects are often found in *Atg* gene knockout mice that also accumulate the autophagy receptor p62. *Atg5* conditional knockout animals develop progressive deficits in motor function and mice lacking *Atg7* in the central nervous system show abnormal limb-clasping reflexes, reduced motor coordination and die within 28 weeks of birth [300, 301].

4.2.6 *Ormdl3*- & *Ormdl1/3* Deficiency Impairs Autophagy in Intestinal Epithelial Cells

Besides being involved in ER homeostasis, autophagy plays a key role in innate immune defense of the intestine by controlling bacterial interactions. Induction of xenophagy in intestinal epithelial cells represents a host defense mechanism against invading microbes [349]. Several studies provide evidence for a link between autophagy gene mutations and IBD. CD-associated polymorphisms in *NOD2*, *ATG16L1* and *IRGM* affect xenophagy and defects in autophagy impair the ability of intestinal epithelial cells to restrict *E. coli* LF82 replication [67]. Our findings support the notion that the autophagy defects identified in *Ormdl3*- and *Ormdl1/3*-deficient mice might interfere with the ability of the intestinal epithelium to clear invading bacteria such as *E. coli* LF82. Consistent with this idea, in the absence of ORMDL3 or ORMDL1/3, we found elevated susceptibility to *E. coli* LF82 infection *in vitro* using iMEFs, *ex vivo* employing freshly isolated crypts and *in vivo*. Epithelial autophagy is triggered by invasive bacteria such as the *E. coli* LF82 strain used in this study, but also by *S. typhimurium* and *E. faecalis* [349]. In contrast, non-invasive bacteria, such as *Lactobacillus salivarius* do not activate autophagy in intestinal epithelial cells [349]. To monitor autophagic flux, we quantified the conversion of LC3BI to its LC3BII form, as a marker for autophagosome formation. ORMDL-deficient cells revealed a marked reduction in LC3 lipidation upon chemical autophagy induction, starvation and most importantly upon bacterial infection. Our findings strongly suggest that increased susceptibility to bacterial colonization observed in *Ormdl3*-deficient mice is not only attributable to the described defects in Paneth and Goblet cell function but also to defective xenophagy. Another distinctive hallmark of *Atg*-deficient cells is the upregulation of p62 levels and the formation of cytosolic p62 aggregates [301, 350]. p62 becomes incorporated into the autophagosome and is degraded upon autolysosome formation, thus serving as marker for autophagic degradation. Inhibition of autophagy correlates with elevated p62 levels, reflecting the autophagic status [351-353]. Vice versa, decreased p62 levels indicate activation of autophagy. Indeed, lack of ORMDL proteins resulted in increased levels of p62 in several tissues, including the brain, lung and ileum. Similar results were observed using *ex vivo* and cell culture approaches. However, a more detailed analysis will be necessary to exclude transcriptional upregulation or defective proteasomal degradation of p62 under the tested conditions. To determine the extent of p62 oligomerization assessing both the Triton X-100-soluble and -insoluble fraction is necessary [354].

4.2.7 ORMDL Proteins Regulate ER membrane Trafficking

Our findings in *Ormdl3*^{-/-} and *Ormdl1*^{-/-}*3*^{-/-} cells and the corresponding *in vivo* model suggest an important role of the ORMDL protein family in modulating ER turnover. We propose that ORMDL proteins, dependent on the cellular requirements, might trigger selective ER degradation via the autophagic machinery.

Due to this intensive crosstalk between autophagy and the secretory pathway (reviewed in Davis et al. [155]), we hypothesized that ORMDL proteins might not only play a role in autophagy but also in regulating protein trafficking. The function of ORMDL proteins in the secretory pathway is supported

by the detected augmented transport of VSVG-GFP from the ER to the Golgi apparatus in *Ormdl3*- and *Ormdl1/3*-deficient iMEFs compared to wild type cells both under basal and stress conditions. Importantly, considering the lack of enhanced UPR activation in *Ormdl3*- and *Ormdl1/3*-deficient mice, combined with the ER expansion in *Ormdl3*^{-/-} and *Ormdl1*^{-/-}*3*^{-/-} intestinal epithelial cells, our results indicate that proteins of the ORMDL family might act as negative regulators of ER-Golgi trafficking. In *S. cerevisiae*, deletion of the lipid-regulator *OPI1* results in ER expansion accompanied by enhanced protein secretion [338, 355]. Whether enhanced secretion actually is a direct consequence of the enlarged ER in *Ormdl3*- and *Ormdl1/3*-deficient cells needs to be further studied.

The endoplasmic reticulum (ER) is the site of calcium storage, secretory protein and lipid biosynthesis. ER volume and activity must match cellular requirements. Stress conditions such as nutrient deprivation, accumulation of misfolded proteins, and infection trigger ER turnover. ER-phagy describes the selective degradation of the endoplasmic reticulum via the autophagy machinery. ER-phagy receptors engage the cytosolic macroautophagy machinery via LC3 interacting (LIR) regions, which associate with ubiquitin-like, cytosolic proteins of the Atg8/LC3/GABARAP family. Notably, upon autophagy induction, we detected co-localization of ORMDL3 with autophagosomal and lysosomal marker proteins. In line with these findings, overexpressed ORMDL3 interacted with LC3 suggesting the presence of LIR motifs within the amino acid sequence of ORMDL3. Indeed, bioinformatic protein sequence analysis of the ORMDL protein family identified several possible LIR motifs [356]. Remarkably, three of the identified motifs are conserved in all human and murine ORMDL proteins. Two identified possible LIR motifs, starting at amino acid 43 or 101, respectively, exhibit the core consensus sequence [F]xx[I/V]. The third predicted LIR motif, [G/A]-[M/T]-[Y]-[I/V]-[F]-[L], ranges from amino acid 59 to 64. The residues marked in bold (positions 3 and 6) represent the most crucial residues for the interaction with LC3 [356]. In this context, the topology of the ORMDL protein family must be considered. In yeast, transmembrane segment prediction identifies four transmembrane domains [181]. Likewise, Phyre²-based protein sequence analysis of the human and murine ORMDL proteins predicts four membrane-spanning domains [357]. On the contrary, based on experimental evidence, Cantero-Recasens et al. [182] propose a topology model for human ORMDL3 consisting of two transmembrane domains, with the N- and C-terminus facing the cytoplasm and a large loop within the ER lumen. Depending on the topology of ORMDL proteins, the LIR motif ranging from amino acid 101 to 104, which probably localizes in the cytoplasm, might be essential for the interaction with LC3. However, detailed future studies will be required to elucidate the topology and to confirm the functional relevance of the predicted LIR motifs in the ORMDL protein family.

The complex ER structure is comprised of ER tubules and ER sheets characterized by the presence of key proteins involved in ER-shaping and function [358, 359]. For example, CLIMP-63 (microtubule-binding 63 kDa cytoskeleton-linking membrane protein) localizes to ER sheets, while reticulon domain-containing proteins RTN1-4 are mainly found at ER tubules. In mammalian cells, ER subdomains are degraded by selective autophagy, facilitated by specific receptors. The ER-phagy receptor FAM134B, a member of the reticulon-homology-domain-containing FAM134 family, mediates the turnover of ER sheets [150]. In contrast, the long isoform of the reticulon family member RTN3 (RTN3L) functions as a selective receptor for the degradation of ER tubules [151]. SEC62, part of the SEC61 translocon complex [360], facilitates ER-phagy during recovery from ER stress [154]. Recently, CCPG1, an ER-resident transmembrane protein that can bind to Atg8-family proteins and to FIP200 was described as ER-phagy receptor [152]. Remarkably, ER stress induces transcription of *CCPG1* providing a direct connection between ER stress and ER-phagy. *In vivo*, CCPG1 protects against hyper-accumulation of

insoluble proteins within the ER of pancreatic acinar cells [152]. Recently, it was shown the lack of the ER-phagy receptor Rtn3 does not affect the general morphology of the ER [151]. In contrast, in the absence of *Ormdl3* we found a pronounced ER expansion under basal conditions in highly secretory cells illustrating the important role of ORMDL3 in ER homeostasis. Likewise, Khaminets et al. [150] observed ER expansions in *Fam134b*^{-/-} mice at 10 months of age in sensory neurons not present in wild-type controls. Comparably, in *CCPG1*-deficient mice, acinar cells exhibit a dilated ER lumen filled with trapped protein aggregates. Importantly, in strong contrast to our data, the observed ER dilatation in *CCPG1* hypomorphic mice correlated with enhanced UPR activation [152]. Similar to the selective autophagy receptors FAM134B and RTN3, we observed autophagy dependent regulation of ORMDL protein levels. Moreover, the lack of ORMDL proteins impaired starvation induced turnover of the ER sheet marker proteins TRAP α and CLIMP63 and the ER tubules marker RTN4B. Therefore, similar to the described function of FAM134B [150], we propose that ORMDL proteins are crucial for constitutive and starvation-induced ER-phagy.

Our findings support the notion that ORMDL proteins are essential for ER homeostasis *in vitro* and *in vivo*. We propose that ORMDL proteins regulate the fate of ER fragments. The observed direct interaction between ORMDL3 and the autophagic machinery suggests that ORMDL proteins promote the delivery of ER fragments to autophagosomes for lysosomal degradation. However, the molecular mechanism that enables ORMDL proteins to modulate ER-Golgi trafficking is part of ongoing investigations. Absence of ORMDL proteins or lack of oligomeric complexes might alter ER structure facilitating the recruitment of COPII components and directing ER membrane fragments towards the formation of COPII vesicles. Notably, COPII vesicle formation has been shown to be dependent on the lipid composition [361], and thus lipid modifications induced by the presence or absence of ORMDL proteins could affect budding. Alternatively, enlarged ER membrane structures in *Ormdl3*- and *Ormdl1/3*-deficient cells might facilitate COPII vesicle formation, thereby enhancing ER-Golgi trafficking. Likewise, how ORMDL proteins facilitate ER-phagy needs to be explored in more detail. Similar to what has been described for RTN3, clustering of ORMDL proteins might facilitate the fragmentation of ER fragments and their selective degradation. Oligomerization of ORMDL proteins might then recruit the autophagy machinery and direct ER fragments towards ER-phagy. In yeast, Breslow et al. [198] et al described both the formation of homo-oligomers and hetero-oligomeric structures. Likewise, mammalian ORMDLs have been found to generate heteromeric and homomeric complexes [199]. The more pronounced ER expansion in *Ormdl1/3* double deficient mice compared to *Ormdl3*^{-/-} animals implies that both ORMDL1 and ORMDL3 mediate ER-phagy. The function of ORMDL2 in selective ER degradation still needs to be investigated. However, based on the amino acid homology and the presence of similar LIR motifs in all three ORMDL proteins, we assume that ORMDL2 might be equally involved in ER-phagy.

As alternative mechanism, conformational changes could unmask the LIR motif in ORMDL proteins favoring selective ER degradation. Post-translational modification might present another way to regulate the function of ORMDL proteins. Many LIR motifs are preceded by threonine or serine residues and phosphorylation of these amino acids is known to increase LC3 affinity [362, 363].

In conclusion, ORMDL proteins are essential for cellular homeostasis by regulating ER turnover. This is particularly relevant *in vivo*, where lack of ORMDL1 and ORMDL3 impairs autophagic flux, interferes with ER morphology, impairs the structure and function of highly secretory cells and ultimately causes progressive neurodegeneration. Thus, our studies propose a novel function of the ORMDL protein family as regulators of ER fate. While lack of ORMDL proteins enhances ER-Golgi trafficking, our data

suggest that ORMDL proteins might serve as ER-phagy receptors by directly interacting with the autophagic machinery to initiate selective degradation of ER fragments. Thus, future studies are warranted to uncover the molecular regulation of the two proposed opposing functions of ORMDL proteins.

4.3 Conclusions & Future Perspectives

Genome-wide association studies (GWAS) have identified *ORMDL3* as a genetic risk factor of CD and UC [38, 39]. Although impaired bacterial handling is considered to underlie IBD, the role of the IBD risk gene *ORMDL3* in shaping host-microbe interaction has not been addressed so far. This study sheds light on the function of *ORMDL3* in modulating host-microbe interactions and cellular homeostasis in the intestine.

Our *in vivo* studies revealed that *Ormdl3*- and *Ormdl1/3*-deficiency, respectively, impair body growth and simultaneous deletion of *Ormdl1*, *Ormdl2* and *Ormdl3* causes embryonic lethality. Yet, the function of ORMLD proteins in embryonic development and organogenesis remains to be assessed and is subject of ongoing investigation. In this context, conditional knockout models including Tamoxifen-induced deletion of *Ormdl1*, *Ormdl2* and *Ormdl3* and specific deletion of all three *Ormdl* genes in intestinal epithelial cells might represent key tools to determine the function of ORMDL proteins in pre- and postnatal development and to decipher the overlapping functions of the three ORMDL proteins.

This thesis reveals a microbiota-driven transcriptional repression of *Ormdl3* in germ-free-raised mice compared to wild-type mice. *In vitro*, we discovered a repressive effect of TLR4 signaling on the promoter activity of *Ormdl3*. With regard to the transcriptional regulation of *ORMDL3*, little is known and a more detailed analysis of TLR4-regulated *ORMDL3* activity is required.

On a cellular level, lack of *ORMDL3* or *ORMDL1/3* disturbs the structure and homeostasis of highly secretory cell types including Paneth and Goblet cells, thereby compromising mucosal defense. It will be important to elucidate whether the detected reduced *Muc2* expression in *Ormdl3* deficient mice impairs the mucus layer. Of note, functional defects of Paneth and Goblet cells might alter the microbial composition making 16S rDNA profiling of *Ormdl3*^{+/+}, *Ormdl3*^{-/-} and *Ormdl1*^{-/-}*3*^{-/-} feces crucial. In line with impaired function of Paneth and Goblet cells, we find that *Ormdl3*-deficient mice are more susceptible to bacterial colonization. Importantly, we demonstrate that xenophagy is compromised in the absence of *ORMDL3*.

Our findings in *Ormdl3*^{-/-} and *Ormdl1*^{-/-}*3*^{-/-} cells and the corresponding *in vivo* models suggest a role of the ORMDL protein family in modulating ER turnover. Highly secretory cells in the intestine showed a massive dilation of the ER lumen. Surprisingly, at the same time, we did not detect any signs of increased ER stress and UPR activation neither *in vitro* nor *in vivo*. In light of these findings, we propose a possible role of ORMDL proteins in regulating ER turnover. We propose that ORMDL proteins might function as selective ER-phagy receptors directing ER fragments towards the autophagy machinery for degradation. We detected an interaction of *ORMDL3* with the autophagy machinery including LC3. Protein sequence analysis of the ORMDL protein family discovered several possible LIR motifs. However, detailed future studies are necessary to validate the functional relevance of the predicted LIR motifs and to decipher the molecular mechanism of ORMDL-mediated ER turnover. Likewise, the function of *ORMDL2* in ER membrane trafficking has not been explored in this study. Based on the high

amino acid homology and the presence of similar LIR motifs in all three ORMDL proteins, we propose that ORMDL2 is equally involved in ER turnover.

In light of impaired ER-phagy and xenophagy in the absence of ORMDL3, future studies might elucidate the possible crosstalk of ER-phagy and xenophagy. Strikingly, ER-phagy is induced by bacteria [364] and both xenophagy and ER-phagy engage the autophagic core machinery. Up to now, ATG7, ATG14, ATG16L1, BCN1, and FIP200 have been shown to be required for bacterial-induced ER-phagy [364]. ORMDL proteins may function as ER sensors detecting specific stress conditions such as bacterial infection. In turn, ORMDL proteins might trigger bacterial-induced ER-phagy.

In conclusion, ORMDL proteins are important for cellular homeostasis by modulating ER membrane trafficking. *In vivo*, lack of ORMDL1 and ORMDL3 compromises autophagic flux, affects the ER morphology and function of highly secretory cells and impairs bacterial handling. Thus, we discover a crucial role of ORMDL proteins in shaping host-microbe interactions by regulating ER turnover and cellular homeostasis in the intestine.

5 Summary

The endoplasmic reticulum (ER) provides a critical environment for secretory protein folding pivotal for maintaining cellular homeostasis. The accumulation of unfolded or misfolded proteins within the ER provokes ER stress, which in turn induces the unfolded protein response (UPR) mediated by ATF6 α and the two transmembrane protein kinases PERK and IRE1 α . Remarkably, the UPR is closely intertwined with autophagy and bacterial sensing and increasing evidence has emerged that the so far identified IBD risk genes converge in these interconnected pathways.

Noteworthy, ER stress and UPR activation are commonly found characteristics of the intestinal epithelium of IBD patients. However, while the modulation of the PERK and the IRE1 pathway of the UPR and their function in intestinal inflammation have been extensively explored, the regulation of ATF6 α signaling has remained poorly understood. Deciphering the mechanisms of physiological ATF6 α signaling is key not only to our understanding of ATF6 α signaling in intestinal inflammation but also to identify targets enabling the modulation of the ATF6 α pathway. In *Chapter 3* of this study, we elucidate the regulation of ATF6 α signaling using a stringent high-throughput siRNA screening approach targeting the human druggable genome. RNAi screening identified 15 suppressors and 7 activators of ATF6 α signaling. We identified the regulatory subunit of the casein kinase 2 (CSNK2B) as inducer of ATF6 α signaling. Our data suggests that CSNK2B mediates its effect on the ATF6 α pathway upstream of the ATF6 α cleavage event at the Golgi complex. Our data implies that CSNK2B facilitates the transport of ATF6 α from the ER to the Golgi apparatus by promoting COPII vesicle formation. Moreover, we identified the acyl-CoA synthetase long chain family member 1 (ACSL1) as activator of the ATF6 α pathway. We detected co-localization of ATF6 α and ACSL1 and mechanistic studies imply that ACSL1 facilitates ATF6 α signaling independently from the cleavage event at the Golgi complex. Remarkably, we show that impairment in either UPR or autophagy function in intestinal epithelial cells results in the compensatory upregulation of ATF6 α signaling. Our findings indicate that hyperactivation of the ATF6 α branch functions as compensatory mechanism in intestinal epithelial cells with impaired autophagy or defective UPR signaling. Notably, we detected ATF6 α mediated activation of NF- κ B signaling along with enhanced *Tnfa* expression. Thus, interfering with hyperactive ATF6 α signaling via inhibition of the identified ATF6 α signaling inducers ACSL1 and CSNK2B might represent a suitable pharmacological approach in intestinal inflammation.

In *Chapter 4* of this study, the role of ORMDL3 in intestinal homeostasis is examined. ORMDL3, which localizes to the ER, has been suggested to control various cellular processes including the UPR. Genome-wide association studies (GWAS) have identified *ORMDL3* as a genetic risk factor for IBD. While the inability to control intestinal bacteria is considered to underlie IBD, the role of ORMDL3 in shaping host-microbe interaction is unclear. This study sheds light on the role of ORMDL3 in bacterial handling. We find that *Ormdl3*-deficient mice are more susceptible to adherent-invasive *E. coli* colonization. Notably, the lack of ORMDL3 affects the structure and function of highly secretory cell types including Paneth and Goblet cells, thereby compromising mucosal defense mechanisms. We show that xenophagy, essential for limiting bacterial replication, is impaired in the absence of ORMDL3. Vice versa, this thesis reveals a microbiota-driven transcriptional repression of *Ormdl3* in germ free raised mice compared to wild type mice. *In vitro*, we discovered a repressive effect of TLR4 signaling on the promoter activity of *Ormdl3*.

In vivo, we demonstrate that *Ormdl3* and *Ormdl1/3* deficiency affects body growth and that simultaneous deletion of *Ormdl1*, *Ormdl2* and *Ormdl3* causes embryonic lethality. Remarkably, highly

secretory cells in the intestine of *Ormdl3* and *Ormdl1^{-/-}3^{-/-}* mice exhibit a massive dilation of the ER lumen implicating a role of ORMDL proteins in regulating ER turnover. Strikingly, no signs of elevated ER stress and UPR activation were detected neither *in vitro* nor *in vivo*. Instead, we observed increased ER-Golgi trafficking and impaired degradation of ER fragments in the absence of ORMDL1 and ORMDL3. In light of these findings, we propose that ORMDL proteins might function as selective ER-phagy receptors directing ER fragments towards lysosomal degradation.

Collectively, the findings of this thesis underline the extensive crosstalk between the UPR and autophagy. Both pathways and their synergistic interactions within the intestinal epithelium are essential for cellular homeostasis. Insights provided in this study may contribute to the development of new therapeutic approaches in IBD.

6 Zusammenfassung

Im Endoplasmatischen Retikulum (ER) findet die Faltung von Transmembran- und sekretorischen Proteinen statt. Damit ist das ER entscheidend an der Aufrechterhaltung der zellulären Homöostase beteiligt. Die Anhäufung von falsch- oder nicht gefalteten Proteinen innerhalb des ER löst sogenannten ER Stress aus, der wiederum die *unfolded protein response* (UPR) Signalwege aktiviert. Die Aktivierung des UPRs erfolgt über ATF6 α und die beiden Kinasen PERK und IRE1 α . Dabei ist der UPR eng mit der Autophagie und der Detektion von Bakterien verknüpft. Interessanterweise zeigten Forschungsergebnisse der letzten Jahre, dass zahlreiche CED (chronisch entzündliche Darmerkrankungen) Risikogene an diesen Signalwegen beteiligt sind.

ER Stress und die Aktivierung der UPR finden sich charakteristischerweise im intestinalen Epithel von CED Patienten. Während die Regulation des PERK- und des IRE1-Zweiges der UPR sowie deren Funktion in intestinalen Entzündungsprozessen intensiv untersucht wurden, ist über die Regulation des ATF6 α Signalweges relativ wenig bekannt.

Dabei kommt der Entschlüsselung der Regulation des ATF6 α Signalweges sowie dessen Beteiligung an Entzündungsvorgängen im intestinalen Epithel eine Schlüsselrolle zu. Ein besseres Verständnis dieses Signalweges und dessen regulatorischen Komponenten könnte außerdem ein Eingreifen in diesen Signalweg ermöglichen. In *Kapitel 3* dieser Arbeit werden die Ergebnisse des hier durchgeführten siRNA Screens vorgestellt, dessen Ziel es war, Aktivatoren und Repressoren des ATF6 α Signalweges zu identifizieren. Mit Hilfe dieses Screens konnten wir 15 Inhibitoren sowie 7 Aktivatoren des ATF6 α Signalweges identifizieren. Unter anderem wurde die regulatorische Untereinheit der Casein Kinase 2 (CSNK2B) als Aktivator des ATF6 α Signalweges identifiziert. Die hier gewonnenen Ergebnisse legen nahe, dass CSNK2B die COPII Vesikelbildung erleichtert und damit den Transport von ATF6 α vom ER zum Golgi-Apparat fördert. Des Weiteren wurde ACSL1 (*acyl-CoA synthetase long chain family member 1*) als Aktivator des ATF6 α Signalweges entdeckt. Wir konnten eine Kolo-kalisation von ATF6 α und ACSL1 beobachten und weiterführenden Analysen deuten darauf hin, dass ACSL1 unabhängig von der Spaltung von ATF6 am Golgi-Apparat diesen Signalweg beeinflusst. Darüber hinaus konnten wir zeigen, dass eine Beeinträchtigung der UPR oder der Autophagie in intestinalen Epithelzellen zu einer kompensatorischen Heraufregulation des jeweils anderen Signalweges führt. Unsere Ergebnisse deuten darauf hin, dass die Hyperaktivierung des ATF6 α Signalwegs einen kompensatorischen Mechanismus darstellt, der aktiv wird, wenn entweder der Autophagieprozess eingeschränkt ist oder einer der beiden anderen UPR Zweige beeinträchtigt ist. Außerdem konnten wir zeigen, dass der ATF6 α Zweig der UPR zur Aktivierung von NF- κ B führt, wodurch die Synthese von proinflammatorischen Zytokinen wie TNF α induziert wird. Aufgrund dieser Beobachtungen könnte die Eindämmung der Hyperaktivierung des ATF6 α Signalweges durch die Inhibition der positiven Regulatoren ACSL1 und CSNK2B einen möglichen therapeutischen Ansatz bei der Behandlung von CED darstellen.

In *Kapitel 4* dieser Arbeit wird die Funktion von ORMDL3 in der Homöostase des intestinalen Epithels untersucht. ORMDL3, lokalisiert in der ER Membran, wurde bereits mit der Regulation zahlreicher zellulärer Prozesse wie der UPR in Verbindung gebracht. Außerdem wurde ORMDL3 in Genomweiten Assoziationsstudien (GWAS) als Risikogen für die Entstehung von CED identifiziert. Als eine der Ursachen für die Entstehung von CED wird eine gestörte Immunantwort auf das Mikrobiom diskutiert. Dabei wurde bisher nie untersucht, welche Funktion ORMDL3 bei der Interaktion zwischen dem Wirt und dessen Mikrobiom spielt. In dieser Arbeit wurde die Rolle von ORMDL3 im Umgang und der Kontrolle des Mikrobioms näher untersucht. Wir konnten zeigen, dass *Ormdl3*-defiziente Mäuse

anfälliger für eine Besiedelung mit einem adhärenen *E. coli* Stamm sind. Die Abwesenheit von ORMDL3 schädigt die Struktur und Funktion von sekretorischen Zellen wie Paneth und Goblet Zellen, wodurch wiederum antibakterielle Abwehrmechanismen beeinträchtigt sind. Interessanterweise konnten wir durch den Vergleich der *Ormdl3* Expression von konventionell und keimfrei gehaltenen Mäusen beobachten, dass die Expression von *Ormdl3* durch das Mikrobiom unterdrückt wird. *In vitro* beobachteten wir eine repressive Wirkung des TLR4 Signalweges auf die Expression von *Ormdl3*.

Unsere Daten zeigen außerdem, dass eine Defizienz in *Ormdl3* oder ein gleichzeitiges Fehlen von *Ormdl1* und *Ormdl3* das Körperwachstum beeinträchtigt. Darüber hinaus stellten wir fest, dass eine gleichzeitige Deletion von *Ormdl1*, *Ormdl2* und *Ormdl3* embryonal lethal ist. Interessanterweise wiesen die sekretorischen Zellen im Darm der *Ormdl3*^{-/-} und der *Ormdl1*^{-/-}*Ormdl3*^{-/-} Mäuse eine massive Expansion des ER Lumens auf. Überraschenderweise zeigten die Tiere aber keine Zeichen von erhöhtem ER Stress oder gesteigerter UPR Aktivierung. Dagegen konnten wir eine erhöhte Proteintransportrate vom ER zum Golgi-Apparat und gleichzeitig einen gestörten Abbau von ER Fragmenten beobachten. In Anbetracht dieser Ergebnisse vermuten wir, dass ORMDL Proteine als selektive Rezeptoren fungieren, die ER Fragmente dem Autophagieprozess zuführen.

Zusammenfassend illustrieren die Ergebnisse dieser Arbeit die intensiven Überschneidungen, die zwischen der UPR und Autophagie stattfinden. Beide Signalwege sowie deren synergistische Interaktion innerhalb des intestinalen Epithels sind entscheidend an der Aufrechterhaltung der zellulären Homöostase beteiligt. Die in dieser Arbeit vorgestellten Erkenntnisse könnten zur Entwicklung neuer Therapiestrategien bei der Behandlung von CED beitragen.

7 References

1. Kaser, A., S. Zeissig, and R.S. Blumberg, *Inflammatory bowel disease*. *Annu Rev Immunol*, 2010. **28**: p. 573-621.
2. Spekhorst, L.M., et al., *Performance of the Montreal classification for inflammatory bowel diseases*. *World J Gastroenterol*, 2014. **20**(41): p. 15374-81.
3. Podolsky, D.K., *Inflammatory bowel disease*. *N Engl J Med*, 2002. **347**(6): p. 417-29.
4. Bandzar, S., S. Gupta, and M.O. Platt, *Crohn's disease: a review of treatment options and current research*. *Cell Immunol*, 2013. **286**(1-2): p. 45-52.
5. Sandborn, W.J., et al., *Vedolizumab as induction and maintenance therapy for Crohn's disease*. *N Engl J Med*, 2013. **369**(8): p. 711-21.
6. Colombel, J.F., et al., *Adalimumab induces deep remission in patients with Crohn's disease*. *Clin Gastroenterol Hepatol*, 2014. **12**(3): p. 414-22 e5.
7. Colombel, J.F., et al., *Infliximab, azathioprine, or combination therapy for Crohn's disease*. *N Engl J Med*, 2010. **362**(15): p. 1383-95.
8. Cosnes, J., et al., *Epidemiology and natural history of inflammatory bowel diseases*. *Gastroenterology*, 2011. **140**(6): p. 1785-94.
9. Molodecky, N.A., et al., *Increasing incidence and prevalence of the inflammatory bowel diseases with time, based on systematic review*. *Gastroenterology*, 2012. **142**(1): p. 46-54 e42; quiz e30.
10. Thia, K.T., et al., *An update on the epidemiology of inflammatory bowel disease in Asia*. *Am J Gastroenterol*, 2008. **103**(12): p. 3167-82.
11. Franke, A., et al., *Genome-wide association study for ulcerative colitis identifies risk loci at 7q22 and 22q13 (IL17REL)*. *Nat Genet*, 2010. **42**(4): p. 292-4.
12. Franke, A., et al., *Genome-wide meta-analysis increases to 71 the number of confirmed Crohn's disease susceptibility loci*. *Nat Genet*, 2010. **42**(12): p. 1118-25.
13. Anderson, C.A., et al., *Meta-analysis identifies 29 additional ulcerative colitis risk loci, increasing the number of confirmed associations to 47*. *Nat Genet*, 2011. **43**(3): p. 246-52.
14. Jostins, L., et al., *Host-microbe interactions have shaped the genetic architecture of inflammatory bowel disease*. *Nature*, 2012. **491**(7422): p. 119-24.
15. Khor, B., A. Gardet, and R.J. Xavier, *Genetics and pathogenesis of inflammatory bowel disease*. *Nature*, 2011. **474**(7351): p. 307-17.
16. Halme, L., et al., *Family and twin studies in inflammatory bowel disease*. *World J Gastroenterol*, 2006. **12**(23): p. 3668-72.
17. Thompson, N.P., et al., *Genetics versus environment in inflammatory bowel disease: results of a British twin study*. *BMJ*, 1996. **312**(7023): p. 95-6.
18. Yang, H., et al., *Familial empirical risks for inflammatory bowel disease: differences between Jews and non-Jews*. *Gut*, 1993. **34**(4): p. 517-24.
19. Orholm, M., et al., *Concordance of inflammatory bowel disease among Danish twins. Results of a nationwide study*. *Scand J Gastroenterol*, 2000. **35**(10): p. 1075-81.
20. Halfvarson, J., et al., *Inflammatory bowel disease in a Swedish twin cohort: a long-term follow-up of concordance and clinical characteristics*. *Gastroenterology*, 2003. **124**(7): p. 1767-73.
21. Hugot, J.P., et al., *Association of NOD2 leucine-rich repeat variants with susceptibility to Crohn's disease*. *Nature*, 2001. **411**(6837): p. 599-603.
22. Ogura, Y., et al., *A frameshift mutation in NOD2 associated with susceptibility to Crohn's disease*. *Nature*, 2001. **411**(6837): p. 603-6.
23. Travassos, L.H., et al., *Nod1 and Nod2 direct autophagy by recruiting ATG16L1 to the plasma membrane at the site of bacterial entry*. *Nat Immunol*, 2010. **11**(1): p. 55-62.
24. Hampe, J., et al., *A genome-wide association scan of nonsynonymous SNPs identifies a susceptibility variant for Crohn disease in ATG16L1*. *Nat Genet*, 2007. **39**(2): p. 207-11.

25. Rioux, J.D., et al., *Genome-wide association study identifies new susceptibility loci for Crohn disease and implicates autophagy in disease pathogenesis*. Nat Genet, 2007. **39**(5): p. 596-604.
26. Wellcome Trust Case Control, C., *Genome-wide association study of 14,000 cases of seven common diseases and 3,000 shared controls*. Nature, 2007. **447**(7145): p. 661-78.
27. Murthy, A., et al., *A Crohn's disease variant in Atg16l1 enhances its degradation by caspase 3*. Nature, 2014. **506**(7489): p. 456-62.
28. Cadwell, K., et al., *A key role for autophagy and the autophagy gene Atg16l1 in mouse and human intestinal Paneth cells*. Nature, 2008. **456**(7219): p. 259-63.
29. Lassen, K.G., et al., *Atg16L1 T300A variant decreases selective autophagy resulting in altered cytokine signaling and decreased antibacterial defense*. Proc Natl Acad Sci U S A, 2014. **111**(21): p. 7741-6.
30. McCarroll, S.A., et al., *Deletion polymorphism upstream of IRGM associated with altered IRGM expression and Crohn's disease*. Nat Genet, 2008. **40**(9): p. 1107-12.
31. Parkes, M., et al., *Sequence variants in the autophagy gene IRGM and multiple other replicating loci contribute to Crohn's disease susceptibility*. Nat Genet, 2007. **39**(7): p. 830-2.
32. Singh, S.B., et al., *Human IRGM induces autophagy to eliminate intracellular mycobacteria*. Science, 2006. **313**(5792): p. 1438-41.
33. Brest, P., et al., *A synonymous variant in IRGM alters a binding site for miR-196 and causes deregulation of IRGM-dependent xenophagy in Crohn's disease*. Nat Genet, 2011. **43**(3): p. 242-5.
34. Ellinghaus, D., et al., *Association between variants of PRDM1 and NDP52 and Crohn's disease, based on exome sequencing and functional studies*. Gastroenterology, 2013. **145**(2): p. 339-47.
35. Adolph, T.E., et al., *Paneth cells as a site of origin for intestinal inflammation*. Nature, 2013. **503**(7475): p. 272-6.
36. Kaser, A., et al., *XBP1 links ER stress to intestinal inflammation and confers genetic risk for human inflammatory bowel disease*. Cell, 2008. **134**(5): p. 743-56.
37. Zheng, W., et al., *Evaluation of AGR2 and AGR3 as candidate genes for inflammatory bowel disease*. Genes Immun, 2006. **7**(1): p. 11-8.
38. Barrett, J.C., et al., *Genome-wide association defines more than 30 distinct susceptibility loci for Crohn's disease*. Nat Genet, 2008. **40**(8): p. 955-62.
39. McGovern, D.P., et al., *Genome-wide association identifies multiple ulcerative colitis susceptibility loci*. Nat Genet, 2010. **42**(4): p. 332-7.
40. Moffatt, M.F., et al., *Genetic variants regulating ORMDL3 expression contribute to the risk of childhood asthma*. Nature, 2007. **448**(7152): p. 470-3.
41. Zhao, F., et al., *Disruption of Paneth and goblet cell homeostasis and increased endoplasmic reticulum stress in Agr2^{-/-} mice*. Dev Biol, 2010. **338**(2): p. 270-9.
42. Ott, S.J., et al., *Reduction in diversity of the colonic mucosa associated bacterial microflora in patients with active inflammatory bowel disease*. Gut, 2004. **53**(5): p. 685-93.
43. Wu, G.D., et al., *Linking long-term dietary patterns with gut microbial enterotypes*. Science, 2011. **334**(6052): p. 105-8.
44. David, L.A., et al., *Diet rapidly and reproducibly alters the human gut microbiome*. Nature, 2014. **505**(7484): p. 559-63.
45. Castiglione, F., et al., *Risk factors for inflammatory bowel diseases according to the "hygiene hypothesis": a case-control, multi-centre, prospective study in Southern Italy*. J Crohns Colitis, 2012. **6**(3): p. 324-9.
46. Timm, S., et al., *Place of upbringing in early childhood as related to inflammatory bowel diseases in adulthood: a population-based cohort study in Northern Europe*. Eur J Epidemiol, 2014. **29**(6): p. 429-37.
47. Ni, J., et al., *Gut microbiota and IBD: causation or correlation?* Nat Rev Gastroenterol Hepatol, 2017. **14**(10): p. 573-584.

48. Manichanh, C., et al., *The gut microbiota in IBD*. Nat Rev Gastroenterol Hepatol, 2012. **9**(10): p. 599-608.
49. Wlodarska, M., A.D. Kostic, and R.J. Xavier, *An integrative view of microbiome-host interactions in inflammatory bowel diseases*. Cell Host Microbe, 2015. **17**(5): p. 577-91.
50. Kostic, A.D., R.J. Xavier, and D. Gevers, *The microbiome in inflammatory bowel disease: current status and the future ahead*. Gastroenterology, 2014. **146**(6): p. 1489-99.
51. Kaur, N., et al., *Intestinal dysbiosis in inflammatory bowel disease*. Gut Microbes, 2011. **2**(4): p. 211-6.
52. Sokol, H., et al., *Low counts of Faecalibacterium prausnitzii in colitis microbiota*. Inflamm Bowel Dis, 2009. **15**(8): p. 1183-9.
53. Willing, B., et al., *Twin studies reveal specific imbalances in the mucosa-associated microbiota of patients with ileal Crohn's disease*. Inflamm Bowel Dis, 2009. **15**(5): p. 653-60.
54. Llopis, M., et al., *Lactobacillus casei downregulates commensals' inflammatory signals in Crohn's disease mucosa*. Inflamm Bowel Dis, 2009. **15**(2): p. 275-83.
55. Issa, M., et al., *Impact of Clostridium difficile on inflammatory bowel disease*. Clin Gastroenterol Hepatol, 2007. **5**(3): p. 345-51.
56. Thomson, J.M., et al., *Enterohepatic helicobacter in ulcerative colitis: potential pathogenic entities?* PLoS One, 2011. **6**(2): p. e17184.
57. Kaakoush, N.O., H.M. Mitchell, and S.M. Man, *Role of emerging Campylobacter species in inflammatory bowel diseases*. Inflamm Bowel Dis, 2014. **20**(11): p. 2189-97.
58. Darfeuille-Michaud, A., et al., *High prevalence of adherent-invasive Escherichia coli associated with ileal mucosa in Crohn's disease*. Gastroenterology, 2004. **127**(2): p. 412-21.
59. Darfeuille-Michaud, A., et al., *Presence of adherent Escherichia coli strains in ileal mucosa of patients with Crohn's disease*. Gastroenterology, 1998. **115**(6): p. 1405-13.
60. Miquel, S., et al., *Complete genome sequence of Crohn's disease-associated adherent-invasive E. coli strain LF82*. PLoS One, 2010. **5**(9).
61. Nash, J.H., et al., *Genome sequence of adherent-invasive Escherichia coli and comparative genomic analysis with other E. coli pathotypes*. BMC Genomics, 2010. **11**: p. 667.
62. Conte, M.P., et al., *Adherent-invasive Escherichia coli (AIEC) in pediatric Crohn's disease patients: phenotypic and genetic pathogenic features*. BMC Res Notes, 2014. **7**: p. 748.
63. Hornef, M., *Pathogens, Commensal Symbionts, and Pathobionts: Discovery and Functional Effects on the Host*. ILAR J, 2015. **56**(2): p. 159-62.
64. Boudeau, J., et al., *Invasive ability of an Escherichia coli strain isolated from the ileal mucosa of a patient with Crohn's disease*. Infect Immun, 1999. **67**(9): p. 4499-509.
65. Darfeuille-Michaud, A., *Adherent-invasive Escherichia coli: a putative new E. coli pathotype associated with Crohn's disease*. Int J Med Microbiol, 2002. **292**(3-4): p. 185-93.
66. Bringer, M.A., et al., *Replication of Crohn's disease-associated AIEC within macrophages is dependent on TNF-alpha secretion*. Lab Invest, 2012. **92**(3): p. 411-9.
67. Lapaquette, P., M.A. Bringer, and A. Darfeuille-Michaud, *Defects in autophagy favour adherent-invasive Escherichia coli persistence within macrophages leading to increased pro-inflammatory response*. Cell Microbiol, 2012. **14**(6): p. 791-807.
68. De la Fuente, M., et al., *Escherichia coli isolates from inflammatory bowel diseases patients survive in macrophages and activate NLRP3 inflammasome*. Int J Med Microbiol, 2014. **304**(3-4): p. 384-92.
69. Agus, A., et al., *Understanding host-adherent-invasive Escherichia coli interaction in Crohn's disease: opening up new therapeutic strategies*. Biomed Res Int, 2014. **2014**: p. 567929.
70. Carvalho, F.A., et al., *Crohn's disease adherent-invasive Escherichia coli colonize and induce strong gut inflammation in transgenic mice expressing human CEACAM*. J Exp Med, 2009. **206**(10): p. 2179-89.
71. Small, C.L., et al., *Persistent infection with Crohn's disease-associated adherent-invasive Escherichia coli leads to chronic inflammation and intestinal fibrosis*. Nat Commun, 2013. **4**: p. 1957.

72. Drouet, M., et al., *AIEC colonization and pathogenicity: influence of previous antibiotic treatment and preexisting inflammation*. *Inflamm Bowel Dis*, 2012. **18**(10): p. 1923-31.
73. Nguyen, H.T., et al., *Crohn's disease-associated adherent invasive Escherichia coli modulate levels of microRNAs in intestinal epithelial cells to reduce autophagy*. *Gastroenterology*, 2014. **146**(2): p. 508-19.
74. Lapaquette, P., et al., *Crohn's disease-associated adherent-invasive E. coli are selectively favoured by impaired autophagy to replicate intracellularly*. *Cell Microbiol*, 2010. **12**(1): p. 99-113.
75. Homer, C.R., et al., *ATG16L1 and NOD2 interact in an autophagy-dependent antibacterial pathway implicated in Crohn's disease pathogenesis*. *Gastroenterology*, 2010. **139**(5): p. 1630-41, 1641 e1-2.
76. Clapham, D.E., *Calcium signaling*. *Cell*, 2007. **131**(6): p. 1047-58.
77. Fagone, P. and S. Jackowski, *Membrane phospholipid synthesis and endoplasmic reticulum function*. *J Lipid Res*, 2009. **50 Suppl**: p. S311-6.
78. Hamasaki, M., et al., *Autophagosomes form at ER-mitochondria contact sites*. *Nature*, 2013. **495**(7441): p. 389-93.
79. Sevier, C.S. and C.A. Kaiser, *Formation and transfer of disulphide bonds in living cells*. *Nat Rev Mol Cell Biol*, 2002. **3**(11): p. 836-47.
80. Tu, B.P. and J.S. Weissman, *Oxidative protein folding in eukaryotes: mechanisms and consequences*. *J Cell Biol*, 2004. **164**(3): p. 341-6.
81. Saibil, H., *Chaperone machines for protein folding, unfolding and disaggregation*. *Nat Rev Mol Cell Biol*, 2013. **14**(10): p. 630-42.
82. Schroder, M. and R.J. Kaufman, *The mammalian unfolded protein response*. *Annu Rev Biochem*, 2005. **74**: p. 739-89.
83. Lee, C. and J. Goldberg, *Structure of coatamer cage proteins and the relationship among COPI, COPII, and clathrin vesicle coats*. *Cell*, 2010. **142**(1): p. 123-32.
84. Sato, K. and A. Nakano, *Mechanisms of COPII vesicle formation and protein sorting*. *FEBS Lett*, 2007. **581**(11): p. 2076-82.
85. Barlowe, C., et al., *COPII: a membrane coat formed by Sec proteins that drive vesicle budding from the endoplasmic reticulum*. *Cell*, 1994. **77**(6): p. 895-907.
86. Walter, P. and D. Ron, *The unfolded protein response: from stress pathway to homeostatic regulation*. *Science*, 2011. **334**(6059): p. 1081-6.
87. Zhang, K. and R.J. Kaufman, *From endoplasmic-reticulum stress to the inflammatory response*. *Nature*, 2008. **454**(7203): p. 455-62.
88. Cox, J.S., C.E. Shamu, and P. Walter, *Transcriptional induction of genes encoding endoplasmic reticulum resident proteins requires a transmembrane protein kinase*. *Cell*, 1993. **73**(6): p. 1197-206.
89. Tirasophon, W., A.A. Welihinda, and R.J. Kaufman, *A stress response pathway from the endoplasmic reticulum to the nucleus requires a novel bifunctional protein kinase/endoribonuclease (Ire1p) in mammalian cells*. *Genes Dev*, 1998. **12**(12): p. 1812-24.
90. Wang, X.Z., et al., *Cloning of mammalian Ire1 reveals diversity in the ER stress responses*. *EMBO J*, 1998. **17**(19): p. 5708-17.
91. Korennykh, A.V., et al., *The unfolded protein response signals through high-order assembly of Ire1*. *Nature*, 2009. **457**(7230): p. 687-93.
92. Yoshida, H., et al., *XBP1 mRNA is induced by ATF6 and spliced by IRE1 in response to ER stress to produce a highly active transcription factor*. *Cell*, 2001. **107**(7): p. 881-91.
93. Lee, A.H., N.N. Iwakoshi, and L.H. Glimcher, *XBP-1 regulates a subset of endoplasmic reticulum resident chaperone genes in the unfolded protein response*. *Mol Cell Biol*, 2003. **23**(21): p. 7448-59.
94. Hassler, J.R., et al., *The IRE1alpha/XBP1s Pathway Is Essential for the Glucose Response and Protection of beta Cells*. *PLoS Biol*, 2015. **13**(10): p. e1002277.

95. Hollien, J. and J.S. Weissman, *Decay of endoplasmic reticulum-localized mRNAs during the unfolded protein response*. Science, 2006. **313**(5783): p. 104-7.
96. Bertolotti, A., et al., *Dynamic interaction of BiP and ER stress transducers in the unfolded-protein response*. Nat Cell Biol, 2000. **2**(6): p. 326-32.
97. Harding, H.P., Y. Zhang, and D. Ron, *Protein translation and folding are coupled by an endoplasmic-reticulum-resident kinase*. Nature, 1999. **397**(6716): p. 271-4.
98. Harding, H.P., et al., *An integrated stress response regulates amino acid metabolism and resistance to oxidative stress*. Mol Cell, 2003. **11**(3): p. 619-33.
99. Vattem, K.M. and R.C. Wek, *Reinitiation involving upstream ORFs regulates ATF4 mRNA translation in mammalian cells*. Proc Natl Acad Sci U S A, 2004. **101**(31): p. 11269-74.
100. Harding, H.P., et al., *Regulated translation initiation controls stress-induced gene expression in mammalian cells*. Mol Cell, 2000. **6**(5): p. 1099-108.
101. Palam, L.R., T.D. Baird, and R.C. Wek, *Phosphorylation of eIF2 facilitates ribosomal bypass of an inhibitory upstream ORF to enhance CHOP translation*. J Biol Chem, 2011. **286**(13): p. 10939-49.
102. Song, B., et al., *Chop deletion reduces oxidative stress, improves beta cell function, and promotes cell survival in multiple mouse models of diabetes*. J Clin Invest, 2008. **118**(10): p. 3378-89.
103. Marciniak, S.J., et al., *CHOP induces death by promoting protein synthesis and oxidation in the stressed endoplasmic reticulum*. Genes Dev, 2004. **18**(24): p. 3066-77.
104. Haze, K., et al., *Mammalian transcription factor ATF6 is synthesized as a transmembrane protein and activated by proteolysis in response to endoplasmic reticulum stress*. Mol Biol Cell, 1999. **10**(11): p. 3787-99.
105. Shen, J. and R. Prywes, *ER stress signaling by regulated proteolysis of ATF6*. Methods, 2005. **35**(4): p. 382-9.
106. Wu, J., et al., *ATF6alpha optimizes long-term endoplasmic reticulum function to protect cells from chronic stress*. Dev Cell, 2007. **13**(3): p. 351-64.
107. Yamamoto, K., et al., *Transcriptional induction of mammalian ER quality control proteins is mediated by single or combined action of ATF6alpha and XBP1*. Dev Cell, 2007. **13**(3): p. 365-76.
108. Yoshida, H., et al., *Identification of the cis-acting endoplasmic reticulum stress response element responsible for transcriptional induction of mammalian glucose-regulated proteins. Involvement of basic leucine zipper transcription factors*. J Biol Chem, 1998. **273**(50): p. 33741-9.
109. Yoshida, H., et al., *ATF6 activated by proteolysis binds in the presence of NF-Y (CBF) directly to the cis-acting element responsible for the mammalian unfolded protein response*. Mol Cell Biol, 2000. **20**(18): p. 6755-67.
110. Martindale, J.J., et al., *Endoplasmic reticulum stress gene induction and protection from ischemia/reperfusion injury in the hearts of transgenic mice with a tamoxifen-regulated form of ATF6*. Circ Res, 2006. **98**(9): p. 1186-93.
111. Adachi, Y., et al., *ATF6 is a transcription factor specializing in the regulation of quality control proteins in the endoplasmic reticulum*. Cell Struct Funct, 2008. **33**(1): p. 75-89.
112. Bernales, S., K.L. McDonald, and P. Walter, *Autophagy counterbalances endoplasmic reticulum expansion during the unfolded protein response*. PLoS Biol, 2006. **4**(12): p. e423.
113. Deuring, J.J., et al., *Genomic ATG16L1 risk allele-restricted Paneth cell ER stress in quiescent Crohn's disease*. Gut, 2014. **63**(7): p. 1081-91.
114. Diamanti, M.A., et al., *IKKalpha controls ATG16L1 degradation to prevent ER stress during inflammation*. J Exp Med, 2017. **214**(2): p. 423-437.
115. Kouroku, Y., et al., *ER stress (PERK/eIF2alpha phosphorylation) mediates the polyglutamine-induced LC3 conversion, an essential step for autophagy formation*. Cell Death Differ, 2007. **14**(2): p. 230-9.

116. Ogata, M., et al., *Autophagy is activated for cell survival after endoplasmic reticulum stress*. Mol Cell Biol, 2006. **26**(24): p. 9220-31.
117. Schrader, E.K., K.G. Harstad, and A. Matouschek, *Targeting proteins for degradation*. Nat Chem Biol, 2009. **5**(11): p. 815-22.
118. Kaur, J. and J. Debnath, *Autophagy at the crossroads of catabolism and anabolism*. Nat Rev Mol Cell Biol, 2015. **16**(8): p. 461-72.
119. Mizushima, N., T. Yoshimori, and Y. Ohsumi, *The role of Atg proteins in autophagosome formation*. Annu Rev Cell Dev Biol, 2011. **27**: p. 107-32.
120. Mizushima, N., et al., *Autophagy fights disease through cellular self-digestion*. Nature, 2008. **451**(7182): p. 1069-75.
121. Cuervo, A.M. and E. Wong, *Chaperone-mediated autophagy: roles in disease and aging*. Cell Res, 2014. **24**(1): p. 92-104.
122. Wang, C.W. and D.J. Klionsky, *The molecular mechanism of autophagy*. Mol Med, 2003. **9**(3-4): p. 65-76.
123. Lucocq, J. and D. Walker, *Evidence for fusion between multilamellar endosomes and autophagosomes in HeLa cells*. Eur J Cell Biol, 1997. **72**(4): p. 307-13.
124. Stromhaug, P.E., et al., *Purification and characterization of autophagosomes from rat hepatocytes*. Biochem J, 1998. **335** (Pt 2): p. 217-24.
125. Eskelinen, E.L., *Maturation of autophagic vacuoles in Mammalian cells*. Autophagy, 2005. **1**(1): p. 1-10.
126. Lamb, C.A., T. Yoshimori, and S.A. Tooze, *The autophagosome: origins unknown, biogenesis complex*. Nat Rev Mol Cell Biol, 2013. **14**(12): p. 759-74.
127. Levine, B., N. Mizushima, and H.W. Virgin, *Autophagy in immunity and inflammation*. Nature, 2011. **469**(7330): p. 323-35.
128. Mizushima, N., et al., *A protein conjugation system essential for autophagy*. Nature, 1998. **395**(6700): p. 395-8.
129. Hanada, T., et al., *The Atg12-Atg5 conjugate has a novel E3-like activity for protein lipidation in autophagy*. J Biol Chem, 2007. **282**(52): p. 37298-302.
130. Hemelaar, J., et al., *A single protease, Apg4B, is specific for the autophagy-related ubiquitin-like proteins GATE-16, MAP1-LC3, GABARAP, and Apg8L*. J Biol Chem, 2003. **278**(51): p. 51841-50.
131. Tanida, I., T. Ueno, and E. Kominami, *LC3 conjugation system in mammalian autophagy*. Int J Biochem Cell Biol, 2004. **36**(12): p. 2503-18.
132. Kabeya, Y., et al., *LC3, a mammalian homologue of yeast Apg8p, is localized in autophagosomal membranes after processing*. EMBO J, 2000. **19**(21): p. 5720-8.
133. Klionsky, D.J. and S.D. Emr, *Autophagy as a regulated pathway of cellular degradation*. Science, 2000. **290**(5497): p. 1717-21.
134. Klionsky, D.J., et al., *Guidelines for the use and interpretation of assays for monitoring autophagy (3rd edition)*. Autophagy, 2016. **12**(1): p. 1-222.
135. Hanna, R.A., et al., *Microtubule-associated protein 1 light chain 3 (LC3) interacts with Bnip3 protein to selectively remove endoplasmic reticulum and mitochondria via autophagy*. J Biol Chem, 2012. **287**(23): p. 19094-104.
136. Korac, J., et al., *Ubiquitin-independent function of optineurin in autophagic clearance of protein aggregates*. J Cell Sci, 2013. **126**(Pt 2): p. 580-92.
137. Kraft, C., et al., *Mature ribosomes are selectively degraded upon starvation by an autophagy pathway requiring the Ubp3p/Bre5p ubiquitin protease*. Nat Cell Biol, 2008. **10**(5): p. 602-10.
138. Mochida, K., et al., *Receptor-mediated selective autophagy degrades the endoplasmic reticulum and the nucleus*. Nature, 2015. **522**(7556): p. 359-62.
139. Pankiv, S., et al., *p62/SQSTM1 binds directly to Atg8/LC3 to facilitate degradation of ubiquitinated protein aggregates by autophagy*. J Biol Chem, 2007. **282**(33): p. 24131-45.
140. Thurston, T.L., et al., *Galectin 8 targets damaged vesicles for autophagy to defend cells against bacterial invasion*. Nature, 2012. **482**(7385): p. 414-8.

141. Rogov, V., et al., *Interactions between autophagy receptors and ubiquitin-like proteins form the molecular basis for selective autophagy*. Mol Cell, 2014. **53**(2): p. 167-78.
142. Stolz, A., A. Ernst, and I. Dikic, *Cargo recognition and trafficking in selective autophagy*. Nat Cell Biol, 2014. **16**(6): p. 495-501.
143. Kirkin, V., et al., *A role for ubiquitin in selective autophagy*. Mol Cell, 2009. **34**(3): p. 259-69.
144. Watson, R.O., P.S. Manzanillo, and J.S. Cox, *Extracellular M. tuberculosis DNA targets bacteria for autophagy by activating the host DNA-sensing pathway*. Cell, 2012. **150**(4): p. 803-15.
145. Manzanillo, P.S., et al., *The ubiquitin ligase parkin mediates resistance to intracellular pathogens*. Nature, 2013. **501**(7468): p. 512-6.
146. Delgado, M.A., et al., *Toll-like receptors control autophagy*. EMBO J, 2008. **27**(7): p. 1110-21.
147. Huang, J. and J.H. Brummel, *Bacteria-autophagy interplay: a battle for survival*. Nat Rev Microbiol, 2014. **12**(2): p. 101-14.
148. Wurzer, B., et al., *Oligomerization of p62 allows for selection of ubiquitinated cargo and isolation membrane during selective autophagy*. Elife, 2015. **4**: p. e08941.
149. Chargui, A., et al., *Subversion of autophagy in adherent invasive Escherichia coli-infected neutrophils induces inflammation and cell death*. PLoS One, 2012. **7**(12): p. e51727.
150. Khaminets, A., et al., *Regulation of endoplasmic reticulum turnover by selective autophagy*. Nature, 2015. **522**(7556): p. 354-8.
151. Grumati, P., et al., *Full length RTN3 regulates turnover of tubular endoplasmic reticulum via selective autophagy*. Elife, 2017. **6**.
152. Smith, M.D., et al., *CCPG1 Is a Non-canonical Autophagy Cargo Receptor Essential for ER-Phagy and Pancreatic ER Proteostasis*. Dev Cell, 2018. **44**(2): p. 217-232 e11.
153. Schuck, S., C.M. Gallagher, and P. Walter, *ER-phagy mediates selective degradation of endoplasmic reticulum independently of the core autophagy machinery*. J Cell Sci, 2014. **127**(Pt 18): p. 4078-88.
154. Fumagalli, F., et al., *Translocon component Sec62 acts in endoplasmic reticulum turnover during stress recovery*. Nat Cell Biol, 2016. **18**(11): p. 1173-1184.
155. Davis, S., J. Wang, and S. Ferro-Novick, *Crosstalk between the Secretory and Autophagy Pathways Regulates Autophagosome Formation*. Dev Cell, 2017. **41**(1): p. 23-32.
156. Joo, J.H., et al., *The Noncanonical Role of ULK/ATG1 in ER-to-Golgi Trafficking Is Essential for Cellular Homeostasis*. Mol Cell, 2016. **62**(4): p. 491-506.
157. Zoppino, F.C., et al., *Autophagosome formation depends on the small GTPase Rab1 and functional ER exit sites*. Traffic, 2010. **11**(9): p. 1246-61.
158. Kihara, A., et al., *Two distinct Vps34 phosphatidylinositol 3-kinase complexes function in autophagy and carboxypeptidase Y sorting in Saccharomyces cerevisiae*. J Cell Biol, 2001. **152**(3): p. 519-30.
159. Budovskaya, Y.V., et al., *The Ras/cAMP-dependent protein kinase signaling pathway regulates an early step of the autophagy process in Saccharomyces cerevisiae*. J Biol Chem, 2004. **279**(20): p. 20663-71.
160. Chan, E.Y. and S.A. Tooze, *Evolution of Atg1 function and regulation*. Autophagy, 2009. **5**(6): p. 758-65.
161. Cadwell, K., et al., *Virus-plus-susceptibility gene interaction determines Crohn's disease gene Atg16L1 phenotypes in intestine*. Cell, 2010. **141**(7): p. 1135-45.
162. Bogaert, S., et al., *Involvement of endoplasmic reticulum stress in inflammatory bowel disease: a different implication for colonic and ileal disease?* PLoS One, 2011. **6**(10): p. e25589.
163. Sato, T., et al., *Paneth cells constitute the niche for Lgr5 stem cells in intestinal crypts*. Nature, 2011. **469**(7330): p. 415-8.
164. Ayabe, T., et al., *Secretion of microbicidal alpha-defensins by intestinal Paneth cells in response to bacteria*. Nat Immunol, 2000. **1**(2): p. 113-8.
165. Hansson, G.C., *Role of mucus layers in gut infection and inflammation*. Curr Opin Microbiol, 2012. **15**(1): p. 57-62.

166. Olszak, T., et al., *Protective mucosal immunity mediated by epithelial CD1d and IL-10*. Nature, 2014. **509**(7501): p. 497-502.
167. Cao, S.S., et al., *The unfolded protein response and chemical chaperones reduce protein misfolding and colitis in mice*. Gastroenterology, 2013. **144**(5): p. 989-1000 e6.
168. Liu, B., et al., *Essential roles of grp94 in gut homeostasis via chaperoning canonical Wnt pathway*. Proc Natl Acad Sci U S A, 2013. **110**(17): p. 6877-82.
169. Brandl, K., et al., *Enhanced sensitivity to DSS colitis caused by a hypomorphic Mbtps1 mutation disrupting the ATF6-driven unfolded protein response*. Proc Natl Acad Sci U S A, 2009. **106**(9): p. 3300-5.
170. Llarena, M., et al., *Different mechanisms of recognition and ER retention by transmembrane transcription factors CREB-H and ATF6*. Traffic, 2010. **11**(1): p. 48-69.
171. Cao, S.S., et al., *Phosphorylation of eIF2alpha is dispensable for differentiation but required at a posttranscriptional level for paneth cell function and intestinal homeostasis in mice*. Inflamm Bowel Dis, 2014. **20**(4): p. 712-22.
172. Namba, T., et al., *Positive role of CCAAT/enhancer-binding protein homologous protein, a transcription factor involved in the endoplasmic reticulum stress response in the development of colitis*. Am J Pathol, 2009. **174**(5): p. 1786-98.
173. Zhang, K., et al., *The unfolded protein response sensor IRE1alpha is required at 2 distinct steps in B cell lymphopoiesis*. J Clin Invest, 2005. **115**(2): p. 268-81.
174. Iwawaki, T., et al., *Function of IRE1 alpha in the placenta is essential for placental development and embryonic viability*. Proc Natl Acad Sci U S A, 2009. **106**(39): p. 16657-62.
175. Tsuru, A., et al., *Negative feedback by IRE1beta optimizes mucin production in goblet cells*. Proc Natl Acad Sci U S A, 2013. **110**(8): p. 2864-9.
176. Martino, M.B., et al., *The ER stress transducer IRE1beta is required for airway epithelial mucin production*. Mucosal Immunol, 2013. **6**(3): p. 639-54.
177. Bertolotti, A., et al., *Increased sensitivity to dextran sodium sulfate colitis in IRE1beta-deficient mice*. J Clin Invest, 2001. **107**(5): p. 585-93.
178. Wang, Z., Y. Hao, and A.W. Lowe, *The adenocarcinoma-associated antigen, AGR2, promotes tumor growth, cell migration, and cellular transformation*. Cancer Res, 2008. **68**(2): p. 492-7.
179. Tschurtschenthaler, M., et al., *Defective ATG16L1-mediated removal of IRE1alpha drives Crohn's disease-like ileitis*. J Exp Med, 2017. **214**(2): p. 401-422.
180. Zhang, Q., et al., *Commensal bacteria direct selective cargo sorting to promote symbiosis*. Nat Immunol, 2015. **16**(9): p. 918-26.
181. Hjelmqvist, L., et al., *ORMDL proteins are a conserved new family of endoplasmic reticulum membrane proteins*. Genome Biol, 2002. **3**(6): p. RESEARCH0027.
182. Cantero-Recasens, G., et al., *The asthma-associated ORMDL3 gene product regulates endoplasmic reticulum-mediated calcium signaling and cellular stress*. Hum Mol Genet, 2010. **19**(1): p. 111-21.
183. Hsu, K.J. and S.E. Turvey, *Functional analysis of the impact of ORMDL3 expression on inflammation and activation of the unfolded protein response in human airway epithelial cells*. Allergy Asthma Clin Immunol, 2013. **9**(1): p. 4.
184. Barrett, J.C., et al., *Genome-wide association study and meta-analysis find that over 40 loci affect risk of type 1 diabetes*. Nat Genet, 2009. **41**(6): p. 703-7.
185. Kurreeman, F.A., et al., *Use of a multiethnic approach to identify rheumatoid- arthritis-susceptibility loci, 1p36 and 17q12*. Am J Hum Genet, 2012. **90**(3): p. 524-32.
186. Dobbins, S.E., et al., *Allergy and glioma risk: test of association by genotype*. Int J Cancer, 2011. **128**(7): p. 1736-40.
187. Tomita, K., et al., *Variants in the 17q21 asthma susceptibility locus are associated with allergic rhinitis in the Japanese population*. Allergy, 2013. **68**(1): p. 92-100.
188. Hirschfield, G.M., et al., *Variants at IRF5-TNPO3, 17q12-21 and MMEL1 are associated with primary biliary cirrhosis*. Nat Genet, 2010. **42**(8): p. 655-7.

189. Laukens, D., et al., *Evidence for significant overlap between common risk variants for Crohn's disease and ankylosing spondylitis*. PLoS One, 2010. **5**(11): p. e13795.
190. Levy, D., et al., *Genome-wide association study of blood pressure and hypertension*. Nat Genet, 2009. **41**(6): p. 677-87.
191. Han, S., et al., *Orm1 and Orm2 are conserved endoplasmic reticulum membrane proteins regulating lipid homeostasis and protein quality control*. Proc Natl Acad Sci U S A, 2010. **107**(13): p. 5851-6.
192. Miller, M., et al., *ORMDL3 is an inducible lung epithelial gene regulating metalloproteases, chemokines, OAS, and ATF6*. Proc Natl Acad Sci U S A, 2012. **109**(41): p. 16648-53.
193. Mekahli, D., et al., *Endoplasmic-reticulum calcium depletion and disease*. Cold Spring Harb Perspect Biol, 2011. **3**(6).
194. Brini, M., et al., *The plasma membrane calcium pump in health and disease*. FEBS J, 2013. **280**(21): p. 5385-97.
195. Miller, M., et al., *ORMDL3 transgenic mice have increased airway remodeling and airway responsiveness characteristic of asthma*. J Immunol, 2014. **192**(8): p. 3475-87.
196. Carreras-Sureda, A., et al., *ORMDL3 modulates store-operated calcium entry and lymphocyte activation*. Hum Mol Genet, 2013. **22**(3): p. 519-30.
197. Maceyka, M. and S. Spiegel, *Sphingolipid metabolites in inflammatory disease*. Nature, 2014. **510**(7503): p. 58-67.
198. Breslow, D.K., et al., *Orm family proteins mediate sphingolipid homeostasis*. Nature, 2010. **463**(7284): p. 1048-53.
199. Kiefer, K., et al., *Coordinated regulation of the orosomucoid-like gene family expression controls de novo ceramide synthesis in mammalian cells*. J Biol Chem, 2015. **290**(5): p. 2822-30.
200. Siow, D., et al., *ORMDL/serine palmitoyltransferase stoichiometry determines effects of ORMDL3 expression on sphingolipid biosynthesis*. J Lipid Res, 2015. **56**(4): p. 898-908.
201. Siow, D.L. and B.W. Wattenberg, *Mammalian ORMDL proteins mediate the feedback response in ceramide biosynthesis*. J Biol Chem, 2012. **287**(48): p. 40198-204.
202. Sims, K., et al., *Kdo2-lipid A, a TLR4-specific agonist, induces de novo sphingolipid biosynthesis in RAW264.7 macrophages, which is essential for induction of autophagy*. J Biol Chem, 2010. **285**(49): p. 38568-79.
203. Harvald, E.B., A.S. Olsen, and N.J. Faergeman, *Autophagy in the light of sphingolipid metabolism*. Apoptosis, 2015. **20**(5): p. 658-70.
204. Ma, X., et al., *ORMDL3 contributes to the risk of atherosclerosis in Chinese Han population and mediates oxidized low-density lipoprotein-induced autophagy in endothelial cells*. Sci Rep, 2015. **5**: p. 17194.
205. Wang, S., et al., *ORMDL orosomucoid-like proteins are degraded by free-cholesterol-loading-induced autophagy*. Proc Natl Acad Sci U S A, 2015. **112**(12): p. 3728-33.
206. Dang, J., et al., *ORMDL3 Facilitates the Survival of Splenic B Cells via an ATF6alpha-Endoplasmic Reticulum Stress-Beclin1 Autophagy Regulatory Pathway*. J Immunol, 2017. **199**(5): p. 1647-1659.
207. Gade, P., et al., *An IFN-gamma-stimulated ATF6-C/EBP-beta-signaling pathway critical for the expression of Death Associated Protein Kinase 1 and induction of autophagy*. Proc Natl Acad Sci U S A, 2012. **109**(26): p. 10316-21.
208. Zalckvar, E., et al., *DAP-kinase-mediated phosphorylation on the BH3 domain of beclin 1 promotes dissociation of beclin 1 from Bcl-XL and induction of autophagy*. EMBO Rep, 2009. **10**(3): p. 285-92.
209. Heazlewood, C.K., et al., *Aberrant mucin assembly in mice causes endoplasmic reticulum stress and spontaneous inflammation resembling ulcerative colitis*. PLoS Med, 2008. **5**(3): p. e54.
210. Shkoda, A., et al., *Interleukin-10 blocked endoplasmic reticulum stress in intestinal epithelial cells: impact on chronic inflammation*. Gastroenterology, 2007. **132**(1): p. 190-207.

211. Treton, X., et al., *Altered endoplasmic reticulum stress affects translation in inactive colon tissue from patients with ulcerative colitis*. *Gastroenterology*, 2011. **141**(3): p. 1024-35.
212. Deuring, J.J., et al., *Absence of ABCG2-mediated mucosal detoxification in patients with active inflammatory bowel disease is due to impeded protein folding*. *Biochem J*, 2012. **441**(1): p. 87-93.
213. Sato, T., et al., *Single Lgr5 stem cells build crypt-villus structures in vitro without a mesenchymal niche*. *Nature*, 2009. **459**(7244): p. 262-5.
214. Sato, T. and H. Clevers, *Growing self-organizing mini-guts from a single intestinal stem cell: mechanism and applications*. *Science*, 2013. **340**(6137): p. 1190-4.
215. Fujii, S., et al., *PGE2 is a direct and robust mediator of anion/fluid secretion by human intestinal epithelial cells*. *Sci Rep*, 2016. **6**: p. 36795.
216. Miyoshi, H. and T.S. Stappenbeck, *In vitro expansion and genetic modification of gastrointestinal stem cells in spheroid culture*. *Nat Protoc*, 2013. **8**(12): p. 2471-82.
217. Mullis, K.B. and F.A. Faloona, *Specific synthesis of DNA in vitro via a polymerase-catalyzed chain reaction*. *Methods Enzymol*, 1987. **155**: p. 335-50.
218. Lowry, O.H., et al., *Protein measurement with the Folin phenol reagent*. *J Biol Chem*, 1951. **193**(1): p. 265-75.
219. Schmidt, H., et al., *Enrichment and analysis of secretory lysosomes from lymphocyte populations*. *BMC Immunol*, 2009. **10**: p. 41.
220. Dutta, B., et al., *An interactive web-based application for Comprehensive Analysis of RNAi-screen Data*. *Nat Commun*, 2016. **7**: p. 10578.
221. Yu, G., et al., *clusterProfiler: an R package for comparing biological themes among gene clusters*. *OMICS*, 2012. **16**(5): p. 284-7.
222. Smidt, K., et al., *SLC30A3 responds to glucose- and zinc variations in beta-cells and is critical for insulin production and in vivo glucose-metabolism during beta-cell stress*. *PLoS One*, 2009. **4**(5): p. e5684.
223. Schwab, M.E., *Functions of Nogo proteins and their receptors in the nervous system*. *Nat Rev Neurosci*, 2010. **11**(12): p. 799-811.
224. Dixon, S.J., et al., *Ferroptosis: an iron-dependent form of nonapoptotic cell death*. *Cell*, 2012. **149**(5): p. 1060-72.
225. Wang, Y., et al., *Activation of ATF6 and an ATF6 DNA binding site by the endoplasmic reticulum stress response*. *J Biol Chem*, 2000. **275**(35): p. 27013-20.
226. Mao, W., et al., *Cardiomyocyte apoptosis in autoimmune cardiomyopathy: mediated via endoplasmic reticulum stress and exaggerated by norepinephrine*. *Am J Physiol Heart Circ Physiol*, 2007. **293**(3): p. H1636-45.
227. Schindler, A.J. and R. Schekman, *In vitro reconstitution of ER-stress induced ATF6 transport in COPII vesicles*. *Proc Natl Acad Sci U S A*, 2009. **106**(42): p. 17775-80.
228. Koreishi, M., et al., *CK2 phosphorylates Sec31 and regulates ER-To-Golgi trafficking*. *PLoS One*, 2013. **8**(1): p. e54382.
229. Kramer, A., et al., *Small molecules intercept Notch signaling and the early secretory pathway*. *Nat Chem Biol*, 2013. **9**(11): p. 731-8.
230. Niederreiter, L., et al., *ER stress transcription factor Xbp1 suppresses intestinal tumorigenesis and directs intestinal stem cells*. *J Exp Med*, 2013. **210**(10): p. 2041-56.
231. Liu, T., et al., *NF-kappaB signaling in inflammation*. *Signal Transduct Target Ther*, 2017. **2**.
232. Rana, T.M., *Illuminating the silence: understanding the structure and function of small RNAs*. *Nat Rev Mol Cell Biol*, 2007. **8**(1): p. 23-36.
233. Boutros, M. and J. Ahringer, *The art and design of genetic screens: RNA interference*. *Nat Rev Genet*, 2008. **9**(7): p. 554-66.
234. Grimm, S., *The art and design of genetic screens: mammalian culture cells*. *Nat Rev Genet*, 2004. **5**(3): p. 179-89.
235. Adamson, B., et al., *A Multiplexed Single-Cell CRISPR Screening Platform Enables Systematic Dissection of the Unfolded Protein Response*. *Cell*, 2016. **167**(7): p. 1867-1882 e21.

236. Muller, P., et al., *Identification of JAK/STAT signalling components by genome-wide RNA interference*. *Nature*, 2005. **436**(7052): p. 871-5.
237. Lipinski, S., et al., *RNAi screening identifies mediators of NOD2 signaling: implications for spatial specificity of MDP recognition*. *Proc Natl Acad Sci U S A*, 2012. **109**(52): p. 21426-31.
238. Friedman, A. and N. Perrimon, *A functional RNAi screen for regulators of receptor tyrosine kinase and ERK signalling*. *Nature*, 2006. **444**(7116): p. 230-4.
239. Echeverri, C.J., et al., *Minimizing the risk of reporting false positives in large-scale RNAi screens*. *Nat Methods*, 2006. **3**(10): p. 777-9.
240. Birmingham, A., et al., *3' UTR seed matches, but not overall identity, are associated with RNAi off-targets*. *Nat Methods*, 2006. **3**(3): p. 199-204.
241. Ma, Y., et al., *Prevalence of off-target effects in Drosophila RNA interference screens*. *Nature*, 2006. **443**(7109): p. 359-63.
242. Sledz, C.A. and B.R. Williams, *RNA interference and double-stranded-RNA-activated pathways*. *Biochem Soc Trans*, 2004. **32**(Pt 6): p. 952-6.
243. Judge, A.D., et al., *Sequence-dependent stimulation of the mammalian innate immune response by synthetic siRNA*. *Nat Biotechnol*, 2005. **23**(4): p. 457-62.
244. Kim, J.H., T.M. Lewin, and R.A. Coleman, *Expression and characterization of recombinant rat Acyl-CoA synthetases 1, 4, and 5. Selective inhibition by triacsin C and thiazolidinediones*. *J Biol Chem*, 2001. **276**(27): p. 24667-73.
245. Van Horn, C.G., et al., *Characterization of recombinant long-chain rat acyl-CoA synthetase isoforms 3 and 6: identification of a novel variant of isoform 6*. *Biochemistry*, 2005. **44**(5): p. 1635-42.
246. Yamamoto, K., et al., *Induction of liver steatosis and lipid droplet formation in ATF6alpha-knockout mice burdened with pharmacological endoplasmic reticulum stress*. *Mol Biol Cell*, 2010. **21**(17): p. 2975-86.
247. Singh, A.B., et al., *SREBP2 Activation Induces Hepatic Long-chain Acyl-CoA Synthetase 1 (ACSL1) Expression in Vivo and in Vitro through a Sterol Regulatory Element (SRE) Motif of the ACSL1 C-promoter*. *J Biol Chem*, 2016. **291**(10): p. 5373-84.
248. Faust, M., et al., *Localization of individual subunits of protein kinase CK2 to the endoplasmic reticulum and to the Golgi apparatus*. *Mol Cell Biochem*, 2001. **227**(1-2): p. 73-80.
249. Pinna, L.A. and J.E. Allende, *Protein kinase CK2 in health and disease: Protein kinase CK2: an ugly duckling in the kinome pond*. *Cell Mol Life Sci*, 2009. **66**(11-12): p. 1795-9.
250. Hanif, I.M., et al., *Casein Kinase II: an attractive target for anti-cancer drug design*. *Int J Biochem Cell Biol*, 2010. **42**(10): p. 1602-5.
251. Cozza, G., F. Meggio, and S. Moro, *The dark side of protein kinase CK2 inhibition*. *Curr Med Chem*, 2011. **18**(19): p. 2867-84.
252. Wang, G., et al., *CK2 signaling in androgen-dependent and -independent prostate cancer*. *J Cell Biochem*, 2006. **99**(2): p. 382-91.
253. Hosoi, T., et al., *Inhibition of casein kinase 2 modulates XBP1-GRP78 arm of unfolded protein responses in cultured glial cells*. *PLoS One*, 2012. **7**(6): p. e40144.
254. Manni, S., et al., *Protein kinase CK2 protects multiple myeloma cells from ER stress-induced apoptosis and from the cytotoxic effect of HSP90 inhibition through regulation of the unfolded protein response*. *Clin Cancer Res*, 2012. **18**(7): p. 1888-900.
255. Sarno, S., et al., *Selectivity of 4,5,6,7-tetrabromobenzotriazole, an ATP site-directed inhibitor of protein kinase CK2 ('casein kinase-2')*. *FEBS Lett*, 2001. **496**(1): p. 44-8.
256. Palmiter, R.D. and L. Huang, *Efflux and compartmentalization of zinc by members of the SLC30 family of solute carriers*. *Pflugers Arch*, 2004. **447**(5): p. 744-51.
257. Palmiter, R.D., et al., *ZnT-3, a putative transporter of zinc into synaptic vesicles*. *Proc Natl Acad Sci U S A*, 1996. **93**(25): p. 14934-9.
258. Rawson, R.B., *The site-2 protease*. *Biochim Biophys Acta*, 2013. **1828**(12): p. 2801-7.
259. Angebault, C., et al., *Recessive Mutations in RTN4IP1 Cause Isolated and Syndromic Optic Neuropathies*. *Am J Hum Genet*, 2015. **97**(5): p. 754-60.

260. Venkatesh, K., et al., *The Nogo-66 receptor homolog NgR2 is a sialic acid-dependent receptor selective for myelin-associated glycoprotein*. J Neurosci, 2005. **25**(4): p. 808-22.
261. Wang, K.C., et al., *Oligodendrocyte-myelin glycoprotein is a Nogo receptor ligand that inhibits neurite outgrowth*. Nature, 2002. **417**(6892): p. 941-4.
262. Murayama, K.S., et al., *Reticulons RTN3 and RTN4-B/C interact with BACE1 and inhibit its ability to produce amyloid beta-protein*. Eur J Neurosci, 2006. **24**(5): p. 1237-44.
263. Niederost, B., et al., *Nogo-A and myelin-associated glycoprotein mediate neurite growth inhibition by antagonistic regulation of RhoA and Rac1*. J Neurosci, 2002. **22**(23): p. 10368-76.
264. Fournier, A.E., B.T. Takizawa, and S.M. Strittmatter, *Rho kinase inhibition enhances axonal regeneration in the injured CNS*. J Neurosci, 2003. **23**(4): p. 1416-23.
265. Lehmann, M., et al., *Inactivation of Rho signaling pathway promotes CNS axon regeneration*. J Neurosci, 1999. **19**(17): p. 7537-47.
266. Yu, J.X., L. Chao, and J. Chao, *Prostasin is a novel human serine proteinase from seminal fluid. Purification, tissue distribution, and localization in prostate gland*. J Biol Chem, 1994. **269**(29): p. 18843-8.
267. Costa, F.P., et al., *Prostasin, a potential tumor marker in ovarian cancer--a pilot study*. Clinics (Sao Paulo), 2009. **64**(7): p. 641-4.
268. Vallet, V., et al., *An epithelial serine protease activates the amiloride-sensitive sodium channel*. Nature, 1997. **389**(6651): p. 607-10.
269. Uchimura, K., et al., *The serine protease prostaticin regulates hepatic insulin sensitivity by modulating TLR4 signalling*. Nat Commun, 2014. **5**: p. 3428.
270. Nakamura, K., et al., *[Inhibitory effects of sepimostat mesilate (FUT-187) on the activities of trypsin-like serine proteases in vitro]*. Yakugaku Zasshi, 1995. **115**(3): p. 201-12.
271. Maekawa, A., et al., *Camostat mesilate inhibits prostaticin activity and reduces blood pressure and renal injury in salt-sensitive hypertension*. J Hypertens, 2009. **27**(1): p. 181-9.
272. Amodeo, G.F., et al., *Charged residues distribution modulates selectivity of the open state of human isoforms of the voltage dependent anion-selective channel*. PLoS One, 2014. **9**(8): p. e103879.
273. Cheng, E.H., et al., *VDAC2 inhibits BAK activation and mitochondrial apoptosis*. Science, 2003. **301**(5632): p. 513-7.
274. Roy, S.S., et al., *VDAC2 is required for truncated BID-induced mitochondrial apoptosis by recruiting BAK to the mitochondria*. EMBO Rep, 2009. **10**(12): p. 1341-7.
275. Szabadkai, G., et al., *Chaperone-mediated coupling of endoplasmic reticulum and mitochondrial Ca²⁺ channels*. J Cell Biol, 2006. **175**(6): p. 901-11.
276. De Stefani, D., et al., *VDAC1 selectively transfers apoptotic Ca²⁺ signals to mitochondria*. Cell Death Differ, 2012. **19**(2): p. 267-73.
277. Lee, K., J. Kerner, and C.L. Hoppel, *Mitochondrial carnitine palmitoyltransferase 1a (CPT1a) is part of an outer membrane fatty acid transfer complex*. J Biol Chem, 2011. **286**(29): p. 25655-62.
278. Yagoda, N., et al., *RAS-RAF-MEK-dependent oxidative cell death involving voltage-dependent anion channels*. Nature, 2007. **447**(7146): p. 864-8.
279. Wang, Y.Q., et al., *The Protective Role of Mitochondrial Ferritin on Erastin-Induced Ferroptosis*. Front Aging Neurosci, 2016. **8**: p. 308.
280. Hasler, R., et al., *Uncoupling of mucosal gene regulation, mRNA splicing and adherent microbiota signatures in inflammatory bowel disease*. Gut, 2017. **66**(12): p. 2087-2097.
281. Palmieri, O., et al., *Systematic analysis of circadian genes using genome-wide cDNA microarrays in the inflammatory bowel disease transcriptome*. Chronobiol Int, 2015. **32**(7): p. 903-16.
282. Koch, S., et al., *Protein kinase CK2 is a critical regulator of epithelial homeostasis in chronic intestinal inflammation*. Mucosal Immunol, 2013. **6**(1): p. 136-45.
283. Pahl, H.L. and P.A. Baeuerle, *Expression of influenza virus hemagglutinin activates transcription factor NF-kappa B*. J Virol, 1995. **69**(3): p. 1480-4.

284. Meyer, M., et al., *Hepatitis B virus transactivator MHBst: activation of NF-kappa B, selective inhibition by antioxidants and integral membrane localization*. EMBO J, 1992. **11**(8): p. 2991-3001.
285. Urano, F., et al., *Coupling of stress in the ER to activation of JNK protein kinases by transmembrane protein kinase IRE1*. Science, 2000. **287**(5453): p. 664-6.
286. Hu, P., et al., *Autocrine tumor necrosis factor alpha links endoplasmic reticulum stress to the membrane death receptor pathway through IRE1alpha-mediated NF-kappaB activation and down-regulation of TRAF2 expression*. Mol Cell Biol, 2006. **26**(8): p. 3071-84.
287. Deng, J., et al., *Translational repression mediates activation of nuclear factor kappa B by phosphorylated translation initiation factor 2*. Mol Cell Biol, 2004. **24**(23): p. 10161-8.
288. Tam, A.B., et al., *ER stress activates NF-kappaB by integrating functions of basal IKK activity, IRE1 and PERK*. PLoS One, 2012. **7**(10): p. e45078.
289. Nakajima, S., et al., *Selective abrogation of BiP/GRP78 blunts activation of NF-kappaB through the ATF6 branch of the UPR: involvement of C/EBPbeta and mTOR-dependent dephosphorylation of Akt*. Mol Cell Biol, 2011. **31**(8): p. 1710-8.
290. Yamazaki, H., et al., *Activation of the Akt-NF-kappaB pathway by subtilase cytotoxin through the ATF6 branch of the unfolded protein response*. J Immunol, 2009. **183**(2): p. 1480-7.
291. McElhinny, J.A., et al., *Casein kinase II phosphorylates I kappa B alpha at S-283, S-289, S-293, and T-291 and is required for its degradation*. Mol Cell Biol, 1996. **16**(3): p. 899-906.
292. Romieu-Mourez, R., et al., *Protein kinase CK2 promotes aberrant activation of nuclear factor-kappaB, transformed phenotype, and survival of breast cancer cells*. Cancer Res, 2002. **62**(22): p. 6770-8.
293. Coleman, O.I., et al., *Activated ATF6 Induces Intestinal Dysbiosis and Innate Immune Response to Promote Colorectal Tumorigenesis*. Gastroenterology, 2018.
294. Levin, A.D., M.E. Wildenberg, and G.R. van den Brink, *Mechanism of Action of Anti-TNF Therapy in Inflammatory Bowel Disease*. J Crohns Colitis, 2016. **10**(8): p. 989-97.
295. Pan, W.H., et al., *Exposure to the gut microbiota drives distinct methylome and transcriptome changes in intestinal epithelial cells during postnatal development*. Genome Med, 2018. **10**(1): p. 27.
296. Sommer, F., et al., *Site-specific programming of the host epithelial transcriptome by the gut microbiota*. Genome Biol, 2015. **16**: p. 62.
297. Ramanan, D., et al., *Bacterial sensor Nod2 prevents inflammation of the small intestine by restricting the expansion of the commensal Bacteroides vulgatus*. Immunity, 2014. **41**(2): p. 311-24.
298. VanDussen, K.L., et al., *Genetic variants synthesize to produce paneth cell phenotypes that define subtypes of Crohn's disease*. Gastroenterology, 2014. **146**(1): p. 200-9.
299. Liu, B., et al., *Irgm1-deficient mice exhibit Paneth cell abnormalities and increased susceptibility to acute intestinal inflammation*. Am J Physiol Gastrointest Liver Physiol, 2013. **305**(8): p. G573-84.
300. Hara, T., et al., *Suppression of basal autophagy in neural cells causes neurodegenerative disease in mice*. Nature, 2006. **441**(7095): p. 885-9.
301. Komatsu, M., et al., *Loss of autophagy in the central nervous system causes neurodegeneration in mice*. Nature, 2006. **441**(7095): p. 880-4.
302. Liang, C.C., et al., *Neural-specific deletion of FIP200 leads to cerebellar degeneration caused by increased neuronal death and axon degeneration*. J Biol Chem, 2010. **285**(5): p. 3499-509.
303. Crosnier, C., D. Stamataki, and J. Lewis, *Organizing cell renewal in the intestine: stem cells, signals and combinatorial control*. Nat Rev Genet, 2006. **7**(5): p. 349-59.
304. Kaser, A. and R.S. Blumberg, *Autophagy, microbial sensing, endoplasmic reticulum stress, and epithelial function in inflammatory bowel disease*. Gastroenterology, 2011. **140**(6): p. 1738-47.

305. Cote, F., J.F. Collard, and J.P. Julien, *Progressive neuronopathy in transgenic mice expressing the human neurofilament heavy gene: a mouse model of amyotrophic lateral sclerosis*. Cell, 1993. **73**(1): p. 35-46.
306. Mangiarini, L., et al., *Exon 1 of the HD gene with an expanded CAG repeat is sufficient to cause a progressive neurological phenotype in transgenic mice*. Cell, 1996. **87**(3): p. 493-506.
307. Wang, J., et al., *Ypt1/Rab1 regulates Hrr25/CK1delta kinase activity in ER-Golgi traffic and macroautophagy*. J Cell Biol, 2015. **210**(2): p. 273-85.
308. Davis, S., et al., *Sec24 phosphorylation regulates autophagosome abundance during nutrient deprivation*. Elife, 2016. **5**.
309. Ishihara, N., et al., *Autophagosome requires specific early Sec proteins for its formation and NSF/SNARE for vacuolar fusion*. Mol Biol Cell, 2001. **12**(11): p. 3690-702.
310. Presley, J.F., et al., *ER-to-Golgi transport visualized in living cells*. Nature, 1997. **389**(6646): p. 81-5.
311. Barton, E.R., et al., *Deletion of muscle GRP94 impairs both muscle and body growth by inhibiting local IGF production*. FASEB J, 2012. **26**(9): p. 3691-702.
312. Ostrovsky, O., et al., *Glucose regulated protein 94 is required for muscle differentiation through its control of the autocrine production of insulin-like growth factors*. Biochim Biophys Acta, 2010. **1803**(2): p. 333-41.
313. Li, Y., et al., *PERK eIF2alpha kinase regulates neonatal growth by controlling the expression of circulating insulin-like growth factor-I derived from the liver*. Endocrinology, 2003. **144**(8): p. 3505-13.
314. Zhang, P., et al., *The PERK eukaryotic initiation factor 2 alpha kinase is required for the development of the skeletal system, postnatal growth, and the function and viability of the pancreas*. Mol Cell Biol, 2002. **22**(11): p. 3864-74.
315. Conway, K.L., et al., *Atg16l1 is required for autophagy in intestinal epithelial cells and protection of mice from Salmonella infection*. Gastroenterology, 2013. **145**(6): p. 1347-57.
316. Reimold, A.M., et al., *An essential role in liver development for transcription factor XBP-1*. Genes Dev, 2000. **14**(2): p. 152-7.
317. Luo, S., et al., *GRP78/BiP is required for cell proliferation and protecting the inner cell mass from apoptosis during early mouse embryonic development*. Mol Cell Biol, 2006. **26**(15): p. 5688-97.
318. Wanderling, S., et al., *GRP94 is essential for mesoderm induction and muscle development because it regulates insulin-like growth factor secretion*. Mol Biol Cell, 2007. **18**(10): p. 3764-75.
319. Jin, R., et al., *Mechanisms elevating ORMDL3 expression in recurrent wheeze patients: role of Ets-1, p300 and CREB*. Int J Biochem Cell Biol, 2012. **44**(7): p. 1174-83.
320. Qiu, R., et al., *Signal transducer and activator of transcription 6 directly regulates human ORMDL3 expression*. FEBS J, 2013. **280**(9): p. 2014-26.
321. Ahmed, S.T. and L.B. Ivashkiv, *Inhibition of IL-6 and IL-10 signaling and Stat activation by inflammatory and stress pathways*. J Immunol, 2000. **165**(9): p. 5227-37.
322. Ahmed, S.T., et al., *Inhibition of IL-6 signaling by a p38-dependent pathway occurs in the absence of new protein synthesis*. J Leukoc Biol, 2002. **72**(1): p. 154-62.
323. Niemand, C., et al., *Activation of STAT3 by IL-6 and IL-10 in primary human macrophages is differentially modulated by suppressor of cytokine signaling 3*. J Immunol, 2003. **170**(6): p. 3263-72.
324. Zhuang, L.L., et al., *All-trans retinoic acid modulates ORMDL3 expression via transcriptional regulation*. PLoS One, 2013. **8**(10): p. e77304.
325. Wang, X.H., et al., *Mechanisms and roles by which IRF-3 mediates the regulation of ORMDL3 transcription in respiratory syncytial virus infection*. Int J Biochem Cell Biol, 2017. **87**: p. 8-17.
326. Woo, C.W., et al., *Adaptive suppression of the ATF4-CHOP branch of the unfolded protein response by toll-like receptor signalling*. Nat Cell Biol, 2009. **11**(12): p. 1473-80.

327. Bandow, K., et al., *Molecular mechanisms of the inhibitory effect of lipopolysaccharide (LPS) on osteoblast differentiation*. *Biochem Biophys Res Commun*, 2010. **402**(4): p. 755-61.
328. Strober, W., I. Fuss, and P. Mannon, *The fundamental basis of inflammatory bowel disease*. *J Clin Invest*, 2007. **117**(3): p. 514-21.
329. Glasser, A.L., et al., *Adherent invasive Escherichia coli strains from patients with Crohn's disease survive and replicate within macrophages without inducing host cell death*. *Infect Immun*, 2001. **69**(9): p. 5529-37.
330. Lim, Y.J., et al., *Endoplasmic reticulum stress pathway-mediated apoptosis in macrophages contributes to the survival of Mycobacterium tuberculosis*. *PLoS One*, 2011. **6**(12): p. e28531.
331. Bergstrom, K.S., et al., *Muc2 protects against lethal infectious colitis by disassociating pathogenic and commensal bacteria from the colonic mucosa*. *PLoS Pathog*, 2010. **6**(5): p. e1000902.
332. Burger-van Paassen, N., et al., *Mucin Muc2 deficiency and weaning influences the expression of the innate defense genes Reg3beta, Reg3gamma and angiogenin-4*. *PLoS One*, 2012. **7**(6): p. e38798.
333. Sheng, Y.H., et al., *Mucins in inflammatory bowel diseases and colorectal cancer*. *J Gastroenterol Hepatol*, 2012. **27**(1): p. 28-38.
334. Shaffer, A.L., et al., *XBP1, downstream of Blimp-1, expands the secretory apparatus and other organelles, and increases protein synthesis in plasma cell differentiation*. *Immunity*, 2004. **21**(1): p. 81-93.
335. Sriburi, R., et al., *Coordinate regulation of phospholipid biosynthesis and secretory pathway gene expression in XBP-1(S)-induced endoplasmic reticulum biogenesis*. *J Biol Chem*, 2007. **282**(10): p. 7024-34.
336. Diakopoulos, K.N., et al., *Impaired autophagy induces chronic atrophic pancreatitis in mice via sex- and nutrition-dependent processes*. *Gastroenterology*, 2015. **148**(3): p. 626-638 e17.
337. Antonucci, L., et al., *Basal autophagy maintains pancreatic acinar cell homeostasis and protein synthesis and prevents ER stress*. *Proc Natl Acad Sci U S A*, 2015. **112**(45): p. E6166-74.
338. Schuck, S., et al., *Membrane expansion alleviates endoplasmic reticulum stress independently of the unfolded protein response*. *J Cell Biol*, 2009. **187**(4): p. 525-36.
339. Sriburi, R., et al., *XBP1: a link between the unfolded protein response, lipid biosynthesis, and biogenesis of the endoplasmic reticulum*. *J Cell Biol*, 2004. **167**(1): p. 35-41.
340. Reimold, A.M., et al., *Plasma cell differentiation requires the transcription factor XBP-1*. *Nature*, 2001. **412**(6844): p. 300-7.
341. Lee, A.H., et al., *XBP-1 is required for biogenesis of cellular secretory machinery of exocrine glands*. *EMBO J*, 2005. **24**(24): p. 4368-80.
342. Wang, M., et al., *Essential role of the unfolded protein response regulator GRP78/BiP in protection from neuronal apoptosis*. *Cell Death Differ*, 2010. **17**(3): p. 488-98.
343. Wiest, D.L., et al., *Membrane biogenesis during B cell differentiation: most endoplasmic reticulum proteins are expressed coordinately*. *J Cell Biol*, 1990. **110**(5): p. 1501-11.
344. Feldman, D., R.L. Swarm, and J. Becker, *Ultrastructural study of rat liver and liver neoplasms after long-term treatment with phenobarbital*. *Cancer Res*, 1981. **41**(6): p. 2151-62.
345. Voeltz, G.K., et al., *A class of membrane proteins shaping the tubular endoplasmic reticulum*. *Cell*, 2006. **124**(3): p. 573-86.
346. Klopfenstein, D.R., F. Kappeler, and H.P. Hauri, *A novel direct interaction of endoplasmic reticulum with microtubules*. *EMBO J*, 1998. **17**(21): p. 6168-77.
347. Salinas, S., et al., *Hereditary spastic paraplegia: clinical features and pathogenetic mechanisms*. *Lancet Neurol*, 2008. **7**(12): p. 1127-38.
348. Hubner, C.A. and I. Kurth, *Membrane-shaping disorders: a common pathway in axon degeneration*. *Brain*, 2014. **137**(Pt 12): p. 3109-21.
349. Benjamin, J.L., et al., *Intestinal epithelial autophagy is essential for host defense against invasive bacteria*. *Cell Host Microbe*, 2013. **13**(6): p. 723-34.

350. Takamura, A., et al., *Autophagy-deficient mice develop multiple liver tumors*. *Genes Dev*, 2011. **25**(8): p. 795-800.
351. Komatsu, M., et al., *Essential role for autophagy protein Atg7 in the maintenance of axonal homeostasis and the prevention of axonal degeneration*. *Proc Natl Acad Sci U S A*, 2007. **104**(36): p. 14489-94.
352. Wang, Q.J., et al., *Induction of autophagy in axonal dystrophy and degeneration*. *J Neurosci*, 2006. **26**(31): p. 8057-68.
353. Bartlett, B.J., et al., *p62, Ref(2)P and ubiquitinated proteins are conserved markers of neuronal aging, aggregate formation and progressive autophagic defects*. *Autophagy*, 2011. **7**(6): p. 572-83.
354. Komatsu, M., et al., *Homeostatic levels of p62 control cytoplasmic inclusion body formation in autophagy-deficient mice*. *Cell*, 2007. **131**(6): p. 1149-63.
355. de Ruijter, J.C., E.V. Koskela, and A.D. Frey, *Enhancing antibody folding and secretion by tailoring the *Saccharomyces cerevisiae* endoplasmic reticulum*. *Microb Cell Fact*, 2016. **15**: p. 87.
356. Jacomin, A.C., et al., *iLIR database: A web resource for LIR motif-containing proteins in eukaryotes*. *Autophagy*, 2016. **12**(10): p. 1945-1953.
357. Kelley, L.A., et al., *The Phyre2 web portal for protein modeling, prediction and analysis*. *Nat Protoc*, 2015. **10**(6): p. 845-58.
358. Shibata, Y., G.K. Voeltz, and T.A. Rapoport, *Rough sheets and smooth tubules*. *Cell*, 2006. **126**(3): p. 435-9.
359. Shibata, Y., et al., *Mechanisms determining the morphology of the peripheral ER*. *Cell*, 2010. **143**(5): p. 774-88.
360. Conti, B.J., et al., *Cotranslational stabilization of Sec62/63 within the ER Sec61 translocon is controlled by distinct substrate-driven translocation events*. *Mol Cell*, 2015. **58**(2): p. 269-83.
361. Melero, A., et al., *Lysophospholipids Facilitate COPII Vesicle Formation*. *Curr Biol*, 2018. **28**(12): p. 1950-1958 e6.
362. Birgisdottir, A.B., T. Lamark, and T. Johansen, *The LIR motif - crucial for selective autophagy*. *J Cell Sci*, 2013. **126**(Pt 15): p. 3237-47.
363. Wild, P., D.G. McEwan, and I. Dikic, *The LC3 interactome at a glance*. *J Cell Sci*, 2014. **127**(Pt 1): p. 3-9.
364. Moretti, J., et al., *STING Senses Microbial Viability to Orchestrate Stress-Mediated Autophagy of the Endoplasmic Reticulum*. *Cell*, 2017. **171**(4): p. 809-823 e13.

8 Supplement

8.1 List of Abbreviations

AGR2	encoding the anterior gradient protein-2
AIEC	adherent-invasive <i>E. coli</i>
ATCC	American Type Culture Collection
ATF4	activating transcription factor 4
ATF6	activating transcription factor 6
ATF6 α (N)	N-terminal fragment of ATF6 α
ATG7	autophagy related 7
ATG16L1	autophagy related 16 like 1
BIP	binding-immunoglobulin protein
BMDM	bone marrow-derived macrophages
BSA	bovine serum albumin
BW	body weight
bZIP	basic leucine zipper
Ca ²⁺	calcium
<i>CALCOCO2</i>	<i>calcium binding and coiled-coil domain 2</i>
CD	Crohn's disease
cDNA	complimentary DNA
CEACAM6	cell adhesion molecule 6
CED	chronisch-entzündliche Darmerkrankungen
CHOP	CCAAT-enhancer-binding homologous protein
CHX	cycloheximide
CoA	coenzyme A
CO-IP	Co-immunoprecipitations
CREBH	cAMP responsive element-binding protein CXCL1 chemokine (C-X-C motif) ligand 1
DAI	disease activity index
DAPK1	death associated protein kinase 1
DMSO	dimethylsulfoxide
DNA	deoxyribonucleic acid
DNAJC3	DnaJ heat shock protein family (Hsp40) member C3
DSS	dextran sulfate sodium
DTT	ditriothreitol
ECL	enhanced chemiluminescence
<i>E. coli</i>	<i>Escherichia coli</i>
EDTA	ethylenediaminetetraacetic acid
eIF2 α	eukaryotic translation initiation factor 2 α
EndoH	endoglycosidase H
ERN1/2	Endoplasmic Reticulum to nucleus signaling 1/2
eQTL	expression quantitative trait loci
ER	endoplasmic reticulum
ERAD	ER-associated protein degradation
ERK	extracellular signal-regulated kinase
ERSE	ER stress response element
FIP200	FAK family kinase interacting protein of 200 kDa
FL	full length
FRT	flippase recognition target FSC forward scatter
GADD34	growth-arrest DNA damage gene 34
GH	growth hormone
GRP78	78-kDa glucose-regulated protein

GRP94	94-kDa glucose-regulated protein
GWAS	genome-wide association studies
HE	hematoxylin and eosin
HRP	horseradish peroxidase
HSC70	heat shock cognate 70 kDa protein
IBD	inflammatory bowel disease
IEC	intestinal epithelial cell
IFN γ	interferon gamma
IGF1	insulin-like growth factor 1
IHC	immunohistochemistry
IKK α	I κ B kinase α
IL	interleukin
IRE1	inositol-requiring kinase 1
IRGM	immunity Related GTPase M
JNK	c-Jun-N-terminal kinase
kDa	kilodalton
KO	knockout
LC3	microtubule-associated protein 1 light chain 3
LIR	LC3 interacting region
Lyz1	lysozyme 1
Mbtps1	membrane-bound transcription factor S1P-encoding gene
MEF	mouse embryonic fibroblasts
MOPS	4-Morpholinepropanesulfonic acid
mRNA	messenger ribonucleic acids
Muc2	mucin 2
NDP52	nuclear dot protein 52kDa
NeoR	neomycin resistance
NFY	nuclear transcription factor
NF- κ B	nuclear factor kappa-light-chain-enhancer of activated B cells
NOD2	nucleotide-binding oligomerization domain-containing protein 2
NRF2	nuclear factor erythroid 2-related factor
OASIS	old astrocyte specifically induced substance
OPTN	Optineurin
ORMDL	orosomuroid 1 (<i>Saccharomyces cerevisiae</i>)-like protein
p36ATF6 α	36 kDa fragment of ATF6 α
p50ATF6 α	50 kDa fragment of ATF6 α
p58IPK	protein kinase inhibitor of 58 kDa
p62/SQSTM1	Sequestosome 1
PBA	4-phenylbutyrate PBS phosphate-buffered saline
PCR	polymerase chain reactions
p-eIF2 α	phosphorylated form of eIF2 α
PE	phosphatidylethanolamine
PERK	double-stranded RNA-activated protein kinase (PKR)-like ER kinase
PP1	protein phosphatase 1
PuroR	puromycin resistance
PVDF	polyvinylidene difluoride
qPCR	quantitative real-time PCR
RIDD	regulated IRE1-dependent decay of mRNA
RLU	relative light units
RT	reverse transcriptase
S1P	site 1 protease
S2P	site 2 protease

SARs	selective autophagy receptors
SDS-PAGE	sodium dodecyl sulfate polyacrylamide gel electrophoresis
SEM	standard error of the mean
SERCA2B	sarcoplasmic/endoplasmic reticulum calcium ATPase 2
SiRNA	small interfering RNA
SNP	single nucleotide polymorphisms
SPT	serine palmitoyltransferase
SPTLC1	serine palmitoyltransferase, long chain base subunit 1
STAT3	signal transducer and activator of transcription 3
TEMED	tetramethylethylenediamine
TG	thapsigargin
TLR	Toll-like receptor
TM	tunicamycin
TNBS	trinitrobenzene sulfonic acid
TNF α	tumor necrosis factor alpha
TRAF2	tumor necrosis factor receptor-associated factor 2
TRAP α	translocon-associated protein alpha
TUDCA	tauroursode-oxycholate
UBD	ubiquitin-binding domain
UC	ulcerative colitis
ULK1	Unc-51-like kinase 1
Untr	untreated
UPR	unfolded protein response
UPRE	unfolded protein response element
WT	wild type
XBP1	X-box binding protein 1
sXBP1	spliced XBP1

8.2 Buffers and Solutions

Table 11: List of applied buffers and solutions.

buffer or solution	composition or company
10x TAE buffer	Carl Roth, Karlsruhe, Germany, cat. nr. T845.2
10x TBS	200 mM Tris (pH 7.6), 1.37 M sodium chloride
10x TGS buffer	25 mM Tris (pH 8.3), 192 mM glycine, 0.1 % (w/v) SDS
5x SDS loading dye	250 mM Tris (pH 6.8), 10 % (w/v) SDS, 50 % (v/v) glycerol, 500 mM DTT
Anode buffer 1	30 mM Tris, 20 % (v/v) methanol
Anode buffer 2	300 mM Tris, 20 % (v/v) methanol
Blocking solution	5 % (w/v) non-fat dry milk in TTBS
Cathode buffer	25 mM Tris, 20 % (v/v) methanol, 40 mM 6-amino-ncaproic acid
Cell fractionation 1	10 mM HEPES (pH 7.9), 10 mM potassium chloride, 1.5 mM magnesium chloride, 10 mM sodium fluoride
Cell fractionation 2	20 mM HEPES (pH 7.9), 420 mM sodium chloride, 1.5 mM magnesium chloride, 0.2 mM EDTA, 25 % (v/v) glycerol, 10 mM sodium fluoride
CO-IP binding and washing buffer	PBS, 0.02 % (v/v) Tween20
CO-IP elution buffer	50 mM Glycin (pH 2.8)
DNA loading dye	50 % (v/v) glycerol, 0.1 % (w/v) bromophenol blue, 0.1 % (w/v) xylene cyanol
ECL substrate	GE Healthcare, Freiburg, Germany, cat. nr. RPN2109
FCS	PAA Laboratories/ GE Healthcare, Freiburg, Germany, cat. nr. PAA A15-151
Ketanest S 25mg/ml, 10ml	Pfizer, New York, USA
Loading gel	0.5 M Tris (pH 6.8), 0.4 % (w/v) SDS
MOPS SDS Running Buffer (20X)	Novex/Life Technologies, Darmstadt, Germany, cat. nr. NP001
OPTI-MEM	Gibco/Life Technologies, Darmstadt, Germany, cat. nr. 31985-047
PBS	8 g/l sodium chloride, 0.2 g/l potassium chloride, 1.56 g/l disodium phosphate, 0.24 g/l monopotassium phosphate, pH 7.4
RIPA	150 mM sodium chloride, 1 % (v/v) NP40, 0.5 % (w/v) deoxycholic acid, 0.1 % (w/v) SDS, 50 mM Tris (pH 8.0)
Rompun	Bayer, Leverkusen, Germany
Separation buffer	1.5 M Tris (pH 8.8), 0.4 % (w/v) SDS
SmartLadder	Eurogentec, Cologne, Germany, cat. nr. MW-1700-10
Stacking buffer	0.5 M Tris (pH 8.8), 0.4 % (w/v) SDS
Stripping buffer	62.5 mM Tris (pH 6.8), 2 % (w/v) SDS
SYBR Safe DNA gel stain	Life Technologies, Darmstadt, Germany cat. nr. S33102
TEA	10 mM Tris, 1 mM EDTA
TTBS	1x TBS, 0.1 % (v/v) Tween20

8.3 Media

Table 12: List of applied media.

Media	Composition or company
DMEM	Gibco/Life Technologies, Darmstadt, Germany cat. nr. 41966-029
DMEM Glutamax	Gibco/Life Technologies, Darmstadt, Germany cat. nr. 61965-059
LB Agar	10 g/l tryptone, 5 g/l yeast extract, 5 g/l sodium chloride, 15 g/l agar
LB Medium	10 g/l tryptone, 5 g/l yeast extract, 5 g/l sodium chloride
MEF medium	DMEM Glutamax, 1x Penicillin/Streptomycin, 1x NEAA, MEM
NEAA, MEM	Invitrogen/Thermo Scientific, Bremen, Germany cat nr. 11140-035

8.4 Chemicals

Table 13: List of applied chemicals.

chemical	company
2-Mercaptoethanol	Sigma-Aldrich, Munich, Germany
6-amino-n-caproic acid	Sigma-Aldrich, Munich, Germany
Acrylamide Bis Sol.30%	Bio-Rad, Munich, Germany
Ammonium persulfate (APS)	Sigma-Aldrich, Munich, Germany
Amphotericin	PAA Laboratories/ GE Healthcare, Freiburg, Germany
Ampicillin	Sigma-Aldrich, Munich, Germany
Bovine serum albumin (BSA)	Carl Roth, Karlsruhe, Germany
Bromophenol blue	Sigma-Aldrich, Munich, Germany
Deoxycholic acid	Sigma-Aldrich, Munich, Germany
Dimethylsulfoxid (DMSO)	Sigma-Aldrich, Munich, Germany
Dithiothreitol (DTT)	Th. Geyer, Renningen, Germany
DSS reagent grade, molecular weight 36000-50000	MP Biomedicals, Illkirch Cedex, France
Dynabeads Protein G	Life Technologies, Darmstadt, Germany
EDTA	Sigma-Aldrich, Munich, Germany
Ethanol	Merck, Darmstadt, Germany
Glycerol	Carl Roth, Karlsruhe, Germany
Glycine	Carl Roth, Karlsruhe, Germany
HEPES	Sigma-Aldrich, Munich, Germany
Isopropanol	Merck, Darmstadt, Germany
Kanamycin	Merck, Darmstadt, Germany
LE Agarose	Biozyme, Hessisch Oldendorf, Germany
Magnesium chloride	Merck, Darmstadt, Germany
Methanol	Merck, Darmstadt, Germany
Monopotassium phosphate	Sigma-Aldrich, Munich, Germany
Non-fat dry milk (NFDM)	Bio-Rad, Munich, Germany
Nonidet p 40 substitute	Sigma-Aldrich, Munich, Germany
Penicilin/Streptomycin	Life Technologies, Darmstadt, Germany
Potassium chloride	Sigma-Aldrich, Munich, Germany
Potassium dihydrogen phosphate	Merck, Darmstadt, Germany
RNase-free water	Qiagen, Hilden, Germany
Sodium chloride	Merck, Darmstadt, Germany
Sodium dodecyl sulfate (SDS)	Carl Roth, Karlsruhe, Germany
Sodium fluoride	Sigma-Aldrich, Munich, Germany
Sodium phosphate dibasic	Sigma-Aldrich, Munich, Germany
SYBR safe	Life Technologies
Tetramethylethylenediamine (TEMED)	Sigma-Aldrich, Munich, Germany
TRIS	Merck, Darmstadt, Germany
Triton-X	Sigma-Aldrich, Munich, Germany
Tween20	Carl Roth, Karlsruhe, Germany
Xylene cyanol	Sigma-Aldrich, Munich, Germany

8.5 Enzymes & Inhibitors

Table 14: List of applied enzymes.

enzyme	company
Endonuclease H	New England Biolabs
GoTaq™ polymerase	Promega, Mannheim, Germany
Proteinase K	Thermo Scientific, Bremen, Germany
RNase-free DNase Set	Qiagen, Hilden, Germany
Trypsin/EDTA	Life Technologies

Table 15: List of applied small molecules.

inhibitor	company
AEBSF (4-(2-Aminoethyl) benzenesulfonyl fluoride hydrochloride)	Calbiochem, Darmstadt, Germany
Bafilomycin A	Enzo Life Sciences GmbH, Lörrach, Germany
Camostat mesylate	Sigma-Aldrich, Munich, Germany
Cycloheximide (CHX)	Sigma-Aldrich, Munich, Germany
Erastin	Cayman, Hamburg, Germany
Halt™ combined protease and phosphatase inhibitor	Thermo Scientific, Bremen, Germany
Simvastatin	Sigma-Aldrich, Munich, Germany
TBB	Tocris, Bristol, United Kingdom
TPEN	Cayman, Hamburg, Germany
Triacsin C	Enzo Life Sciences GmbH, Lörrach, Germany
Tunicamycin (TM)	Calbiochem, Darmstadt, Germany

8.6 Kits

Table 16: List of applied kits.

kit	company
Dual-luciferase® reporter assay system	Promega, Mannheim, Germany
GeneJET Plasmid Miniprep Kit	Thermo Scientific, Bremen, Germany
Maxima H Minus First Strand cDNA Synthesis Kit	Thermo Scientific, Bremen, Germany
PureLink® HiPure Plasmid Filter Midiprep Kit	Life Technologies, Darmstadt, Germany
QIAshredder	Qiagen, Hilden, Germany
Rapid DNA Ligation Kit	Roche, Mannheim, Germany
Rat/Mouse Growth hormone ELISA kit	EMD Millipore, Schwalbach, Germany
RNeasy Mini Kit	Qiagen, Hilden, Germany
Roti Histokit	Carl Roth, Karlsruhe, Germany
SYBR® Select Master Mix	Life Technologies, Darmstadt, Germany

8.7 Plasmids and Oligonucleotides

Table 17: List of plasmids used in this study.

plasmid	generated by
p3xFLAG-ATF6	Chen <i>et al.</i> , 2002; purchased from Addgene, Cambridge, USA, cat. nr.11975
pCMV-HA-EGFP	Gateway cloning
pCMV-HA-hORMDL1	Gateway cloning
pCMV-HA-hORMDL3	Gateway cloning
pGL3-ERSE	restriction enzyme based cloning using BglII and KpnI
pRL-TK	purchased from Promega, Mannheim, Germany, cat. nr. E2241

All oligonucleotides were generated and desalted by Microsynth AG (Balgach, Switzerland). All sequences are shown from 5' to 3' direction.

Table 18: List of applied oligonucleotides with their sequences.

target	species	forward sequence	reverse sequence
Ormdl1 PCR WT	murine	AACGTTAGTGCTGTTTGGACA CACG	AACATGCTTCCCTATACTGTGC CACT
Ormdl1 PCR KO	murine	CCCCAAAAGTGTATGCTCAC GACA	TCCCTATACTGTGCCCACTAC CCATTGT
Ormdl3 PCR WT	murine	CTTCATCCGTTGTTGCTTGC	TCCCCTACAGATCTCCTGAGG
Ormdl3 PCR KO	murine	CTTCATCCGTTGTTGCTTGC	TCACAGTGCCAGTAGGAAACC
Ormdl3 PCR cond	murine	CTTCATCCGTTGTTGCTTGC	TCCCCTACAGATCTCCTGAGG
Ormdl3 PCR cre	murine	GTGTGGGACAGAGAACAAACC	ACATCTTCAGTTCTGCGGG
<i>Ormdl1</i>	murine	ACTCACTGGGAACAGCTGGA	ATTCCAAAGATGCGAACACC
<i>Ormdl2</i>	murine	CTTTTGACACATTGGGAGCA	GGTAGCTTAGGCAGCAGCAC
<i>Ormdl3</i>	murine	GTGGCATCTGGCTCTCCTAC	TGAGCACAGTCATCAAGGACA
<i>Gapdh</i>	murine	CCGGGGCTGGCATTGCTCTCA	CTTGCTCAGTGTCCCTTGCTGG GG
<i>Xbp1</i>	murine	GAACCAGGAGTTAAGAACACG	AGGCAACAGTGTGACAGAGTCC
<i>Cxcl1</i>	murine	GCTGGGATTCACCTCAAGAA	TGGGGACACCTTTTAGCATC
<i>Tnfa</i>	murine	TCACACTCAGATCATCTTCTC	AGACTCCTCCCAGGTATATG
<i>Atf6a</i>	murine	ATGCCAGTGTCCCAGCAAAA	TCCCCCAGTGACTGCAAGAA
<i>Grp94</i>	murine	TGGGTCAAGCAGAAAGGAGG	TCTCTGTTGCTTCCCAGCTTT
<i>Atf4</i>	murine	ATGGCCGGCTATGGATGAT	CGAAGTCAAACCTTTTCAGATC CATT
<i>Chop</i>	murine	CTGCCTTTCACCTTGGAGA	CGTTTCCTGGGGATGAGATA
<i>Gadd34</i>	murine	CTGCAAGGGGCTGATAAGAG	AGGGGTCAGCCTTGTTTTCT
<i>ORMDL1</i>	human	CTGACCAGGGTAAAGCAAGG	TCCAAAGATCCGAACACCAT
<i>ORMDL2</i>	human	CATACGGTGAAAGGGACACC	CGGCAGCAGTACACTTAGCA
<i>ORMDL3</i>	human	GTGGCATCTGGCTCTCCTAC	TGAGCACAAAATGGATCTGG
<i>GAPDH</i>	human	GGCATGGCCTCCGTGTCCC	TGCCAGCCCCAGCGTCAAAG

Table 19: Overview of applied TaqMan probes.

target	species	company	catalog number
<i>ACSL1</i>	human	Life Technologies, Darmstadt, Germany	00960561
<i>Acs11</i>	murine	Life Technologies, Darmstadt, Germany	00484217
<i>Atf4</i>	murine	Life Technologies, Darmstadt, Germany	00515325
<i>Atf6</i>	murine	Life Technologies, Darmstadt, Germany	01295317
<i>ATF6</i>	human	Life Technologies, Darmstadt, Germany	00232586
<i>CSNK2B</i>	human	Life Technologies, Darmstadt, Germany	00365635
<i>Csnk2b</i>	murine	Life Technologies, Darmstadt, Germany	00487216
<i>Dnajc3</i>	murine	Life Technologies, Darmstadt, Germany	01226332
<i>Hspa5</i>	murine	Life Technologies, Darmstadt, Germany	00517690
<i>Hsp90b1</i>	murine	Life Technologies, Darmstadt, Germany	00441926
<i>Muc2</i>	murine	Life Technologies, Darmstadt, Germany	00458299
<i>Gapdh</i>	murine	Life Technologies, Darmstadt, Germany	99999915
<i>Lyz1</i>	murine	Life Technologies, Darmstadt, Germany	00657323
<i>ORMDL1</i>	human	Life Technologies, Darmstadt, Germany	00212847
<i>ORMDL2</i>	human	Life Technologies, Darmstadt, Germany	00374752
<i>ORMDL3</i>	human	Life Technologies, Darmstadt, Germany	00918021
<i>Ormdl1</i>	murine	Life Technologies, Darmstadt, Germany	00523629
<i>Ormdl2</i>	murine	Life Technologies, Darmstadt, Germany	00452481
<i>Ormdl3</i>	murine	Life Technologies, Darmstadt, Germany	00787910
<i>Tnfa</i>	murine	Life Technologies, Darmstadt, Germany	00443258
<i>Xbp1</i>	murine	Life Technologies, Darmstadt, Germany	03464496

8.8 Antibodies

All primary antibodies used for western blotting were diluted in TTBS containing 5 % (w/v) bovine serum albumin (BSA) or 5 % (w/v). Secondary antibodies used in this study were diluted in non-fat dry milk.

Table 20: Primary antibodies used in this study.

antibody	dilution	company	catalog number
ATF6 α	1:1000	GenScript, Piscataway, USA	commissioned work
cl. ATF6 α	1:500	Acris, Herford, Germany	SM7007P
ATG16L1	1:1000	MBL International, Woburn, USA	M150-3
β -Actin	1:1000	Sigma-Aldrich, Munich, Germany	A-5441
CHOP	1:500	Cell Signaling Technology, Leiden, The Netherlands	5554
CLIMP63	1:2000	Proteintech, Manchester, United Kingdom	16686-1-AP
GAPDH	1:1000	Santa Cruz Biotechnology, Heidelberg, Germany	sc-365062
GFAP	1:1000	Abcam, Cambridge, United Kingdom	ab68428
GFP	1:1000	Cell Signaling Technology, Leiden, The Netherlands	2956
GRP78	1:2000	Abcam, Cambridge, United Kingdom	ab21685
GRP94	1:1000	Cell Signaling Technology, Leiden, The Netherlands	20292
HA	1:1000	Roche, Mannheim, Germany	11 867 423 001
IBA1	1:1000	Abcam, Cambridge, United Kingdom	ab107159
LAMP2	1:1000	Abcam, Cambridge, United Kingdom	ab25339
LC3	1:1000	Cell Signaling Technology, Leiden, The Netherlands	3868
LPS	1:2000	Abcam, Cambridge, United Kingdom	ab35654
Lysozyme	1:1000	Abcam, Cambridge, United Kingdom	ab108508
ORMDL1/2/3	1:500	Santa Cruz Biotechnology, Heidelberg, Germany	sc-161143
P58IPK	1:1000	Cell Signaling Technology, Leiden, The Netherlands	2940
P62	1:1000	Cell Signaling Technology, Leiden, The Netherlands	8025
peIF2 α	1:500	Cell Signaling Technology, Leiden, The Netherlands	3398
RTN4	1:2000	Abcam, Cambridge, United Kingdom	ab47085
TRAP α	1:1000	Abcam, Cambridge, United Kingdom	Ab126607

Table 21: Secondary antibodies used in this study.

antibody	dilution	company	catalog number
mouse HRP	1:5000	Amersham Biosciences, Glattbrugg, Switzerland	NA931V
rabbit HRP	1:5000	Amersham Biosciences, Glattbrugg, Switzerland	NA934V
goat HRP	1:5000	Sigma-Aldrich, Munich, Germany	A5420
Alexa Fluor 488	1:400	Thermo Scientific, Bremen, Germany	A11029
goat α -mouse			
Alexa Fluor 488-	1:400	Thermo Scientific, Bremen, Germany	A11070
goat α -rabbit			
Alexa Fluor 555-	1:400	Thermo Scientific, Bremen, Germany	A21424
goat α -mouse			
Alexa Fluor 555-	1:400	Thermo Scientific, Bremen, Germany	A21430
goat α -rabbit			

8.9 Devices & Consumables

Table 22: Devices used in this study.

devices	company
7900 HT Fast Real-Time PCR System	Applied Biosystems/Life Technologies, Darmstadt, Germany
96-well thermocycler	Applied Biosystems/Life Technologies, Darmstadt, Germany
ABI PRISM® 3700 sequencer	Applied Biosystems/Life Technologies, Darmstadt, Germany
Analytic balance 870-15	Kern, Balingen, Germany
Assistant Mini-Centrifuge SPROUT	Heathrow Scientific, Nottingham , United Kingdom
Automated developer machine	Agfa, Mortsel, Belgium
Axio Imager.Z1	Zeiss, Jena, Germany
Cellometer Auto T4 Plus	PeqLab Biotechnologie GmbH, Erlangen, Germany
Centrifuge for 15/50 ml tubes: Megafuge 16R	Thermo Scientific, Bremen, Germany
Centrifuge for Eppendorf tubes: Fresco 21	Thermo Scientific, Bremen, Germany
Certomat MV, vortex mixer	B. Braun Biotech Internat., Melsungen, Germany
ChemiDoc XRS Imaging System	Bio-Rad, Munich, Germany
Confocal microscope: TCS SP5	Leica Microsystems, Wetzlar, Germany
Electronic pipet filler	Eppendorf, Hamburg, Germany
Eppendorf Research®, adjustable volume pipette	Eppendorf, Hamburg, Germany
FACSCalibur flow cytometer	BD Biosciences, Heidelberg, Germany
GeneAmp PCR System 9700	Applied Biosystems/Life Technologies, Darmstadt, Germany
Gentle-MACS™ Dissociator	Miltenyi Biotec, Bergisch Gladbach, Germany
Incubator for cell lines	Binder, Tuttlingen, Germany
Incubator for <i>E.coli</i> in media: Orbital Incubator SI50	Stuart Equipment, Staffordshire, United Kingdom
Incubator for <i>E.coli</i> on agar plates: Incucell 111	MMM Group, Planegg, Germany
Laminar flow workbench HERASafe KS	Thermo Scientific, Bremen, Germany
Leica RM 2255 microtome	Leica Microsystems, Wetzlar, Germany
Magnetic stirrer C-MAG HS 7 IKAMAG	IKA, Staufen, Germany
Microwave R-239	SHARP, Hamburg, Germany
Mini-Sub Cell GT	Bio-Rad, Munich, Germany
Molecular Imager ChemiDoc XRS Imaging System	Bio-Rad, Munich, Germany
NanoDrop ND-1000 spectrophotometer	PeqLab Biotechnologie GmbH, Erlangen, Germany
Power Pac 300	Bio-Rad, Munich, Germany
SympHony Benchtop Meters	VWR, Darmstadt, Germany
Tecan Infinite F200 pro plate reader	Tecan, Männedorf, Switzerland
Thermomixer compact 5350	Eppendorf, Hamburg, Germany
Trans-Blot® Turbo™ Transfer System	Bio-Rad, Munich, Germany
Tube roller SRT6	Stuart Equipment, Staffordshire, United Kingdom
Vortex-Genie 2 Variable Speed	Sartorius, Göttingen, Germany
Water bath 1003	GFL, Burgwedel, Germany
Water purification system	TKA, Niederelbert, Germany
Wide Mini ReadySub-Cell GT	Bio-Rad, Munich, Germany
XCell SureLock® Mini-Cell	Life Technologies, Darmstadt, Germany

Table 23: List of consumables used in this study.

consumable	company
0.5 ml, 1.5 ml and 2 ml reaction tubes	Sarstedt, Nümbrecht, Germany
1 ml syringes	BD Biosciences, Heidelberg, Germany
100 ml culture flasks	Schott, Mainz, Germany
15 ml and 50 ml tubes	Sarstedt, Nümbrecht, Germany
26G needles	B. Braun, Melsungen, Germany
Blot paper	Bio-Rad, Munich, Germany
Chemiluminescence hyperfilm	Applied Biosystems/Life Technologies, Darmstadt, Germany
Glass beads	Carl Roth, Karlsruhe, Germany
HistoBond	Paul Marienfeld GmbH& Co. KG
MicroAmp Optical 384-Well Reaction Plates	Applied Biosystems
Microvette 500 (Potassium-EDTA)	Sarstedt, Nümbrecht, Germany
NuPAGE® Bis-Tris gel	Life Technologies, Darmstadt, Germany
Pipette tips and filter tips	Sarstedt, Nümbrecht, Germany
Pipette tips for electronic pipette	Biohit, Göttingen, Germany
Polyvinylidene difluoride (PVDF) membranes	Bio-Rad, Munich, Germany
Rotilabo 0.22 µm syringe filter	Carl Roth, Karlsruhe, Germany
Serological pipettes	Sarstedt, Nümbrecht, Germany
Surgical disposable scalpels	B. Braun, Melsungen, Germany
Tissue culture dishes 96-, 24- and 6well	Sarstedt, Nümbrecht, Germany

Table 24: List of candidates identified in the primary screen.

GeneSymbol	mean	max	min	median	sd
ATF6	-15.229	-6.802	-23.17	-15.715	8.194816
POLR2K	-12.5627	-4.234	-21.929	-11.525	8.893021
SHARP	-8.21567	-5.098	-11.616	-7.933	3.268181
CSNK2B	-7.02367	-1.492	-15.74	-3.839	7.639238
NETO2	-6.04367	-3.384	-10.179	-4.568	3.629904
MMP3	-5.59667	-0.993	-12.685	-3.112	6.229438
TLR4	-5.482	-0.99	-13.845	-1.611	7.249223
RAN	-5.294	-3.525	-8.2	-4.157	2.536431
TRIM61	-4.876	-1.715	-10.874	-2.039	5.196946
PARP2	-3.896	0.172	-7.356	-4.504	3.80065
BTAF1	-3.42	-1.474	-6.998	-1.788	3.102614
SLC30A3	-3.396	0.434	-9.92	-0.702	5.678429
ACSL1	-3.357	-1.665	-5.103	-3.303	1.719636
IL17R	-3.22367	0.738	-9.182	-1.227	5.252771
NALP11	-3.20833	-0.569	-5.909	-3.147	2.670528
CYP51A1	-3.13533	-0.372	-7.469	-1.565	3.800173
MGC8685	-2.992	0.274	-9.18	-0.07	5.361725
POLR2F	-1.96167	3.341	-6.452	-2.774	4.946779
MTM1	-1.89833	2.035	-4.978	-2.752	3.583588
SNF1LK	-1.324	1.051	-3.853	-1.17	2.455624
PRDM10	-0.97533	3.954	-5.924	-0.956	4.939028
GNG7	-0.89067	1.232	-4.019	0.115	2.766184
SBK1	-0.61	0.881	-1.698	-1.013	1.335896
SLC35D2	-0.58733	4.999	-6.641	-0.12	5.834055
PLCL1	-0.54767	0.568	-1.19	-1.021	0.969884
ALG12	-0.38567	7.562	-5.499	-3.22	6.976569
FARSLB	-0.25333	0.252	-1.014	0.002	0.670511
SOCS5	0.044667	1.298	-2.266	1.102	2.003494
INPP5B	0.311	1.302	-0.958	0.589	1.155363
RNF34	0.322667	4.676	-1.901	-1.807	3.77039
ZNF265	0.324	3.193	-1.705	-0.516	2.55476
NKTR	0.406333	2.704	-0.994	-0.491	2.005669
ODF1	0.427	12.276	-7.302	-3.693	10.41899
MGAT4B	0.452667	1.492	-0.944	0.81	1.256698
NFIC	0.473667	2.085	-1.922	1.258	2.115513
INPP5E	0.614667	1.46	-0.561	0.945	1.050214
ATP5J	0.645333	6.821	-4.03	-0.855	5.578916
C5R1	0.657	1.91	-0.508	0.569	1.2114
GPR158L1	0.692333	3.648	-5.191	3.62	5.095135
PPP1R14A	0.702333	9.11	-6.782	-0.221	7.986133
UNC5D	0.805667	3.359	-4.063	3.121	4.218068
K-ALPHA-1	0.814667	1.954	-0.543	1.033	1.262737
NAGK	0.829	5.274	-1.831	-0.956	3.874264
LGR7	0.833	4.371	-2.825	0.953	3.599501
PTPRD	0.87	2.007	-0.028	0.631	1.038339

PAFAH1B1	0.971333	14.155	-9.975	-1.266	12.21959
EZH1	1.053667	3.707	-1.882	1.336	2.805176
CYP27A1	1.074	3.768	-3.337	2.791	3.851146
RPA1	1.185667	6.565	-5.527	2.519	6.155278
DHODH	1.193667	2.824	-1.133	1.89	2.068362
KLK11	1.236667	2.769	-0.128	1.069	1.45576
MYST2	1.237333	5.265	-1.634	0.081	3.591919
DDX48	1.238333	3.566	-2.342	2.491	3.146903
TNFRSF9	1.250667	4.831	-1.208	0.129	3.171905
TIMM8B	1.288	2.517	-0.486	1.833	1.573935
ARF3	1.298333	4.02	-0.082	-0.043	2.357113
SHMT1	1.322667	4.218	-3.24	2.99	3.998805
CELSR3	1.328667	5.476	-0.922	-0.568	3.596055
GRM4	1.354667	2.957	-1.521	2.628	2.495827
BIRC5	1.595333	5.942	-1.126	-0.03	3.804003
KLK1	1.660667	4.024	-1.451	2.409	2.813167
CCKBR	1.686	7.634	-1.619	-0.957	5.161743
HM13	1.705	6.523	-1.156	-0.252	4.196921
TTK	1.721333	6.035	-0.535	-0.336	3.73707
PTER	1.772667	3.328	0.709	1.281	1.376987
UNC5C	1.848	5.757	-0.644	0.431	3.427698
MSH5	1.856667	2.679	0.723	2.168	1.014485
GPR173	1.942	4.697	-1.952	3.081	3.46775
LOC115294	1.946333	4.813	0.141	0.885	2.510322
AOC2	1.965	11.033	-8.834	3.696	10.04598
CCR3	2.053333	4.913	-1.961	3.208	3.579513
MGST2	2.143667	10.759	-3.935	-0.393	7.668404
PA2G4	2.227667	5.313	-3.335	4.705	4.826993
FUSIP1	2.381667	5.865	0.078	1.202	3.068559
PLA2G6	2.393333	6.347	-0.595	1.428	3.570258
MGC15668	2.396333	6.453	-0.758	1.494	3.689212
SFRS7	2.47	6.807	-4.748	5.351	6.293221
AKR1B10	2.49	12.173	-3.965	-0.738	8.53954
RBP2	2.499667	4.064	1.682	1.753	1.355217
SLC22A17	2.598	4.578	0.972	2.244	1.828878
FLJ22054	2.622333	6.341	-0.288	1.814	3.387619
MTCH2	2.647	13.433	-3.377	-2.115	9.362238
SCO1	2.652667	5.257	-1.722	4.423	3.811453
CSNK1D	2.749	4.425	0.122	3.7	2.303748
TRIM43	2.848	3.715	2.021	2.808	0.847708
CPSF2	2.879	6.304	-1.154	3.487	3.765991
ADAMTS13	2.885667	6.303	-1.056	3.41	3.707413
MKNK2	2.911333	4.791	0.717	3.226	2.055147
PIK3R2	2.954667	10.981	-3.589	1.472	7.397293
GABRB2	3.050333	14.924	-4.103	-1.67	10.3546
MYO9B	3.122	7.577	0.161	1.628	3.92725
FOLR3	3.133667	15.273	-3.931	-1.941	10.55995

MYF6	3.365667	6.002	2.018	2.077	2.283322
KRTHA3A	3.684667	14.854	-3.454	-0.346	9.79696
HMGCS2	3.74	15.112	-2.51	-1.382	9.864577
TXNDC5	3.952333	12.355	-0.366	-0.132	7.277863
ELA2B	3.962	8.272	-0.285	3.899	4.278848
PTCH2	3.981	4.754	2.567	4.622	1.226337
PVRL2	4.078667	13.918	-2.773	1.091	8.73739
GPR107	4.152667	10.018	-1.668	4.108	5.843128
VCP	4.478333	6.028	2.486	4.921	1.812017
TBDN100	4.529667	15.906	-1.244	-1.073	9.852565
QPCT	4.568333	14.04	-0.232	-0.103	8.202958
AGXT2L1	4.822	14.135	-0.406	0.737	8.085517
SSBP1	4.838333	9.216	1.453	3.846	3.975498
KIAA1173	4.861333	13.406	0.061	1.117	7.418712
PPIL2	4.879333	12.599	-0.219	2.258	6.799178
CCNG1	4.91	16.289	-1.426	-0.133	9.875687
CRYL1	4.931333	16.357	-1.188	-0.375	9.903264
ESRRBL1	4.999667	11.639	0.478	2.882	5.874127
CREB5	5.070333	8.078	0.82	6.313	3.785209
GTF2A1	5.073	14.515	-1.702	2.406	8.43104
TESK1	5.104667	9.248	1.553	4.513	3.88147
TAPBP	5.234667	11.491	-3.006	7.219	7.449425
GPR110	5.267	15.786	-1.186	1.201	9.187571
ATP5A1	5.334333	13.316	-0.048	2.735	7.050995
RUVBL1	5.339667	8.119	3.928	3.972	2.407074
KCNH5	5.381333	13.374	0.089	2.681	7.042134
P66beta	5.565333	18.092	-2.077	0.681	10.93571
PIP3AP	6.054333	18.406	-0.518	0.275	10.7042
ELP3	6.238667	15.378	1.2	2.138	7.928778
CAMK1D	6.287333	13.363	2.71	2.789	6.127834
SLC20A2	6.318667	17.814	-1.808	2.95	10.23556
SNRPD1	6.414667	11.96	-0.718	8.002	6.486343
LOXL2	6.424333	21.054	-0.932	-0.849	12.66973
VDAC2	6.491	17.132	0.95	1.391	9.218014
MSI2	6.496333	17.038	-0.3	2.751	9.255928
HIAT1	6.717333	15.662	1.105	3.385	7.829744
KIAA0759	6.744667	16.502	-1.303	5.035	9.024784
ATP6V1H	7.049	18.051	-0.84	3.936	9.822706
BCS1L	7.427333	17.407	-0.772	5.647	9.219338
NUP62	7.565333	24.206	-1.369	-0.141	14.42431
SMARCA3	7.798333	15.551	1.896	5.948	7.013028
GRK7	7.822	21.456	-1.764	3.774	12.12773
FLJ11164	7.871	20.986	0.762	1.865	11.3713
PRSS8	7.953333	27.247	-3.585	0.198	16.81553
RTN4IP1	7.979667	22.685	-0.606	1.86	12.79474
TPST1	8.023667	21.153	0.271	2.647	11.43223
SUPT6H	8.763333	27.383	-3.967	2.874	16.4839

LBR	9.104333	30.364	-2.834	-0.217	18.45785
ADCY5	9.405667	26.521	-1.297	2.993	14.97672
PPIA	9.440333	29.734	-4.756	3.343	18.03533
TRIP	9.604667	30.346	-2.006	0.474	18.00527
CCKAR	9.613667	28.044	-0.867	1.664	16.01123
UBL5	9.893	17.217	5.022	7.44	6.456966
PRPF8	10.242	14.565	2.397	13.764	6.805764
SNRPB	10.36767	23.36	1.819	5.924	11.43736
GCKR	10.577	27.842	-0.879	4.768	15.21619
RANBP2L1	10.707	24.868	2.423	4.83	12.3227
GABRG1	11.21333	30.373	-0.056	3.323	16.67855
TREM2	13.59633	28.583	-0.277	12.483	14.46218
SYVN1	13.853	28.209	0.805	12.545	13.74874
WIG1	16.24567	31.245	-0.534	18.026	15.96413
RAB3IP	17.21233	45.207	0.867	5.563	24.35753
ACTN4	21.06767	36.646	1.979	24.578	17.59807
AKAP9	21.14767	65.968	-2.278	-0.247	38.82883
YWHAQ	22.59633	49.14	-0.67	19.319	25.06621

Table 25: List of candidates identified in the second screen.

GeneSymbol	mean	max	min	median	sd
ATF6	-15.229	-6.802	-23.17	-15.715	8.194816
POLR2K	-12.5627	-4.234	-21.929	-11.525	8.893021
SHARP	-8.21567	-5.098	-11.616	-7.933	3.268181
CSNK2B	-7.02367	-1.492	-15.74	-3.839	7.639238
NETO2	-6.04367	-3.384	-10.179	-4.568	3.629904
MMP3	-5.59667	-0.993	-12.685	-3.112	6.229438
TLR4	-5.482	-0.99	-13.845	-1.611	7.249223
RAN	-5.294	-3.525	-8.2	-4.157	2.536431
TRIM61	-4.876	-1.715	-10.874	-2.039	5.196946
PARP2	-3.896	0.172	-7.356	-4.504	3.80065
BTA1F1	-3.42	-1.474	-6.998	-1.788	3.102614
SLC30A3	-3.396	0.434	-9.92	-0.702	5.678429
ACSL1	-3.357	-1.665	-5.103	-3.303	1.719636
IL17R	-3.22367	0.738	-9.182	-1.227	5.252771
NALP11	-3.20833	-0.569	-5.909	-3.147	2.670528
CYP51A1	-3.13533	-0.372	-7.469	-1.565	3.800173
MGC8685	-2.992	0.274	-9.18	-0.07	5.361725
CCR3	2.053333	4.913	-1.961	3.208	3.579513
MGST2	2.143667	10.759	-3.935	-0.393	7.668404
PA2G4	2.227667	5.313	-3.335	4.705	4.826993
FUSIP1	2.381667	5.865	0.078	1.202	3.068559
PLA2G6	2.393333	6.347	-0.595	1.428	3.570258
MGC15668	2.396333	6.453	-0.758	1.494	3.689212
SFRS7	2.47	6.807	-4.748	5.351	6.293221
AKR1B10	2.49	12.173	-3.965	-0.738	8.53954
RBP2	2.499667	4.064	1.682	1.753	1.355217
SLC22A17	2.598	4.578	0.972	2.244	1.828878
FLJ22054	2.622333	6.341	-0.288	1.814	3.387619
MTCH2	2.647	13.433	-3.377	-2.115	9.362238
SCO1	2.652667	5.257	-1.722	4.423	3.811453
CSNK1D	2.749	4.425	0.122	3.7	2.303748
TRIM43	2.848	3.715	2.021	2.808	0.847708
CPSF2	2.879	6.304	-1.154	3.487	3.765991
ADAMTS13	2.885667	6.303	-1.056	3.41	3.707413
MKKNK2	2.911333	4.791	0.717	3.226	2.055147
PIK3R2	2.954667	10.981	-3.589	1.472	7.397293
GABRB2	3.050333	14.924	-4.103	-1.67	10.3546
MYO9B	3.122	7.577	0.161	1.628	3.92725
FOLR3	3.133667	15.273	-3.931	-1.941	10.55995
MYF6	3.365667	6.002	2.018	2.077	2.283322
KRTHA3A	3.684667	14.854	-3.454	-0.346	9.79696
HMGCS2	3.74	15.112	-2.51	-1.382	9.864577
TXNDC5	3.952333	12.355	-0.366	-0.132	7.277863
ELA2B	3.962	8.272	-0.285	3.899	4.278848
PTCH2	3.981	4.754	2.567	4.622	1.226337

PVRL2	4.078667	13.918	-2.773	1.091	8.73739
GPR107	4.152667	10.018	-1.668	4.108	5.843128
VCP	4.478333	6.028	2.486	4.921	1.812017
TBDN100	4.529667	15.906	-1.244	-1.073	9.852565
QPCT	4.568333	14.04	-0.232	-0.103	8.202958
AGXT2L1	4.822	14.135	-0.406	0.737	8.085517
SSBP1	4.838333	9.216	1.453	3.846	3.975498
KIAA1173	4.861333	13.406	0.061	1.117	7.418712
PPIL2	4.879333	12.599	-0.219	2.258	6.799178
CCNG1	4.91	16.289	-1.426	-0.133	9.875687
CRYL1	4.931333	16.357	-1.188	-0.375	9.903264
ESRRBL1	4.999667	11.639	0.478	2.882	5.874127
CREB5	5.070333	8.078	0.82	6.313	3.785209
GTF2A1	5.073	14.515	-1.702	2.406	8.43104
TESK1	5.104667	9.248	1.553	4.513	3.88147
TAPBP	5.234667	11.491	-3.006	7.219	7.449425
GPR110	5.267	15.786	-1.186	1.201	9.187571
ATP5A1	5.334333	13.316	-0.048	2.735	7.050995
RUVBL1	5.339667	8.119	3.928	3.972	2.407074
KCNH5	5.381333	13.374	0.089	2.681	7.042134
P66beta	5.565333	18.092	-2.077	0.681	10.93571
PIP3AP	6.054333	18.406	-0.518	0.275	10.7042
ELP3	6.238667	15.378	1.2	2.138	7.928778
CAMK1D	6.287333	13.363	2.71	2.789	6.127834
SLC20A2	6.318667	17.814	-1.808	2.95	10.23556
SNRPD1	6.414667	11.96	-0.718	8.002	6.486343
LOXL2	6.424333	21.054	-0.932	-0.849	12.66973
VDAC2	6.491	17.132	0.95	1.391	9.218014
MSI2	6.496333	17.038	-0.3	2.751	9.255928
HIAT1	6.717333	15.662	1.105	3.385	7.829744
KIAA0759	6.744667	16.502	-1.303	5.035	9.024784
ATP6V1H	7.049	18.051	-0.84	3.936	9.822706
BCS1L	7.427333	17.407	-0.772	5.647	9.219338
NUP62	7.565333	24.206	-1.369	-0.141	14.42431
SMARCA3	7.798333	15.551	1.896	5.948	7.013028
GRK7	7.822	21.456	-1.764	3.774	12.12773
FLJ11164	7.871	20.986	0.762	1.865	11.3713
PRSS8	7.953333	27.247	-3.585	0.198	16.81553
RTN4IP1	7.979667	22.685	-0.606	1.86	12.79474
TPST1	8.023667	21.153	0.271	2.647	11.43223
SUPT6H	8.763333	27.383	-3.967	2.874	16.4839
LBR	9.104333	30.364	-2.834	-0.217	18.45785
ADCY5	9.405667	26.521	-1.297	2.993	14.97672
PPIA	9.440333	29.734	-4.756	3.343	18.03533
TRIP	9.604667	30.346	-2.006	0.474	18.00527
CCKAR	9.613667	28.044	-0.867	1.664	16.01123
UBL5	9.893	17.217	5.022	7.44	6.456966

PRPF8	10.242	14.565	2.397	13.764	6.805764
SNRPB	10.36767	23.36	1.819	5.924	11.43736
GCKR	10.577	27.842	-0.879	4.768	15.21619
RANBP2L1	10.707	24.868	2.423	4.83	12.3227
GABRG1	11.21333	30.373	-0.056	3.323	16.67855
TREM2	13.59633	28.583	-0.277	12.483	14.46218
SYVN1	13.853	28.209	0.805	12.545	13.74874
WIG1	16.24567	31.245	-0.534	18.026	15.96413
RAB3IP	17.21233	45.207	0.867	5.563	24.35753
ACTN4	21.06767	36.646	1.979	24.578	17.59807
AKAP9	21.14767	65.968	-2.278	-0.247	38.82883
YWHAQ	22.59633	49.14	-0.67	19.319	25.06621

Table 26: List of final hits identified in the third screen.

GeneSymbol	EntrezID	Replicate1.mean	Replicate1.max	Replicate1.min	Replicate1.median	Replicate1.sd
POLR2K	5440	-5.30767	-4.568	-6.06	-5.295	0.746081
SPEN	23013	-5.18767	-4.938	-5.362	-5.263	0.221811
RAN	5901	-4.67367	-3.301	-5.822	-4.898	1.275384
SLC30A3	7781	-3.284	-2.074	-3.92	-3.858	1.048349
CSNK2B	1460	-2.58767	0.13	-5.863	-2.03	3.03517
ACSL1	2180	-2.351	-2.138	-2.522	-2.393	0.195415
CYP51A1	1595	-2.03967	-1.494	-2.441	-2.184	0.489721
GTF2A1	2957	2.148333	3.214	1.227	2.004	1.001332
ATP6V1H	51606	2.877667	3.922	1.171	3.54	1.490307
PRPF8	10594	3.245	4.391	2.111	3.233	1.140047
SNRPB	6628	3.943667	6.318	1.152	4.361	2.608163
RTN4IP1	84816	4.011333	7.391	1.161	3.482	3.148551
MFSD14A	64645	4.04	5.812	1.163	5.145	2.513776
SUPT6H	6830	4.289333	8.937	0.937	2.994	4.154325
SRSF7	6432	4.319333	6.415	2	4.543	2.215982
UBL5	59286	5.473	7.23	3.224	5.965	2.047818
VDAC2	7417	5.762	7.753	3.534	5.999	2.119461
PRSS8	5652	6.567333	10.381	2.38	6.941	4.013567
SNRPD1	6632	6.742	11.686	1.822	6.718	4.932044
LOC100996657	1.01E+08	6.954667	8.239	5.154	7.471	1.606006
GABRB2	2561	7.488333	9.984	5.513	6.968	2.280465
NUP62	23636	9.588333	13.815	7.112	7.838	3.678356

8.10 Acknowledgments

First and foremost, I would like to thank my supervisor Prof. Philip Rosenstiel for offering me the opportunity to pursue this PhD and for continuing to support me through to the end.

Thank you for your effort, your ideas, and your guidance which allowed me to work independently and grow as a researcher.

I would also like to thank the other members of my PhD committee, Prof. Dr. Thomas Röder and Prof. Dr. Andre Franke, for kindly agreeing to evaluate my thesis and for their willingness to be part of my evaluation committee.

I am also very thankful to Dr. Philipp Arnold who has been a great collaborator and shed light on the function of ORMDL proteins.

I gratefully acknowledge the funding sources that provided the financial support for this research: the Collaborative Research Centre 877 (Proteolysis as a Regulatory Event in Pathophysiology) as well as the ZMB Young Scientist Grant.

I would like to sincerely thank the many people who not only made this research possible but also made the journey to completing it such an enjoyable and rewarding experience.

I owe many thanks to Dr. Jan Kuiper for providing many valuable insights and much helpful advice over the years. I am especially thankful to Dr. Marlene Jentsch for introducing me into the fabulous world of ORMDL proteins and to Dr. Anne Luzius for her guidance and support. I am grateful to Dr. Simone Lipinski and Dr. Konrad Aden for the opportunity to work with you the past years and for all the insightful input. I would also like to acknowledge Dr. Nina Sommer for her help in the animal experiment and Dr. med. Go Ito for his help and support in culturing organoids.

I am especially thankful to the cell biology technicians: Sabine, Melanie, Dorina, Steffi, Maren, Karina, Tatjana, Katha and Tanja. This work would not have been successful without your profound knowledge, dedication and help.

To Antonella, Berith, Anna & Helene - I cannot express my gratitude enough for all your help, support, and most importantly friendship!

Thank you to all the past and present members of the Cell Biology group, colleagues and friends at the IKMB for your advice, friendship and support.

Last but not least, thank you to Martin and my family for encouraging me to pursue my dreams. I am eternally grateful for your love, your time, advice, effort and support.

Curriculum Vitae STEPHANIE STENGEL

Date of birth: 18.07.1990

Place of birth: Crailsheim

Nationality: German

Contact: stephanie_stengel@web.de

WORK EXPERIENCE

Since 05/2015

Institute of Clinical Molecular Biology, Kiel University & University Hospital Schleswig-Holstein, Germany

Doctoral Researcher

- Studying disease pathogenesis in inflammatory bowel disease (IBD) *in vitro* and *in vivo*
- Analysis of the role of IBD risk genes in shaping hostmicrobiome interactions
- Drug testing on 3D cell culture models derived from murine tissue and human biopsies
- RNAi screening

12/2014 - 04/2015

Research Center for Infectious Diseases, Würzburg University, Germany

Research Assistant

- Characterizing a bacterial protein and its function
- Drug target testing for the development of new antibiotics

09/2013 - 12/2013

Institute of Cancer Sciences, Glasgow University, Scotland

ERASMUS Research Internship

- Establishing a murine 3D *in vitro* model for breast cancer research

03/2013 - 05/2013

Kneipp, Ochsenfurt, Germany

Internship in Research & Development

11/2010 - 01/2011

Rudolf Virchow Center, Würzburg University, Germany

Research Assistant

Role of pro-inflammatory signaling in autoimmune diseases

EDUCATION

Since 05/2015

Institute of Clinical Molecular Biology, Kiel University & University Hospital Schleswig-Holstein, Germany

PhD candidate and member of the Integrated Research Training Group (IRTG) of the Collaborative Research Centre 877

Thesis title: On the Role of ER Homeostasis and Autophagy in Intestinal Inflammation

10/2012 - 11/2014

Würzburg University, Germany

Master in Biomedicine (MSc) (Final grade: 1.1)

Master-Thesis: Characterization of the interacting domains of the scaffold protein that organizes lipid rafts in bacteria

10/2009 - 08/2012

Würzburg University, Germany

Bachelor in Biomedicine (BSc) (Final grade: 1.5)

Bachelor-Thesis: Evolution of resistance to antimycotics in *Candida albicans*

06/2009

Albert-Schweitzer-Gymnasiums Crailsheim
Allgemeine Hochschulreife (final grade: 1.1)

RELEVANT SKILLS

Languages	German (native speaker) English (fluent) Spanish (basic) French (basic)
Software	MS Office (excellent) Adobe Illustrator (good) ImageJ (good)
Certificates	Statistics in science Flow cytometry

AWARDS

10/2017	ZMB Young Scientists Grant 2017 for Doctoral Students 10.000€ for my research project
09/2017	Travel Grant 25 th UEG Week 2017, Barcelona, Spain

SELECTED CONFERENCE CONTRIBUTIONS

10/2017	United European Gastroenterology (UEG) week, Barcelona, Spain
10/2015	7th DGfI Autumn school: Current Concepts in Immunology, Merseburg
10/2014	5 th ASM Conference on Cell-Cell Communication in Bacteria, San Antonio, Texas

PUBLICATIONS

Aden, K., Tran, F., Ito, G., Sheibani-Tezerji, R., Lipinski, S., Kuiper, J.W., Tschurtschenthaler, M., Saveljeva, S., Bhattacharyya, J., Hasler, R., Bartsch, K., Luzius, A., Jentsch, M., Falk-Paulsen, M., **Stengel, S.T.**, Welz, L., Schwarzer, R., Rabe, B., Barchet, W., Krautwald, S., Hartmann, G., Pasparakis, M., Blumberg, R.S., Schreiber, S., Kaser, A., and Rosenstiel, P. (2018). ATG16L1 orchestrates interleukin-22 signaling in the intestinal epithelium via cGAS-STING. *J Exp Med*.

Garcia-Fernandez, E., Koch, G., Wagner, R.M., Fekete, A., **Stengel, S.T.**, Schneider, J., Mielich-Suss, B., Geibel, S., Markert, S.M., Stigloher, C., and Lopez, D. (2017). Membrane Microdomain Disassembly Inhibits MRSA Antibiotic Resistance. *Cell* 171, 1354-1367 e1320.

Stengel, S., Messner, B., Falk-Paulsen, M., Sommer, N., and Rosenstiel, P. (2017). Regulated proteolysis as an element of ER stress and autophagy: Implications for intestinal inflammation. *Biochim Biophys Acta Mol Cell Res* 1864, 2183-2190.

Koch, G., Wermser, C., Acosta, I.C., Kricks, L., **Stengel, S.T.**, Yepes, A., and Lopez, D. (2017). Attenuating *Staphylococcus aureus* Virulence by Targeting Flotillin Protein Scaffold Activity. *Cell Chem Biol* 24, 845-857 e846.

Koch, G., Yepes, A., Forstner, K.U., Wermser, C., **Stengel, S.T.**, Modamio, J., Ohlsen, K., Foster, K.R., and Lopez, D. (2014). Evolution of resistance to a last-resort antibiotic in *Staphylococcus aureus* via bacterial competition. *Cell* 158, 1060-1071.

8.12 Eidesstattliche Erklärung

Hiermit erkläre ich, Stephanie Tanja Stengel, an Eides statt, dass ich die vorliegende Arbeit unter der wissenschaftlichen Leitung von Prof. Dr. Philip Rosenstiel selbstständig und ohne fremde Hilfe verfasst habe. Die Abhandlung stellt nach Form und Inhalt meine eigene Arbeit dar und ich habe außer der Beratung meiner Betreuer, Prof. Dr. Philip Rosenstiel und Dr. Jan Kuiper, keine weitere Hilfe in Anspruch genommen.

Weiterhin habe ich keine anderen als die von mir angegebenen Quellen und Hilfsmittel benutzt und die den verwendeten Werken wörtlich und inhaltlich entnommenen Stellen als solche kenntlich gemacht. Die Arbeit wurde unter der Einhaltung der Regeln guter wissenschaftlicher Praxis der Deutschen Forschungsgemeinschaft erstellt. Auszüge der Dissertation wurden bereits in Posterbeiträgen veröffentlicht.

Ich versichere, dass ich weder an der Christian-Albrechts-Universität zu Kiel noch anderweitig versucht habe, eine Dissertation einzureichen oder mich einer Promotionsprüfung zu unterziehen.

Hiermit erkläre ich, dass mir kein akademischer Grad entzogen wurde.

Kiel, den

Stephanie Tanja Stengel